Neuron-specific characteristics of miR135b- and miR137-mediated translational regulation

Thesis submitted for the degree of

Doctor of Philosophy

at the University of Leicester

By

Karishma Joshi BSc

Department of Neuroscience, Psychology and Behaviour

University of Leicester

August 2020

Abstract

Neuron-specific characteristics of miR135b- and miR137-mediated translational regulation – Karishma Joshi

microRNAs are small, non-coding post-transcriptional regulators of gene expression that target specific mRNAs, typically effecting translational repression coupled to degradation. In contrast, previous work within the Luthi-Carter laboratory has shown that neuron-enriched microRNAs, including miR135b and miR137, co-exist with their targets, many of which encode proteins with important synaptic functions.

Neurons are highly polarised, interconnecting cells that form complex brain networks. The site of neurotransmission, the synapse, allows the directional flow of electrical and chemical signals via specialised neuronal subdomains, i.e. from the axon to dendritic fields. mRNA transport and local translation is one of several mechanisms modulating synaptic strength, in a phenomenon known as neuronal plasticity.

In this thesis, I test the hypothesis that neuronal microRNAs, miR135b and miR137, operate via non-degrading target interactions. In addition, I explore a related hypothesis and demonstrate that miR135b- and miR137-target interactions display characteristics consistent with a role in RNA transport to synapses, including their interaction with relevant RNA binding proteins.

My analyses provide strong evidence for non-degrading miR135b- and miR137-target interactions, by demonstrating that both microRNAs co-exist with, and in some cases positively modulate the levels of, their target mRNAs. Moreover, under the conditions of my experiments, overexpression of miR137 led to an increase, rather than a decrease, in the levels of its target proteins. Furthermore, I show that miR135b and miR137 and their targets coexist in MOV10-positive complexes, consistent with a role in translational repression during mRNA transport to pre- or postsynaptic fields. Although not expressly demonstrated, the association of miR135b and miR137 with MOV10 in this context strongly implicates these complexes in signal-dependent modulation of local protein translation to regulate synaptic and neuronal connectivity. The regulation of miR135b- and miR137-target interactions may therefore explain their previous associations with dysfunctional neuronal connectivity giving rise to human neurological and neuropsychiatric conditions.

Acknowledgements

First and foremost, I would like to thank both of my supervisors. Prof. Ruth Luthi-Carter, for being encouraging, supportive and for always providing me with endless guidance from the moment I first met you. Ruth has taught me to always stand up for myself and for what I believe in, and to have belief in my own ability. Thank you for putting up with my incessant questions and need for double-checking, my frustrations and importantly, celebrating the successes. Thank you for all your guidance whilst writing my thesis mid-pandemic, the insight you have provided to this project has been invaluable! I hear PhDs are often emotional rollercoasters, but I am glad that you were there to guide me through. Thank you to the members of the Luthi-Carter lab, past and present for teaching me, and for being a great team.

A massive thank you to Dr Volko Straub, my co-supervisor, for your help, guidance and support throughout my PhD. Thank you for always providing me with an alternate perspective to my research. Thank you for teaching me, helping me with my ImageJ/FIJI analysis, providing me with opportunities to teach, and always allowing me to borrow antibodies.

I would additionally like to express my gratitude to Prof. Flaviano Giorgini for being on my thesis panel for the last three years. Thank you for your encouragement, all your suggestions and for helping me set (and be okay with) realistic expectations.

Thank you to the Department of Neuroscience, Psychology and Behaviour for the help and facilities which have been essential to my research. I am grateful for the opportunities to participate on various committees within the Department during my PhD – from Health & Safety, Equality, Diversity & Inclusion to Brain Awareness Day 2019. I am thankful to have worked alongside so many great people during my time in NPB.

Thank you to Dr Kees Straatman, of the Advanced Imaging Facility at the University of Leicester for your help and guidance with my microscopy. I would like to express my gratitude to Prof. Martin Bushell for allowing me access to his lab's polysome profiling equipment, and to Dr Ewan Smith for teaching me how to use it all (and, importantly, how to clean up sucrose messes).

My husband, Jay – thank you for making all the bad science days feel better, stopping me replying to emails on holiday and mostly for being my biggest support. Thank you for supporting me through my anxieties and always encouraging me. I couldn't have done it without you believing in me and promising me that my experiments would eventually work (even though I'm sure, that you were never sure they would)!

A huge thank you to my amazing family. My parents, for their love and always allowing me the freedom to pursue whatever I felt was right and having total confidence in me, even when I am often convinced that I am a total imposter! Mum – for ringing me every evening to make sure I'll be home at a decent time, and for all the dinners! Dad – for asking me questions about my work, and really trying to understand what it is I am working on (we've made up a tonne of analogies to help with this). My brother, Jay, for your never-ending belief in me, I appreciate it more than I let on. Thank you to my parents- and siblings-in-law for their unconditional support and encouragement. Thank you to my cousins for being a wonderful bunch and all the fun-filled weekends.

My friends in 330 (and beyond) – 'the duct tape to my sanity' and 'my PhD survival kit'. Thank you for keeping me sane and for allowing me to rant, cry and laugh. Thank you for joining me (without complaint) on my 'OCD tour' of the lab before leaving in the evenings. To be surrounded and inspired by so many amazing people, with the best minds but most importantly the kindest hearts, was a true privilege. Cake Friday, the whiteboard, the bunting, the cheese, the snacks, the coffee, Halloween… The past few years would have been much harder without being surrounded by so many friends. My friends, Aarti and Azraa, thank you for the food and wine dates and always being there for me.

Thank you to the students who I have supervised over the years. My first real opportunity teaching was when I had barely begun my PhD; in the years that followed, I've supervised undergraduate students, master's students and work experience/summer placement students in the lab, as well as demonstrating and teaching on undergraduate Biological Science courses. My time spent teaching has been invaluable. I couldn't imagine this experience without meeting all the wonderful students who I had the privilege to introduce (often for the first time) to the world of research. I hope I can continue to inspire more young minds in the future.

Contents

List of Figures

List of Tables

List of Abbreviations

3': Three Prime

5': Five Prime

Aβ: Amyloid-Beta

Ab-Ag: Antibody-Antigen

Ago: Argonaute

AMPA: α-amino-3-hydroxy-5-methyl-4-isoxazolepropionic acid

Ankrd12: Ankyrin Repeat Domain 12

APP: Amyloid Precursor Protein

ARE: AU-rich Element

ASD: Autism Spectrum Disorder

Atp1b1: ATPase Na+/K+ Transporting Subunit Beta 1

bDNA: Branched DNA

Bsn: Bassoon

BSA: Bovine Serum Albumin

CAMKII: Ca^{2+}/Calmodulin Dependent Protein Kinase

CCR4-NOT: Carbon Catabolite Repression—Negative On TATA-less

cDNA: complementary DNA

DIV: Days In-Vitro

DMEM: Dulbecco's Modified Eagle Medium

DNA: Deoxyribonucleic Acid

DTT: Dithiothreitol

eIF: Eukaryotic Initiation Factor

Fam126b: Family with Sequence Similarity 126 Member B

FBS: Foetal Bovine Serum

FISH: Fluorescence In-Situ Hybridisation

FMRP: Fragile-X Mental Retardation Protein

FUS: Fused in Sarcoma

GABA: Gamma Aminobutyric Acid

Gabra1: Gamma Aminobutyric Acid Type A Receptor Subunit Alpha 1

GAT-1: GABA Transporter 1

GFP: Green Fluorescent Protein

GTP: Guanosine Triphosphate

HCl: Hydrochloric Acid

ICC: Immunocytochemistry

ID: Intellectual Disability

IMP1: IGF2 mRNA binding protein 1

IP: Immunoprecipitation

KCl: Potassium Chloride

LB: Luria-Bertani

Lrrn3: Leucine Rich Repeat Neuronal 3

LTP: Long-Term Potentiation

LTD: Long-Term Depression

m^7G: 7-methylguanosine

mRNA: messenger RNA

MEF2A: Myocyte Enhancing Factor 2A

$MgCl_2$: Magnesium Chloride

miR124: microRNA 124

miR135b: microRNA 135b

miR137: microRNA 137

***MIR137HG*:** microRNA 137 Host Gene

MOV10: Moloney Leukaemia Virus 10 Protein

NaCl: Sodium Chloride

NaOH: Sodium Hydroxide

NMDA: N-methyl-D-aspartate

Nsg1: Neuronal Vesicle Trafficking Associated 1

PABP: Poly-A Binding Protein

PAN: Poly(A) Nuclease

PBS: Phosphate Buffered Saline

PCR: Polymerase Chain Reaction

PEI: Polyethylenimine

PFA: Paraformaldehyde

Pre-microRNA: Precursor microRNA

Pri-microRNA: Primary microRNA transcript

PSD95: Postsynaptic Density Protein 95

Ptpn5: Protein Tyrosine Phosphatase Non-Receptor Type 5

RIMs: Rab3-interacting Molecules

REST: RE1-Silencing Transcription Factor

RISC: RNA Induced Silencing Complex

RBP: RNA Binding Protein

RNA: Ribonucleic Acid

RNAi: RNA interference

RT: Reverse Transcription

SDS: Sodium Dodecyl Sulphate

SDS-PAGE: Sodium Dodecyl Sulphate Polyacrylamide Gel Electrophoresis

SEM: Standard Error of the Mean

Sept3: Septin 3

Slc6a1: Solute Carrier Family 6 Member 1

SMA: Spinal Muscular Atrophy

SMN: Survival Motor Neuron

SNP: Single Nucleotide Polymorphism

SOD2: Superoxide Dismutase 2

Ssr2: Signal Sequence Receptor 2

Syt1: Synaptotagmin 1

TBS: Tris Buffered Saline 0.1% Tween

TBS-T: Tris Buffered Saline - 0.1% Tween

TDMD: Target Directed microRNA Degradation

TDP-43: TAR DNA Binding Protein 43

TEMED: Tetramethylethylenediamine

TMMP: Target-mediated microRNA Protection

tRNA: Transfer RNA

qPCR: Quantitative Polymerase Chain Reaction

Vamp2: Vesicle Associated Membrane Protein 2

XRN1: 5’ – 3’ Exoribonuclease 1

XRN2: 5’ – 3’ Exoribonuclease 2

ZBP1: Zip-code Binding Protein 1

1 Chapter 1: Introduction

1.1 Cellular organisation of the nervous system

The brain is made up of roughly 100 billion neurons, which are interconnected to form an intricate network (Herculano-Houzel, 2009). Neurons are highly polarised cells that connect electrically and chemically over relatively long distances. The structural wiring of neuronal networks underlies brain function. Electrical conductivity occurs along neuronal processes, the dendrites and axons. The contacts between neurons, called synapses, act as the site of chemical communication between neuronal cells. Synapses are intercellular junctions that connect the output field (axon) of one neuron to the input field (dendrite or other postsynaptic membrane) of the next neuron in the series, via the release of chemical messengers called neurotransmitters. Neurons differ in the type of neurotransmitter they release; in the brain these are predominantly glutamate, which is excitatory, or gamma-aminobutyric acid (GABA), which is inhibitory, thereby governing the effect of that neuron in its circuit (Südhof, 2018).

The polar organisation of neuronal subdomains with different functional roles is crucial for the directional conveyance of information through the brain. Axons and their presynaptic terminals must be specified to perform the vesicular release of neurotransmitters, whilst postsynaptic fields e.g. along dendrites, require the correct trafficking and anchoring of suitable neurotransmitter receptors (Takano et al., 2015). Physical aspects of synaptic connections also require polar organisation and maintenance, including the expression of cell adhesion molecules, such as presynaptic neurexins and postsynaptic neuroligins, and components of the synaptic cytoskeleton, which help govern synaptic morphology and strength (Poulopoulos et al., 2009, Südhof, 2018).

The polar organisation of neurons therefore requires the differential synthesis and trafficking of specialised macromolecules along axons and dendrites. This sometimes demands transport of macromolecules over long intracellular distances. For example, ATP-dependent transport of components required for the local synthesis and packaging of neurotransmitters into vesicles, such as enzymes and vesicle proteins, must be shuttled down long axonal processes to presynaptic terminals. Likewise, voltage gated

calcium channels must be expressed at the presynapse to allow electrogenic signals to be converted into calcium-dependent neurotransmitter release into the synaptic cleft (Sudhof, 2012). This release occurs at presynaptic active zones composed of scaffold proteins such as Bassoon (Bsn), Rab3-Interacting Molecules (RIMs) and Munc13, which also require targeted biosynthesis and/or transport (Sudhof, 2012, Gundelfinger et al., 2015).

In the recipient neuron neurotransmitters are received by postsynaptic fields. Sometimes highly structured, dendrites receive input signals which are detected by the presence of neurotransmitter receptors (Südhof, 2018). In excitatory synapses, ionotropic glutamate receptors (e.g. AMPA and NMDA receptors) are organised in postsynaptic densities, which concentrate these receptors using a network of scaffolding proteins (e.g. PSD95) and harbour other effectors necessary for subsequent signals to be propagated (such as voltage-gated ion channels and kinases) (Feng and Zhang, 2009, Sheng and Kim, 2011).

Inhibitory synapses contain different sets of adhesion and scaffolding proteins, such as Neuroligin-2, which is thought to function in GABA-A receptor recruitment, and gephyrin, which interacts with glycine receptors (Varoqueaux et al., 2004, Poulopoulos et al., 2009, Sheng and Kim, 2011).

In either case, the receipt of a neurotransmitter triggers a voltage change in the corresponding postsynaptic field – depolarisation at excitatory synapses or hyperpolarisation in inhibitory synapses, respectively. There are also parallel activities of other signalling cascades that reside in the postsynaptic membrane, such as kinases (e.g. CAMKII) and small GTPases (Sheng and Kim, 2011). Specific combinations of signalling activities and transient states of signalling events at a synapse govern the amplitude of the corresponding response, otherwise known as synaptic strength. The ability to regulate the synaptic strength over time is a phenomenon known as synaptic plasticity. Synaptic plasticity can either strengthen or weaken the connection between neurons; these two major forms of synaptic plasticity are known as long-term potentiation (LTP) and long-term depression (LTD), respectively. In LTP, high-frequency stimulation of the synapse increases synaptic strength whereas in LTD, low frequency

neuronal stimulation depresses synaptic strength (Malenka and Bear, 2004). Synaptic plasticity is a key property of neuronal cells that underpins learning and memory.

1.2 Cell polarity-dependent regulation of neuronal gene and protein expression

The majority of cellular DNA, and therefore largest number of genes, reside in the nucleus. In neuronal cells the nucleus forms part of the cell body, which is situated between the dendrite(s) and the axon(s). Messenger RNA (mRNA) is transported out of the nucleus to direct the synthesis of proteins necessary for neuronal function. Pre-mRNA is transcribed from DNA by RNA polymerase II, capped with 7-methylguanosine at the 5' end (5' m^7G), spliced to remove intronic sequences and polyadenylated at the 3' end to form the mature mRNA (Fong and Bentley, 2001). The mature mRNA is then exported to the cytoplasm, where it is either translated, degraded or translationally repressed to be transported (Martin and Ephrussi, 2009, Doyle and Kiebler, 2011).

Translation of the mRNA requires the 43S preinitiation complex, which consists of the ternary complex (comprised of an initiator methionine tRNA, GTP, and eukaryotic initiator factor 2 (eIF2)), eIF3, eIF1, eIF1A, eIF5 and the 40S small ribosomal unit (Jackson et al., 2010, Fukao et al., 2014). The 43S preinitiation complex attaches to the 5' m^7G cap, facilitated by the eIF4F translation initiation complex consisting of eIF4E, eIF4A and eIF4G proteins (Jackson et al., 2010). eIF4G is a scaffold protein that binds eIF4A, eIF4E, Poly(A) Binding Protein (PABP) and eIF43. PABP attaches to the polyadenylated 3' end of the mRNA and interacts directly at the 5' end with the eIF4G subunit of the eIF4F complex, whose eIF4E subunit is bound directly to the 5' cap, thereby circularising the mRNA (Wells et al., 1998). eIF4A helicases, in combination with eIF4B and eIF4H, facilitate unwinding of the 5' secondary structure of the mRNA to be translated, which enables ribosomal scanning. The preinitiation complex then scans the 5' untranslated region (UTR) until it locates the start codon, which leads to 48S preinitiation complex formation and encourages recruitment of the 60S large ribosomal subunit, thereby forming the translationally competent 80S ribosome complex (Wells et al., 1998, Jackson et al., 2010). This is followed by the elongation phase of translation, where the nascent polypeptide chain is extended until a stop codon is reached (King and Gerber, 2016,

Schuller and Green, 2018). A high fraction of neuronal mRNAs are translated within the neuronal cell body.

Neuronal proteins synthesised within the cell body may subsequently be transported to different cellular sub-compartments; this is governed by a process of protein sorting into different cargo vesicles to be transported via the neuronal cytoskeleton (Burack et al., 2000). Differential protein localisation is necessary to specify and maintain the dendritic versus axonal properties required for the directionality of neuronal communication. Experiments utilising heterologously expressed GFP fusion proteins have illustrated that axonal and dendritic proteins can be sorted at the cell body or proximal dendrite into distinct vesicles, to correctly target them to their respective sites of action (Bentley and Banker, 2016). The correct targeting of synaptic proteins is crucial to neuronal function and viability. For example, activation of synaptic NMDA receptors modulates synaptic plasticity and neuroprotection, whereas activation of extrasynaptic NMDA receptors causes neuronal cell death (Hardingham et al., 2002, Hardingham and Bading, 2010).

In addition to the directional transport of proteins, parallel machinery exists to selectively target mRNAs to dendritic versus axonal compartments (Zappulo et al., 2017). Upon their exit from the nucleus, mRNAs can be sorted and packaged into specialised RNA granules that are selectively transported to axonal or dendritic compartments. In neurons, a large fraction of axon- and dendrite-localised mRNAs can be related to synaptic functions. Furthermore, mRNAs and ribosomes have been observed to be localised in perisynaptic domains where they engage to fulfil local protein synthesis (Buffington et al., 2014). Local translation of mRNAs encoding synaptic proteins is believed to be a key component of signal-dependent neuronal plasticity.

1.3 Neuronal mRNA transport

As described above, maintenance of neuronal polarity requires differential distribution of mRNAs and proteins. mRNA production is almost exclusively confined to the neuronal cell body, as are the bulk population of translating ribosomes. Therefore, it is generally believed that mRNA transport is reserved for special conditions in which protein synthesis needs to be tightly controlled spatiotemporally. Synaptic plasticity, a phenomenon involved in learning and memory, is believed to rely heavily on localised

protein synthesis to modulate electrical or structural properties of neuronal connections in a signal-dependent manner (Fernandez-Moya et al., 2014).

mRNA targeting to neuronal subdomains has been shown to occur through cis- elements or 'zip-codes' within their 3' UTRs which are recognised by RNA binding proteins (RBPs) that regulate transcript stability as well as localisation (Martin and Ephrussi, 2009, Doyle and Kiebler, 2011).

RNA transport has been studied in a variety of model systems. In budding yeast, *Saccharomyces cerevisiae*, the *ASH1* mRNA is recruited into a transport granule through a process that is dependent on sequences in the *ASH1* 3' UTR and She RBPs (Bertrand et al., 1998). *ASH1* mRNA is transported to and restricted at the bud, to be selectively expressed in daughter cells, which is crucial for mate type switching (Bertrand et al., 1998). In *Drosophila,* mRNAs including *bicoid* and *nanos* are asymmetrically localised to the anterior and posterior ends of the embryo, respectively, and are involved in patterning this axis (Kiebler and Bassell, 2006).

Wilhelm and Vale (1993) proposed a model where RNAs and RBPs would be assembled into 'RNA transport particles' which are anchored to the local cytoskeleton. Neuronal RNA transport granules are thought to contain the cargo mRNA, RBPs and motor proteins such as KIF5, the kinesin heavy chain (Krichevsky and Kosik, 2001, Kosik and Krichevsky, 2002, Kanai et al., 2004, Bramham and Wells, 2007). The observed velocity of RNA transport granules is also consistent with the movement being facilitated by kinesin and dynein (Wilhelm and Vale, 1993).

Other identified components of RNA granules include Staufen and FMRP (Kanai et al., 2004). Interestingly, in the process of characterising of neuronal RNA granules, Elvira and colleagues identified an RBP they called Zipcode Binding Protein (ZBP1, now known as IMP1) (Elvira et al., 2006). IMP1 translationally represses and regulates *β-actin* mRNA transport selectively along axons to neuronal growth cones, a process that is stimulated by the neurotrophin NT-3 (Zhang et al., 2001, Kiebler and Bassell, 2006, Elvira et al., 2006). Deletion of the IMP1-binding sequence in the *β-actin* mRNA, which they called the 'zipcode' sequence, impaired this transport. Also, Src mediated phosphorylation of IMP1 allowed *β-actin* mRNA to be released, and translated near the growth cone

(Hüttelmaier et al., 2005). Moreover, IMP1 protein expression was shown to be necessary for NT-3-regulated neurite outgrowth, showing that *β-actin* mRNA transport and localised translation was crucial to this process (Hüttelmaier et al., 2005). IMP1 further interacts with a microtubule molecular motor, KIF11, thus coupling *β-actin* mRNA transport along microtubules and its translational regulation (Song et al., 2015).

The Kiebler group discovered that dendritically localised *CAMKIIα*, *MAP2* and *β-actin* mRNAs are sorted into distinct populations of RNA granules, also supporting the existence of sequence-specific targeting events (Tubing et al., 2010, Mikl et al., 2011). Curiously only a small number of RNA molecules were detected per granule (Mikl et al., 2011). This mechanism could also account for such mRNAs being needed for highly specialised neuronal functions and thereby governed by different regulatory events.

A variety of different RBPs have been implicated in neuronal mRNA transport and signal-dependent translation. Dysfunctions in some of these RBPs have been implicated in human diseases. For example, mutations in FMRP and SMN cause Fragile-X Syndrome and Spinal Muscular Atrophy (SMA), respectively, and manifest cellularly as defective translational regulation and mRNA transport to dendritic and axonal subregions (Fallini et al., 2012, Mazroui et al., 2002). TDP-43 has role in regulating RNA splicing and neuronal RNA transport, and its malfunction is implicated in several interrelated neuropathologies, including motor neuron disease and frontotemporal dementia (Mackenzie and Rademakers, 2008, Alami et al., 2014, Prasad et al., 2019).

Moreover, a discrete network of RBPs appear to have interconnected roles in neuronal mRNA transport and translation. For example, FMRP is known to be associated with MOV10, which is involved in regulating signal-dependent translation in discrete neuronal subdomains (Mazroui et al., 2002, Ashraf et al., 2006, Banerjee et al., 2009, Fallini et al., 2012, Kenny et al., 2014, Kute et al., 2019). Moreover, SMN is known to interact with both IMP1 and FMRP (Piazzon et al., 2008, Fallini et al., 2014, Khalil et al., 2018).

1.4 What are microRNAs?

Small non-coding RNAs regulate post-transcriptional gene expression, giving rise to the complexity of gene products differentially expressed throughout an organism. Included

in this class of small non-coding RNAs are small interfering RNAs (siRNAs), PIWI interacting RNAs (piRNAs) and microRNAs (Ha and Kim, 2014). This thesis will focus on microRNAs, a distinct subset of small non-coding RNAs which regulate gene expression through post-transcriptional mechanisms.

Neurons express a set of microRNAs that are believed to regulate and maintain their post-mitotic differentiation (Johnston and Hobert, 2003, Yoo et al., 2011, He et al., 2012, Jovičić et al., 2013). microRNAs are also implicated in local regulation of mRNAs at neuronal synapses to modulate synaptic plasticity (Schratt et al., 2006, Banerjee et al., 2009). This thesis follows on from previous work by the Luthi-Carter lab that examines unique aspects of microRNA mediated gene regulation in neuronal cells and considers how these may promote specialised neuronal functions.

The first 21 nucleotide microRNA to be discovered was lin-4 in *C. elegans* (Lee et al., 1993, Wightman et al., 1993). Lin-4 was shown to negatively regulate the expression of lin-14 protein by complementary base pairing to the 3' UTR of *lin-14* mRNA (subsequently defined as its mRNA 'target'). lin-4 was determined to serve a crucial regulatory step in early larval development. A second *C. elegans* microRNA, let-7 and its target *lin-41* were subsequently shown to regulate the transition from larval to adult states (Reinhart et al., 2000). It was then proposed that lin-4 and let-7 RNAs be referred to as small temporal RNAs (stRNAs) due to their roles in developmental timing (Pasquinelli et al., 2000).

The regulation afforded by lin-4 and let-7 was observed to depend on their base-pairing to complementary sequences within the 3' UTRs of their mRNA targets. At this point let-7 and its interaction with *lin-41* were determined to be conserved in *Drosophila melanogaster, Danio rerio* and in humans in a variety of different tissues (Pasquinelli et al., 2000). The evolutionarily conserved sequences and functions of let-7 microRNA and its targets led to further investigation of the extent to which small non-coding RNAs might represent an important undocumented aspect of eukaryotic gene regulation.

Soon after, it was discovered by three groups simultaneously that a large class of small non-coding RNAs resembling lin-4 and let-7 existed, and were given the name microRNAs owing to their small size (Lau et al., 2001, Lee and Ambros, 2001, Lagos-

Quintana et al., 2001). These studies employed cDNA cloning to identify many additional microRNAs in *C.elegans.* These new data identified that the microRNAs derived from longer RNA stem-loop precursors of around ~70 nucleotides, and other characteristics that indicated that they were products of Dicer (~21 – 24 nucleotides in length and containing a 5' monophosphate and a 3' hydroxyl group) (Lau et al., 2001, Lagos-Quintana et al., 2001). These groups also showed that mature microRNAs could derive from either the 5' or 3' arm of its stem-loop precursor (Lau et al., 2001, Lee and Ambros, 2001). Bioinformatic analyses further identified conserved microRNAs in a number of other host genomes (Lagos-Quintana et al., 2001). These findings combined with earlier evidence convinced the field that microRNAs served important functions as post-transcriptional gene regulators (Lee et al., 1993, Reinhart et al., 2000, Pasquinelli et al., 2000, Lee and Ambros, 2001, Lau et al., 2001, Lagos-Quintana et al., 2001).

1.4 microRNA biogenesis

microRNAs are encoded within introns of protein coding genes, within intergenic regions or in an orientation which is anti-sense to protein-coding genes (Lau et al., 2001, Lee and Ambros, 2001, Lagos-Quintana et al., 2001). microRNA precursors are transcribed by RNA polymerase II; these transcripts are called primary-microRNAs (pri-microRNAs) (Lee et al., 2004, Filipowicz et al., 2008). microRNAs within introns can be transcribed together with their host genes, whereas the other classes of microRNA would require independent transcription (Lee et al., 2004). Some microRNA genes are clustered together and are transcribed as a poly-cistronic precursor which is then further processed (Bartel, 2004).

The pri-microRNA transcript is usually over 1-kilobases long and is structured into a stem-loop with single-stranded flanking sequences (Ha and Kim, 2014) (**Figure 1.1** displays a schematic of microRNA biogenesis). The microprocessor complex formed of Drosha and DGCR8 (Pasha in *Drosophila*) processes the pri-microRNA before it exits the nucleus. DGCR8 recruits pri-microRNAs via specific RNA binding domains, to be processed by Drosha, an RNAse III-type endonuclease; the microprocessor complex selectively cleaves pri-microRNAs in two places to produce a stem-loop with a 2 nucleotide 3' overhang called the precursor microRNA (pre-microRNA) (Han et al., 2004,

Ha and Kim, 2014). Human and *Drosophila* pri-microRNAs contain conserved motifs that govern their Drosha and DGCR8 processing. These motifs are not present in *C. elegans* pri-microRNAs and thus they cannot be processed by human or *Drosophila* S2 cells (Auyeung et al., 2013).

The resulting pre-microRNA is 70 – 100 nucleotides long and is exported out of the nucleus to the cytoplasm via exportin5 and RAN-GTP which interact with the microprocessor-generated 3' overhang (Ha and Kim, 2014). In the cytoplasm, the pre-microRNA is processed by Dicer, another RNAse III-type endonuclease, with assistance from the Transactivation Response-Element RNA-Binding Protein (TRBP, loquacious in *Drosophila*) (Ha and Kim, 2014). Dicer cleaves the pre-microRNA on both strands of its stem to produce a microRNA duplex of ~21 nucleotides with a 2 nucleotide 3' overhang (Lau et al., 2001, Bartel, 2004).

With the aid of chaperone proteins, the microRNA duplex is loaded onto the RNA induced silencing complex (RISC) (Iwasaki et al., 2010). One of the two strands, sometimes called the 'passenger strand' is degraded, whereas the other strand, sometimes called the 'guide strand' remains associated to RISC. The strand with the least thermodynamically stable 5' end and/or containing a 5' Uracil is usually selected to be the 'guide strand' (Ha and Kim, 2014). However, there are instances where the guide and passenger strands are present in equal numbers or which undergo 'arm-switching'; here the microRNA isoforms are denoted by -5p or -3p depending on which arm of the microRNA duplex is present (Griffiths-Jones et al., 2011).

RISC is a multiprotein complex including Argonaute (Ago) proteins. There are 4 members of the Ago protein family in humans, all of which are around ~100kDa in size and share a common architecture (Kosik, 2006). Ago proteins have 4 domains: An N-terminal domain, a PAZ domain, a MID domain and a PIWI domain; these together form two lobes connected by linkers (Gebert and MacRae, 2019). The N-terminal and PAZ domains bind the 3' end of the microRNA, whilst the MID and PIWI domains hold the 5' end. Ago1 – 4 are involved in microRNA mediated mRNA regulation, though only Ago2 exhibits nuclease activity (Liu et al., 2004, Kosik, 2006, Filipowicz et al., 2008).

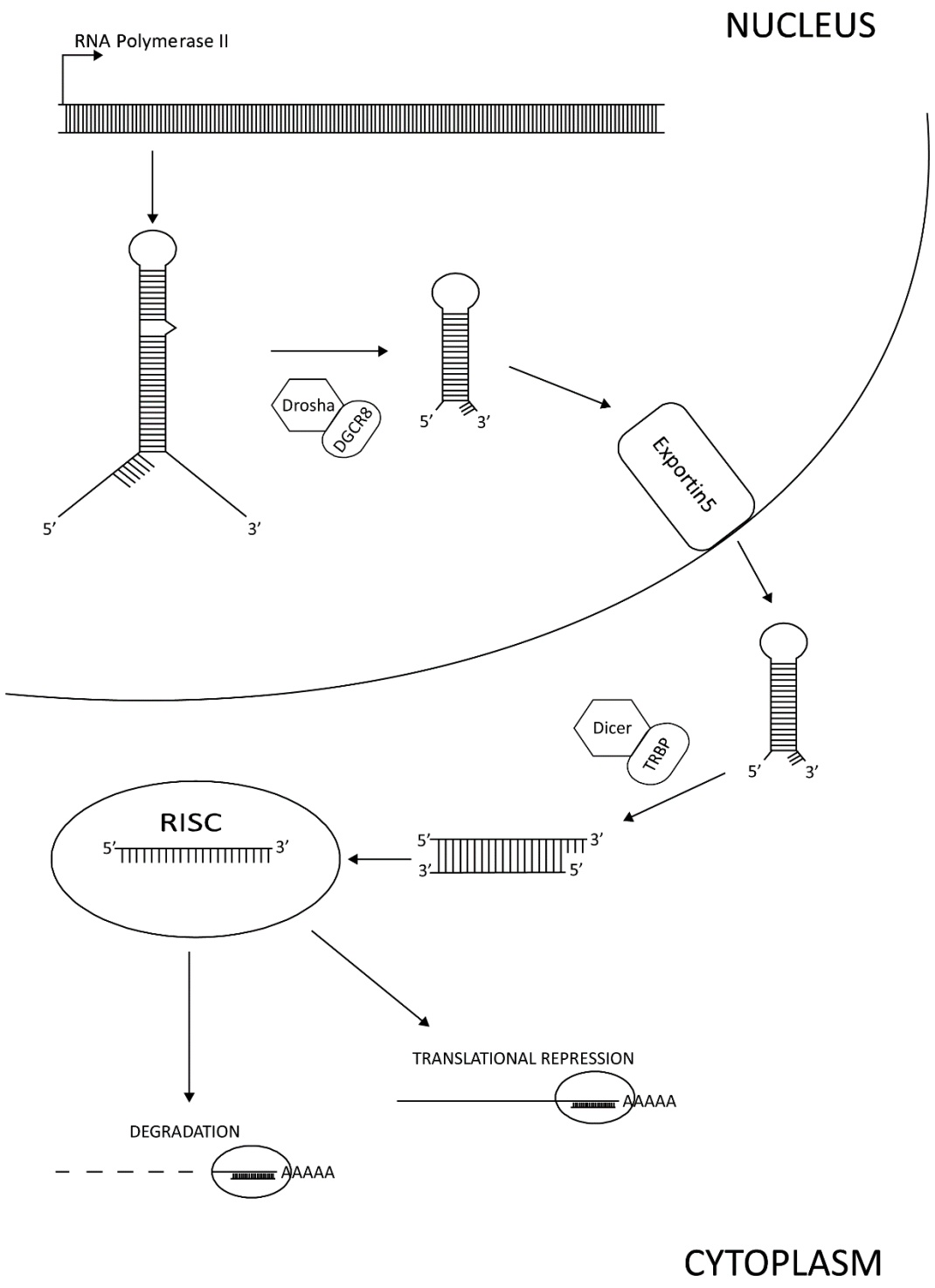

Figure 1.1: A schematic depicting the biogenesis of microRNAs. microRNAs are transcribed by RNA polymerase II either from their own promoters or within the introns of protein coding genes; the resulting pri-microRNA transcript is processed into pre-microRNA by the microprocessor complex consisting of Drosha and DCGR8. The 70 – 100 nucleotide pre-microRNA is exported out of the nucleus into the cytoplasm by exportin5-RAN•GTP, where it is further processed into the 21-nucleotide long microRNA-microRNA duplex by Dicer and TRBP. One strand of which is degraded and the other is loaded onto the RISC complex to direct target degradation or translational repression.

1.5 Mechanisms of microRNA mediated mRNA regulation

The microRNA-loaded RISC goes on to recruit mRNAs which contain complementary 'target sequences'; the microRNA-mRNA binding subsequently translationally represses and/or degrades the target mRNAs. Nucleotides 2 – 8 at the 5' end of the microRNA make up the seed sequence that is crucial for target recognition (Bartel, 2009). Seed sequences are complementary to a ~7 nucleotide target sequence in the mRNA, which is typically, but not always, located in its 3' UTR (Bartel, 2009). It has been suggested that Ago binding exposes nucleotides 2 – 4 of the microRNA seed to the cytosol in a helical conformation, to create an transient association with mRNAs harbouring a complementary sequence; the association is stabilised if the mRNA contains a full target sequence (Chandradoss et al., 2015).

microRNAs exhibit a heterogeneous range of observed target pairings. The thermodynamic stabilities of these variable pairings are generally believed to correlate with the strengths of their effects on mRNA regulation. According to this convention, the rank order of complementary pairings occur between: i) nucleotides 2 – 8 with an additional adenosine opposite nucleotide 1, ii) nucleotides 2 – 8 only, iii) nucleotides 2 – 7 with the adenosine opposite nucleotide 1, and iv) nucleotides 2 – 7 only (Lewis et al., 2005). The additional adenosine is recognised by a binding site on Ago via hydrogen bonding to water (Schirle et al., 2015). No further sequence complementarity between the microRNA and its mRNA target is typically required (Lewis, et al., 2005). Despite this, complementarity to the microRNA nucleotides 13 – 16 has been noted (Grimson et al., 2007). Other factors have also been identified to govern target recognition, for example, the distance of the seed region from the 3'UTR, the proximity of the target sequence to the stop codon and whether there are multiple of the same microRNA's binding sites in proximity to each other (Grimson et al., 2007). A single microRNA-charged RISC can undertake many rounds of mRNA targeting; therefore, one microRNA molecule can have a large impact on the stability of its target mRNA population. Non-canonical sites, which are not matched to the microRNA seed, are reported to exist but the functionality of these sites has been debated (Agarwal et al., 2015).

The expression levels of canonical microRNAs are anti-correlated to those of their target mRNAs due to tight coupling of translational repression to target degradation (Baek et

al., 2008, Guo et al., 2010, Eichhorn et al., 2014, Jin and Xiao, 2015). Both activities can be ascribed to the microRNA-loaded RISC. Canonical microRNA mediated target regulation occurs in two steps, where the mRNA must be translationally repressed to subsequently allow mRNA degradation (Wilczynska and Bushell, 2015).

GW182 proteins are known to be important scaffolds in directing microRNA mediated post-transcriptional regulation, bringing together Argonaute proteins and downstream effectors to allow efficient coupling between deadenylation, decapping and degradation (Jonas and Izaurralde, 2015). A microRNA-RISC complex typically leads to deadenylation through recruitment of the PAN2-PAN3 and CCR4-NOT deadenylase complexes by GW182 (Jonas and Izaurralde, 2015). GW182 binds PAN3 which mediates the further recruitment of PAN2 and additionally interacts with the CCR4-NOT complex via two of its subunits (NOT9 and NOT1) (Braun et al., 2013, Chen et al., 2014a, Wilczynska and Bushell, 2015). The shortening of the poly(A) tail by deadenylases renders an mRNA vulnerable to decay (Garneau et al., 2007). Hence, deadenylation is followed by decapping by decapping protein 2 and its cofactors, finally leading to 5’ to 3’ mRNA degradation through the exoribonuclease, XRN1 (Fabian and Sonenberg, 2012, Jonas and Izaurralde, 2015).

GW182 proteins also interact with PABP, a protein which usually protects the 3’ poly(A) tail, to promote translational repression (Krol et al., 2010, Braun et al., 2013, Wilczynska and Bushell, 2015). Though PABP predominantly protects mRNAs from deadenylation, it can also be involved in recruiting the PAN2-PAN3 deadenylase to microRNA-RISC complexes. One model shows that that PAN2-PAN3 deadenylation occurs to an extent whereby PABP can no longer bind the poly(A) tail, leading to subsequent degradation by CCR4-NOT (Wolf and Passmore, 2014). Another group showed that PABP facilitates the interaction between a microRNA-loaded RISC complex and its mRNA target, after which PABP may dissociate independently of deadenylation, thereby exposing the poly(A) tail and allowing deadenylase binding (Moretti et al., 2012). Other evidence holds that GW182-facilitated recruitment of CCR4-NOT decreases PABP association from the poly(A) tail (Zekri et al., 2013). In addition, the RISC complex interacts with a variety of RBPs and helicases which might work in conjunction to regulate mRNA translational repression and/or mRNA degradation (Bartel, 2004, Kosik, 2006, Krol et al., 2010).

There are contradictory findings in the literature as to whether microRNAs repress their targets during translational initiation or elongation, as evidenced by a lack of mRNA entering translation, or stalled polyribosomes, respectively (Pillai et al., 2005, Nottrott et al., 2006, Petersen et al., 2006, Mathonnet et al., 2007, Gu and Kay, 2010). A very significant paper by another Leicester group, Meijer et al., (2013), demonstrated that microRNA mediated mRNA repression and degradation could only occur during translation initiation and was reliant on the helicase eIF4A2 of the eIF4F translation initiation complex. eIF4F-independent reporter transcripts were neither translationally repressed nor degraded – suggesting that mRNA degradation might be downstream from translational repression. Moreover, Meijer et al. (2013) also showed that eIF4A2 has a role distinct from translation initiation; immunoprecipitation of eIF4A2 demonstrated association with the CCR4-NOT complex through its MIF4G domain that shares homology with translation initiation factor eIF4G of the eIF4F complex. This suggested a mechanism by which eIF4A2 itself might be involved in microRNA mediated translational repression by blocking the binding of eIF4G.

Though GW182 facilitates the coupling of a microRNA-loaded RISC to the deadenylation and degradation machineries, this protein is also implicated in regulating microRNA mediated translational repression. GW182's interaction with PABP during microRNA mediated translational repression has been shown to abrogate mRNA circularisation and thereby prevent translation initiation (Wolf and Passmore, 2014). In agreement with this, there is further evidence to suggest that GW182 also interferes with translation initiation by decreasing target mRNA associations with PABP and translation initiation factors eIF4G and eIF4E (Zekri et al., 2013). However microRNA mediated translational repression can also occur independently of PABP (Fukaya and Tomari, 2011). This suggests that there may be multiple protein-protein interactions involved in microRNA mediated translational repression (Iwakawa and Tomari, 2015).

To date, microRNAs have been primarily observed to direct both the translational repression and consequent degradation of most of their targets, whilst only a small proportion of mRNAs are thought to be translationally repressed only (Larsson and Nadon, 2013, Eichhorn et al., 2014). The balance of regulation a microRNA imparts on its target mRNA, e.g. coupled repression and degradation versus repression only, may

be due to multiple different factors, and may be adapted to the requirements of a cell at a given time. Importantly, it has been shown that microRNA mediated translational repression of mRNA targets can be reversed to allow regulated protein translation, in which case repression must necessarily be uncoupled from mRNA degradation.

1.6 Neuronal microRNAs and targets demonstrate unique expression characteristics

microRNAs are essential for neuronal function, from regulating brain development through to synaptic plasticity (Schratt et al., 2006, Kosik, 2006). Conditional deletion of Dicer in the CNS during neural development has consequent effects on neuronal differentiation and brain architecture. These perturbations of brain structure result in phenocopies of human neurological and/or psychiatric disorders (Sakamoto and Crowley, 2018). Moreover, some human brain diseases have been linked genetically to microRNA-producing loci.

The Luthi-Carter group has previously shown that brain microRNAs are expressed in a highly cell-type specific manner. microRNAs restricted to neural cell subtypes have been shown to have roles in neural cell specification, particularly among neurons, astrocytes and oligodendrocytes, which all arise from a common stem cell precursor (Jovičić et al., 2013). The Luthi-Carter lab's data have also suggested that the continued cell-type-specific production of microRNAs following developmental milestones plays a role in maintaining neural cell identity. This mechanism is proposed to ensure that each specialised neural cell type only expresses proteins appropriate to its functions.

An additional line of evidence from the Luthi-Carter laboratory also underpins the hypotheses that I pursued in my project. In contrast to the canonical model which suggests that microRNAs and their mRNA targets demonstrate reciprocal patterns of expression, our lab's previous results have shown that the levels of the majority of neuronal microRNAs positively correlate with their mRNA targets (Jovičić, 2011). These analyses were conducted in primary cortical neuronal cultures. First, separate mRNA and microRNA profiles were collected for neurons, astrocytes, oligodendrocytes and microglia. Then mRNA targets of neuronal- or glial-enriched microRNAs were predicted using Ago CLIP-Seq data combined with four microRNA-target prediction algorithms.

Jovičić (2011) found that 38 of 53 neuronal microRNAs were positively correlated to their mRNA targets in neurons versus astrocytes. Of these, 26 microRNAs also showed a significant positive correlation with their targets in neurons versus oligodendrocytes (Jovičić, 2011). In contrast, only one microRNA, miR124, showed a significant negative correlation with its targets in the same comparisons. The microRNAs with neuron-expressed targets included miR135b and miR137. Overexpression of miR135b and miR137 further confirmed that their presence did not lead to the degradation of their mRNA targets (Jovičić, 2011). Instead, ribosome immunoprecipitations demonstrated that miR135b and miR137 targets were significantly less associated with translating ribosomes (Jovičić, 2011). This indicates that these neuron-enriched microRNAs are sequestering their targets in a translationally arrested state without diminishing target mRNA abundance.

Jovičić's results (2011) suggest the existence of a class of neuronal microRNAs that primarily operate through translational repression in the absence of mRNA degradation. I further postulate that this regime supports reversible inhibition suitable for the facilitation of mRNA transport and/or signal-dependent protein translation.

1.7 A possible role for microRNAs in mRNA transport

RBPs can act either cooperatively with microRNAs, facilitating their interaction with targets, or competitively, by binding in close proximity and obscuring each other's recognition sites (Ciafrè and Galardi, 2013). Several groups have identified differential distributions of mRNAs, microRNAs and RBPs in neuronal soma and neurites (Kye et al., 2007, Zappulo et al., 2017, Khalil et al., 2018). Moreover, there is an enrichment of RBPs within neurites which may interact with cis-elements within the UTRs of mRNAs to be transported (Zappulo et al., 2017). microRNAs and their precursors have also been shown to be present in neurites (Schratt, 2009, Sambandan et al., 2017). However, the extent to which microRNAs might systematically play a role in RNA transport is far less studied.

1.8 microRNAs as possible regulators of synaptic plasticity

microRNA mediated mRNA degradation has also been shown to be involved in modulating synaptic plasticity. Brain microRNA expression profiles have been reported to change following learning and behaviour paradigms and brain epileptiform activity (Jimenez-Mateos et al., 2011, Thomas et al., 2018). microRNAs have also been observed to degrade specific mRNAs encoding neurotransmitter receptors and ion channel proteins known to regulate neuronal excitability and thereby modulating the strength and connectivity of neuronal circuits (Saba et al., 2012, Gross et al., 2016).

Another line of evidence shows that signal-dependent microRNA induction can be a crucial facet of the regulation of neuronal plasticity. For example, the neural activity-dependent transcription factor CREB is implicated in synaptic facilitation by inducing the transcription of the pri-miR212/132 microRNA cluster following synaptic stimulation and regulating mRNA targets including *MeCP2*, an activity-dependent repressor of transcription (Vo et al., 2005, Remenyi et al., 2010, Tognini and Pizzorusso, 2012). Furthermore, the neurotrophin BDNF both relieves miR134 repression of *Limk1* whilst increasing transcription of pri-miR134 following the activation of transcription factor Mef2 (Fiore et al., 2009).

Signal-dependent translational regulation is known to result in long lasting changes in synaptic morphology and excitability. Evidence to support microRNA mediated translational repression in synaptic plasticity is more limited, however. I postulated that microRNA-operated regimes of translational repression might be more prevalent than previously appreciated. I considered the examples below to explore possible mechanisms of microRNA mediated effects on synaptic strength via the translational regulation of proteins involved in synaptic signalling.

miR134 is a brain specific microRNA that targets *Limk1* mRNA to regulate synaptic actin polymerisation and modulate dendritic spine volume (Schratt et al. 2006). Overexpression of miR134 increases *Limk1*-mediated translational repression which consequently decreases dendritic spine volume. Conversely, this translational repression is reversed upon BDNF treatment through its canonical TrkB and mTOR

signalling pathway, suggesting a specific signal-dependent microRNA mediated mechanism for modulating synaptic structure (Schratt et al., 2006).

Armitage, the *Drosophila* orthologue of MOV10, has been associated with microRNA-regulated memory formation (Ashraf et al., 2006). Acetylcholinergic activity in the *Drosophila* memory centre causes proteasome-mediated degradation of Armitage and simultaneously releases *CAMKII* from microRNA mediated repression. The increased translation of *CAMKII* facilitates future activity at the corresponding synapse (Ashraf et al., 2006). Subsequent experiments in rat hippocampal neurons also uncovered an analogous NMDA receptor-mediated degradation of RISC-associated MOV10 and relief from microRNA mediated inhibition of translation of *CAMKII* (Schratt et al., 2006, Banerjee et al., 2009). A similar effect was described for miR138, which targets a depalmitoylating enzyme (*Lypla1*) to regulate Rho-dependent signalling pathways (Banerjee et al., 2009). The work by Ashraf et al., (2006) and Banerjee et al., (2009) provide clear evidence that microRNAs may work in conjunction with RBPs to regulate translational repression and de-repression. The reversal of translational repression of microRNA targets might be especially important in neurons where the target proteins might be needed in a specific cellular sub-compartment, such as dendritic spines, to modulate synaptic plasticity (Schratt, 2009).

1.9 Current understanding of the neurobiologies of miR135b and miR137 in neural tissues

1.9.1 miR135b

miR135b is encoded in the first intron of the *LEMD1* gene on chromosome 1 region 1q32.1, a susceptibility locus for bipolar disorder (Khatri and Subramanian, 2013, Issler et al., 2014).

Though the majority of research on miR135b is focused on its roles as an oncogenic microRNA, it does also have known roles in the brain. miR135b is reported to influence neuronal morphology and is particularly implicated in axonal growth and regeneration (van Battum et al., 2018). miR135b expression decreases throughout the process of cortical development but increases again in the adult (van Battum et al., 2018).

Overexpression of miR135b significantly increases neurite outgrowth and branching, an effect attributed to the negative regulation of its target *KLF4* which otherwise inhibits axon growth and regeneration (van Battum et al., 2018).

miR135b has been shown to have links to several neuropsychiatric and neurodegenerative disorders. In addition to being genomically associated with bipolar disorder, overexpression of miR135b has been shown to reduce depression-like phenotypes by increasing synaptic serotoninergic signalling by downregulating both a serotonin transporter (*Slc6a4*) and a serotonin receptor (*Htr1a*) in the raphe nucleus (Issler et al., 2014). Increasing the level of miR135b increased the level of serotonin the synaptic cleft, implicating this microRNA as an endogenous serotonin reuptake inhibitor (Issler et al., 2014).

More recently, miR135b has been shown to modulate fear memory expression in stress-resilient animals in a model of post-traumatic stress disorder (Sillivan et al., 2019). miR135b has also been shown to regulate *DISC1*, variants of which comprise risk factors for neuropsychiatric diseases including schizophrenia and mood disorders (Rossi et al., 2014); miR135b is unable to target the 3'UTR of the *rs11122396 G* allele of *DISC1*, which might explain the functional deficit associated with this variant (Rossi et al., 2014).

Differential expression of miR135b has been described in iPSC-derived neurons from Parkinson's disease patients (Tolosa et al., 2018). Further investigation into this expression might provide interesting insights into miR135b's role within this neurodegenerative condition.

miR135b has also been shown to be neuroprotective in Alzheimer's disease by regulating *BACE1*, a protein involved in the formation of brain β-amyloid (Zhang et al., 2016); miR135b was reduced in Alzheimer's disease versus control blood samples, whereas miR135b overexpression had positive effects on the proliferation on hippocampal stem cells, and resulted in increased performance in learning and memory tasks in rodents (Zhang et al., 2016).

1.9.2 miR137

miR137 is highly expressed in early brain development. The miR137 host gene (*MIR137HG*) is located within an intergenic region on chromosome 1, 1p21.3 (Sakamoto and Crowley, 2018). Microdeletions and single nucleotide polymorphisms (SNPs) in the *MIR137HG* have been associated with autism spectrum disorder (ASD), intellectual disability (ID) and schizophrenia (Thomas et al., 2018). Therefore, the potential to modulate the activities of miR137 could be a useful therapeutic in these disorders (Sakamoto and Crowley, 2018).

In mouse models, knock-out of miR137 is embryonic lethal between E4.5 and 11.5. A conditional knock-out of miR137 that decreases its expression to 50% in mice presents with ASD-like behaviours (Cheng et al., 2018). miR137 regulates neuronal gene expression during embryonic stem cell differentiation; it is present in high levels in the rat brain during later developmental stages and plays a role in adult neurogenesis and neuronal maturation (Sakamoto and Crowley, 2018).

Patients presenting with ID with features of ASD with additional speech delay harbour a hemizygous microdeletion at 1p21.3, which results in decreased levels of pre- and mature miR137 and an accompanied increase in miR137's mRNA targets (Willemsen et al., 2011). The microdeletions which lead to ASD and ID phenotypes are distinct from the SNPs observed giving rise to schizophrenia, however (Thomas et al., 2018).

Ripke et al., (2011) demonstrated a SNP in the *MIR137HG* (*rs1625579*) and 4 other loci containing predicted miR137 targets to have a significant associations with schizophrenia. *Rs1625579* decreases the abundance of miR137 in the brain, and experimental deficits in miR137 and its targets show defective neuronal morphology and connectivity (Sakamoto and Crowley, 2018). While the major allele (T) at the schizophrenia risk loci *rs1625579* decreases miR137 levels, the minor allele (G) is protective against schizophrenia relative to the major allele and increases miR137 levels (Thomas et al., 2018).

Surprisingly, however, transgenic mice that overexpress miR137 in neurons under the Thy-1 promoter also displayed schizophrenia-associated phenotypes, including social and cognitive deficits and altered pathways (Arakawa et al., 2019). Overexpression of

miR137 in the dentate gyrus of mice via lentiviral transduction led to a consequent downregulation of its mRNA and protein targets, including Syt1, Nsf and Cplx1, all of which regulate presynaptic vesicle release. These targets were also reported to be downregulated in schizophrenia brains post-mortem (Siegert et al., 2015). Consistent with this finding, miR137 overexpression leads to presynaptic deficits manifesting as decreased vesicle density, LTP, and hippocampal learned behaviours (Siegert et al., 2015). These phenotypes were predicted to be a result of mRNA target dysfunction, where they showed Syt1 overexpression was able to rescue the phenotypes caused by miR137 overexpression (Siegert et al., 2015).

In contrast, He et al., (2018a) showed miR137 overexpression to impair synapse formation and synaptic transmission in cultured rat hippocampal neurons without affecting Syt1 or Cplx1 protein expression. Moreover, Syt1 overexpression did not rescue the detrimental effects of miR137 overexpression in the hippocampus (He et al., 2018a).

Taken together, these results suggest that miR137 requires tight temporal and spatial regulation and may regulate synaptic transmission through several different targets.

1.10 Rationale and Statement of Aims

miR135b and miR137 are neuron-enriched microRNAs with links to neurological and psychiatric conditions. In addition to their human genetic associations, many of the validated targets of miR135b and miR137 have important synaptic functions. However, much of the evidence to date suggests that these microRNAs carry out their roles by negatively regulating the expression of their mRNA targets. This contrasts with data from our lab showing that a large number of neuron-enriched microRNAs, including miR135b and miR137, co-exist with their mRNA targets (Jovičić, 2011).

Previous work in the Luthi-Carter laboratory by Jovičić (2011) highlighted that neuronal microRNAs 135b and 137 were positively correlated with their neuronal mRNA targets via bioinformatic analyses, which is contrary to the widely reported mechanism of microRNA action. Moreover, Jovičić (2011) demonstrated that these mRNA targets were sequestered away from translating ribosomes. However, neither the direct interactions

nor the function(s) of this potential co-existence between neuronal microRNAs and their targets were explored in previous work.

In this thesis I will further explore the unique microRNA-mRNA expression relationships of miR135b and miR137 in order to elucidate possible functions of these microRNAs involving facilitatory regulation of their targets.

Hypothesis 1: A specialised group of neuronal microRNAs, exemplified by miR135b and miR137, mediate non-degrading microRNA-target interactions.

I examined the effects of lentiviral mediated overexpression of microRNAs 135b and 137 in neuronal cultures to determine the consequences on the abundances of their target mRNA and/or protein levels. This provided further proof of non-degrading microRNA-target interactions. Furthermore, target protein levels remained unchanged, or in some cases increased.

Hypothesis 2: microRNA-mRNA target interactions of miR135b and miR137 display characteristics consistent with their transport to synapses in RNA granules.

These studies elucidated specific microRNA-target-RBP interactions in cellular fractions consistent with localisation to RNA granules. Moreover, the specific RBPs associated with miR135b- and 137-target complexes are known to fulfil roles in RNA transport and neuronal signal-dependent translational regulation.

2 Chapter 2: Materials and Methods

2.1 Neuronal cell culture

2.1.1 Coating plates with poly-L-lysine hydrobromide and poly-D-lysine hydrobromide

100 x 15 mm culture dishes (Nunclon™ Delta, Cat No. 150350) were each coated with 5 ml of a 0.1 mg/ml solution of Poly-L-Lysine Hydrobromide (Sigma-Aldrich®, Cat No P274-100 mg) in distilled water. 24 well plates (Thermo Scientific™ Nunc™ Cell-Culture Treated Multidish, Cat No. 142475) containing coverslips (13 mm No. 1.5, VWR™ Cat No. 631-0150) were coated with 300 µl per well of 0.1 mg/ml Poly-D-Lysine Hydrobromide (Sigma-Aldrich®, Cat No. P0899-10 mg) in Boric Acid Buffer. 24 well plates without coverslips were coated with 300 µl per well of 0.1 mg/ml Poly-L-Lysine Hydrobromide in Boric Acid Buffer. Culture dishes were left to coat overnight at room temperature in a tissue culture hood. The following day the Poly-L-Lysine Hydrobromide or Poly-D-Lysine Hydrobromide solutions were removed from the plates, before washing plates twice in distilled water and leaving to air dry at room temperature in a tissue culture hood.

2.1.2 Dissection of cortical neurons from E16 Sprague-Dawley embryonic pups

An embryonic day 10 (E10) timed pregnant Sprague-Dawley rat dam was obtained from Charles River Laboratories. The dam was euthanised by Schedule 1 procedure at E16.5 by isoflurane anaesthesia followed by cervical dislocation and severing of the femoral artery. The uterus of the dam was removed from the abdomen and placed in ice cold DMX buffer (Dulbecco's Phosphate Buffered Saline (PBS) supplemented with 100 U/ml Penicillin-Streptomycin (Gibco®, Cat No. 15140122), 10 mM HEPES (Gibco®, Cat No. 11560496) and 2% Glucose). The embryos were removed from the embryonic sac and culled by schedule 1 procedure where they were decapitated, and their heads placed in ice cold DMX buffer. Within a laminar flow hood, the embryonic brains were removed from the skull, detached from the brainstem and the hemispheres separated. Meninges were removed from the hemispheres. The cortices and hippocampi were separated from the rest of the brain and collected in separate dishes containing DMX buffer. After collecting cortical and hippocampal tissue from all dissected embryos, the total tissue collected was transferred into a 50 ml falcon tube. The DMX buffer was aspirated, and

the tissue was digested with 0.025% Trypsin in PBS at 37°C for 10 minutes with agitation every 2-3 minutes. The trypsin solution was removed, and the tissue was washed once with Neurobasal Medium (Gibco®, Cat No. 21103049) supplemented with 10% Horse Serum to stop the enzymatic digestion of the tissue. The tissue was mechanically dissociated in 5 ml Neurobasal Medium with 10% Horse Serum followed by centrifugation at 300 G for 5 minutes to pellet the cells. The supernatant was removed, and the cell pellet was resuspended in an appropriate volume of Neurobasal Medium supplemented with 2% B27 (Gibco®, Cat No. 17504044), 100 U/ml Penicillin-Streptomycin (Gibco®, Cat No. 15140122) and 0.5 mM L-Glutamine (Gibco®, Cat No. 25030081). The resulting cell suspension was passed through a cell strainer (Fisherbrand, Cat No. 22363549) to remove any debris.

2.1.3 Cell counting

A 1:10 cell suspension was used to count cells, i.e. 10 µl of cell suspension was added to 80 µl of medium and 10µl of Trypan Blue solution. 10 µl of this was pipetted into a haemocytometer, and the cells were counted at a 10x magnification using a light microscope. Live, unstained cells contained fully within 4 x 16 square corner grids were counted and an average was calculated. This was multiplied by the dilution factor and 10000 to give the number of cells/ml.

2.1.4 Plating neuronal cells

Cortical neurons were plated at a density of $5x10^6$ cells/10 ml in a 100 mm dish, and $3x10^5$ cells/ml in a final volume of 600 µl per well in a 24 well plate (both with and without coverslips) all in Neurobasal Medium supplemented with 2% B27, 100 U/ml Penicillin-Streptomycin and 0.5 mM L-Glutamine. Hippocampal neurons were plated at a density of $3x10^5$ cells/ml in a final volume of 600 µl per well in a 24 well plate in Neurobasal Medium supplemented with 2% B27, 100 U/ml Penicillin-Streptomycin, 0.5 mM L-Glutamine and 25 µM Glutamate. After 48 hours in culture, the media was removed from the hippocampal cells and replaced with supplanted Neurobasal Medium without additional Glutamate supplementation. Cells were incubated at 37°C and 5% CO_2, with half of their media changed on a weekly basis.

2.1.5 Plating low-density neuronal cultures

Cortical neuronal cell suspensions were plated in Neurobasal Medium supplemented with 2% B27, 0.5 mM Penicillin-Streptomycin and 0.5 mM L-Glutamine and 10% heat-inactivated horse serum to stimulate glial cell growth to support the low-density cultures. Low density cortical neurons were plated at a density of $1x10^4$ cells/ml in a final volume of 600 µl per well in a 24 well plate (both with and without coverslips). Cells were incubated at 37°C and 5% CO_2, with a complete media change at DIV7 to supplemented Neurobasal Medium without heat-inactivated horse serum, and half the media changed on a weekly basis thereafter.

2.2 Lentiviral vector production and lentiviral transduction of neuronal cells

2.2.1 Plasmid preparation

XL-10-Gold Ultracompetent bacterial cells (Stratagene, Cat No. 200314) were thawed on ice. 25 µl of bacterial cells were incubated with 1 µl of β-Mercaptoethanol for 10 minutes on ice and mixed every 2 minutes. 50 ng of DNA (either SIN-PGK-miR124, SIN-PGK-miR135b, SIN-PGK-miR137) was added to the cells, followed by a 30-minute incubation on ice. The bacterial cells were then subject to heat shock in a water bath for 30 seconds at 42°C, then placed on ice for 2 minutes. 225 µl of Luria-Bertani (LB) broth pre-heated to 42°C was added to the cells, before incubation for 1 hour at 37°C with 300 RPM shaking. Transformed bacteria were streaked onto LB + Ampicillin plates and incubated at 37°C. A colony was picked from each plate to inoculate 300 ml LB broth + Ampicillin. Plasmids were purified using Macherey-Nagel NucleoBond® PC500 Maxiprep Kit (Cat No. 740574.50).

2.2.2 Lentiviral vector production using HEK293FT cells

HEK293FT cells were cultured in 175 cm^2 flasks (Corning, Cat No. 431080) in Dulbecco's Modified Eagle Medium (DMEM) (Biowest, Cat No. L0106-500) supplemented with 10% Foetal Bovine Serum (FBS), 1 mM Sodium Pyruvate (Gibco®, Cat No. 11360070), 0.1 mM Non-Essential Amino Acids (Gibco®, Cat No. 11140050), 2 mM L-Glutamine (Gibco®, Cat

No. 25030081), 100 U/ml Penicillin-Streptomycin (Gibco®, Cat No. 15140122) and 500 µg/ml Geneticin (G418) (Sigma-Aldrich®, Cat No. A1720-5G). Cells were cultured at 37˚C and 5% CO_2.

Lentiviral vectors were produced using a 4-plasmid transfection system (the plasmid of interest, pCMV DR, pMDG and pRSV-Rev). Prior to transfection, the HEK293FT cells were seeded at a density of 3 x 10^6 cells into 100 x 17 mm culture dishes. The following day, the cells were transfected in a 3:1 ratio of Polyethylenimine (PEI) to DNA. For 20 x 100 mm dishes 750 µg of PEI was added to a final volume of 10 ml in serum free DMEM in a 50 ml falcon tube. Alongside, 250 µg of DNA containing: 99 µg Plasmid of Interest, 99 µg pCMV DR, 29 µg pMDG and 23 µg pRSV-Rev was added to serum free DMEM in another falcon tube to a final volume of 10 ml. Both tubes were incubated at room temperature for 5 minutes, the contents of both tubes were then combined with each other, vortexed for 10 seconds, and incubated for a further 15 minutes at room temperature. 1 ml of PEI/DNA mixture was added to one plate in a dropwise manner and incubated for a minimum of 6 hours prior to a complete media change. The plates were then incubated for 48 hours at 37˚C and 5% CO_2, prior to harvesting the virus.

2.2.3 Harvesting virus

Beckman ultracentrifuge tubes and pots were washed with 75% ethanol and distilled water then left to dry. The media was collected from the cells (containing the lentiviral vector) and centrifuged at 1000 RPM for 10 minutes to remove cell debris. The resulting supernatant was subjected to ultracentrifugation at 19000 RPM for 90 minutes at 4°C. Viral pellets were resuspended in 300 µl 1% Bovine Serum Albumin (BSA) in PBS and stored at -80°C until use.

2.2.4 Quantification of lentiviral concentration

RETROtek HIV-1 p24 Antigen ELISA (Zeptometrix, Cat No. 0801111), an immunobased assay, was used to detect and quantify the amount of HIV-1 p24 antigen within the resulting sample.

2.2.5 Lentiviral mediated transduction of microRNAs in cortical neuronal cells

At DIV14, cortical and hippocampal cell cultures were transduced with lentiviral vectors to overexpress microRNAs of interest (miR124, miR135b or miR137) at a concentration of 25 ng p24 antigen/ml in supplemented Neurobasal Medium. Half of the culture medium was replaced with fresh culture medium at 24 hours post-transduction. Previous work in the Luthi-Carter lab has shown microRNA overexpression via lentiviral transduction to be at its optimum at 14 days post-lentiviral transduction (Jovicic, 2011).

2.3 RNA extraction from cortical neuronal cultures overexpressing microRNAs of interest

At DIV28 (14 days after lentiviral transduction) RNA was extracted from cortical neurons overexpressing microRNAs of interest within 24 well plates. All steps were carried out within a fume cupboard. Firstly, media was removed from each well and 500 µl of TRI Reagent® (Sigma-Aldrich®, Cat No. 93289) was added to the well, cells were scraped using a pipette tip. TRI Reagent® containing cell lysate was transferred into an Eppendorf tube. This was repeated for all wells. Samples were left at room temperature for a minimum of 5 minutes. 100 µl of chloroform (Honeywell™, Cat No. C2432-25ML) was added to each tube, prior to shaking for 15 seconds. Samples were left to equilibrate for 2 – 15 minutes at room temperature, followed by centrifugation at 12000 G for 15 minutes at 4˚C. The aqueous phase was transferred into a new Eppendorf tube, and 250 µl of isopropanol was added. The tubes were inverted to mix and left to equilibrate for 5 – 10 minutes at room temperature. Samples were centrifuged again at 12000 G for 10 minutes at 4˚C. The supernatant was removed, and the resultant RNA pellet was washed with 500 µl of 75% ethanol and vortexed. Samples were centrifuged at 7500 G for 5 minutes at 4˚C. The ethanol was aspirated from the samples, and the RNA pellets were left to dry at room temperature for 10 minutes. This was followed by resuspension in 20 µl of molecular biology grade water (Sigma-Aldrich®, Cat No. W4502-1L). The samples were left to shake at 55˚C for 10 minutes and stored at -80˚C. RNA yield, 260:230 and 260:280 were read on Thermo Scientific™ Nanodrop™ 8000.

If RNA quality was poor (260:230 and 260:280 < 1), samples were subject to ethanol precipitation (1 volume of molecular biology grade water, 1/10th volume of 3 M sodium

acetate pH 5.2 (Sigma-Aldrich®, Cat No. S2889-250G), 2.5 volume of 100% ethanol and 1 µl of GlycoBlue Co-precipitant (Thermo Scientific™, Cat No. AM9515)) overnight at -20˚C. The following day, the samples were centrifuged at 14000 RPM for 30 minutes at 4°C, the supernatant was removed, and the pellet washed with 800 µl 75% ethanol and vortexed to detach the pellet from the tube wall. This was followed by centrifugation, again, at 14000 RPM for 10 minutes at 4°C. The supernatant was removed, and the residual ethanol was aspirated off before resuspending the pellet in 20 µl of molecular biology grade water.

2.4 Sucrose gradient fractionation of cortical neuronal cells

2.4.1 Preparing sucrose gradients

10% – 50% w/v sucrose solutions (in 5% increments) were prepared in 1x sucrose gradient buffer (0.3 M NaCl, 15 mM $MgCl_2$, 15 mM Tris-HCl pH 7.5, 0.1 mg/ml cycloheximide, 1 mg/ml heparin and 2mM DTT). 1.1 ml of sucrose (highest density first) was layered into a 12 ml Polyallomer tubes (Thermo Scientific™, Cat No. 03699), frozen on dry ice, before adding the subsequent layer. This was repeated until all layers were added. Gradients were stored at -80°C. Prior to use, gradients were kept at 4°C overnight to thaw and equilibrate.

2.4.2 Harvesting cells

At DIV28 (14 days after lentiviral transduction) cortical neuronal cells were treated with 100 µl cycloheximide (Sigma-Aldrich®, Cat No. C1988) (10 mg/ml stock solution in PBS) to achieve a final concentration of 0.1 mg/ml cycloheximide. The cells were incubated at 37°C for 3 minutes to arrest translation. From this point onwards, the cells were kept on ice. The media was removed, and cells were washed with cold 0.1 mg/ml cycloheximide in PBS. Cells were lysed with lysis buffer (1% Triton X-100, 500 U/ml Ribolock RNAse Inhibitor, 0.3 M NaCl, 15 mM $MgCl_2$, 15 mM Tris-HCl pH 7.5, 0.1 mg/ml cycloheximide, 1 mg/ml heparin and 2 mM DTT), and gently scraped. 1 ml of lysis buffer was used per 10 x 100 mm culture dishes. The cell lysate was transferred into an Eppendorf and incubated on ice for 10 minutes, before being transferred to a

microcentrifuge and centrifuged at 10000 G for 10 minutes at 4°C. The supernatant was collected in a separate Eppendorf.

2.4.3 Ultracentrifugation

The cleared lysate was applied to the top of a thawed sucrose gradient and the tubes were balanced to 0.01 g. The gradients were placed in pre-cooled ultracentrifuge buckets, sealed and attached to a SW40Ti rotor. The gradients were subject to ultracentrifugation at 36000 RPM for 2 hours at 4°C (Beckman Coulter, Optima XPN).

2.4.4 Polyribosome profiling on Foxy Jr fractionation system

The sucrose gradients were fractionated with continuous monitoring with a 254 nm UV spectrophotometer (Teledyne Isco). Samples were passed through the spectrophotometer. This was facilitated by a pump adding a solution of 60% sucrose stained with bromophenol blue at a rate of 1.1 ml/minute to the bottom of the tube, corresponding to each 5% step in the gradient. A polyribosome profile was generated for each gradient.

For RNA extraction, equal fractions of 1.1 ml were collected in 3 parts 7.7 M Guanidine HCl (Sigma), mixed thoroughly, before adding 4 parts 100% ethanol and mixing again.

For protein extraction, 1.1 ml fractions were manually collected from the top of the gradient into individual 15 ml falcon tubes and kept on ice.

2.5 RNA extraction from sucrose gradient fractionation

RNA samples were kept precipitating at -20°C in 7.7 M Guanidine HCl and ethanol until required (minimum overnight). The samples were centrifuged at 3500 G for 50 minutes at 4°C. The supernatant was carefully discarded. The resulting pellet was resuspended in molecular biology grade water, and ethanol precipitated (1 volume of molecular biology grade water, 1/10th volume of 3 M sodium acetate pH 5.2, 2.5 volume of 100% ethanol and 1 µl of GlycoBlue co-precipitant) overnight at -20°C. The following day, the samples were centrifuged at 14000 RPM for 30 minutes at 4°C. The supernatant was removed, the pellet washed with 800 µl of 75% ethanol and vortexed to detach the pellet from the tube wall. This was followed by centrifugation at 14000 RPM for 10

minutes at 4°C. The supernatant was removed, and residual ethanol was aspirated. The pellet was resuspended in 1.5 M lithium chloride and 1 µl of GlycoBlue co-precipitant and allowed to precipitate overnight at 4°C.

The following day, the samples were centrifuged at 14000 RPM for 30 minutes at 4°C, the supernatant was removed, and the pellet washed with 800 µl 75% ethanol and vortexed as done previously. The RNA pellet was ethanol precipitated as above, overnight at -20°C.

The following day, the samples were centrifuged at 14000 RPM for 30 minutes at 4°C, the supernatant was removed, and the pellet washed twice with 800 µl 75% ethanol, as previously described. The supernatant was removed, the samples were briefly subject to centrifugation again and any residual ethanol was aspirated. Samples were left to air dry for 10 minutes prior to resuspending in 20 µl molecular biology grade water. The samples were shaken at 300 RPM for 10 minutes at 55°C. RNA yield, 260:230 and 260:280 were read on Thermo Scientific™ Nanodrop™ 8000.

2.6 Reverse transcription

cDNA for the quantification of the microRNAs of interest was synthesised using TaqMan™ MicroRNA Reverse Transcription Kit (Applied Biosystems™, Cat No. 4366596) containing MultiScribe™ Reverse Transcriptase. microRNA specific primers were utilised

	Volume per Reaction (µl)
dNTPs (100 mM)	0.15
10x RT Buffer	1.5
RNase Inhibitor 20 U/µl)	0.19
MultiScribe™ Reverse Transcriptase	0.75
Molecular Biology Grade H_2O	4.41
RNA sample (150 ng)	5
5x RT primer	3

Table 2.1: TaqMan™ MicroRNA Reverse Transcription components per reaction

for miR124 (Thermo Scientific™, mmu-miR-124, Assay ID: 001182), miR135b (Thermo Scientific™, hsa-miR-135b, Assay ID: 002261, Cat No. 4427975) and miR137 (Thermo Scientific™, mmu-miR137, Assay ID: 001129, Cat No. 4427975).

Temperature	Time
16°C	30 minutes
42°C	30 minutes
85°C	5 minutes
4°C	Hold

Table 2.2: TaqMan™ microRNA Reverse Transcription cycling conditions in SensoQuest LabCycler

	Volume per Reaction (µl)
dNTPs (100 mM)	0.8
10x Random Primers	2
10x RT Buffer	2
MultiScribe™ Reverse Transcriptase	0.75
Molecular Biology Grade H_2O	9.45
RNA (100 – 300 ng)	5

Table 2.3: High Capacity cDNA Reverse Transcription components per reaction

cDNA to detect microRNA target mRNAs was synthesised by utilising the High Capacity cDNA Reverse Transcription kit (Applied Biosystems™, Cat No. 4368814) containing MultiScribe™ Reverse Transcriptase. 100 – 300 ng of RNA was used per reverse transcription in a 20 µl reaction.

Temperature	Time
25°C	10 minutes
37°C	120 minutes
85°C	5 minutes
4°C	Hold

Table 2.4: High Capacity cDNA Reverse Transcription cycling conditions in SensoQuest LabCycler

Temperature	Time	
95°C	10 minutes	
95°C	15 seconds	**Cycles**
60°C	60 seconds	(50 Cycles)

Table 2.5: microRNA TaqMan™ qPCR reaction composition

2.7 QPCR

To quantitate the abundance of mature microRNAs of interest, TaqMan™ Universal MasterMix II, no UNG (Applied Biosystems™, Cat No. 4440040) was utilised with cDNA from the TaqMan™ RT reaction and microRNA specific primers for miR124, miR135b and miR137. The quantitative-PCR was carried out using the using the Roche LightCycler® 480.

qPCR	Volume for Single Well (µl)	Volume for Triplicate (µl)
TaqMan™ Universal MasterMix II, no UNG	10	36
H2O	7.67	27.61
cDNA	1.33	4.8
TaqMan™ Small RNA assay (20x)	1	1 µl/well

Table 2.6: TaqMan™ Universal MasterMix II, no UNG qPCR cycling conditions in Roche LightCycler® 480

cDNA produced from the high capacity reverse transcription was used to carry out quantitative-PCR to detect for microRNA target mRNAs, using the Roche LightCycler® 480. To quantitate the microRNA targets, Power SYBR Green PCR Master Mix (Applied Biosystems™, Cat No. 4367659) was utilised. Primers were designed according to mRNA sequences (**Table 2.9**). A master mix containing 5 µl SYBR Green, 2 µl forward and 2 µl reverse primer per well was prepared, 9 µl of master mix was added to each well followed by 1 µl of cDNA (1 ng) (**Table 2.7**).

LightCycler® 480 white 384 well plates were used to run qPCR reactions (Roche, 04729749001). The plates were briefly subject to centrifugation before sealing with Absolute qPCR Plate Seals (Thermo Scientific, Cat No. AB-1170) prior to loading into the Roche LightCycler® 480.

	Volume for Single Well (µl)
SYBR Green	5
Forward Primer (1 µM)	2
Reverse Primer (1 µM)	2
cDNA (1 ng)	1

Table 2.7: SYBR green qPCR reaction composition

Temperature	**Time**	
95°C	10 minutes	
95°C	15 seconds	**Cycles**
60°C	60 seconds	(50 Cycles)

Table 2.8: SYBR green qPCR cycling conditions in Roche LightCycler® 480

	mRNA target	**Forward Primer**	**Reverse Primer**
miR124	Early Growth Response 1 (*Egr1*)	TTA TCC CAGCCA AAC TAC CC	ACA AGG CCA CTG ACT AGG C
	Nuclear Receptor Subfamily 4 Group A Member 1 (*Nr4a1*)	GCC TCC TCC ACA TCT TCT TC	ACA GGG TCT CGT CTA ATG GG
miR135b	ATPase Na+/K+ Transporting Subunit Beta 1 (*Atp1b1*)	GGC ATC TTC ATC GGG ACC AT	GGG TCA TTA GGA CGG AAG GAA A

	Bassoon (*Bsn*)	CCG AGG AGT CTG CCA AAG AGA G	GGC AGT GTC CGC TTC ACC TTG
	Neuronal Vesicle Trafficking Associated 1 (*Nsg1*)	GAC ACC ATT CCT CTG ATG ACG C	ATG CTG ACG GTG AAC TCG GCT A
	Signal Sequence Receptor 2 (*Ssr2*)	CCT CCA GAA GAC TTC GGC ATT G	AGT AAC CAG CTT TGA GAG GAC G
	(Vesicle Associated Membrane Protein 2 (*Vamp2*)	GAC AAA ACA GAA TCC CCC TAA TTC	AGT CGA ACC TCT AGC AAG GAT GA
miR137	Ankyrin Repeat Domain 12 (*Ankrd12*)	CAG AGA CAG AGG AGT TGG AGT TGC T	AGG CTT TGG CTT CCA CAG ACG
	Neuronal-specific Septin 3 (*Sept3*)	AAG CGA TTG GGC ATG TGA TAG	GCC TGG CGT GTC GAT GA
	Leucine-rich Repeat Neuronal Protein 3 (*Lrrn3*)	GAT TCT CTG TTC TGT GTG GAC C	TAA GAG GGA GGC AGA TTT CCA T
	Synaptotagmin 1 (*Syt1*)	GCT TTG AAG TTC CGT TCG AG	CAA CGA AGA CTT TGC CGA TG
	Protein Tyrosine Phosphatase Non-Receptor Type 5 (*Ptpn5*)	CAC TGT TCC CCG ATC ATT GTT	TGG CGA TGA AGC ACC CG
	Solute Carrier Family 6 Member 1 (*Slc6a1*)	GTC AAG GTG CAG AAG AAG GCT G	AAC CTC CAT ACA TTG CCC AGG

	Gamma-Aminobutyric Acid Type A Receptor Subunit Alpha 1 (*Gabra1*)	ATT CTC TCC CAA GTC TCC TTC TG	GGC ACT GAT ACT CAA GGT TGT CAT
	Family with Sequence Similarity 126 Member B (*Fam126b*)	ACT CCA ACA GTG CCG AGA ATC	GGA CTC CTC TCC TCC ATT TAG ACC
Housekeeping	βIII-Tubulin (*TUBB3*)	GTC ATC AGT GAC GAG CAT GG	GGC CTG AAT AGG TGT CCA AA
	β-Actin (*ACTB*)	TCT CAG CTG TGG TGG TGA AG	AGC CAT GTA CGT AGC CAT C
	Fox3 (*RBFOX3*)	TCC CAA CTT ACG GAG CGG CA	CAA GAG AGT GGT GGG AAC GC

Table 2.9: Primer sequences to detect mRNA targets in SYBR Green qPCR

2.8 Protein extraction

2.8.1 Protein extraction from sucrose gradient fractionation

9 volumes of 100% methanol were added to each of the 1.1 ml fractions collected from the sucrose gradient fractionation. Samples were left to precipitate overnight at -20°C. The following day, samples were centrifuged at 4400 RPM for 1 hour at 4°C. The supernatant was aspirated. Protein pellets were resuspended in 80 µl of 1x SDS-PAGE (SDS Polyacrylamide Gel Electrophoresis) Loading Buffer (0.25 M Tris-HCl pH 6.8, 0.5 M DTT, 10% Sodium Dodecyl Sulphate (SDS), 50% Glycerol and 0.5% Bromophenol Blue). Samples were heated to 75°C for 10 minutes before storing at -20°C prior to SDS-PAGE.

2.8.2 Protein Extraction from Cortical Neurons Cultured on 100 mm dishes

Media was removed from each 100 mm dish, and cells were gently washed once with PBS. Cells were kept on ice. Residual PBS was removed from each of the plates. 500 µl of 1x SDS-PAGE loading buffer was added to each 100 mm culture dish, the cells were gently scraped and transferred to an Eppendorf on ice. The protein lysate was sonicated

for 10 – 15 seconds. Samples were heated to 75°C for 10 minutes, before storing at -20°C.

2.8.3 Protein extraction from hippocampal neurons cultured on 24 well plates

Media was removed from the cells, and PBS was added to each well to wash the cells. PBS was removed from two wells at a time to prevent drying. 100 µl of 1x SDS-PAGE loading buffer was added to one well, cells were scraped using a pipette tip and the 100 µl of 1x SDS-PAGE loading buffer was transferred to the second well. The cells were scraped again, before transferring the full 100 µl to a fresh Eppendorf on ice. This was repeated for all wells. The protein lysate was sonicated for 10 – 15 seconds. Samples were heated to 75°C for 10 minutes, before storing at -20°C.

2.9 Western blotting

2.9.1 Preparing gels

Gels were prepared and run utilising the BioRad Mini-PROTEAN® 3 cell system. The glass plates (short plate and spacer plate) were rinsed in 1% SDS to remove any residual gel and/or dirt, then rinsed with distilled water. A 7.5% gel was utilised for proteins with a large molecular weight and a 10% gel for proteins with a smaller molecular weight (this was empirically determined, stacking and separating gel compositions shown in **Table 2.10 and 2.11**). The separating gel was poured first and overlaid with isopropanol whilst the gel was polymerising. After polymerisation, the isopropanol was removed, the gel rinsed generously with double distilled water and the stacking gel poured on top, with the addition of the comb. If gels weren't to be used imminently, they were wrapped in blue paper roll soaked in running buffer and sealed in a plastic bag to prevent dehydration. Gels were used within 48 hours of preparation.

2.9.2 Running gels and transferring proteins to a nitrocellulose membrane

Protein samples were thawed and heated to 75°C for 10 minutes and vortexed. Protein samples were run on the gel for the appropriate length of time (considering the molecular weight of the protein of interest) along with a pre-stained protein ladder (Precision Plus Dual Colour Standards, Bio-Rad, Cat No. 1610374) at 100 V in 1x SDS-

PAGE running buffer. Proteins were transferred onto a nitrocellulose membrane using the Bio-Rad Criterion Blotter for 20 or 30 minutes in ice cold CAPs buffer, pH 11, 20% methanol.

2.9.3 Confirmation of transfer and blocking

To validate protein transfer, the membrane was incubated with Ponceau-S for 5 minutes, then rinsed with distilled water. The membrane was de-stained with TBS-T. To quantitate the total protein which had been transferred, the membrane was incubated with REVERT Total Protein Stain (LI-COR®) for 5 minutes at room temperature. The membrane was rinsed twice for 30 seconds with REVERT Wash Buffer (LI-COR®, 6.7% v/v Glacial Acetic Acid, 30% v/v Methanol in water) then scanned in the 700 nm channel with the LI-COR® Odyssey Infrared Imager, prior to destaining with REVERT reversal solution (LI-COR®, 0.1 M NaOH, 30% v/v Methanol in water) for a maximum of 10 minutes. Total protein was quantified using LI-COR® Image Studio™ Lite. The membranes were blocked in 0.2 µm filtered 5% BSA TBS-T for a minimum time of 1 hour at room temperature.

Stacking Gel	**4 gels, 1.5 mm spacer**
Buffer (Tris 0.5 M pH 6.8, 0.4% SDS)	5 ml
Acrylamide (30%)	2.7 ml
Water	12 ml
Ammonium Persulfate (10% w/v)	200 µl
TEMED	20 µl

Table 2.10: Composition of stacking gels for SDS-PAGE.

Separating Gel	**7.5% Gel (2 gels, 1.5 mm spacer)**	**10% Gel (2 gels, 1.5 mm spacer)**
Buffer (Tris 1.5 M pH 8.8, 0.4% SDS)	5 ml	5 ml
Acrylamide (40%)	3.75 ml	5 ml

Water	11.05 ml	9.8 ml
Ammonium Persulfate (10% w/v)	200 µl	200 µl
TEMED	20 µl	20 µl

Table 2.11: Composition of separating gels for SDS-PAGE

1 L w/v 10x SDS-PAGE Running Buffer
144.1 g Glycine
100 ml 10% SDS
30.3 g Tris Base
(1x SDS-PAGE Running Buffer: 1-part 10x SDS-PAGE Running Buffer with 9 parts H_2O)

Table 2.12: Composition of SDS-PAGE running buffer

2.9.4 Antibody staining

The membrane was incubated with the appropriate primary antibody (concentration according to the manufacturer or empirically determined – **Table 2.14**) in blocking solution at 4°C with gentle agitation overnight. The following day, the membranes were washed 3 x 5 minutes in TBS-T, prior to incubation with the appropriate LI-COR® IRDye secondary antibody, IR800 or IR680 (**Table 2.15**), in 5% BSA-TBS-T for 1 hour at room temperature whilst protected from light. The membranes were washed 3 x 5 minutes in TBS-T prior to being scanned with the LI-COR® Odyssey Infrared Imager. Western blot bands were quantified using LI-COR® Image Studio™ Lite.

1 L w/v 10x Tris-Buffered Saline (TBS)
24 g Tris Base
88 g NaCl
Adjust to pH 7.6 with HCl
(1x TBS-T: 1-part 10x TBS with 9 parts H_2O + 0.1% Tween-20)

Table 2.13: Composition of 10x TBS for blocking and antibody incubation

2.10 Immunocytochemistry

2.10.1 Cell fixation

Culture medium was removed from the neuronal cells. Cells were fixed in 4% Paraformaldehyde (PFA)/PBS for 5 minutes at room temperature in a fume cupboard. 4% PFA/PBS was removed from the cells and they were washed 3x in PBS prior to blocking and antibody staining. If cells were not to be stained imminently, they were stored in PBS with 0.02% Sodium Azide at 4°C.

2.10.2 Staining

Cells were blocked and permeabilised for 20 minutes at room temperature in a solution of 4% Goat Serum, 0.3% Triton X-100 in PBS. Cells were incubated with the primary antibody at the appropriate concentration (**Table 2.14**) overnight in blocking solution. The following day, cells were washed and incubated with the secondary antibody at the appropriate concentration (**Table 2.15**) (with 1:10000 Hoescht, with cells in plates without coverslips) in 2% Goat Serum in PBS for 90 minutes at room temperature. Coverslips were mounted onto slides with Fluromount-G with DAPI, firstly at room temperature for a minimum of 2 hours prior to transferring to 4˚C in the dark.

Company	**Antibody**	**Catalogue Number**	**Host**	**Dilution**
abcam®	βIII-Tubulin	ab18207	Rabbit	1:1000
abcam®	eIF4A1	ab31217	Rabbit	1:500
abcam®	eIF4A2	ab31218	Rabbit	1:1000
Cell Signalling Technology®	eIF4G	#2498S	Rabbit	1:500
abcam®	FMRP	ab191411	Rabbit	1:10000
Cell Signalling Technology®	IMP1	#D33A2	Rabbit	1:1000
Cell Signalling Technology®	PABP	#4992S	Rabbit	1:1000

Cell Signalling Technology®	SOD2	#D9V9C	Rabbit	1:1000
Proteintech®	MOV10	10370-1-AP	Rabbit	1:1000/1:500
BD Biosciences	SMN	610646	Mouse	1:5000/1:250
abcam®	Syt1	ab13259	Mouse	1:500
Proteintech®	Gabra1	12410-1-AP	Rabbit	1:1000
Proteintech®	Ptpn5	14515-1-AP	Rabbit	1:500
abcam®	Vamp2	ab185966	Rabbit	1:1000
Proteintech®	Atp1b1	15192-1-AP	Rabbit	1:3000
Proteintech®	Bsn	2777-1-AP	Rabbit	1:500
abcam®	Nr4a1	ab109180	Rabbit	1:1000
Sigma-Aldrich®	Egr1	AV31141	Rabbit	1 µg/ul
Agilent Dako	GFAP	Z0334	Rabbit	1:400
Sigma-Aldrich®	NeuN	MAB377	Mouse	1:100
abcam®	Tau	ab80579	Mouse	1:500
Sigma-Aldrich®	MAP2	ab5543	Chicken	1:5000

Table 2.14: Primary antibodies utilised for western blotting and immunocytochemistry.

Company	Antibody	Catalogue Number	Host	Target	Dilution
Invitrogen™	AlexaFluor 647	A21244	Goat	Rabbit	1:1000
Invitrogen™	AlexaFluor 647	A21235	Goat	Mouse	1:1000
Invitrogen™	AlexaFluor 594	A11042	Goat	Chicken	1:1000
Invitrogen™	AlexaFluor 564	A11035	Goat	Rabbit	1:1000
Invitrogen™	AlexaFluor 488	A11029	Goat	Mouse	1:1000

Invitrogen™	AlexaFluor 488	A11008	Goat	Rabbit	1:1000
LI-COR®	IRDye 800	92532211	Goat	Rabbit	1:10000
LI-COR®	IRDye 800	92532210	Goat	Mouse	1:10000
LI-COR®	IRDye 680	92668073	Donkey	Rabbit	1:5000
LI-COR®	IRDye 680	92668079	Goat	Mouse	1:10000

Table 2.15: Secondary antibodies utilised for immunocytochemistry and western blotting

2.11 Combined Fluorescence In-Situ Hybridisation and Immunocytochemistry (FISH/ICC)

In order to simultaneously detect our microRNAs of interest, their mRNA targets and potential RNA binding proteins of interest, the ViewRNA® Cell Plus Assay (Thermo Scientific™, Cat No. 88-190000-99) was utilised.

2.11.1 Temperature validation

The ViewRNA® Temperature Validation Kit (Thermo Scientific™, Cat No. QVC0523) was used to validate the temperature of the humidifying incubator to be used for the experiment. A hydrophobic barrier was created on a glass slide using a hydrophobic barrier pen. A Type-K beaded probe was secured over the hydrophobic barrier and plugged into the digital thermometer. The region within the hydrophobic barrier was filled with water, and the slide with attached Type-K probe placed onto a rack inside the incubator set at 40°C. 30 minutes later the temperature was recorded. This was repeated in 3 additional locations within the incubator. The temperature was adjusted according to the recorded temperatures to maintain the temperature in the incubator at 40 ± 1°C. Prior to each FISH/ICC experiment the temperature in the incubator was validated.

2.11.2 Immunocytochemistry

Low density cortical neurons cultured on coverslips were removed from incubation at 37˚C and 5% CO_2 and transferred to a new 24 well plate. Coverslips were fixed and permeabilised using the ViewRNA® Fixation/Permeabilisation Solution for 30 minutes at

room temperature. The Fixation/Permeabilisation solution was prepared by combining equal parts of component A and component B. Following this, cells were washed 3 times with PBS Wash Buffer (PBS and 1:100 100x RNAse Inhibitor) prior to blocking with ViewRNA® Blocking/Antibody Diluent and 1:100 RNAse Inhibitor for 20 minutes at room temperature in a humidified tray.

Primary antibodies (MOV10 1:500 and SMN 1:250, **Table 2.14**) were diluted in 400 µl ViewRNA® Blocking/Antibody Diluent and 1:100 RNAse Inhibitor and incubated with the cells for 1 hour at room temperature in a humidified staining tray. The cells were washed three times in PBS Wash Buffer before incubation for 1 hour at room temperature in a humidified staining tray with the appropriate AlexaFluor 647 secondary antibodies (**Table 2.15**) diluted 1:1000 in 400 µl ViewRNA® Blocking/Antibody Diluent and 1:100 RNAse Inhibitor.

2.11.3 Fixation and FISH

Cells were washed three times with PBS Wash Buffer, then fixed with ViewRNA® Fixation Solution (1-part solution B: 7 parts solution A) for 1 hour at room temperature in a humidified staining tray.

Cells were washed again with PBS Wash Buffer. Cells were maintained in the last wash whilst preparing the ViewRNA® probe sets specific to the microRNAs (miR135b or miR137) and mRNAs of interest (*Vamp2*, *Bsn* or *Syt1*) (see **Table 2.16** for details). The RNA probe-sets hybridise to their targets by ~20 oligonucleotide pairs. Moreover, microRNA probe-sets are designed to have an increased melting temperature to increase the specificity of their binding (Manufacturer's Protocol).

ViewRNA® probe sets were thawed at room temperature, then kept on ice. The ViewRNA® Cell Plus Probe Set Diluent was equilibrated to 40°C in a temperature equilibrated incubator. Probe sets were diluted 1:100 in a final volume of 400 µl per coverslip in the pre-warmed Probe Set Diluent. The last PBS wash was removed, and the coverslips were overlaid with 400 µl of the diluted probe sets. The coverslips were hybridised with probe sets for 2 hours at 40°C in a humidified staining tray.

Company	Target	Type	Catalogue Number
Thermo Scientific™	hsa-miR135b-5p	1 (AlexaFluor 546)	VM1-10075-VCP
Thermo Scientific™	hsa-miR137-3p	1 (AlexaFluor 546)	VM1-10522-VCP
Thermo Scientific™	*Vamp2* (Rat)	4 (AlexaFluor 488)	VC4-3145095
Thermo Scientific™	*Bsn* (Rat)	4 (AlexaFluor 488)	VC4-3144301
Thermo Scientific™	*Syt1* (Rat)	4 (AlexaFluor 488)	VC4-3145689

Table 2.16: Probe Sets for ViewRNA® Cell Plus Assay

Coverslips were washed 5 times in ViewRNA® Cell Plus Wash Buffer Solution (1:333 Wash Component 1 and 1:200 Wash Component 2 in distilled water) prior to overlaying with 800 µl of the wash buffer solution and storing in a humidified staining tray in the dark at 4°C overnight.

2.11.4 Branched DNA (bDNA) amplification

The following day, all samples were pre-warmed to room temperature from storing at 4°C. ViewRNA® Cell Plus Amplifier Diluent and ViewRNA® Cell Plus Label Probe Diluent were equilibrated to 40°C in a temperature equilibrated incubator for 30 minutes. Simultaneously, the ViewRNA® Cell Plus PreAmplifier Mix, ViewRNA® Cell Plus Amplifier Mix, and ViewRNA® Cell Plus Label Probe Mix were thawed at room temperature, before placing on ice until use.

The ViewRNA® Cell Plus PreAmplifier Mix was diluted 1:25 in 400 µl per coverslip of ViewRNA® Cell Plus Amplifier Diluent and incubated on coverslips for 1 hour at 40°C in a humidified staining tray. Cells were washed 5 times in ViewRNA® Cell Plus Wash Buffer Solution. Then, ViewRNA® Cell Plus Amplifier Mix was diluted 1:25 in 400µl per coverslip of ViewRNA® Cell Plus Amplifier Diluent and incubated on coverslips for 1 hour at 40°C in a humidified staining tray. Cells were again washed 5 times in ViewRNA® Cell Plus Wash Buffer Solution. Finally, ViewRNA® Cell Plus Label Probe Mix was diluted 1:25 in 400 µl per coverslip of ViewRNA® Cell Plus Label Probe Diluent and incubated on coverslips for 1 hour at 40°C in a humidified staining tray. Cells were again washed 5 times in ViewRNA® Cell Plus Wash Buffer Solution. Cells were incubated for 10 minutes in the final wash step.

Cells were washed once in PBS. Coverslips were kept submerged in PBS to avoid drying out whilst mounting. Coverslips were mounted onto glass slides with a drop of Fluoromount-G with DAPI. Slides were left to mount for at least 2 hours at room temperature, prior to transferring to 4˚C. All slides were imaged within 2 days after mounting.

2.11.5 Microscopy and image analysis

Before imaging, slides were equilibrated to room temperature. Slides were imaged on Nikon Eclipse Ti inverted microscope with LED light source for wavelengths 365 nm, 490 nm, 565 nm and 635 nm. The mRNA targets were detectable at 488 nm, the microRNAs were detectable at 488 nm and the RNA binding proteins at 647 nm.

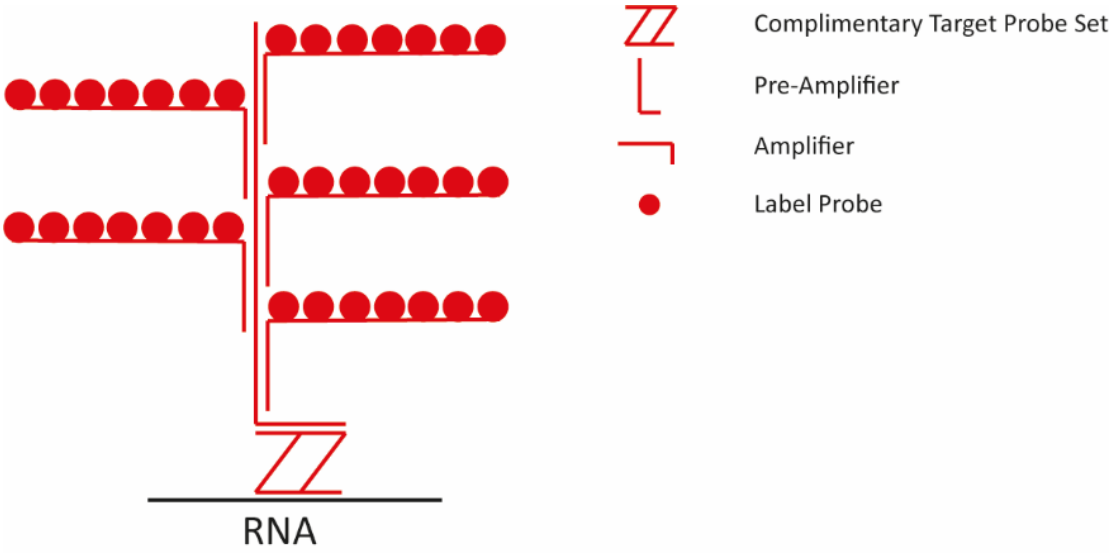

Figure 2.1: Schematic of bDNA amplification. A gene complementary probe set hybridises specifically to the target RNA (either the microRNA or its target mRNAs). Sequentially, pre-amplifier, amplifier and fluorochrome conjugated label probes hybridise to each other. This leads to signal amplification through construction of a tree-like structure to achieve bDNA amplification.

Coverslips were imaged using a Plan Apo TIRF 100x oil objective (NA: 1.49, WD: 0.12 mm, cover glass correction 0.13 – 0.2).

Images were analysed on ImageJ (FIJI) in order to identify individual microRNA, mRNA and RBP puncta and assess the extent of their overlap with each other. Firstly, the macro (**Appendix 1**) prompts the user to set the puncta processing parameters and threshold

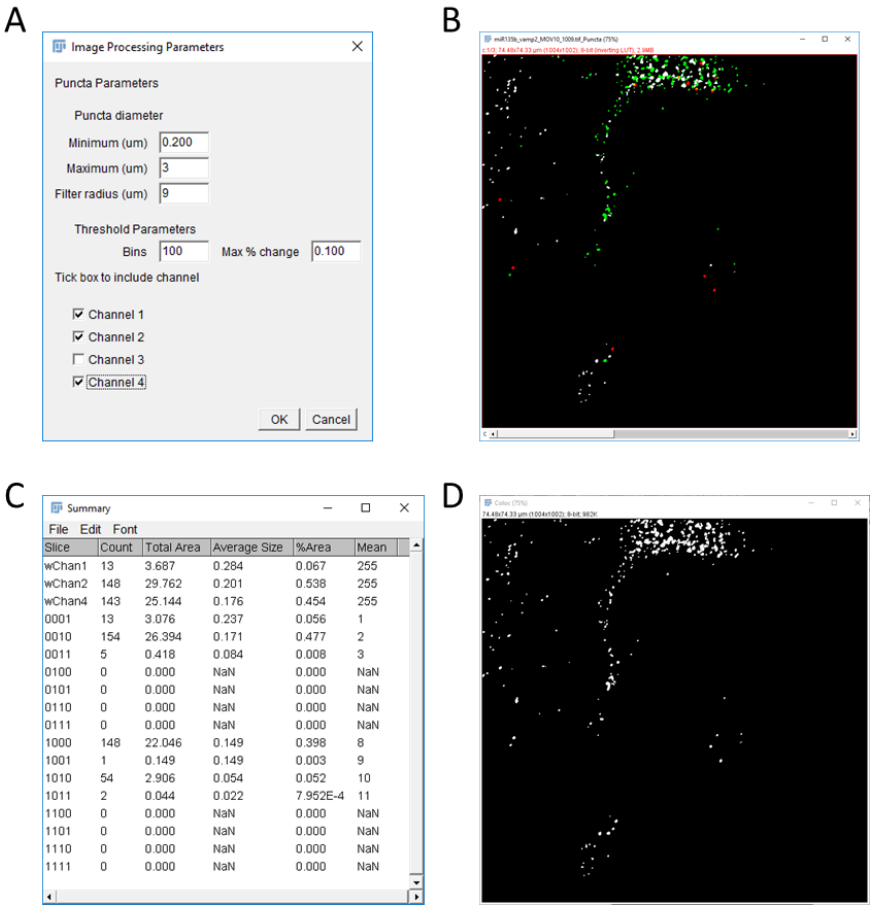

Figure 2.2: ImageJ/FIJI Puncta Analysis Macro Input and Output. A The user sets 'Image Processing Parameters': minimum and maximum puncta diameters (in µm), a filter radius which is used in the Convoluted Background Subtraction (BioVoxxel Update Site). 'Threshold Parameters': bins through which a maximum % change occurs (0.2% between 100 bins) where puncta are easily identified without being eroded. There is an option for the user to select which channels should be included in the analyses, corresponding to channels in which the microRNA, mRNA and protein are imaged in, respectively (R, G, B, Cy5). A median filter is applied prior to thresholding and background subtraction. Finally, a watershed function was applied, and each channel was converted to binary. **B** An example showing the resultant composite image output containing the binary masks of the detected puncta in each channel. **C** The macro produces a summary table that outlines the count, area, average size, % area and mean value of the detected pixels. The first three rows outline the results for each individual channel, the subsequent rows outline the overlapping particles in any of the 4 channels combinations. **D** An example showing the resultant image titled 'Coloc' that combines and codes the binary masks for each channel in a single image.

parameters (**Figure 2.2A**). A convoluted background subtraction was applied via the BioVoxxel Update Site; the filter radius was set by determining the point where background subtraction allowed detection of individual puncta without eroding them. Following this, a median filter was applied to the image prior to applying a threshold

where there was a 0.2% change between 100 bins. Finally, a watershed function was applied, and the identified puncta were analysed. Each of the channels (microRNA, mRNA and RBP) were converted to binary. This allowed subsequent analysis of the overlap in each of the possible combinations of microRNA, mRNA and RBP: number of puncta, total area covered by the puncta, their average size, % area covered by the puncta. The macro additionally produces a composite image output containing the binary masks of the detected puncta in each channel (**Figure 2.2B**) and an image titled 'Coloc' which combines and codes the binary masks for each channel in a single image (**Figure 2.2D**).

The 'Summary' table generated by the macro (**Figure 2.2C**) provides the information whereby the number of individual puncta, potential overlap between microRNA, mRNA and RBP of interest can be quantified and subsequently analysed.

2.12 Immunoprecipitation of RNA binding proteins

The Dynabeads Protein G Immunoprecipitation Kit (Thermo Scientific™, Cat No. 10007D) was utilised in order to immunoprecipitate complexes hypothesised to be involved in RNA transport using antibodies against MOV10 and SMN. The manufacturer's protocol was altered slightly as detailed below.

2.12.1 Buffers

10x RPF buffer (3 M NaCl, 150 mM $MgCl_2$, 150 mM Tris-HCl, 1 mg/ml Cycloheximide, 10 mg/ml Heparin and 20 mM DTT) was diluted 1:10 with molecular biology grade water and supplemented with 1% Triton X-100, 100 U/ml Ribolock RNAse Inhibitor in order to make 1x Lysis Buffer.

10x dilution buffer (150 mM $MgCl_2$, 850 mM Tris-HCl, 1 mg/ml Cycloheximide, 10 mg/ml Heparin) was diluted 1:10 with molecular biology grade water and supplemented with 1% Triton X-100, 100 U/ml Ribolock RNAse Inhibitor in order to make 1x dilution buffer.

2.12.2 Cell lysis

Cortical neuronal cells were treated with 100 µl cycloheximide (10 mg/ml stock solution in PBS) to achieve a final concentration of 0.1 mg/ml cycloheximide. Cells were

incubated at 37°C for 3 minutes to arrest translation. From this point onwards the cells were kept on ice. The media was removed, and cells were washed with cold 0.1 mg/ml cycloheximide in PBS. Cells were lysed with lysis buffer and gently scraped. 3 x 100 mm dishes were lysed with 300 µl of Lysis Buffer for 1 x immunoprecipitation experiment.

The cell lysate was transferred into an Eppendorf and incubated on ice for 10 minutes, before being transferred to a microcentrifuge and centrifuged at 10000 G for 10 minutes at 4°C. The supernatant was collected in a separate Eppendorf and diluted 1:2 with Dilution Buffer (600 µl total volume). 1/10th of the lysate was saved as an input fraction and stored at -20°C.

2.12.3 Binding of antibody to lysate

4 µg Antibody or 4 µg IgG Control Antibody (Mouse IgG: Sigma-Aldrich, Cat No. I5381, Rabbit IgG: Sigma-Aldrich, Cat No. I5006) was added to the diluted lysate and subject to inverting rotation at 4°C overnight.

2.12.4 Binding of antigen-antibody complex to Dynabeads Protein G

Dynabeads were completely resuspended by rotation for 5 minutes, then 150 µl of beads were transferred to an Eppendorf, placed on the DynaMag™-2 and the supernatant was removed. The Dynabeads were washed in 200 µl Ab Binding & Washing Buffer. The Dynabeads were incubated for 2 hours with the Antibody-Antigen (Ab-Ag) complex with inverting rotation at 4°C. Thereafter, the tubes containing the Dynabeads-Ab-Ag complex was placed on the DynaMag™-2 and the supernatant was collected in a separate tube. The Dynabeads-Ab-Ag complex was washed 3 times, using 600 µl Washing Buffer for each wash.

2.12.5 Elution of antibody-antigen complex

For immunoprecipitated samples used for western blot the Dynabeads-Ab-Ag complex was resuspended in 100 µl of 1x SDS-PAGE Loading Buffer, heated to 75°C for 10 minutes. The beads were removed by placing on the DynaMag™-2 prior to SDS-PAGE. SDS-PAGE was carried out as outlined above.

For RNA precipitation from the immunoprecipitated products, 3 volumes of 7.7 M Guanidine HCl was added to the Dynabeads-Ab-Ag complex or input, mixed, then 4 volumes of 100% ethanol were added, and samples were thoroughly mixed again. The samples were kept at -20°C (minimum overnight). Following this, the beads were removed using the DynaMag™-2. Both input and immunoprecipitated samples were subject to ethanol precipitation, lithium chloride precipitation and ethanol precipitation again, as previously described, in order to precipitate the RNA.

2.12.6 Reverse transcription and qPCR to confirm microRNA and/or target mRNA enrichment

RNA from input samples were diluted 1:10. 6 µl of RNA from input and 6 µl of RNA from the immunoprecipitated product were subject to reverse transcription using the microRNA Reverse Transcription kit using microRNA specific primers, as previously described, to detect for enrichment of either miR135b and/or miR137. The resultant cDNA was used to carry out a qPCR using TaqMan™ Universal MasterMix II, no UNG and microRNA specific primers, as described above. If there was an enrichment of either microRNA, 6 µl of RNA from input and 6 µl of RNA from the immunoprecipitated product were subject to reverse transcription using the High Capacity Reverse Transcription Kit, as previously described. The resultant cDNA was used to carry out a qPCR using Power SYBR Green PCR Master Mix and mRNA specific primers. This was used to quantify an enrichment, if at all, of mRNA targets of interest.

2.13 Data analysis

Data were analysed using Microsoft Excel and GraphPad Prism 7. Two-group comparisons were conducted using Two-Way ANOVA and one-tailed or two-tailed (as appropriate) Student's t-tests or Mann-Whitney U-tests to determine statistical significance. Bonferroni correction was utilised to correct for multiple testing. Comparisons with $p < 0.05$ (95% threshold) were considered statistically significant. All data are presented as mean ± standard error of the mean (SEM).

3 Chapter 3: Defining expression relationships between neuronal microRNAs and their mRNA and protein targets

3.1 Introduction

microRNAs are important post-transcriptional regulators of gene expression. microRNAs usually bind to and negatively regulate the stability of their mRNA targets and thereby also decrease the levels of target proteins (Bartel, 2004, Eichhorn et al., 2014). The mature microRNA is loaded onto the RISC complex where it exposes its 'seed sequence' to engage mRNA targets by complementary base pairing (Pratt and MacRae, 2009). The prevalent model for microRNA mediated gene regulation invokes translational repression closely coupled to mRNA degradation, with both activities being coordinated by the RISC complex and its downstream effectors (Guo et al., 2010, Eichhorn et al., 2014, Baek et al., 2008, Jin and Xiao, 2015). These include the GW182 scaffold protein, which can bring together the necessary enzymes to catalyse deadenylation, decapping and degradation of the mRNA (Braun et al., 2013).

Whereas in most contexts microRNA mediated mRNA targeting has been observed to predominantly achieve mRNA target degradation, previous results from the Luthi-Carter laboratory show that in neurons, a highly specialised, electrically active cell type, microRNA levels positively correlate to those of their target mRNAs (Jovičić, 2011). These microRNAs included miR135b and miR137 (Jovičić, 2011). When miR135b or miR137 were overexpressed in neurons, there was no change in their target mRNAs' overall abundance, but a significant decrease of their targets associated with translating ribosomes was observed (Jovičić, 2011). This would suggest that neuronal microRNAs are sequestering their mRNA targets in a translationally arrested state without degrading them. I set out to explore this possibility further, and to test whether the microRNA would influence the level of the target protein.

I therefore analysed the effect of miR135b and miR137 overexpression on mRNA target abundance for a wide selection of targets by qPCR and analysed the corresponding effect of microRNA overexpression on levels of target proteins using western blotting. Overexpression of miR124 was used as an example of a canonical microRNA for comparison.

Whilst mainly characterised as an oncogenic microRNA, miR135b is genomically associated with bipolar disorder and is implicated in several neuropsychiatric and neurodegenerative disorders. miR135b has previously been reported to mitigate depression-like phenotypes (Issler et al., 2014). Moreover, miR135b has been shown to be neuroprotective in Alzheimer's disease by negatively regulating BACE1, a protein involved in the accumulation of β-amyloid (Zhang et al., 2016).

miR137 is a brain-enriched microRNA, of which embryonic or early postnatal knockout is lethal (Crowley et al., 2015). Several known miR137 targets have roles in regulating pre- and postsynaptic activity (Thomas et al., 2018). Microdeletions and SNPs in the miR137 host gene (*MIR137HG*) have known links to ASD, ID, and schizophrenia, primarily through a decrease in miR137 expression (Thomas et al., 2018).

miR124 is also a brain-enriched microRNA, but one that has been shown in numerous previous contexts to degrade its target mRNAs (Sun et al., 2015). miR124 is wholly conserved between humans and animal models, including rats and mice (Sun et al., 2015). miR124 is understood to fine-tune gene expression in the brain by targeting mRNAs that promote a non-neuronal identity, therefore maintaining a neuronal phenotype in the cells in which it is expressed (Neo et al., 2014).

In the following experiments, microRNAs were overexpressed in primary embryonic rat neuronal cultures at DIV14 through transduction with lentiviral vectors at a concentration of 25ng/ml. At DIV28 the cultured cells were harvested for either RNA or protein (**Materials and Methods**). The resultant RNA was subject to reverse transcription and qPCR analysis to quantify the microRNA abundance and target mRNA abundance. The resultant protein lysate was subject to immunoblotting in order to detect and quantify relative target protein levels.

3.2 What are the effects of microRNA overexpression on target mRNA levels in neurons?

3.2.1 Validation of lentiviral vectors to transduce neurons and overexpress microRNAs of interest

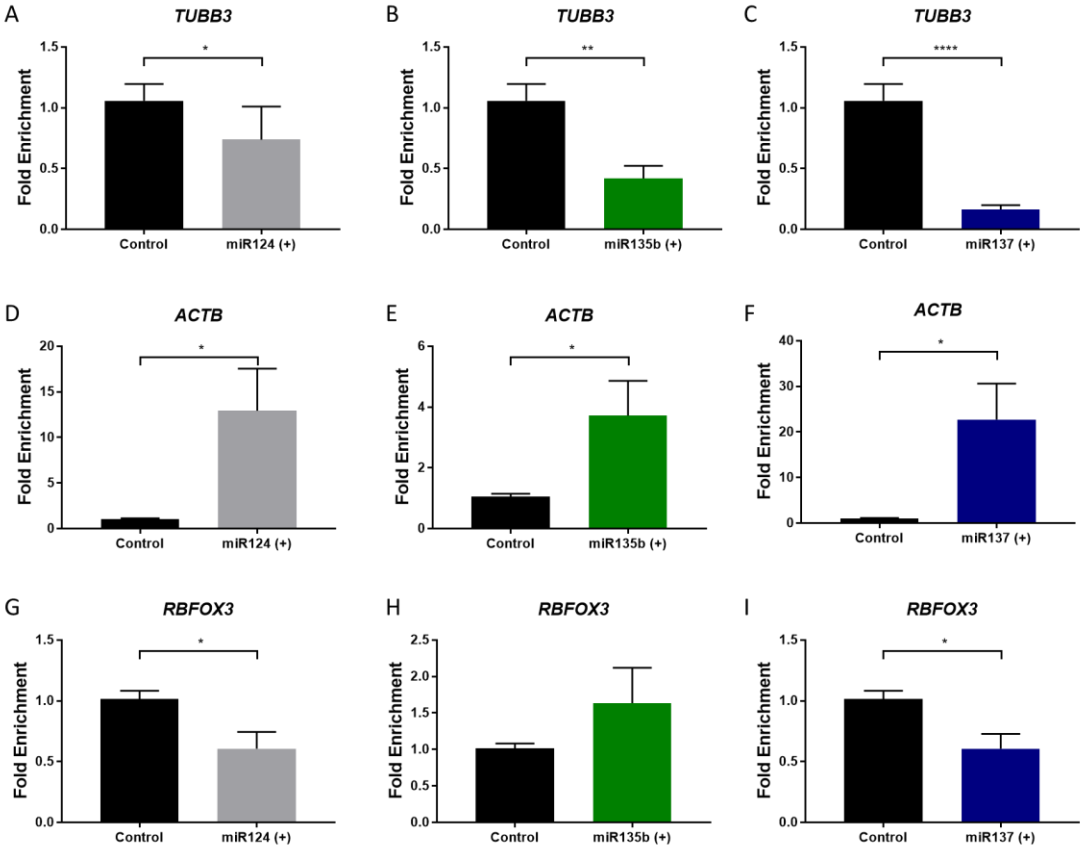

Figure 3.1: Effect of microRNA overexpression on *TUBB3, ACTB* and *RBFOX3* mRNA abundance. There was a significant decrease in *TUBB3* mRNA abundance when normalised to the geometric means of *ACTB* and *RBFOX3* mRNA levels following **A** miR124 ($p < 0.05$), **B** miR135b ($p < 0.01$) and **C** miR137 ($p < 0.0001$) lentiviral mediated overexpression compared to control untransduced cells (Mann-Whitney U-Test). There was a significant increase in *ACTB* mRNA abundance when normalised to the geometric means of *TUBB3* and *RBFOX3* following **D** miR124 ($p < 0.05$), **E** miR135b ($p < 0.05$) and **F** miR137 ($p < 0.05$) lentiviral mediated overexpression compared to control untransduced cells (unpaired two-tailed t-test). There was a significant decrease in *RBFOX3* mRNA abundance when normalised to the geometric means of *TUBB3* and A*CTB* following **G** miR124 ($p < 0.05$) and **I** miR137 ($p < 0.05$) lentiviral mediated overexpression compared to control untranduced cells (unpaired two-tailed t-test). There was no difference in **H** *RBFOX3* mRNA abundance following miR135b overexpression compared to control untransduced cells (Mann-Whitney U-Test). N = 10 replicates (5 technical replicates from 2 x E16 dissections). Graphs show mean ± SEM.

Firstly, I aimed to quantify the extent of microRNA overexpression after the lentiviral transductions of primary cortical neurons. Lentiviral vectors expressed primary microRNAs, whereas the TaqMan™ assays used to reverse transcribe and quantify microRNAs selectively detected the mature microRNAs (**Materials and Methods**). This allowed us to evaluate whether the neurons not only took up the transgene, but also processed the pri-microRNA and loaded it onto the RISC complex.

The microRNA abundances were normalised to the geometric means of the levels of *TUBB3*, *ACTB* and *RBFOX3* to control for any potential effect of microRNA overexpression on the abundance of these genes. As highlighted in **Figure 3.1**, lentiviral mediated microRNA overexpression has variable effects on the expression of *TUBB3, ACTB* and *RBFOX3* when compared to control untransduced cortical neuronal cells.

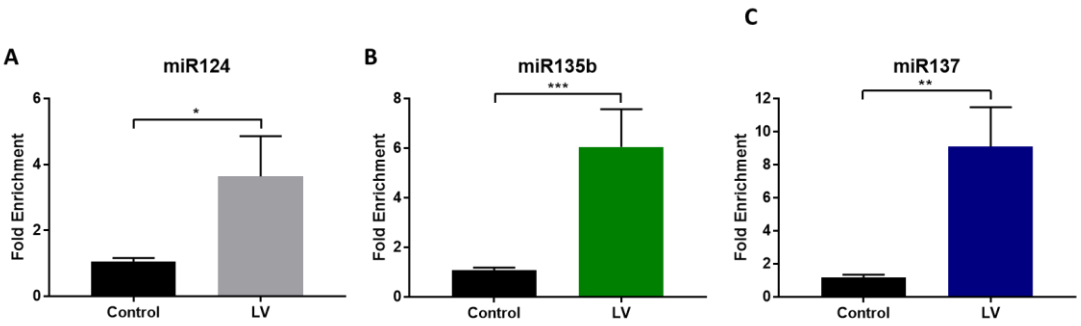

Figure 3.2: Lentiviral transduction of vectors encoding miR124, miR135b and miR137 cause a significant overexpression of all microRNAs in neuronal cultures. Transduction of lentiviral vectors encoding microRNAs in cortical neuronal cultures led to: **A** 3.6-fold enrichment of miR124 ($p < 0.05$, unpaired two tailed t-test) **B** 6.1-fold enrichment in miR135b ($p < 0.001$, Mann-Whitney U Test) and **C** 9.2-fold enrichment in miR137 ($p < 0.01$, unpaired two-tailed t-test). microRNA levels were normalised to the geometric means of the levels of TUBB3, ACTB and RBFOX3 mRNAs. Fold enrichment was calculated by comparison to untransduced control cells. N = 10 replicates (5 technical replicates each from 2 x E16 dissections). Graphs show mean ± SEM.

Figure 3.2 shows that transductions of all three lentiviral vectors resulted in significant increases in mature miR124, miR135b and miR137 levels in cultured cortical neurons to 3.6-, 6.1-, and 9.2-fold of their basal levels compared to uninfected controls, respectively. This showed that the lentiviral transduction worked as expected (**Figure 3.2**).

3.2.2 The effect of miR124 overexpression on target mRNA abundance

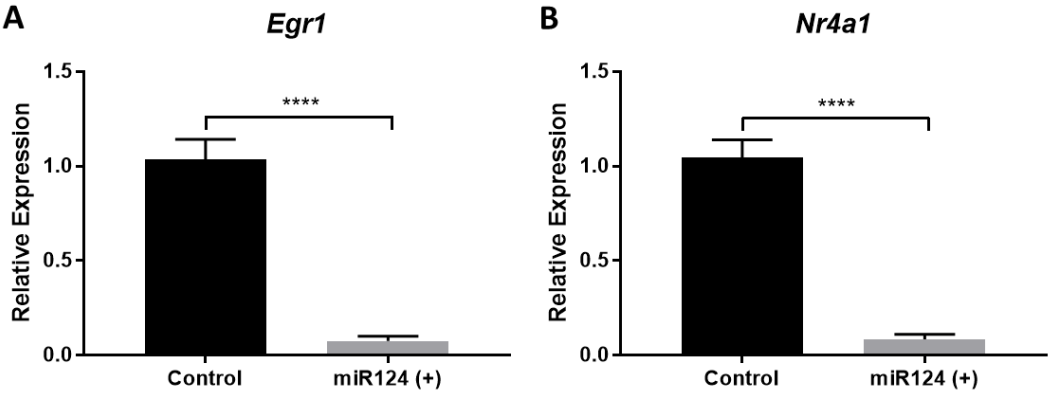

Figure 3.3: Overexpression of miR124 significantly decreases the abundance of its target mRNAs, Egr1 and Nr4a1. Transduction of lentiviral vectors encoding miR124 in cortical neuronal cultures led to a significant decrease in the abundance of miR124 neuronal targets. Two-way ANOVA identified a statistically significant effect of microRNA overexpression on the overall result ($F = 204.49$, $p < 0.0001$). miR124 overexpression led to a statistically significant decrease in **A** *Egr1* ($p < 0.0001$, unpaired two-tailed t-test with Bonferroni correction) and **B** *Nr4a1* ($p < 0.0001$, unpaired two-tailed t-test with Bonferroni correction) to 7.6% and 8.4% of control, respectively. mRNA levels were normalised to the geometric means of the levels of *TUBB3*, *ACTB* and *RBFOX3*. Fold enrichment was calculated by comparison to untransduced control cells. N = 10 replicates (5 technical replicates each from 2 x E16 dissections). Graphs show mean ± SEM.

Since miR124 is known to behave according to the canonical paradigm of negatively regulating its mRNA targets by directing their degradation, we employed this microRNA as a reference in these experiments. We chose to investigate the effect of miR124 overexpression on the corresponding levels of two of its target mRNAs: *Egr1* and *Nr4a1*. Both mRNAs behave as immediate-early genes which are quick to respond to incoming cellular signals by serving as transcription factors that further regulate programmed cellular responses (Bahrami and Drabløs, 2016, Duclot and Kabbaj, 2017). In neurons, this typically comprises a response to excitatory neurotransmission or positive neuromodulation. Egr1 has roles in NMDA-mediated LTP (Duclot and Kabbaj, 2017). Previous studies report this effect is dampened by miR124's downregulation of both the protein and mRNA abundance of Egr1, and inhibiting spatial learning (Duclot and Kabbaj, 2017, Yang et al., 2012b). Nr4a1 is a constitutively active orphan nuclear receptor whose expression is induced by signals such as stress and growth factors known to regulate cellular functions including apoptosis, DNA repair and inflammation by modulating

genes involved in these processes (Tenga et al., 2016, Jeanneteau et al., 2018). *Nr4a1* is also induced by NMDA receptor activation and can regulate synaptic plasticity by negatively regulating genes that govern dendritic spine morphology (Chen et al., 2014b). A previous study has shown that miR124 overexpression leads to a decrease in *Nr4a1* mRNA expression levels compared to a vector control in Daoy cells (a primary medulloblastoma cell line) (Tenga et al., 2016).

Two-Way ANOVA identified a statistically significant effect of miR124 overexpression ($F = 204.49$, $p < 0.0001$). However, the interaction between microRNA overexpression and the mRNA targets was not significant ($F = 0.000323$, $p > 0.05$). As expected, overexpression of miR124 caused a significant decrease of both *Egr1* (**Figure 3.3A**, $p < 0.0001$) and *Nr4a1* (**Figure 3.3B**, $p < 0.0001$) mRNA levels by post-hoc t-test with Bonferroni correction. The mRNA levels of *Egr1* and *Nr4a1* are reduced by more than ten-fold, to 7.6% and 8.4% of control, respectively. These data therefore confirm that miR124 acts in the 'standard' paradigm of primarily degrading its mRNA targets in our experimental system (Bartel, 2004).

3.2.3 The effect of miR135b overexpression on target mRNA abundance

miR135b is one of the microRNAs previously shown by the Luthi-Carter group to positively correlate with its targets rather than degrading them in neurons (Jovičić, 2011). I tested the effects of microRNA overexpression on five miR135b targets: *Atp1b1, Bsn, Nsg1, Ssr2* and *Vamp2*. Four of these targets have important roles in regulating synaptic function.

Atp1b1 codes for the β_1 subunit of Na^+/K^+ ATPase within neurons; its role is to create and maintain an electrochemical gradient across the plasma membrane of cells in order to restore the resting neuronal membrane potential following depolarisation (Johar et al., 2012, Johar et al., 2014).

Bsn is a presynaptic scaffolding protein that regulates neurotransmitter release through the delineation of synaptic active zone release sites (Gundelfinger, Reissner, & Garner, 2015). Bsn might also be directly involved in recruitment of the synaptic vesicles to be released (Hallermann et al., 2010). Mice lacking Bsn show impaired synaptic plasticity along with sensory deficits in hearing and vision (Annamneedi et al., 2018).

Nsg1 (commonly referred to as NEEP21) regulates the trafficking and endocytic recycling of neuronal transferrin and glutamate (GluR2) receptors within dendrites (Steiner et al., 2002, Yap et al., 2017).

The signal sequence receptor, Ssr2 has a general role in protein translocation in the endoplasmic reticulum, including the correct processing of plasma membrane proteins; it is not known to have a specialised neuronal function, but has been previously implicated as a miR135b target (Chinen et al., 1995, Ho et al., 2016, van Battum et al., 2018).

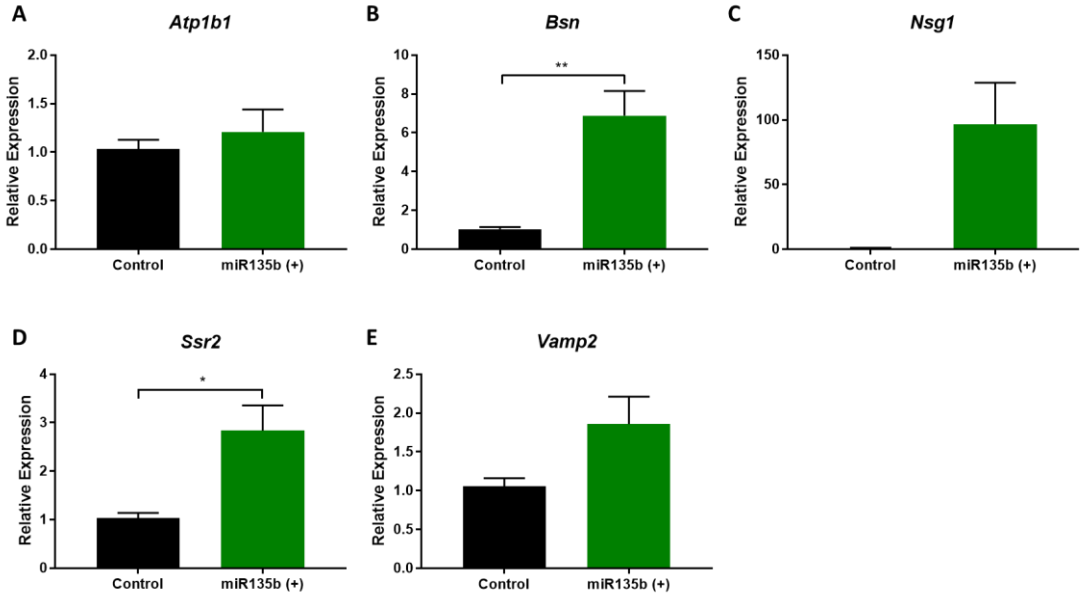

Figure 3.4: Overexpression of miR135b maintains or increases the abundance of its target mRNAs. Two-way ANOVA identified a statistically significant effect of lentiviral mediated miR135b overexpression ($F = 9.44$, $p < 0.01$) and the mRNA targets ($F = 7.61$, $p < 0.0001$) on the overall result. The interaction between miR135b overexpression and the mRNA targets was significant ($F = 7.6$, $p < 0.0001$). Overexpression of miR135b in cortical neuronal cultures had no significant effect ($p > 0.05$) on the mRNA abundance of its targets **A** *Atp1b1*, **C** *Nsg1* and **E** *Vamp2* compared to an uninfected control (two-tailed unpaired t-test with Bonferroni correction). However, overexpressing miR135b led to a causal increase of the mRNA abundance of **B** *Bsn* ($p < 0.01$) and **D** *Ssr2* ($p < 0.05$) (two-tailed unpaired t-test with Bonferroni correction). These results show that miR135b does not operate by degrading its mRNA targets, rather it either maintains mRNA abundance or promotes the creation of mRNA pools to be readily translated. mRNA levels were normalised to the geometric means of the levels of *TUBB3, ACTB* and *RBFOX3*. Fold enrichment was calculated by comparison to untransduced control cells. N = 10 replicates (5 technical replicates each from 2 x E16 dissections). Graphs show mean ± SEM.

Vamp2 (also known as Synaptobrevin-2) has a crucial, well-defined role in the brain as a presynaptic protein which controls synaptic vesicle fusion to the presynaptic membrane in conjunction with Syntaxin1a and SNAP25 (Salpietro et al., 2019). Vamp2 is proteolysed by tetanus toxin, which inhibits neurotransmitter release, further highlighting its role in synaptic connectivity (Schiavo et al., 1992).

In accord with the non-degrading microRNA-target interactions observed by Jovičić (2011), overexpression of miR135b in cortical neurons did not negatively regulate the levels of any of its target mRNAs tested (**Figure 3.4**). This provides additional evidence that miR135b does not degrade its target mRNAs via the canonical paradigm but may regulate their expression in some other manner. In fact, the mean levels of all five of the target mRNAs tested showed increases, and in three of these, the increases were statistically significant when compared to control. These results provided additional evidence that miR135b has a unique relationship with its targets.

Two-Way ANOVA identified a statistically significant effect of miR135b overexpression ($F = 9.44$, $p < 0.01$) and mRNA target ($F = 7.61$, $p < 0.0001$) on the overall result. Moreover, the interaction between microRNA overexpression and the mRNA target was significant ($F = 7.6$, $p < 0.0001$).

There was no change in *Atp1b1, Nsg1* or *Vamp2* mRNA abundance following miR135b overexpression (**Figure 3.4A and 3.4E** $p > 0.05$). These results may nonetheless be considered evidence for non-degrading miR135b-target relationships.

The mRNA levels of miR135b targets *Bsn* ($p < 0.01$, **Figure 3.4B**) and *Ssr2* ($p < 0.05$, **Figure 3.4D**) were significantly increased upon miR135b overexpression post-hoc t-test with Bonferroni correction. These findings are surprising given a lack of precedent for microRNA mediated target protection, rather than degradation. Nonetheless, they are consistent with previous results from our lab (Jovicic 2011).

Taken together, these results are consistent with my hypothesis that miR135b does not direct the degradation of its targets. Two targets showed no significant change in mRNA abundance upon microRNA overexpression, and the other three display a significant increase. This would be consistent with miR135b's holding its targets in a translationally repressed state. Given the synaptic roles of some of these mRNA targets, one scenario

might be the sequestration of these mRNAs into RNA granules to regulate RNA transport; alternatively, this could represent a possible role in creating a synaptic reserve pool of mRNAs for future translation.

3.2.4 The effect of miR137 overexpression on target mRNA abundance

miR137 is another microRNA shown by our group to co-exist with its targets rather than directing their degradation (Jovičić, 2011). To further evaluate miR137-target interactions, target mRNA levels were measured after miR137 overexpression. The mRNA targets investigated were *Ankrd12, Sept3, Lrrn3, Syt1, Ptpn5, Slc6a1, Gabra1* and *Fam126b*, most of which are involved in known synaptic functions. Of these, only *Syt1* has previously been investigated as a miR137 target.

Ankrd12 is an ankyrin repeat domain-containing protein whose specific functions have not yet been elucidated (Bai et al., 2013, Smirnova et al., 2019). Nevertheless, Ankrd12 protein is elevated in the sera of patients suffering from schizophrenia and bipolar disorder and is genetically linked to childhood apraxia of speech (Peter et al., 2016, Smirnova et al., 2019)

The remaining targets have defined roles within the brain. Sept3 is a presynaptic GTPase that regulates neurite outgrowth and the trafficking of synaptic vesicles (Takehashi et al., 2004, Tsang et al., 2008). *Lrrn3* encodes a brain localised leucine-rich-repeat protein whose expression is increased after injury to the cerebral cortex, thereby implicating it in neuroprotection (Ishii et al., 1996, Haines et al., 2005). The target *Fam126b* is a paralogue of the leukodystrophy protein Fam126a, mutations in which lead to the defective formation of the myelin sheath; Fam126b, however, shows a higher expression in neurons compared to oligodendrocytes (Gazzerro et al., 2012, Baskin et al., 2016).

Syt1 protein is a presynaptic calcium sensor that coordinates synaptic vesicle fusion and permits fast neurotransmitter release (Xu et al., 2009, Sudhof, 2013, Baker et al., 2018).

Ptpn5 is a tyrosine kinase that modulates neurotransmission by regulating AMPA and NMDA receptor endocytosis via direct phosphorylation (Lombroso et al., 1991, Boulanger et al., 1995, Yang et al., 2012a). *Slc6a1* encodes the voltage dependent GABA

Transporter 1 (GAT-1) which mediates GABA re-uptake from the synaptic cleft (Carvill et al., 2015, Cai et al., 2019). Mutations in *Slc6a1* can lead to epilepsy and ID (Cai et al., 2019, Jin et al., 2011). *Gabra1*, encoding the alpha-1 subunit of the GABA-A receptor, comprises an additional miR137 target involved in GABAergic neurotransmission which may be mutated in patients with epilepsy (Hernandez et al., 2019).

Consistent with the results obtained by Jovičić (2011), miR137 overexpression did not decrease the levels of any of its target mRNAs investigated (**Figure 3.5**), thereby showing a pattern similar to miR135b, but different from miR124. This result corroborates our hypothesis that this microRNA coexists with its targets without degrading them.

Two-Way ANOVA identified a statistically significant effect of miR137 overexpression ($F = 31.28$, $p < 0.0001$) and the mRNA targets ($F = 2.51$, $p < 0.05$) on the overall result. Moreover, the interaction between miR137 overexpression and the mRNA targets was significant ($F = 2.46$, $p < 0.05$). T-test with Bonferroni correction showed that overexpressing miR137 had no significant effect ($p > 0.05$) on the mRNA levels of its targets *Sept3*, *Lrrn3*, *Ptpn5*, *Slc6a1* and *Gabra1* and *Fam126b* (**Figure 3.5B, C, E, F, G and H**). The remaining mRNAs showed significant increases upon miR137 overexpression. These comprise *Ankrd12* (**Figure 3.5A**, $p < 0.05$) and *Syt1* (**Figure 3.5D**, $p < 0.01$).

Together, these results provide a direct indication that miR137 does not negatively regulate its mRNA targets utilising the canonical microRNA pathway of directing mRNA degradation. The fact that the levels of miR137 are positively correlated with those of its targets instead suggests an interrelated function. Given the known roles of the proteins encoded by miR137's targets (i.e. in neurotransmitter-mediated signalling), we postulate that miR137 might positively regulate synaptic connectivity.

Given the positive regulatory relationships of both miR135b and miR137 to their target mRNAs, I was intrigued to determine what their relationship(s) might be to their target proteins.

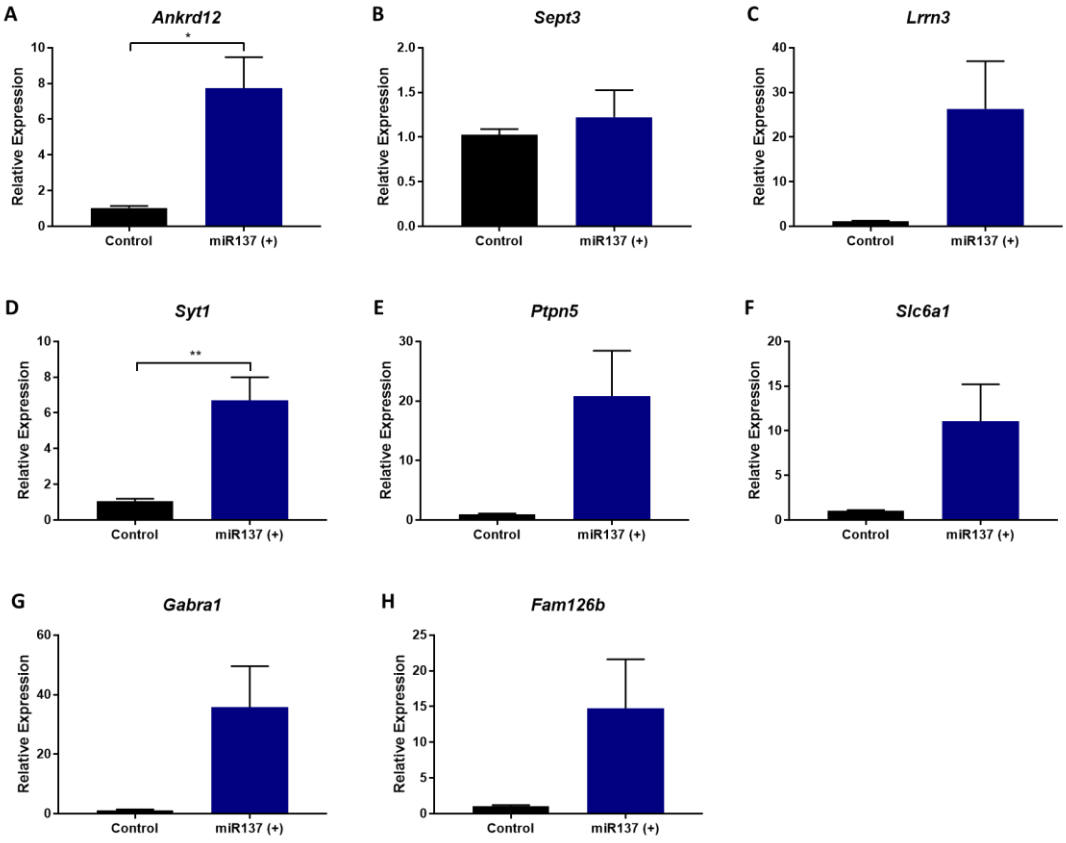

Figure 3.5: Overexpression of miR137 maintains or increases the abundance of its target mRNAs. Two-way ANOVA identified a statistically significant effect of lentiviral mediated miR137 overexpression ($F = 31.28$, $p < 0.0001$) and the mRNA targets ($F = 2.51$, $p < 0.05$) on the overall result. The interaction between miR137 overexpression and the mRNA targets was significant ($F = 2.46$, $p < 0.05$). Overexpression of miR137 in cortical neuronal cultures had no significant effect ($p > 0.05$) on the mRNA abundance of its targets **B** *Sept3*, **C** *Lrrn3,* **E** *Ptpn5*, **F** Slc6a1, **G** *Gabra1* and **H** *Fam126b* compared to an uninfected control (two-tailed unpaired t-test with Bonferroni correction). However, overexpressing miR137 led to an increase of the mRNA abundance of **A** *Ankrd12* ($p < 0.05$), **D** *Syt1* ($p < 0.01$) (two-tailed unpaired t-test with Bonferroni correction). This result suggests that miR137 does not degrade its mRNA targets, rather it either maintains mRNA abundance or promotes the creation of mRNA pools to be readily translated. mRNA levels were normalised to the geometric means of the levels of *TUBB3, ACTB* and *RBFOX3*. Fold enrichment was calculated by comparison to untransduced control cells. N = 10 replicates (5 technical replicates each from 2 x E16 dissections). Graphs show mean ± SEM.

3.3 What are the effects of microRNA overexpression on the levels of target proteins in neurons?

The mRNA data presented above suggested that miR135b and miR137 had the potential to increase the abundances of their target mRNAs, for which there is little or no precedent in the literature. Therefore, I relied on generating new experimental evidence to further characterise these unique microRNA-target relationships at the level of their encoded proteins. Once again, I compared the regulatory activities of miR135b and miR137 to that of the previously characterised 'canonical' neuronal microRNA, miR124, which is known to decrease the abundance of its targets at both the mRNA and protein level.

3.3.1 The effect of miR124 overexpression on target protein abundance

We have established that in our system, overexpression of miR124 in cortical neuronal cells via lentiviral transduction caused a decrease in the mRNA levels of two of its targets, *Nr4a1* and *Egr1*, both of which are immediate-early genes with roles in NMDA mediated synaptic plasticity (Duclot and Kabbaj, 2017, Chen et al., 2014b). Therefore, I subsequently assessed the effect of miR124 overexpression in this system on the levels of the corresponding proteins.

Consistent with the negative regulation of its target mRNAs (**Figure 3.3**), overexpression of miR124 decreased the abundance of its target proteins, Egr1 (**Figure 3.6A**, $p < 0.05$) and Nr4a1 (**Figure 3.6B**, $p < 0.0001$). Compared to the miR124-induced decreases of *Egr1* and *Nr4a1* mRNAs, the fold-changes of the corresponding proteins are notably lower. These results are nonetheless consistent with the previous literature on the behaviour

of miR124 (Tenga et al., 2016, Stark et al., 2005, Duclot and Kabbaj, 2017, He et al., 2018b).

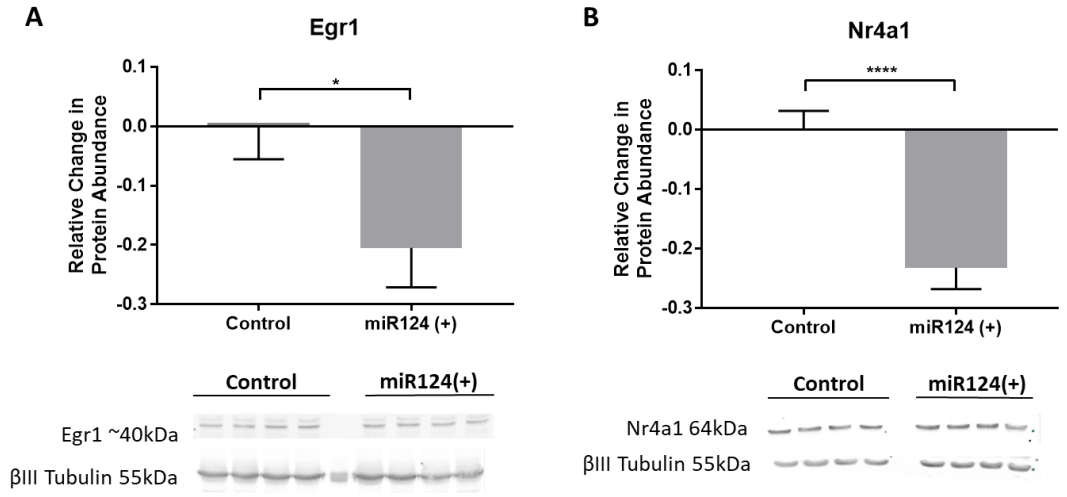

Figure 3.6: miR124 overexpression significantly decreases its targets at the protein level. Cortical neuronal cell cultures overexpressing miR124 were harvested for protein and subject to western blot. Immunoblots were scanned at multiple intensities with the LI-COR Odyssey Infrared Imager. The signal per band was analysed in Image Studio Lite and quantified as a ratio to βIII-tubulin. Overexpression of miR124 significantly decreased the protein abundance of its targets **A** Nr4a1 ($p < 0.0001$, Mann Whitney U test) and **B** Egr1 ($p < 0.05$, unpaired two-tailed t-test). This result shows that miR124 degrades its targets at both the mRNA and protein level. Relative protein abundance was calculated as a difference from untransduced controls. N = 13 from 3 x E16 dissections, data are displayed as mean ± SEM.

3.3.2 The effect of miR135b overexpression on target protein abundance

Having established that miR135b overexpression does not decrease the abundance of several of its mRNA targets (**Figure 3.4**), I wanted to investigate what effect miR135b would have on the corresponding target protein levels.

Interestingly overexpression of miR135b had no significant effect on the abundance of Atp1b1 protein (**Figure 3.7A**, $p > 0.05$); this target had also shown no significant change at the mRNA level. Similarly, the abundance of Vamp2 protein showed no significant difference after miR135b overexpression compared to untransduced controls (**Figure 3.7C**, $p > 0.05$), which paralleled its effect on *Vamp2* mRNA (**Figure 3.4E**). These results suggest that miR135b overexpression does not negatively regulate Atp1b1 and Vamp2 protein abundance by a selective effect on mRNA translation.

miR135b overexpression had no effect on Bsn protein abundance (**Figure 3.7B**, $p > 0.05$); this contrasts with the significant increase which was observed in *Bsn* mRNA after miR135b overexpression (**Figure 3.4B**). Taken together, these findings suggest that overexpression of miR135b may result in an increased pool of *Bsn* mRNA that might not be available for translation; in other words, miR135b does not degrade *Bsn* mRNA but instead might maintain it in a translationally repressed state.

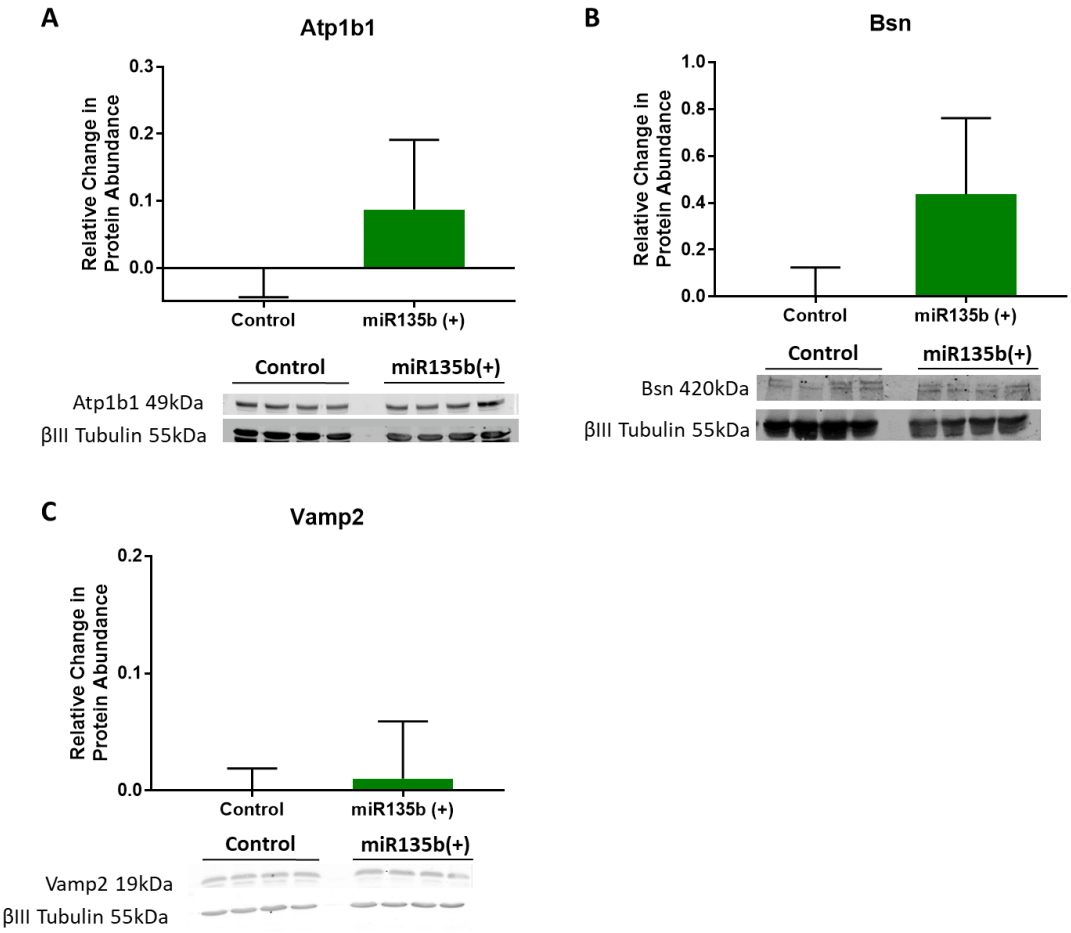

Figure 3.7: Overexpression of miR135b has no significant effect on the protein levels of its targets. Cortical neuronal cell cultures overexpressing miR135b were harvested for protein and subject to western blot. Immunoblots were scanned at multiple intensities with the LI-COR Odyssey Infrared Imager. The signal per band was analysed in Image Studio Lite and quantified as a ratio to βIII-tubulin. Overexpression of miR135b had no significant effect on the abundance of its targets at the protein level **A** Atp1b1 ($p > 0.05$, unpaired two-tailed t-test), **B** Bsn ($p > 0.05$, unpaired two-tailed t-test) and **C** Vamp2 ($p > 0.05$, unpaired two-tailed t-test). This provides further evidence for non-degrading relationships between miR135b and its targets. Relative protein abundance was calculated as a difference from untransduced controls. N = 13 (except for **B** Bsn where n = 8), from 3 x E16 dissections, data are displayed as mean ± SEM.

It was also observed that overexpression of miR135b increased the variation in target protein expression compared to untransduced controls, i.e. increased the standard deviation and standard error of mean: for Atp1b1 (F Test, $p < 0.01$), Bsn (F Test, $p < 0.05$) and Vamp2 (F Test, $p < 0.01$). This could be due to the state of the neurons after lentiviral transduction. Nonetheless, there was no trend in the means to suggest that miR135b overexpression led to decreased target protein abundance.

3.3.3 The effect of miR137 overexpression on target protein abundance

The effect of miR137 overexpression on target protein abundance was also investigated. In this case, we wanted to analyse what effect, if any, an increase in target mRNA abundance might have on target protein abundance upon miR137 overexpression. One possibility that I wished to understand was whether the increase in miR137 mRNA targets represented its ability to translationally repress these mRNAs without degrading them. To this end, miR137 targets Syt1, Ptpn5 and Gabra1 were investigated, all of which have important synaptic functions (**Figure 3.8**).

miR137 overexpression had no significant effect on the protein abundance of either Ptpn5 or Gabra1 (**Figure 3.5**). These results do not support a hypothesis of negative regulation of miR137 target protein expression but remain consistent with the hypothesis that miR137 creates translationally repressed pools of target mRNAs.

Investigation of a third target shows that an overexpression of miR137 increased the abundance of Syt1 at both the mRNA (**Figure 3.5**) and the protein levels (**Figure 3.8C**, $p < 0.001$). This finding contrasts some previously published results in other experimental systems which observed that overexpression of miR137 had either no effect or significantly decreased Syt1 protein abundance in the hippocampus (He et al., 2018a, Siegert et al., 2015). These results might be reconciled by a region-specific effect in the brain, with different regulatory mechanisms in cortical neurons versus hippocampal neurons. Nonetheless, the increase of *Syt1* mRNA and protein observed here suggests that overexpression of miR137 could directly modulate synaptic transmission by stabilising *Syt1* mRNA and facilitating Syt1 protein synthesis.

Whilst overexpression of miR137 did not affect the variability of the data when compared to an uninfected control when investigating the protein abundances of Ptpn5 and Gabra1, there was increased variability when investigating the protein abundance of Syt1 (F test, $p < 0.0001$).

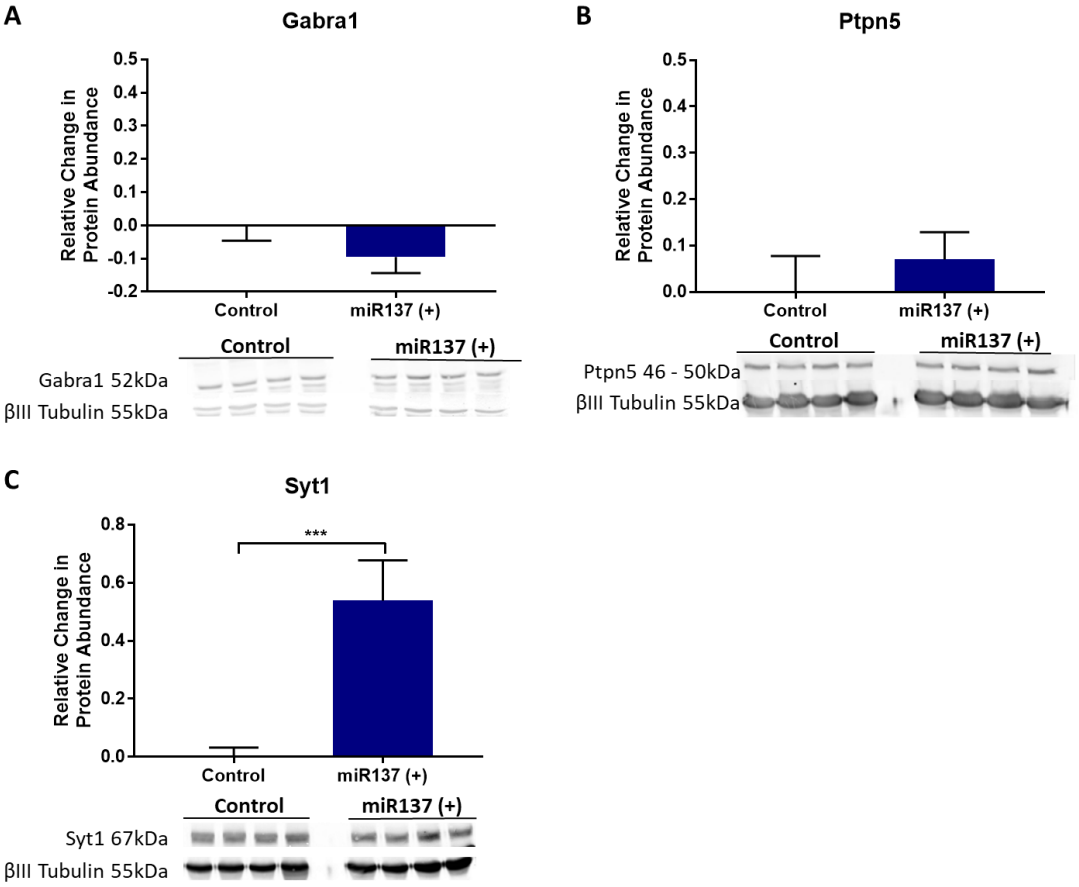

Figure 3.8: Overexpression of miR137 has no effect on the protein abundance of Gabra1 and Ptpn5, whilst significantly increasing the protein abundance of Syt1. Cortical neuronal cell cultures overexpressing miR137 were harvested for protein and subject to western blot. Immunoblots were scanned at multiple intensities with the LI-COR Odyssey Infrared Imager. The signal per band was analysed in Image Studio Lite and quantified as a ratio to βIII-tubulin. Overexpression of miR137 had no significant effect on the abundance of its targets **A** Gabra1 ($p > 0.05$, unpaired two-tailed t-test) and **B** Ptpn5 ($p > 0.05$, unpaired two-tailed t-test) at the protein level. **C** Syt1 protein was significantly increased with miR137 overexpression ($p < 0.001$, unpaired two-tailed t-test). This result provides further evidence for non-degrading relationships between miR137 and its targets. miR137 overexpression increases the protein abundance of the presynaptic calcium sensor Syt1, perhaps to modulate neuronal connectivity. Relative protein abundance was calculated as a difference from control. N = 13, from 3 x E16 dissections, data are displayed as mean ± SEM.

Taken together, these results suggest miR135b and miR137 do not degrade their targets at the mRNA level and do not negatively regulate protein expression in cortical neurons. These contrast with the results obtained for the canonical microRNA, miR124, in the same system, indicating microRNA (rather than cell) specificity of this mode of operation. This provides further evidence that some neuron-enriched microRNAs operate in a unique paradigm in regulating the expression of their targets.

3.4 Comparing the regulatory effects of miR137 in cortical versus in hippocampal neurons.

My results demonstrate that overexpression of miR137 causes a significant increase in its target Syt1 at both the mRNA (**Figure 3.5D**) and protein levels (**Figure 3.8C**) within cortical neuronal cultures. The upregulation in Syt1 mRNA and protein upon miR137 overexpression contrast with results from another study (Siegert et al., 2015). However, a different report found no change in Syt1 protein upon miR137 overexpression (He et al., 2018a). These previous experiments were carried out using hippocampal slices or hippocampal neurons in culture; therefore, I wished to determine whether my distinct results might be explained by having studied neurons from another brain region, particularly since cortical and hippocampal neurons have inherent molecular and circuitry differences.

In order to conduct the experiments as similarly to my previous experiments as possible, I examined Syt1, Gabra1 and Ptpn5 protein levels after miR137 overexpression in E16 rat hippocampal neurons. There was no observed difference in the protein expression of Gabra1 upon miR137 overexpression compared to uninfected controls within hippocampal neurons (**Figure 3.9**, $p > 0.05$). This is consistent with the results observed in cortical neuronal cultures (**Figure 3.8A**).

Contrary to the results obtained in cortical neuronal samples, there was no significant increase in the abundance of Syt1 protein in hippocampal cultures overexpressing miR137 compared to untransduced controls ($p > 0.05$, **Figure 3.9**). These results are in line with those found by He et al., (2018a), in mouse hippocampal cultures but distinct from miR137 overexpression in the hippocampus in vivo (Siegert et al., 2015).

Surprisingly, Ptpn5 protein was significantly increased in hippocampal cultures upon overexpression of miR137 compared to untransduced controls (**Figure 3.9B**, $p < 0.05$). There was no significant effect on miR137 overexpression on Ptpn5 mRNA or protein in cortical neurons (**Figure 3.8B**).

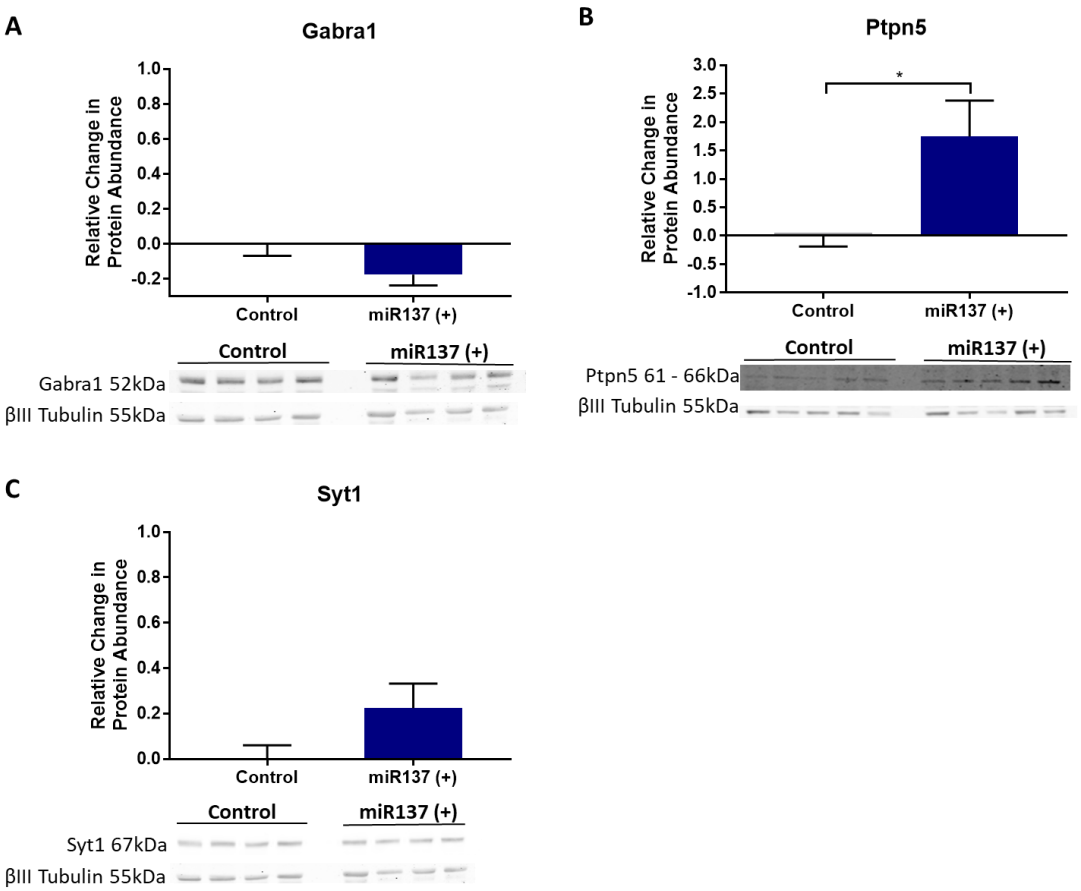

Figure 3.9: Overexpression of miR137 has no effect on the protein abundance of Gabra1 and Syt1, whilst significantly increasing the protein abundance of Ptpn5 in hippocampal neurons. Hippocampal neuronal cell cultures overexpressing miR137 were harvested for protein and subject to western blot. Immunoblots were scanned at multiple intensities with the LI-COR Odyssey Infrared Imager. The signal per band was analysed in Image Studio Lite and quantified as a ratio to β-III-tubulin. Overexpression of miR137 had no significant effect on the abundance of its targets **A** Gabra1 ($p > 0.05$, Mann-Whitney test) and **C** Syt1 ($p > 0.05$, Mann-Whitney test), which contrasts with the results obtained in cortical neuronal cells. **B** Ptpn5 protein abundance was significantly elevated compared to uninfected control ($p < 0.05$, unpaired two-tailed t-test). These results provide evidence for non-degrading relationships between miR137 and its targets in hippocampal neurons, and potential neuronal subtype and/or brain region specific mechanisms of miR137 gene regulation. Relative protein abundance was calculated as a difference from control. N = 18 (except Ptpn5, where N = 14), data are displayed as mean ± SEM.

These results suggest that miR137 overexpression has subtle differential effects on its target protein levels in hippocampal neurons compared to cortical neurons. This might reflect specific aspects of neuronal subtype and/or brain region-specific miR137 regulation.

3.5 Discussion

The results obtained demonstrate that miR135b and miR137 do not decrease the levels of their target mRNAs in our isolated neuronal system. We interpret these results to indicate that miR135b and miR137 may not operate through the canonical microRNA mediated pathway to induce target mRNA degradation.

3.5.1 miR135b and miR137 co-exist with or positively regulate the levels of their mRNA targets

The effects of miR135b and miR137 differed from that of the canonical microRNA, miR124 whose overexpression degraded its mRNA targets, *Egr1* and *Nr4a1*, and decreased the corresponding levels of protein (albeit to a lesser extent) (**Figure 3.3 and 3.6**). This was consistent with the literature, where miR124 has been shown in many contexts to degrade its mRNA targets to maintain neuronal cell identity. For example, miR124 inhibits the gene *PTBP1*, whose role is to inhibit neuronal differentiation (Yeom et al., 2018). Moreover, during neuronal maturation the expression of miR124 as controlled by REST, a transcriptional repressor, is increased to prevent the accumulation of non-neuronal mRNAs (Conaco et al., 2006). REST and miR124 act in a feedback loop, whereby REST inhibits the expression of miR124 in non-neuronal cells but permits its expression in neuronal cells (Conaco et al., 2006).

Within the literature, other groups have reported miR135b and miR137 to negatively regulate their targets, with the dysregulation of these microRNAs leading to cancers, and neuropsychiatric and neurodegenerative diseases. To the contrary, my results highlight the potential for these microRNAs to maintain or increase their target mRNA and/or protein levels. Below I consider the potential functional implications of the positive regulation of these targets.

3.5.1.1 miR135b

Overexpression of miR135b had no effect on the mRNA or protein abundances of its targets *Atp1b1, Nsg1* and *Vamp2* (**Figure 3.4**). These results suggest that miR135b co-exists with these targets, and potentially maintaining their levels of expression. Interestingly, another recent study has shown that an anti-inflammatory compound, Sulforaphane, increases the level of miR135b and the levels of some of its targets including *Atp1b1* in PC-3 cells (Yin et al., 2019). Atp1b1 is one subunit which makes up the heteromeric Na^+/K^+ ATPase in neurons, which is crucial in regulating the electrochemical gradient across the membrane and maintaining the resting membrane potential (Li and Langhans, 2015). This is important in neurons where the influx of sodium is necessary to drive an action potential. A significant decrease in *Atp1b1* expression could have large consequences in neuronal cell excitability, which could explain why miR135b might have a role in maintaining the levels of its expression. A maintenance in *Nsg1* mRNA by miR135b overexpression could perhaps provide a mechanism to modulate neuronal capacity for dendritic receptor trafficking and recycling with a concomitant or signal-dependent increase in Nsg1 protein synthesis (Steiner et al., 2002).

miR135b overexpression maintained the levels of *Vamp2* mRNA and protein compared to untransduced controls (**Figure 3.4E and 3.7C**). Although miR135b overexpression may not increase the capacity of synaptic vesicle fusion by increasing the abundance of Vamp2 mRNA or protein, it might regulate *Vamp2* translation in a more discrete fashion (Salpietro et al., 2019). In corroboration with the result shown in **Figure 3.4E**, *Vamp2* mRNA expression has previously been shown by another group to be unaffected by miR135b transfection into C2C12 cells (myoblast cell line) (Honardoost et al., 2016).

miR135b overexpression significantly increased the expression of *Bsn, Nsg1* and *Ssr2* mRNAs (**Figure 3.4**). None of these genes have been previously investigated as miR135b targets.

Alongside other signal sequence receptor proteins, Ssr2 forms the translocon-associated protein (TRAP) complex (Russo, 2020). The TRAP complex associates with Sec61 to regulate in co-translational translocation to the ER membrane; this process is crucial in

regulating neuronal protein trafficking (Nyathi et al., 2013). The functions of Ssr2 in the endoplasmic reticulum have not been elucidated in context of the brain, therefore the increase in mRNA shown in **Figure 3.4D** upon miR135b overexpression highlight *Ssr2* as an interesting candidate protein to investigate further.

The increase in *Bsn* mRNA upon miR135b overexpression could raise the potential for the definition of presynaptic active zones, which would in turn increase presynaptic capacity for synaptic vesicle recruitment, leading to consequences in synaptic connectivity (Gundelfinger et al., 2015). Curiously there was no significant effect of miR135b overexpression on Bsn protein abundance compared to an uninfected control (**Figure 3.7**). Taken together, the combined mRNA and protein data suggest that miR135b overexpression facilitates an increase in *Bsn* mRNA abundance which is not uniformly translated into protein. This indicates that miR135b might be maintaining the translational silence of *Bsn* mRNA, perhaps during RNA transport. An increase of *Bsn* mRNA by miR135b could alternatively increase the potential for synaptogenesis selectively during neurodevelopment.

3.5.1.2 miR137

My results demonstrated that miR137 overexpression had no significant effect on its targets *Sept3*, *Lrrn3, Ptpn5, Slc6a1, Gabra1* and *Fam126b* mRNA abundances compared to untransduced controls (**Figure 3.5**). However, miR137 overexpression caused an increase in the mRNA levels of its targets: *Ankrd12 and Syt1* (**Figure 3.5**).

miR137 may have functional consequences for GABA-ergic neurotransmission through maintenance of *Slc6a1* and *Gabra1* mRNAs. Mutations in *Slc6a1*, encoding a protein with roles in GABA re-uptake, are shown to cause phenotypes including epilepsy and ID, perhaps through excitotoxicity (Cai et al., 2019). miR137, moreover, has known effects in intellectual disability, and Slc6a1 could be one effector through which this may be mediated (Willemsen et al., 2011). miR137 overexpression maintained the levels of *Gabra1* mRNA with no changes in its protein abundance, perhaps maintaining its translational repression (**Figure 3.5 and 3.8**). Moreover, *Gabra1* mRNA is reported to be decreased in the prefrontal cortex schizophrenic patients, which could correlate with

the presence of SNPs in the *MIR137HG* known to decrease miR137 levels (Ripke et al., 2011, Hoftman et al., 2015).

miR137 overexpression had a similar effect on *Ptpn5* mRNA and protein, consistent with maintaining the translational repression of this mRNA (**Figure 3.5 and 3.8**). Reversal of this translational repression could modulate glutamatergic neurotransmission by increasing AMPA and NMDA receptor endocytosis (Yang et al., 2012a). Extrasynaptic NMDA receptor activation promotes Ptpn5 cleavage to trigger neuronal death, suggesting the regulation of Ptpn5 expression, perhaps by miR137, could be beneficial for neuronal survival (Hardingham and Bading, 2010).

Though its functional roles in the brain are unclear, Ankrd12 is known be increased in the serum of schizophrenic patients (Smirnova et al., 2019). Further investigating the association of miR137 and *Ankrd12* could be an important step in defining schizophrenic biomarkers (Thomas et al., 2018, Smirnova et al., 2019).

In contrast with other targets and the surrounding literature, miR137 overexpression increased both the mRNA abundance and subsequent protein translation of its target Syt1 within cortical neuron cultures (**Figure 3.5 and 3.8**). This suggests that there may be a target specific miR137-mechanism of action. Syt1 is a presynaptic calcium sensor involved in coordinated neurotransmission; this result suggests that miR137 might directly modulate synaptic plasticity via modulation of *Syt1* gene expression in cortical neurons (Xu et al., 2009). SNPs disrupting *Syt1* function have implications in synaptic vesicle fusion, thus impairing presynaptic transmission; this could have implications for neurodevelopment leading to neurological disorders including schizophrenia (Baker et al., 2018).

3.5.1.2.1 miR137 may regulate target expression in a brain region specific manner

Siegert et al., (2015) overexpressed miR137 in the dorsal dentate gyrus of C57BL/6 mice and observed a decrease in mRNA and protein expression of miR137 targets, including Syt1 (Siegert et al., 2015). He et al., (2018a), overexpressed miR137 in cultured hippocampal neurons from E18 C57BL/6 embryonic mice, however, with no change in Syt1 protein. Siegert et al., (2015) demonstrated that miR137 overexpression caused synaptic deficits, including decreased vesicle number and reduced LTP, however these

phenotypes were rescued by overexpressing miR137-resistant *Syt1*. He et al., (2018a), were unable to replicate these results in cultured hippocampal neurons suggesting that miR137 might not exercise its synaptic effects by regulation of *Syt1* mRNA alone. These studies highlight that there is minimal overlap in the consensus in literature thus far when exploring miR137 targets which may be differentially regulated by changes in microRNA expression (He et al., 2018a).

In contrast to the results obtained in cortical neurons, miR137 overexpression within cultured hippocampal cells had no significant effect on the abundance of Syt1 protein (**Figure 3.9C)**, perhaps suggesting neuronal cell type specific functions. These results recapitulated that shown by He et al., (2018), but were in contrast to Siegert et al., (2015). However, model and age specific molecular mechanisms may have an impact on the results obtained both by myself and the two other studies (Siegert et al., 2015, He et al., 2018a).

Surprisingly, overexpression of miR137 significantly increased the protein abundance of Ptpn5 in hippocampal neurons (**Figure 3.9B**), an effect which was not observed in cortical neuronal cultures. Ptpn5 regulates NMDA and AMPA receptor endocytosis and ERK activation post-NMDA receptor activation; this suggests a potential mechanism for the direct modulation of hippocampal synaptic activity by miR137 overexpression (Yang et al., 2012a).

3.5.2 Unique regulatory roles of miR135b and miR137 on target expression

The results in this chapter suggest that there are three potential outcomes of non-degrading microRNA-target interactions. Firstly, neuronal microRNAs might translationally repress their targets to create a reserve pool of mRNAs to be translated when and where required (an increase in mRNA with no increase in protein upon microRNA overexpression). Secondly, neuronal microRNAs might positively correlate with and facilitate the translation of its targets (an increase in mRNA and protein upon microRNA overexpression). Thirdly, neuronal microRNAs might transiently regulate the translation of certain targets, without affecting their global abundances (no change in mRNA or protein abundances upon microRNA overexpression). We postulate that these microRNA-mRNA interactions might be dependent on the type of neuron or synapse,

the subcellular context and the mRNA target itself. These results provide a basis for further understanding the complexities in the mechanisms of microRNA interactions with their targets.

As one facet of the above, we hypothesise that non-degrading microRNA-target interactions facilitate mRNA transport to sites remote from the cell body within translationally arrested RNA granules. These targets could then be locally translated or held in a translationally repressed pool to modulate signal-dependent translation. Investigating the potential colocalisation of microRNA-mRNA pairs in potential RNA granules, both biochemically and visually, will be crucial in investigating this hypothesis.

4 Chapter 4: Do neuronal microRNAs co-exist with their target mRNAs within distinct neuronal sub-fractions?

4.1 Introduction

My results show that, unlike most previously described microRNAs, miR135b and miR137 do not decrease the levels of their target mRNAs but may instead form non-degrading target interactions. I next sought to establish whether these microRNAs co-exist with their targets within the same neuronal cellular sub-compartments. The co-existence of microRNA-mRNA pairs could represent regulation of mRNA translation during neuritic transport. To achieve this regulation, the pairs would need to be packaged into RNA granules.

mRNA translation requires recruitment of the 40S ribosomal subunit which scans for the start codon; then the 60S ribosomal subunit joins the complex, forming the 80S subunit (Liu and Qian, 2016, King and Gerber, 2016). This is followed by the elongation phase of translation, where the peptide chain is extended until the stop codon is reached, after which the newly formed peptide is released (King and Gerber, 2016, Schuller and Green, 2018). Multiple ribosomes can be arranged on one mRNA facilitating its mass translation into protein, this arrangement of multiple ribosomes on a single mRNA strand is referred to as a polysome.

Sucrose density fractionation of cell lysates separates constituent organelles and other sub-compartments according to their relative density (Raschke et al., 2009). Within a linear gradient of 10 – 50% sucrose, ribosomes can be separated from other cellular components and their associated mRNAs, which are presumably undergoing translation, can be captured. Monitoring the translational ribosome profiles of neuronal cells allows determination of whether microRNAs 135b and 137 and their targets were present in the same cellular sub-fractions and the extent to which they associate with translating ribosomes or other sub-compartments. This permits inferences to whether the microRNA-mRNA pairs might be in physical proximity to each other, and if so, in which compartment they reside.

Within polysome profiles, free ribosomes and the 80S monosome are observed at lower densities of sucrose. Polysomal association with an mRNA increases its density. Therefore mRNAs which are being actively translated will sediment in denser fractions of the sucrose gradient (Liang et al., 2018, Pringle et al., 2019).

RNA granules are reported to be large macromolecular structures in neurons; microRNAs and their targets could be packaged into these translationally silent granules to be transported to sites remote from the cell body i.e. pre- or postsynapse (Krichevsky and Kosik, 2001). This phenomenon could also couple transport and signal-dependent translation, which can be controlled both spatially and temporally (Krichevsky and Kosik, 2001, Schratt et al., 2006).

Early studies investigating neuronal RNA granules elucidated that the granules bore resemblance to aggregated ribosomal clusters, furthermore, these granules colocalised with ribosomal proteins and many different mRNAs (Knowles et al., 1996). Krichevsky and Kosik (2001), using E18 cultured neurons from the rat forebrain, identified that sucrose gradient fractionation showed characteristic RNA peaks corresponding to free ribosomes and polysomes, but additionally showed a heavy peak which sedimented

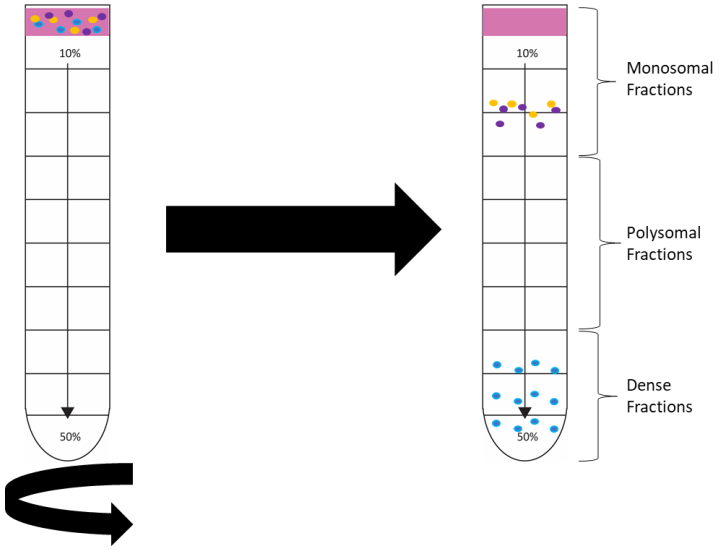

Figure 4.1: Illustration of sucrose gradient fractionation of neuronal cell lysate. Cortical neuronal cell lysate was loaded atop a gradient from 10 – 50% sucrose, and subject to ultracentrifugation. The fractions from the gradient was subject to continuous profiling for UV absorbance at 254 nm to generate a translational profile of the cells. Fractions were collected from the top of the gradient (**Materials and Methods**). Monosomes are present in fractions 0 – 3 (0 - 20% sucrose), polysomes in fractions 3 – 7 (20% - 40% sucrose) and we are considering fractions 7 onwards to be dense (40% - 50% sucrose).

below polysomes. The elements of this heavy peak resembled membrane-less granules made up of tightly packed ribosomes, whose structure was loosened upon depolarisation with KCl, with a concurrent shift in RNA targets to translating fractions (Krichevsky and Kosik, 2001). Krichevsky and Kosik (2001) postulated based on this evidence that RNA granules were translationally silent until their cargoes were released in a signal-dependent manner into translationally competent fractions.

We reasoned that microRNA-mRNA pairs which co-exist within denser fractions of the sucrose gradient could be inferred to exist together within putative RNA granules. This would provide preliminary evidence to suggest that non-degrading microRNA-target interactions might be regulating mRNA stability during transport. We also postulated that translational silencing of mRNAs by microRNAs in RNA granules would limit protein translation to the appropriate time and place in order to serve the specialisation of neuronal sub-compartments and to regulate neuronal connectivity.

4.2 Does miR135b co-exist with its neuronal targets sub-cellularly?

miR135b was shown in our previous experiments to increase the abundances of most of its target mRNAs tested with no consequent effect on the abundances of their encoded proteins. This suggests a protective relationship between miR135b and its mRNA targets, where the microRNA does not direct target degradation. Instead, we hypothesised that this microRNA might be facilitating translational repression during transport and/or creating a reserve pool of mRNA at sites remote from the cell body. In the following experiments, it was evaluated whether microRNA-target pairs might associate with each other in specific cellular sub-compartments. Within the translational profiles, monosomes are present in fractions 0 – 3 shown by a large peak (0 - 20% sucrose), polysomes in fractions 3 – 7 (20% - 40% sucrose) and we are considering fractions 7 onwards to be dense (40% - 50% sucrose) (**Figure 4.2A, 4.2B and 4.2C**).

In control gradients, with no lentiviral transduction, the monosomal peak is on average slightly higher compared to the miR135b overexpressing gradient (**Figure 4.2A, 4.2B and 4.2C**); this could potentially be explained by a relative decrease in translation initiation upon microRNA overexpression. To this end, Meijer et al., (2013) demonstrated that microRNA mediated translational repression of its mRNA targets could only occur during

translation initiation. Consequently, there would be a decrease in 80S (translationally competent) ribosomes upon microRNA overexpression (Chendrimada et al., 2007). Unlike Krichevsky and Kosik (2001), we were unable to see a large peak of UV fluorescence in the denser fractions of the gradient which they identified as the RNA granule fractions; nevertheless, we have made inferences according to distribution in the 40%, 45% and 50% sucrose fractions.

I first examined the distribution of miR135b, both endogenous and following microRNA overexpression (**Figure 4.2**). Endogenous miR135b was present in all fractions from 25 – 50%, with a peak at 40% (**Figure 4.2D**). Therefore, suggesting miR135b is associated with actively translating mRNAs as well as being present in denser fractions which should contain RNA granules. Upon miR135b overexpression, there is a significantly increased abundance of miR135b between control and microRNA overexpressing gradients at both 40% ($p < 0.01$) and 45% ($p < 0.05$). The extent of microRNA overexpression is most evident when comparing both conditions plotted on the same scale (**Figure 4.2F**). There is no change in the abundance of miR135b associated with actively translating fractions, therefore suggesting that microRNA-mRNA interactions within these fractions are similar with and without miR135b overexpression. However, the expression of miR135b after overexpression is consistent with there being a sequestration into RNA granules (Krichevsky and Kosik, 2001).

Despite this, when comparing the proportion of overall miR135b in each fraction in both control and overexpressing gradients, I found no significant differences ($p > 0.05$) in the proportion of the miR135b present in any fraction of the sucrose gradient (**Figure 4.2G, 4.2H** and **4.2I**). This suggests that microRNA overexpression does not alter the fractions which miR135b most preferentially associates with.

In order to test our hypothesis that stable microRNA-mRNA pairs exist in neurons, it was then necessary to examine the localisation of miR135b target mRNAs after sucrose fractionation. Any change in polysome profiles or the distribution of endogenously expressed miR135b and its mRNA targets observed after miR135b overexpression was assessed. This would provide evidence as to whether the microRNA influences the subcellular localisation of its mRNA targets. Conversely, if the main mode of microRNA-mRNA interaction is via degradation as suggested in the literature, then their mRNA

targets might be absent from the fractions in which the microRNAs are strongly

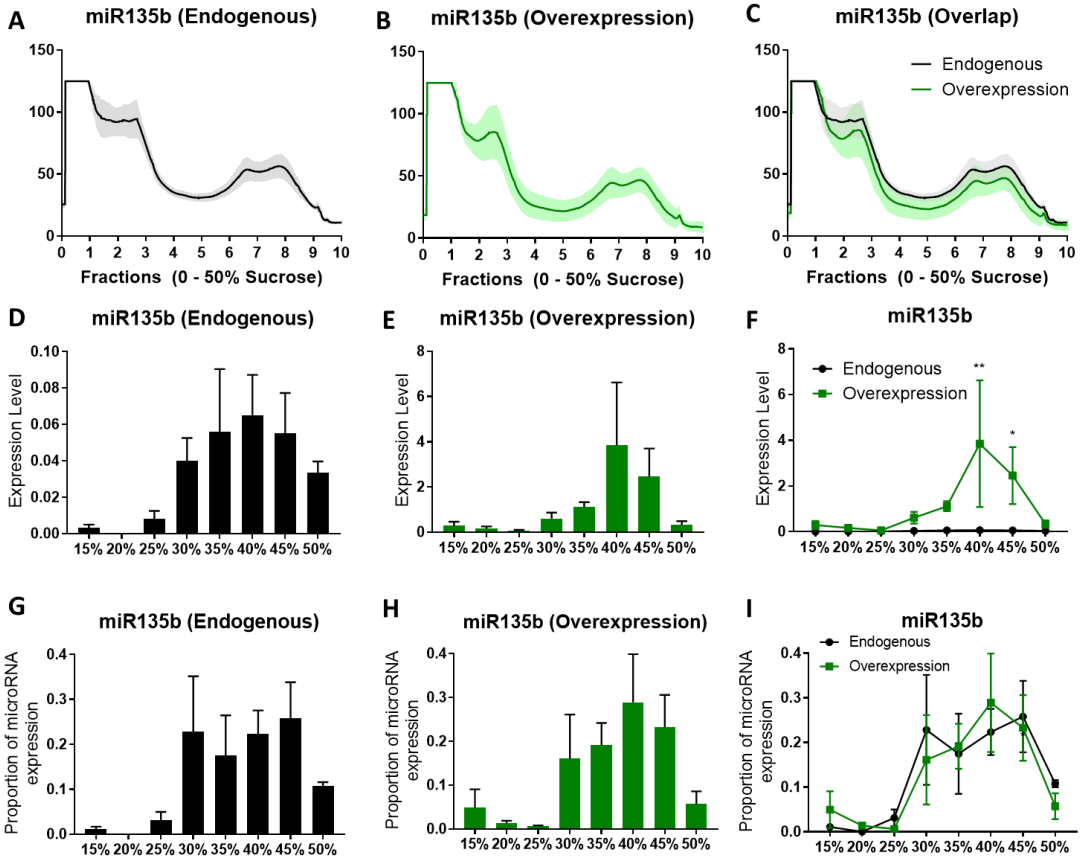

Figure 4.2: Polysome profiles and pattern of sucrose gradient distribution of miR135b in cortical neurons. Cortical neuronal cell cultures were transduced with lentiviral vectors to overexpress miR135b at DIV14, following translational arrest by 100 µg/ml cycloheximide at DIV28, neurons were harvested. Neuronal cell lysate was subject to sucrose density fractionation down a gradient from 10 – 50% sucrose. The fractions from the gradient was subject to continuous profiling for UV absorbance at 254 nm to generate a translational profile of the cells. **A – C** Graphs depict polysome profiles with and without miR135b overexpression, each fraction from 1 - 10 corresponds to each 5% step in the gradient (10 – 50%). **D – F** RNA was extracted from each fraction and reverse transcribed (**Materials and Methods**), microRNA levels were first normalised to total RNA extracted from each fraction, then normalised to the average total sum of expression in endogenous gradients. **D** Shows the endogenous expression level of miR135b after sucrose gradient fractionation in each 5% step in the gradient. **E** Shows the expression of miR135b with overexpression after sucrose gradient fractionation **F** Highlights the effect of miR135b overexpression within the sucrose gradient between endogenous and overexpressing conditions on the same scale. The level of miR135b overexpression is significant between endogenous and overexpression conditions at 40% ($p < 0.01$) and 45% ($p < 0.05$) sucrose (unpaired two-tailed t-test). **G – I** microRNA overexpression does not change the proportion of miR135b present in any fraction of the sucrose gradient (unpaired two-tailed t-test). Data is pooled from 4 biological replicates from 4 x E16 dissections. Graphs show mean ± SEM.

enriched, in this case 40 and 45% sucrose (**Figure 4.2**) (Guo et al., 2010, Eichhorn et al., 2014). However, consistent with my previous results and hypothesis, miR135b's targets are also present at 40% and 45% sucrose fractions after miR135b overexpression (**Figure 4.2 & 4.3**).

In both control and overexpressing conditions, *Atp1b1* is localised across 30% – 50% sucrose fractions, suggesting localisation in both actively translating and granule fractions. Upon miR135b overexpression, there is an overall increase in the abundance of this mRNA, which is statistically significant at 45% sucrose ($p < 0.05$) (**Figure 4.3A**). *Bsn* is predominantly localised in 40 – 45% sucrose fractions in endogenous conditions. Like *Atp1b1*, *Bsn* was increased in denser fractions after miR135b overexpression and showed a statistically significant increase in the 45% fraction ($p < 0.05$) (**Figure 4.3B**).

Ssr2 is present in 25% – 45% sucrose fractions in control conditions, with highest localisation in 40% sucrose. This distribution is shifted towards denser fractions after miR135b overexpression where *Ssr2* mRNA is distributed primarily between the 30% – 50% fractions, with the greatest concentration at 40%. Though *Ssr2* is predominantly localised at 40% with and without miR135b overexpression, there is a statistically significant increase of mRNA present in this fraction upon microRNA overexpression ($p < 0.05$) (**Figure 4.3D**).

These results further highlight a positive, non-degrading relationship between miR135b and its targets, where *Atp1b1*, *Bsn* and *Ssr2* are predominantly present and enriched in fractions where the microRNA itself is compartmentalised in overexpression conditions.

Nsg1 mRNA is distributed throughout translating and dense fractions between 25% – 50% sucrose in both endogenous and miR135b overexpressing conditions (**Figure 4.3C**). Although miR135b overexpression did not lead to a significant change in *Nsg1* mRNA abundance, a qualitative shift of this mRNA towards denser fractions can be observed (**Figure 4.3C**).

Vamp2 differed the most in its density fractionation profile compared to the other miR135b targets analysed. *Vamp2* mRNA is distributed across translating and dense fractions, between 25% – 50% sucrose, with peak localisation at 30%, suggesting this mRNA is largely associated with translating ribosomes (**Figure 4.3E**). miR135b is also

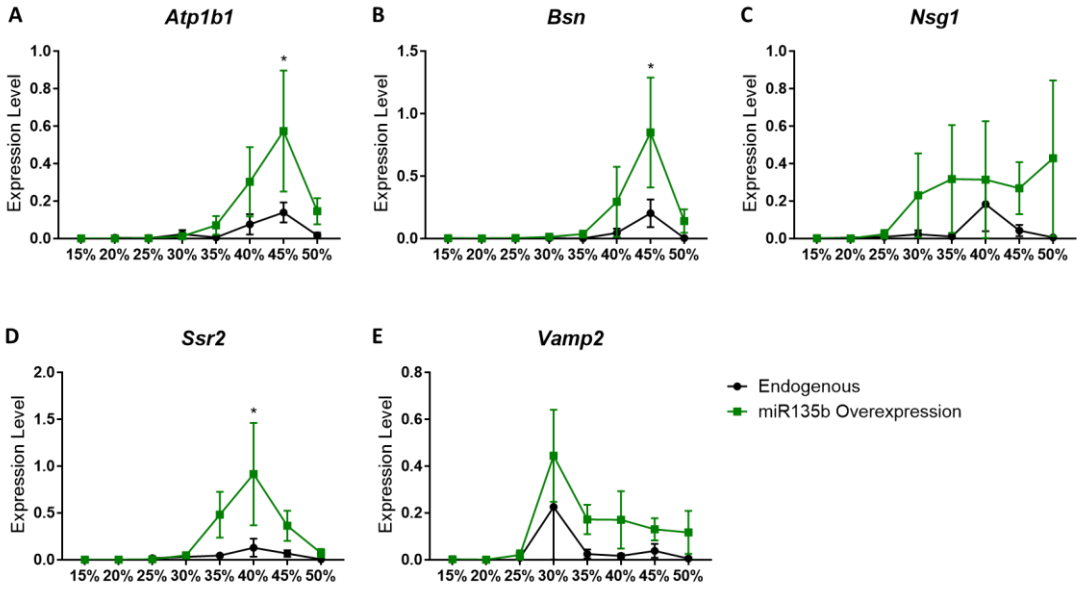

Figure 4.3: The effect of miR135b overexpression on the localisation and abundance of its target mRNAs after sucrose density fractionation. Cortical neuronal cell cultures were transduced with lentiviral vectors to overexpress miR135b at DIV14, following translational arrest by 100 µg/ml cycloheximide at DIV28, neurons were harvested. Neuronal cell lysate was subject to sucrose density fractionation down a gradient from 10 – 50% sucrose. The fractions from the gradient was subject to continuous profiling for UV absorbance at 254 nm to generate a translational profile of the cells. RNA was extracted from each fraction and reverse transcribed (**Materials and Methods**), miR135b target mRNA levels were first normalised to total RNA extracted from each fraction, then normalised to the average total sum of expression in endogenous gradients. Graphs show the expression of miR135b targets within the sucrose gradient with and without miR135b overexpression, within each 5% step in the gradient (15% – 50%). All targets show an average increased abundance and an increased sequestration into denser fractions of the gradient upon miR135b overexpression. **A** There is a significant increase in the abundance of *Atp1b1* at 45% upon miR135b overexpression ($p < 0.05$, unpaired two-tailed t-test) **B** There is a significant difference in the abundance of *Bsn* at 45% upon miR135b overexpression ($p < 0.05$, unpaired two-tailed t-test). **D** There is a significant difference in the abundance of *Ssr2* at 40% upon miR135b overexpression ($p < 0.05$, unpaired two-tailed t-test). **C & E** There is no significant difference ($p > 0.05$, unpaired two-tailed t-test) in the abundance of mRNA targets *Nsg1* and *Vamp2* across the gradient after miR135b overexpression. Data is pooled from 4 biological replicates from 4 x E16 dissections. Graphs show mean ± SEM.

present at 30% sucrose but is not enriched in this fraction in native or overexpressing conditions (**Figure 4.2**). There is no difference in the abundance of *Vamp2* at 30% between with or without miR135b overexpression, suggesting that this mRNA is constitutively actively translated. There is a general trend toward increase in *Vamp2* abundance in denser fractions of the sucrose gradient upon miR135b overexpression,

but this was not statistically significant (**Figure 4.3E**). Since miR135b overexpression also had no effect on the translation of Vamp2 protein (**Figure 6**), it may be inferred that miR135b does not target a large fraction of *Vamp2* mRNA in cortical cells.

Overall, these results strongly suggest that all miR135b targets are actively translated with and without miR135b overexpression, as we observe their localisation in 25% – 40% sucrose fractions and their protein levels are maintained, if not increased (**Figure 4.3**). Together with this, miR135b overexpression led to an increased sequestration of targets into denser fractions, which may represent the paired association of miR135b and its mRNA targets in RNA granules.

As observed from the error bars present in the graphs describing these data (**Figure 4.2 and 4.3**), there is substantial variation from experiment to experiment. In order to achieve a better resolution of microRNA and mRNA distributions, more experiments might be performed.

4.3 Does miR137 co-exist with its targets sub-cellularly?

Our experiments have shown that an overexpression of miR137 largely directs non-degrading relationships with its targets, unlike miR124 which degrades its target mRNAs. We additionally observed that miR137 overexpression increased the protein abundance of two of its targets: Syt1 in cortical neurons and Ptpn5 in hippocampal neurons. These results highlight that this microRNA co-exists with its mRNA targets, which might serve a role in mRNA transport and furthermore positively influence its targets' translation into protein. This unique relationship between miR137 and its targets could also be creating a translationally repressed pool of mRNA targets upon being transported to be translated in a signal-dependent manner. We have already highlighted that many of miR137's targets have important synaptic functions.

To elucidate the localisation of non-degrading microRNA-target interactions we employed sucrose gradient fractionation and polysome profiling. This allowed analysis of the translational profile of the cells along with the localisation of both the microRNA and its targets with and without miR137 overexpression. It would be interesting to elucidate whether the expression profiles of miR137 and its targets are consistent with their potential localisation within RNA granules. Furthermore, the elucidation of any

changes in the localisation of the microRNA and its mRNA targets within the translational profile upon miR137 overexpression may suggest a functional relationship

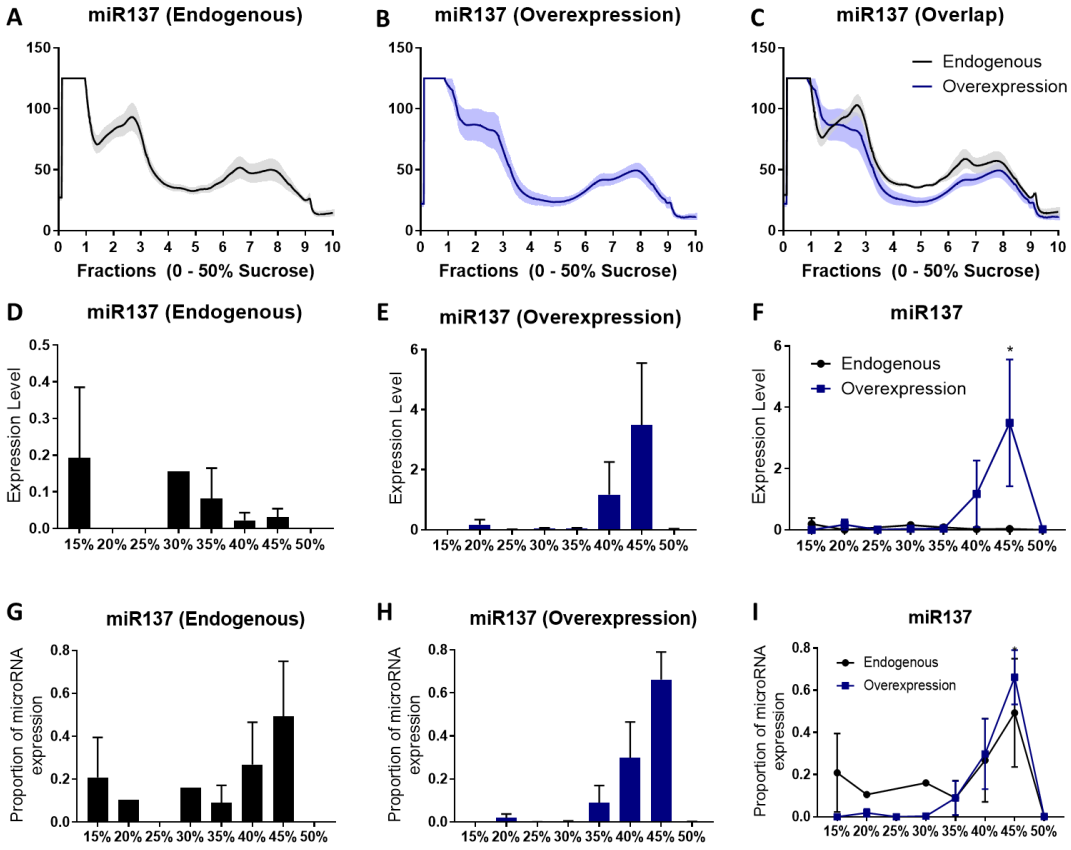

Figure 4.4: Polysome profiles and pattern of sucrose gradient distribution of miR137 in cortical neurons. Cortical neuronal cell cultures were transduced with lentiviral vectors to overexpress miR135b at DIV14, following translational arrest by 100 µg/ml cycloheximide at DIV28, neurons were harvested. Neuronal cell lysate was subject to sucrose density fractionation down a gradient from 10 – 50% sucrose. The fractions from the gradient was subject to continuous profiling for UV absorbance at 254 nm to generate a translational profile of the cells. **A – C** Graphs depicting the polysome profile with and without miR137 overexpression, each fraction from 1 - 10 corresponds to each 5% step in the gradient (10 – 50%). **D – F** RNA was extracted from each fraction and reverse transcribed (Materials and Methods), microRNA levels were first normalised to total RNA extracted from each fraction, then normalised to the average total sum of expression in endogenous gradients. **D** Graph shows the basal expression of miR137 after sucrose gradient fractionation. **E** Shows the expression of miR137 with overexpression after sucrose gradient fractionation **F** Highlights the effect of miR137 overexpression within the sucrose gradient between endogenous and overexpressing conditions. The level of miR137 overexpression is significant between endogenous and overexpressing conditions at 45% ($p < 0.05$, unpaired two-tailed t-test). **G – I** microRNA overexpression does not alter the overall proportion of miR137 present in any fraction of the sucrose gradient (unpaired two-tailed t-test). Data is pooled from 5 biological replicates from 4 x E16 dissections. Graphs show mean ± SEM.

between them. Monosomes are present in fractions 0 – 3 shown by a large peak (0% - 20% sucrose), polysomes in fractions 3 – 7 (20% - 40% sucrose) and dense fractions from 7+ (40% - 50% sucrose) (**Figure 4.4A, 4.4B and 4.4C**).

There are differences in the polysome profiles observed between neuronal cells with and without miR137 overexpression. In control gradients, the 80S monosomal peak is more pronounced. This suggests increased translation initiation in control neuronal cells as opposed those overexpressing miR137 (**Figure 4.4C**). Meijer et al., (2013) showed that microRNA mediated translational repression occurs only during the translation initiation phase, which could explain the observed decrease in 80S ribosome formation upon miR137 overexpression (Chendrimada et al., 2007).

In contrast to Krichevsky and Kosik (2001), we were unable to identify a large peak of absorbance in the denser fractions of the gradient which they identified as the RNA granule peak; we have nonetheless made inferences according to the sucrose density (**Figure 4.4A, 4.4B and 4.4C**).

miR137 is most strongly represented within 15%, 30% and 35% sucrose fractions, but is also present in the denser fractions at 40% – 45% sucrose (**Figure 4.4D**). The peak at 15% could imply that miR137 is exerting its effect on mRNA targets whilst they are undergoing translation initiation, perhaps interfering with eIF4A2 function via the microRNA-loaded RISC complex and associated proteins (Meijer et al., 2013). miR137's distribution upon its own overexpression caused a relatively selective enrichment in the 40% and 45% sucrose fractions (**Figure 4.4E**); the increase of miR137 at 45% compared to the endogenous expression of the microRNA is statistically significant ($p < 0.05$). The profile of miR137 within sucrose gradient fractions after its overexpression is consistent with its localisation in RNA granules (Krichevsky and Kosik, 2001). There is no difference in the abundance of miR137 at any other point in the gradient in control and microRNA overexpressing conditions (**Figure 4.4F**).

Overexpression of miR137 has no significant effect on the proportion of the microRNA present in any fraction of the sucrose gradient following fractionation (**Figure 4.4G**, **4.4H** and **4.4I**). This suggests that microRNA overexpression leads to an increase in miR137 without affecting the overall proportion of the microRNA present within neuronal

subfractions. From these comparisons it is evident that the largest proportion of miR137 is localised in denser fractions of the sucrose gradient both with and without overexpression (**Figure 4.4I**).

Both with and without microRNA overexpression, miR137 targets are most abundantly localised within denser fractions at 40% – 45% sucrose (**Figure 4.5**). However, qualitatively, all miR137 targets demonstrate a shift towards polysomal (translating) fractions upon miR137 overexpression. Interestingly, this is more similar to the localisation of miR137 under control conditions, suggesting that miR137 has a strong influence on target mRNA translation (**Figure 4.4D and 4.5**). The colocalisation of miR137 and its target mRNAs at 40% – 45% increases upon miR137 overexpression (**Figure 4.5**), consistent with compartmentalisation in RNA granules. There is an overlap between the localisation of miR137 and its targets, but this is less pronounced than for miR135b. On the other hand, one might consider that miR137 and its targets have reciprocal influences on each other's compartmentalisation.

Ankrd12 showed a largely similar profile of distribution between control and miR137 overexpressing conditions, where it is primarily localised within denser fractions between 40 – 45% (**Figure 4.5A**). There is no significant difference in the abundance of *Ankrd12* mRNA between any fractions in endogenous and miR137 overexpressing conditions ($p > 0.05$).

Sept3 and *Ptpn5* mRNAs behave quite similarly in their profiles of localisation. Endogenously, these mRNAs are localised throughout the polysomal and dense fractions between 30% – 50% sucrose and are most abundant at 45% (**Figure 4.5B and 4.5E**). After miR137 overexpression there is a leftward shift such that *Sept3* and *Ptpn5* are present in fractions between 25% – 50% sucrose and most abundant at 40% sucrose (**Figure 4.5B and 4.5E**). However, quantitatively, there is no significant difference in the abundance of either mRNA in any fraction in either endogenous or microRNA overexpressing conditions ($p > 0.05$).

Lrrn3 is localised in 30% – 45% sucrose fractions in both endogenous and miR137 overexpressing conditions with a maximum at 45% (**Figure 4.5C**). Whilst there is no significant difference between the abundance of Lrrn3 mRNA in any fraction with our

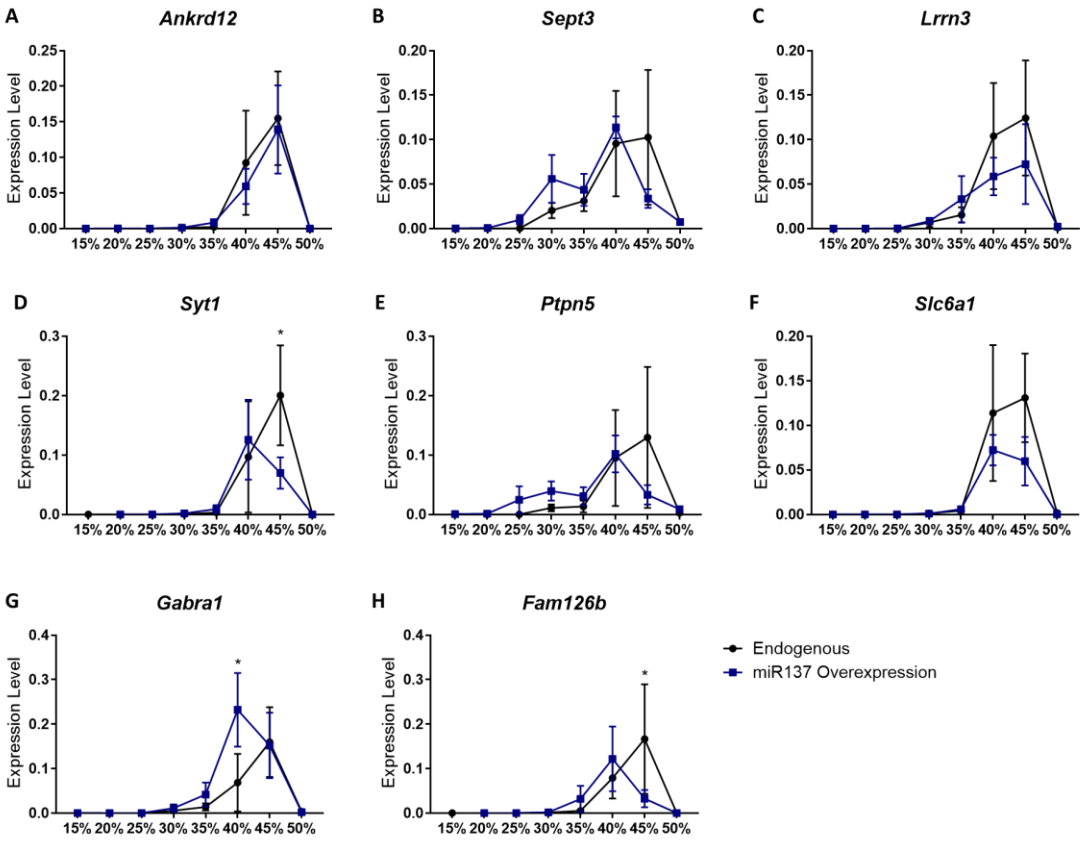

Figure 4.5: The effect of miR137 overexpression on the localisation and abundance of its target mRNAs after sucrose density fractionation. Cortical neuronal cell cultures were transduced with lentiviral vectors to overexpress miR135b at DIV14, following translational arrest by 100 µg/ml cycloheximide at DIV28, neurons were harvested. Neuronal cell lysate was subject to sucrose density fractionation down a gradient from 10 – 50% sucrose. The fractions from the gradient was subject to continuous profiling for UV absorbance at 254 nm to generate a translational profile of the cells. RNA was extracted from each fraction and reverse transcribed (**Materials and Methods**), miR137 target mRNA levels were first normalised to total RNA extracted from each fraction, then normalised to the average total sum of expression in endogenous gradients. Graphs show the expression of miR137 targets within the sucrose gradient with and without miR137 overexpression within each 5% step in the gradient. **A – C**, **E – F** There is generally an observed leftwards shift in the expression profiles of miR137 targets upon overexpression in the sucrose gradient, with no significant difference within any of the fractions between endogenous and miR137 overexpressing conditions. This could suggest a shift towards actively translating fractions. There is a significant decrease of **D** *Syt1* at 45% ($p < 0.05$, unpaired two-tailed t-test) and **H** *Fam126b* at 45% ($p < 0.05$, unpaired two-tailed t-test) upon miR137 overexpression. **G** *Gabra1* is significantly increased on miR137 overexpression at 40% ($p > 0.05$, unpaired two-tailed t-test). There is a consequential leftward shift in the distribution of these mRNAs upon miR137 overexpression, suggesting a redistribution towards translating fractions. Data is pooled from 5 biological replicates from 4 x E16 dissections. Graphs show mean ± SEM.

without miR137 overexpression ($p > 0.05$), miR137 overexpressing gradients showed

increased *Lrrn3* mRNA at 35% sucrose (**Figure 4.5C**), again following a trend in redistribution towards less dense fractions.

Slc6a1 mRNA is present mainly at 40 – 45% sucrose both with and without miR137 overexpression (**Figure 4.4E**). Though *Slc6a1* mRNA abundance is not significantly different in any fraction between the two conditions, there is a general decrease in mRNA abundance in denser fractions and a slight shift where the mRNA is more abundantly expressed at 40% upon miR137 overexpression compared to 45% in endogenous conditions ($p > 0.05$) (**Figure 4.5F**).

Syt1 (**Figure 4.5D**) and *Fam126b* (**Figure 4.5H**) behave in a similar manner with and without miR137 overexpression. Both mRNAs are largely localised to fractions between 40 – 45% sucrose under endogenous conditions, with a significant decrease of these mRNAs at 45% ($p < 0.05$) with a concurrent shift in mRNA abundance towards polysomal fractions after miR137 overexpression.

Gabra1 is localised in fractions between 30% – 45% sucrose in both overexpressing and endogenous conditions; however upon miR137 overexpression we observe a significant increase in the amount of *Gabra1* mRNA at 40% ($p < 0.01$), with an observed shift in the peak of localisation from 45% to 40% (**Figure 4.5G**). Again, this result highlights a redistribution of miR137 mRNA targets away from translationally silent fractions and towards polyribosomal fractions. Interestingly, *Gabra1* is the only miR137 mRNA target to display a significant increase in denser sucrose fractions upon miR137 overexpression.

Overall, miR137 is present in the same fractions as its targets, but this is more pronounced upon its overexpression. Furthermore, overexpression of miR137 increases the propensity of mRNA targets to be expressed within less dense fractions. One possibility is that miR137 increases the fraction of its targets available to be translated into protein. This could indicate a scenario where miR137 triggers a pathway which leads to the movement of its targets out of translationally repressed state to an actively translating state, consistent with the increases in Syt1 and Ptpn5 proteins in cortical and hippocampal cultures, respectively.

As observed from the error bars present in the graphs describing these data (**Figure 4.4 and 4.5**), there is substantial variation from experiment to experiment. In order to

achieve a better resolution of microRNA and mRNA distributions, more experiments might be performed.

4.4 Discussion

Polysome profiling provided a method to analyse the distribution of microRNAs and their mRNA targets in comparison to translating ribosomes. We were able to identify the localisation of miR135b and miR137 and their respective targets in both translating and dense fractions. Furthermore, this methodology permitted analysis of whether microRNAs and their targets were present within the same fractions, providing a proxy for their spatial co-existence, thus their non-degrading relationships. The results obtained show a potential difference in the actions of miR135b versus miR137 based on the observed effects on their target mRNAs' localisation.

Both endogenously and following their overexpression, both miR135b and miR137 were present in low density sucrose fractions, consistent with the inhibition of translation initiation (**Figure 4.2 and 4.3**). Overexpression of both miR135b and miR137 instigated similar observed changes in the overall polysome profiles of the cortical neuronal cells in that both microRNAs caused a decrease in the 80S monosomal peak in the observed polysome profiles (**Figure 4.2 and 4.3**). Previous research has demonstrated that microRNA mediated translational repression occurs during translation initiation. One mechanism by which this occurs is the microRNA directed recruitment of eIF6, which prevents the formation of the 80S initiation complex by inhibiting the binding between the 60S and 40S ribosomal subunits (Chendrimada et al., 2007). Another line of evidence has alternatively inferred that Argonaute proteins, through sequence similarity, might compete with eIF4E for binding to the mRNA cap to initiate translation (Kiriakidou et al., 2007). In an additional study, Meijer et al., (2013) identified a role for the translation initiation factor eIF4A2 in the regime of microRNA mediated translational repression by demonstrating that eIF4A2 could interact with the CCR4-NOT deadenylation complex to the exclusion of binding to eIF4G, thereby inhibiting formation of the eIF4F translation initiation complex (Meijer et al., 2013).

A recent study has shown that neurons have a limited capacity for local protein synthesis within neuronal processes that might be fulfilled by monosome-directed translation to

cater for local protein translation at sites remote from the cell body (Biever et al., 2020). Monosome-directed translation is limited to a single mRNA with a single ribosome, thereby achieving translational flexibility and conservation of the translational machinery. This is consistent with the relatively low abundance of ribosomes in neurites and synapses. Biever et al., (2020) additionally showed that Bsn, a miR135b target, undergoes monosome-directed translation (Biever et al., 2020). This group further speculated that the recruitment of local ribosomes was scalable in a signal-dependent manner to modulate synaptic plasticity (Biever et al., 2020). It would therefore be interesting in future studies to determine whether the 80S peak can be modulated by application of a cue to stimulate the reversal of microRNA mediated translational repression. This would permit elucidation of targets favouring monosomal over polysomal translation.

miR135b and its targets are localised throughout the gradient within the same ribosomal and dense fractions (**Figure 4.2 and 4.3**). miR135b overexpression caused an increased sequestration of both the microRNA itself and its targets into the denser fractions of the gradient (**Figure 4.2 and 4.3**). Moreover, there is a general increase in the abundance of all miR135b targets upon its overexpression (**Figure 4.3**), particularly in 40 – 45%, fractions where the microRNA itself was also enriched (**Figure 4.2 and 4.3**). This could be indicative of a sequestration into RNA granules (**Figure 4.3**). Nonetheless, all targets were still present within ribosomal fractions. miR135b overexpression might maintain constitutive translation, whilst increasing the recruitment of mRNA into translationally silent RNA granules. This is consistent with my results in the previous chapter showing that miR135b overexpression did not have a significant effect on protein abundance (**Figure 3.7**). These results provide further evidence for a cooperative, rather than antagonistic relationship between this microRNA and its targets.

miR137 was endogenously expressed within monosomal and polysomal fractions but showed a selective enrichment into dense fractions upon its overexpression (**Figure 4.4**). However, the proportion of microRNA present in any fraction was unchanged between control and overexpressing gradients (**Figure 4.4**). In contrast, its targets were enriched within denser fractions of the gradient in control conditions and shifted to lighter fractions after miR137 overexpression (**Figure 4.5**). Although somewhat surprising, this

could be considered evidence of a reciprocal effect of miR137 and its targets on each other's localisation.

Combined with the observation of miR137's targets being compartmentalised into dense fractions containing RNA granules, many of these targets have important synaptic functions e.g. *Syt1, Slc6a1, Ptpn5, Gabra1*. It is therefore extremely plausible that these mRNAs are transported to be translated in synaptic terminals.

With miR137 overexpression, its targets were still enriched at 40 – 45%, but the peak of mRNA localisation was shifted leftwards, towards ribosomal fractions (**Figure 4.5**). This observation could perhaps suggest a facilitation of mRNA translation with miR137 overexpression, consistent with an increased abundance of its target proteins.

The differences identified between the behaviours of miR135b and miR137 and their targets in this paradigm might relate to differences in their cellular roles or mechanisms of action. These results suggest that miR135b overexpression both increases the abundance of its mRNA targets and encourages their sequestration into RNA granule containing fractions. This strongly suggests a role for miR135b in facilitating its targets' neuritic transport. The miR135b-target relationship might maintain mRNA silence during transport and could create a pool of translationally repressed mRNA within the correct cellular sub-compartment upon being transported, to be translated in a signal-dependent manner. Perhaps even more surprisingly, however, it also highlights a novel mechanism by which microRNAs can prevent (rather than facilitate) mRNA target degradation.

The results for miR137 reveal an equally interesting and surprising potential mechanism whereby a microRNA might positively (rather than negatively) regulate the translation of its target mRNAs. This is further corroborated by observing that cortical neuron overexpression of miR137 leads to an increase in Syt1 protein cortical neurons (**Figure 3.8**) and an increase in Ptpn5 protein in hippocampal neurons (**Figure 3.9**).

There are slight discrepancies observed between RNA detection in whole cortical neuron lysates (**Chapter 3**) and their recovery from sucrose density fractions with and without microRNA overexpression. These could result from the different collection and

extraction conditions, particularly considering potential differences in RNA stability and treatment with chemical translation inhibitors.

Taken together, these results provide us with further evidence that microRNAs miR135b and miR137 co-exist together with their mRNA targets, as well as preserving rather than preventing their translation. This motivates further exploration of the potential function(s) of this co-existence, particularly with respect to regulating mRNA transport and local translation to modulate neuronal polarity and synaptic connectivity.

5 Chapter 5: Are the effects of neuronal microRNAs miR135b and miR137 specific to their own targets?

5.1 Introduction

Thus far we have established that miR135b and miR137 partake in non-degrading relationships with their mRNA targets in neuronal cells, whereby microRNA overexpression does not decrease the levels of their mRNA targets but might regulate their translation in some other way.

This chapter aims to clarify whether the effects we have observed on mRNA abundance and distribution within sucrose gradients upon miR135b and miR137 overexpression are specific to their own targets. We therefore examined whether miR135b and miR137 overexpression had any effect on the levels of mRNAs that do not contain their respective target sequences.

By way of reminder, target sequences refer to complementarity of the mRNA to nucleotides 2 – 8 of a microRNA, which are designated as its seed sequence. This complementary sequence usually resides in the 3' UTR of the mRNA target, and is sometimes coupled with additional pairing to an adenosine opposite nucleotide 1 (Lewis et al., 2005). mRNA targeting by microRNAs is facilitated by the RISC complex and its associated proteins, such as GW182, to direct microRNA-mRNA interactions and downstream translational repression which may or may not be coupled to mRNA degradation (Liu et al., 2005). Therefore, we would expect miR135b and miR137 not to impart any effect on targets which do not contain a complementary seed sequence.

miR124 was the only neuronal microRNA identified by Jovičić (2011) to uniformly direct degrading microRNA-target interactions. In agreeance with this, my experiments validated that miR124 overexpression directed the degradation of its targets *Egr1* and *Nr4a1*. Egr1 and Nr4a1 are both transcription factors, often behaving as immediate-early genes (Duclot and Kabbaj, 2017, Jeanneteau et al., 2018). The mRNA and protein levels of these targets were significantly decreased after miR124 overexpression compared to untransduced controls in my experiments (**Figure 3.3 and 3.6**), which was consistent with other evidence in the literature (Duclot and Kabbaj, 2017, Tenga et al.,

2016). *Egr1* and *Nr4a1* do not contain the seed sequences necessary for targeting by either miR135b or miR137, however, as manually validated on Ensembl, an online vertebrate genome browser. I specifically verified that the sequences of rat *Egr1* and *Nr4a1* did not contain motifs complementary to the microRNA seed sequence of either miR135b (TATGGCTT) or miR137 (TATTGCT) (Yates et al., 2019).

A lack of effect imparted by miR135b and miR137 on either *Nr4a1* or *Egr1* mRNA levels was further validated using ENCORI (known previously as starBase), an online platform which compiles the data from various different microRNA-target prediction algorithms (including: PITA, RNA22, Diana-microT, miRanda, Pictar and TargetScan) alongside experimental data from Ago CLIP-Seq and degradome sequencing (Li et al., 2014b). Ago CLIP-Seq is achieved by crosslinking argonaute proteins to any bound RNAs, immunoprecipitating these complexes, and subsequently using RNAseq data to map microRNA and mRNA binding sites to define relevant interactions (Chi et al., 2009). In contrast, degradome sequencing detects microRNA target mRNAs which have been cleaved by parallel analysis of RNA ends (German et al., 2009). One caveat of the present analyses is that ENCORI only identifies sequences within the mouse and human genomes, not the rat genome, therefore, there might be slight discrepancies in microRNA-target predictions due to the use of my experimental model. Nonetheless, a high fraction of conserved mouse-human interactions are also observed in rat (Nilsson et al., 2001).

ENCORI predicted hsa-miR135b (human) (PITA and miRanda – 14 Ago CLIP-Seq experiments) and mmu-miR135b (mouse) (PITA and miRanda – 1 Ago CLIP-Seq experiment), to target *Egr1* but neither were predicted to target *Nr4a1*. PITA, RNA22 and PicTar do not consider the rat genome, however further investigation on the microRNA-target prediction algorithms miRanda, Diana-microT and TargetScan did not identify rno-miR135b (rat) to target either *Egr1* or *Nr4a1* (Reczko et al., 2012, John et al., 2004, Agarwal et al., 2015).

With regards to miR137, ENCORI predicted that neither hsa-miR137 (human) and mmu-miR137 (mouse) to target *Nr4a1* or *Egr1*. This was corroborated with manual investigation using miRanda, Diana-microT and TargetScan algorithms to assess any

effect of rno-miR137 (rat) on either *Nr4a1* or *Egr1* (Reczko et al., 2012, John et al., 2004, Agarwal et al., 2015).

To this end, the total cellular abundance of *Egr1* and *Nr4a1* mRNAs following overexpression of either miR135b or miR137 via lentiviral transduction was measured. In addition to this, it was analysed if there were any changes to the distribution of *Egr1* and *Nr4a1* within translational profiles after sucrose density fractionation when comparing untransduced controls and microRNA overexpressing conditions. Should the mRNA abundances and translational profiles of *Egr1* and *Nr4a1* be unaffected by microRNA overexpression, this would suggest that there are no off-target effects of miR135b and/or miR137, and their mechanisms of action are specific to their own mRNA targets harbouring a complementary seed sequence.

5.2 What are the effects of miR135b and miR137 on non-targeted mRNAs?

We had already established that miR135b does not degrade its target mRNAs. Overexpression of miR135b in cortical neuronal cultures significantly increased or had no effect on the abundances of its target mRNAs, with no consequent effect on protein abundance. However, miR135b should have no effect on the levels of either *Egr1* or *Nr4a1*, neither of which contain a complementary seed sequence.

As predicted, overexpression of miR135b had no effect on the level of *Egr1* or *Nr4a1* mRNA (**Figure 5.1**, $p > 0.05$). These results suggest that overexpression of miR135b has no effect on the abundance of either of these targets which do not bear a complementary seed sequence.

Likewise, we predicted that miR137 overexpression would not influence the mRNA levels of miR124 targets, *Egr1* and *Nr4a1*. This is not what was observed, however. There was a significant effect of microRNA overexpression on the overall result (**Figure 5.2,** Two-way ANOVA $F = 38.4$, $p < 0.0001$). In contrast to what was observed for its own targets (**Figure 3.5**), overexpression of miR137 significantly decreased the mRNA

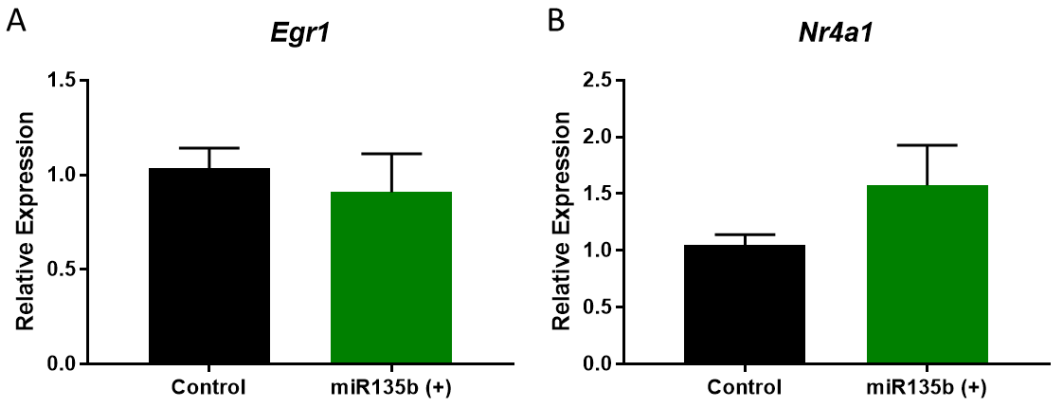

Figure 5.1: Overexpression of miR135b has no significant effect on miR124 target mRNAs Egr1 and Nr4a1. Two-way ANOVA identified that there was no significant effect on miR135b overexpression ($F = 0.75$, $p > 0.05$) or mRNA target on the overall result ($F = 2.15$, $p > 0.05$). There was no interaction between miR135b overexpression and mRNA target ($F = 2.02$, $p > 0.05$). Transduction of lentiviral vectors encoding miR135b in cortical neurons had no effect on miR124 mRNA target abundance of **A** *Egr1* ($p > 0.05$, unpaired two-tailed t-test with Bonferroni correction) and **B** *Nr4a1* ($p > 0.05$, unpaired two-tailed t-test with Bonferroni correction). This suggests no off-target effects. microRNA levels were normalised to the geometric means of the levels of *TUBB3, ACTB* and *RBFOX3* mRNAs. Fold enrichment was calculated by normalising data to control. N = 10 replicates (5 technical replicates each from 2 x E16 dissections). Graphs show mean ± SEM.

abundances of both *Egr1* ($p < 0.01$) and *Nr4a1* ($p < 0.001$) (**Figure 5.2**). In order to further evaluate the apparent regulation of miR137 on these two targets, the sequences of *Egr1* and *Nr4a1* (in rat) were analysed for complementarity to the rno-miR137 (rat) sequence using Ensembl (Hubbard et al., 2002). *Egr1* was found to contain two 5-base sequences complementary to the miR137 seed sequence (positions 2 – 8) and one 8-base, two 6-base and one 5-base sequence matches that extended (partially or entirely) beyond the seed sequence. *Nr4a1* was found not to contain any matches wholly within the seed sequence and three 5-base and one 6-base match only partially within the canonical seed sequence of miR137 (**Table 5.1**).

Previous groups have implemented a technique called CLASH (cross linking, ligation and sequencing of hybrids) to identify a microRNA, its target and their binding site sequences (Helwak et al., 2013). This technique has detected microRNA binding events directed by base-pairing outside the canonical seed region. This non-canonical targeting did not lead to the degradation of the target at either the mRNA or protein levels (Wang, 2014). Non-canonical sites have been postulated to act as microRNA-sponges by sequestering an

microRNA away from its regulated targets (Wang, 2014). This model does not reconcile the results observed with miR137 and *Egr1* or *Nr4a1*, however.

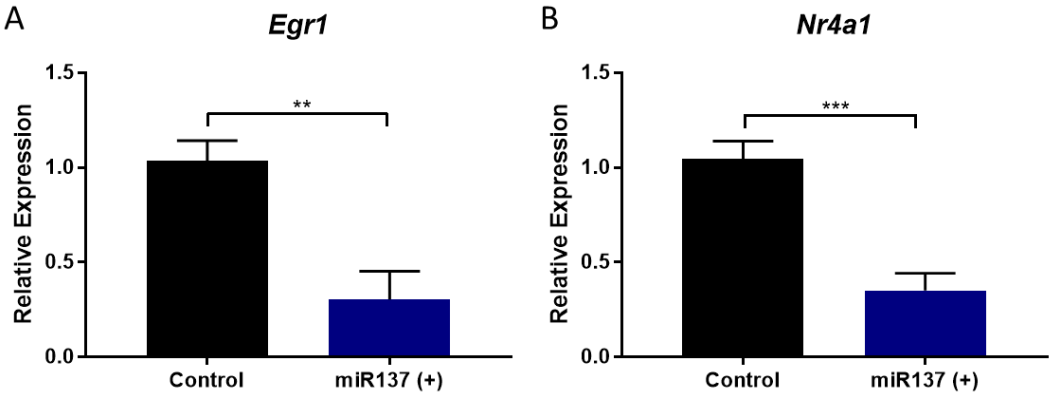

Figure 5.2: Overexpression of miR137 negatively regulates miR124 targets Egr1 and Nr4a1 mRNA. Two-way ANOVA identified a significant effect of miR137 overexpression on the overall result ($F = 38.4$, $p < 0.0001$). There was no effect of mRNA target on the result ($F = 0.06$, $p > 0.05$), nor was there a significant interaction between miR137 overexpression and miR124 mRNA targets ($F = 0.03$, $p > 0.05$). Transduction of lentiviral vectors encoding miR137 degraded the mRNA of miR124 targets **A** *Egr1* ($p < 0.01$, unpaired two-tailed t-test with Bonferroni correction) and **B** *Nr4a1* ($p < 0.001$, unpaired two-tailed t-test with Bonferroni correction). This shows that microRNAs are able to directly or indirectly modulate the abundances of targets which do not bear a complementary seed sequence. microRNA levels were normalised to the geometric means of the levels of *TUBB3, ACTB* and *RBFOX3* mRNAs. Fold enrichment was calculated by normalising data to control. N = 10 replicates (5 technical replicates each from 2 x E16 dissections). Graphs show mean ± SEM.

After elucidating that direct targeting by miR137 was unlikely to explain its apparent diminution of *Egr1* and *Nr4a1* mRNA levels (**Figure 5.2**), I explored the possibility of miR137 targeting mRNAs that may be upstream regulators of *Egr1* or *Nr4a1*.

Interestingly, the TargetScan algorithm predicts rno-miR137 to target *NAB2*, also known as EGR1 binding protein 2. This was additionally corroborated by ENCORI where mmu-miR137 (mouse) additionally targets *NAB2*. NAB2 functions as an endogenous repressor of Egr1; Egr1 acts in a negative feedback loop whereby it stimulates the expression of NAB2 by activating the NAB2 promoter (Bhattacharyya et al., 2013, Kumbrink et al., 2005). Therefore, if miR137 engages in non-degrading relationships with *NAB2* mRNA, perhaps promoting an increase in mRNA and protein, this could strengthen the negative

regulation this protein imparts on *Egr1* mRNA. This could explain the mRNA degradation observed (**Figure 5.2A**) (Bhattacharyya et al., 2013).

Nr4a1 expression in the central nervous system is controlled by transcription factor MEF2A. MEF2A induces *Nr4a1* expression in mammals, which is reported to have

effects on synapse number and development (Chen et al., 2014b, Shalizi et al., 2006). The drosophila orthologue of Nr4a1, Hr38, is also induced by MEF2A suggesting a conserved relationship between the two (Adhikari et al., 2019). TargetScan identified rno-miR137 to target *MEF2A*, whilst ENCORI identified both hsa-miR137 and mmu-miR137 to target *MEF2A*, too. Should this be in the canonical manner of target degradation, this could reconcile the decrease of *Nr4a1* after overexpression of miR137.

An alternate explanation of these effects could be non-canonical targeting of these two mRNAs by miR137 leading to their degradation. Moreover, the prolonged

	Complementary sequences (and lengths) within the mRNA 3'UTR	**Positions of potential hybridization to miR137 sequence**
Egr1	AAGCAA (6mer)	4 – 9
	GTATTCTT (8mer)	10 – 17
	CTTAAG (6mer)	7 – 12
	TAAGC (5mer)	6 – 10
	GCAAT (5mer)	**3 – 7**
	CAATA (5mer)	**2 – 5**
Nr4a1	ATTCT (5mer)	11 – 15
	TTCTT (5mer)	10 – 14
	TCTTA (5mer)	9 – 13
	TTAAGC (6mer)	5 – 10

Table 5.1: Matching sequences within *Egr1* and *Nr4a1* 3'UTRs complementary to miR137. Using Ensembl, a genome database, the 3' UTR's of both *Egr1* (Ensembl, Egr1-201, ENSRNOT00000026303.4) and Nr4a1 (Ensembl, Nr4a1-201, ENSRNOT00000010171.4) were checked for sequences complementary to the miR137 seed sequence (miRbase, MIMAT0000843) all from the rat genome. Sequences in bold represent complementarity to the canonical microRNA seed sequence.

overexpression of microRNAs in neuronal cells may elicit multiple indirect effects. For example, if prolonged miR137 overexpression is making neuronal cells less active there may be a consequent decrease in immediate early gene activation. In any case, the effect of miR137 on these two targets is different to its previously studied targets, which remain stable or are increased after miR137 overexpression.

5.3 Do miR135b and miR137 alter the cellular distributions of non-targeted mRNAs?

Next, the effect of miR135b overexpression on the cellular distributions of *Egr1* or *Nr4a1* was examined by sucrose gradient fractionation of cortical neuronal lysates. Our previous results have highlighted that miR135b overexpression generally caused an increase of its target mRNAs in denser fractions (**Figure 4.3**), consistent with colocalisation in RNA granules (Krichevsky and Kosik, 2001). We therefore sought to elucidate whether this effect of miR135b effects was specific to its own targets or instead potentially have a broader effect on mRNA transport and/or translational regulation.

Egr1 and *Nr4a1* mRNAs showed similar patterns of distribution across the density fractionation gradients in control samples. Egr1 and Nr4a1 are detected in 25 – 50% sucrose fractions, showing enrichment at 45% **(Figure 5.3**). Therefore, whilst being expressed in actively translating fractions, these mRNAs additionally display a distribution within dense fractions consistent with their potential localisation in RNA granules (Krichevsky and Kosik, 2001).

Qualitatively, overexpression of miR135b caused an increase in the abundance of *Nr4a1* mRNA in the 30 – 50% fractions without altering the overall distribution of the mRNA throughout the gradient (**Figure 5.3B**). However, comparison of miR135b overexpression to control lysates did not demonstrate differences ($p > 0.05$).

Though overexpression of miR135b did not change the abundance of *Egr1* mRNA in most fractions, a significant decrease was observed at 45% ($p > 0.01$) (**Figure 5.3A**). This could imply a redistribution of *Egr1* mRNA into denser fractions of the gradient upon miR135b overexpression.

We also examined the effect of miR137 overexpression on the distribution of miR124 targets to compare against the shifts of its own targets towards translationally active fractions (**Figure 4.5**).

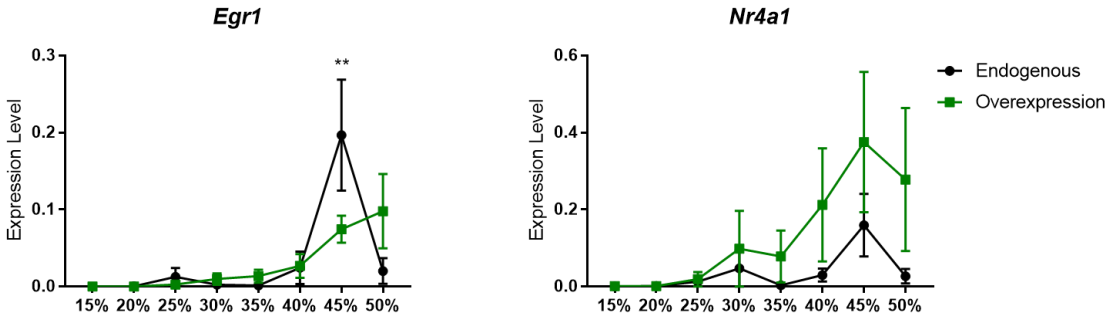

Figure 5.3: The effect of miR135b overexpression on the translational profile of miR124 targets, *Egr1* and *Nr4a1*. Neuronal cell cultures overexpressing miR135b were harvested at DIV28, following translational arrest by 100 µg/ml cycloheximide. Neuronal cell lysate was fractionated through sucrose density ultracentrifugation then subjected to continuous profiling for UV absorbance at 254 nm. RNA was extracted from each fraction and reverse transcribed (**Materials and Methods**), miR124 target mRNA levels were first normalised to total RNA extracted from each fraction, then normalised to the average total sum of expression in endogenous gradients. Graphs show the expression of miR124 targets within the sucrose gradient with and without miR135b overexpression, within each 5% step in the gradient (15% – 50%). **A** There is a significant decrease of *Egr1* at 45% sucrose upon miR135b overexpression ($p < 0.01$, unpaired two-tailed t-test). There was no change in any other fractions. **B** *Nr4a1* is expressed in the same fractions with the same pattern of expression throughout the gradient, there is no significant effect of miR135b overexpression in any fraction throughout the gradient ($p > 0.05$, unpaired two-tailed t-test). Data is pooled from 4 biological replicates from 4 x E16 dissections. Graphs show mean ± SEM.

As in the miR135b experiments, *Egr1* and *Nr4a1* displayed similar distributions in sucrose gradient fractionations with highest levels in the 45% fraction (**Figure 5.4**). As in the previous experiments with whole cell lysates in **Figure 5.2**, miR137 overexpression decreased the overall levels of both mRNAs and, moreover, led to a significant decrease in both *Egr1* ($p < 0.0001$) and *Nr4a1* ($p < 0.05$) in the 45% fraction (**Figure 5.4**).

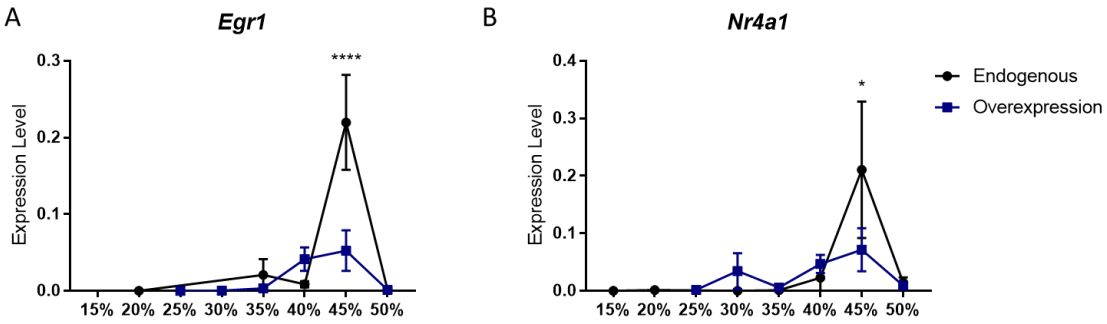

Figure 5.4: The effect of miR137 overexpression on the translational profile of miR124 targets, *Egr1* and *Nr4a1*. Neuronal cell cultures overexpressing miR137 were harvested at DIV28, following translational arrest by 100 µg/ml cycloheximide. Neuronal cell lysate was fractionated through sucrose density ultracentrifugation then subjected to continuous profiling for UV absorbance at 254 nm. RNA was extracted from each fraction and reverse transcribed (**Materials and Methods**), miR124 target mRNA levels were first normalised to total RNA extracted from each fraction, then normalised to the average total sum of expression in endogenous gradients. Graphs show the expression of miR124 targets within the sucrose gradient with and without miR137 overexpression, within each 5% step in the gradient (15%-50%). **A** There is a significant decrease of *Egr1* at 45% sucrose upon miR137 overexpression ($p < 0.0001$, unpaired two-tailed t-test), with no change in any other fraction. **B** *Nr4a1* was also significantly decreased at 45% upon miR137 overexpression ($p < 0.05$, unpaired two-tailed t-test), with no change in any other fraction. Data is pooled from 4 biological replicates from 4 x E16 dissections. Graphs show mean ± SEM.

5.4 Discussion

microRNAs typically exert their effects by binding mRNA targets within their 3'UTRs via their 'seed sequence'; therefore, the canonical rule is that if an mRNA does not harbour a sequence complementary to a microRNA's seed sequence, it will not be targeted by that microRNA. Employing this rule, I analysed the effects of miR135b and miR137 on two mRNAs to which they should not bind.

miR135b overexpression had no significant effect on either *Egr1* or *Nr4a1* mRNA abundances (**Figure 5.1**). This result was as expected and was consistent with various prediction algorithms (miRanda, Diana-microT and TargetScan) (Reczko et al., 2012, John et al., 2004, Agarwal et al., 2015).

Likewise, miR135b overexpression had no significant effect on the distribution of *Nr4a1* in sucrose density gradients (**Figure 5.3B**). This mRNA showed the same pattern of expression throughout the gradient between 25 – 50% sucrose, suggesting a constant association with translating ribosomes and with denser fractions associated with RNA granules, with or without excess miR135b (**Figure 5.3B**). These results corroborate with that seen in **Figure 5.1B**, suggesting that this microRNA has no off-target effect with regards to Nr4a1.

miR135b overexpression did change the profile of *Egr1* expression within the sucrose gradient, this was shown by a significant decrease at 45% ($p < 0.01$) (**Figure 5.3A**). This could suggest an indirect effect upon the distribution of some non-targeted mRNAs.

Overall, however, the present results suggest that miR135b does not have major off-target effects, as exemplified by the levels and distributions of *Egr1* and *Nr4a1* mRNAs.

Unexpectedly, miR137 overexpression negatively regulated the cellular levels of both *Egr1* ($p < 0.01$) and *Nr4a1* ($p < 0.0001$) mRNAs (**Figure 5.2**). Furthermore, this decrease in both *Egr1* ($p < 0.0001$) and *Nr4a1* ($p < 0.05$) was corroborated in the 45% sucrose fraction in the sucrose density fractionation experiments (**Figure 5.4**). This is also the fraction in which miR137 itself is enriched after overexpression, which suggests an anti-correlation. There was also a trend toward an increase in less dense fractions, similar to the qualitative redistribution of miR137's known direct targets (**Figure 4.5**).

Given these results, I considered sequence evidence as to whether miR137 might target *Egr1* and *Nr4a1* directly. Although the possibility of binding outside the miR137 seed sequence cannot be completely excluded, I considered the evidence supporting direct targeting to be weak. Instead I postulated that these effects might be imparted through miR137 targeting mRNAs acting upstream of *Egr1* and *Nr4a1*. miR137 targets *NAB2*, a known endogenous repressor of *Egr1* transcription (Bhattacharyya et al., 2013). Therefore, a facilitatory relationship between miR137 and *NAB2* expression might enhance its negative regulation upon *Egr1* and explain the change in *Egr1* mRNA abundance. Furthermore, miR137 targets *MEF2A*, which positively regulates *Nr4a1* transcription (Adhikari et al., 2019, Chen et al., 2014b, Shalizi et al., 2006). A canonical regulation of *MEF2A* mRNA by miR137 could therefore explain the decrease in *Nr4a1*

mRNA. Although different from the regulation of its known targets studied here, such an effect would be consistent with previous reports of miR137-mediated target mRNA degradation in other contexts (Siegert et al., 2015, Wang et al., 2018, Jia et al., 2016, Cheng et al., 2018, He et al., 2018a).

There is also the possibility that prolonged microRNA overexpression may have consequent effects on neuronal cellular activity. A decrease in activity may concurrently lead to a decrease in immediate early gene (or other) gene expression. Genome wide assessment of microRNA targeting specificity could clarify this going forward.

A broad interpretation of these data would suggest that miR137 can operate in both canonical and non-degrading microRNA regimes. This possibility merits further investigation.

6 Chapter 6: miR135b and miR137 co-distribute with specific RNA binding proteins in neuronal subfractions

6.1 Introduction

Prior biochemical investigations showed that miR135b and miR137 and their respective targets were distributed within overlapping neuronal fractions, both with and without microRNA overexpression. This provided support for my hypothesis that these microRNAs served facilitatory rather than antagonistic activities toward the expression of their targets.

Upon overexpression, both the microRNAs and their targets co-distributed to denser cellular subfractions; this is consistent with their possible incorporation into RNA granules (Krichevsky and Kosik, 2001). However, there were subtle differences in miR135b's and miR137's distribution patterns relative to those of their targets. miR135b overexpression generally increased the abundances of its mRNA targets throughout the gradient, whereas miR137 overexpression shifted the distributions of its targets towards actively translating fractions.

In previous experiments (**Chapter 4**), I focused on describing the RNA components of various neuronal subfractions using sucrose density gradients. In my next series of experiments, I describe the proteins that are present in those same fractions of neuronal cells. I set out to further explore the possible incorporation of miR135b and miR137 and their targets into RNA granules by examining their biochemical co-fractionation with RBPs known to be involved in translational regulation and mRNA transport (Krichevsky and Kosik, 2001).

6.1.1 Proteins investigated to characterise sucrose gradients and to evaluate the neuronal distribution of translational regulatory proteins

Analysing the distribution of various proteins allowed validation of the expected distribution of cellular sub-components within the gradient and consideration of the overall distribution of general translational regulatory proteins. To this end, I analysed the distributions of eIF4A1, eIF4A2, PABP, L10 ribosomal protein and SOD2.

eIF4A1, eIF4A2, PABP and L10 were chosen for their known roles in regulating protein translation. Cap-dependent translation refers to the reliance on a 5' m^7G mRNA cap which protects the mRNA against exonuclease cleavage and serves to recruit and anchor translation initiation factors (Ramanathan et al., 2016). 95 – 97% of mRNAs are translated in a cap-dependent manner; this is mediated by the 43S preinitiation complex made up of the 40S ribosomal unit, an initiator tRNA, GTP and the eIF4F complex (Fukao et al., 2014). The eIF4F complex consists of eIF4E, eIF4A1/4A2, eIF4G and accessory proteins (Malka-Mahieu et al., 2017). eIF4E binds the 5' cap, eIF4A proteins unwind the 5' end of the mRNA to facilitate 43S scanning, and eIF4G acts as a scaffold and circularises the mRNA through interactions with PABP at the 3' poly-A tail (Wells et al., 1998, Sonenberg and Hinnebusch, 2009, Fukao et al., 2014). mRNA circularisation provides a quality control step in which only full and properly formed mRNAs are translated. After the 43S preinitiation complex identifies the start codon, the initiator tRNA is able to dock via complementary base pairing, followed by recruitment of the large 60S ribosomal subunit (Sonenberg and Hinnebusch, 2009). L10 is a component of the 60S ribosomal subunit, which is recruited to the 40S subunit to form the 80S complex to initiate translation (Klauck et al., 2006). L10 is therefore expected to demarcate translating ribosomal fractions.

eIF4A1 and eIF4A2 share 90% sequence homology, and function as ATP-dependent DEAD box helicases to unwind secondary structures at the 5' ends of mRNAs to facilitate ribosome scanning during translation initiation (Lu et al., 2014). Though widely regarded to act interchangeably, evidence suggests that eIF4A1 and eIF4A2 differ in their actions. Whilst both proteins are involved in translation initiation, studies have shown that eIF4A1 might have a preferential role in this process. These proposed differential roles are underpinned by recent evidence to show that eIF4A1 and eIF4A2 have different binding affinities to eIF4G (Wilczynska et al., 2019). EIF4A1 is thought to bind preferentially to eIF4G directly, whilst eIF4A2 is recruited to and binds CNOT1 of the CCR4-NOT deadenylation complex. Importantly, the latter event was further shown to mediate microRNA mediated translational repression (Meijer et al., 2013, Lu et al., 2014, Wilczynska et al., 2019).

PABP functions in protecting the poly(A) tail from nuclease degradation, thereby maintaining mRNA stability (Bernstein et al., 1989). As mentioned previously, PABP also interacts with eIF4G of the eIF4F complex in order to mediate mRNA circularisation during translation, and has been reported to promote 80S ribosome formation (Wells et al., 1998, Kahvejian et al., 2001). A role for PABP has also been elucidated in translation termination, where it helps to identify the stop codon and aids in the recruitment and stabilisation of eukaryotic release factors (Ivanov et al., 2016). Of particular importance is that PABP has also been reported to promote mRNA binding to microRNA-loaded RISC complexes (Moretti et al., 2012). The presence of PABP in dense cellular fractions could further suggest localisation in RNA granules along with microRNAs and their targets to regulate translational repression and mRNA transport, but evidence is scarce on this point.

6.1.2 RBPs with specialised roles in neuronal RNA transport and/or translational regulation

I also sought to investigate the localisation of RBPs that would both help us further localise (or distinguish) RNA granule populations and determine which RBPs might be associated with miR135b- or miR137-target complexes of interest. We focused on RBPs with known associations with RNA granules and involvement in translational regulation in neurons. The investigated proteins comprised IMP1, FMRP, SMN and MOV10.

6.1.2.1 IMP1

Established in regulating β-actin mRNA transport, IMP1 binds to a 54 nucleotide 'zip-code' within β-actin's 3'UTR and maintains it in a translationally repressed state (Kislauskis et al., 1994, Hüttelmaier et al., 2005). When required, e.g. upon neuronal NT-3 stimulation, β-actin mRNA is transported selectively down axons by association with KIF11 (Zhang et al., 2001, Song et al., 2015). This translational repression is reversed once the complex arrives at the neuronal growth cone (e.g. upon Src mediated phosphorylation of IMP1), where β-actin translation and actin polymerisation supports neurite outgrowth (Hüttelmaier et al., 2005). IMP1 has been observed in the same context to be associated with neuronal RNA granules (Elvira et al., 2006).

6.1.2.2 FMRP

In Fragile X Syndrome (FXS), a hereditary intellectual disability disorder, there is silencing of the protein coding gene *FMR1*, with a consequent a decrease in the amount of FMRP protein (Mazroui et al., 2002). FMRP, like IMP1, has been shown to regulate the localisation and translation of mRNAs (Sudhakaran et al., 2014, Wang et al., 2016). The decrease in FMRP, both through mutation and through modelling this phenomenon through null mutation in model systems has been associated with the loss of translational regulation of the mRNAs with which it is associated. This has been observed as both increased target protein levels and a decreased target mRNA association with translating ribosomes (Thomson et al., 2017, Asiminas et al., 2019).

FMRP has also been implicated previously in microRNA mediated regulation of mRNA targets, with one example being the regulation of CAMKII mRNA in the context of synaptic plasticity and long-term memory formation (Sudhakaran et al., 2014, Wang et al., 2016). Most studies characterising FMRP's role in RNA targeting have focussed on the postsynapse; nonetheless, there is some evidence that this RBP may regulate RNA trafficking in the axon, also (Price et al., 2006, Wang et al., 2015).

6.1.3 SMN

SMN, mutations in which are involved in spinal muscular atrophy, has a known role in the localisation and local translation of axonal mRNAs (Wang et al., 2016, Costa and Willis, 2017, Khalil et al., 2018). SMN was originally thought not to bind RNAs directly, due to the lack of a conventional 'RNA interacting motif'; therefore, its mechanism of action was proposed to be primarily through its interaction with other RBPs e.g. IMP1, HuD, TDP-43, FUS and FMRP (Fallini et al., 2012, Khalil et al., 2018, Ottesen et al., 2018). This suggested that the role of SMN was to bring together necessary components to form RNA transport granules. However, recent evidence suggests that SMN may interact with RNAs directly via lysine-rich motifs (Ottesen et al., 2018). A loss of SMN leads to a decrease in axonally localised poly(A)-mRNAs, consistent with a defect in RNA transport (Fallini et al., 2011, Fallini et al., 2012). This is also the mechanism proposed to underlie functional defects in SMA (Khalil et al., 2018).

6.1.4 MOV10

MOV10 is a RISC-associated and neurite-enriched RBP that has been suggested to be involved in the local control of protein translation (Zappulo et al., 2017). The *Drosophila* orthologue of MOV10 is known to aid RISC complex assembly and mRNA transport, and in mammalian systems MOV10 has been shown to interact with Ago proteins to participate in microRNA mediated translational repression (Tomari et al., 2004, Meister et al., 2005, Ashraf et al., 2006). MOV10 has also been implicated in synaptic plasticity and memory by regulating the translation of mRNAs whose products modulate synaptic facilitation (including CAMKII) in an signal-dependent manner; with neuronal activity causing MOV10 degradation and a reversal of microRNA mediated translational repression (Ashraf et al., 2006, Banerjee et al., 2009).

Characterisation of the sucrose gradient and exploration of the localisation of RBPs was designed to produce further insight into the protein complexes with which miR135b-mRNA and miR137-mRNA pairs might interact.

6.2 Characterisation of general translation-related and control protein distributions in neuronal sucrose gradient subfractions

In the gradients used here, monosomal fractions are expected to comprise those containing 0% – 20% sucrose, polysomal fractions 20% – 40% sucrose, and dense RNA granule containing fractions 40% – 50% sucrose. Based on previous experiments by Krichevsky and Kosik (2001), it was expected that members of the eIF4F translation initiation complex would be present in monosomal and polysomal fractions, but largely absent from denser fractions. Similarly, this group showed PABP in fractions associated with single ribosomes and polysomes but not enriched within denser fractions, consistent with its known involvement in translation initiation (Krichevsky and Kosik, 2001). L10 would be expected to be predominantly associated with monosomal and polysomal fractions undergoing active translation. However, Krichevsky and Kosik (2001) did identify RPS6, another ribosomal protein, within denser fractions, and therefore we queried whether L10 might behave similarly.

6.2.1 Sucrose gradient distributions of eIF4A1, eIF4A2, PABP, L10 and SOD2

eIF4A1 and eIF4A2 show similar distributions across the sucrose gradient, being enriched in lighter fractions and less so in polysomal and more dense fractions (**Figure 6.1A and 6.1B**). This is consistent with the presence of eIF4A1 and eIF4A2 in fractions which contain monosomes – where translation is initiated, as opposed to polysomal fractions which are actively translating. Though present, neither of these proteins is enriched within the denser fractions that contain microRNA-mRNA pairs. However, eIF4A1 shows a small peak between 30 – 50% sucrose, whereas eIF4A2 is more uniformly distributed in these denser fractions. Though eIF4A1 shows a second peak in denser fractions, where microRNA-mRNA pairs co-exist, its apparent relative protein abundance is still lower. Consistent with the literature, my experiments indicate that eIF4A2 is more abundant than eIF4A1 in cortical neurons (**Figure 6.1A and 6.1B**) (Galicia-Vázquez et al., 2012).

PABP levels were low in 0% – 20% sucrose fractions, which is somewhat surprising given its known role in translation initiation (**Figure 6.1C**) (Kahvejian et al., 2001). Its localisation was consistently observed in 25 – 50% sucrose fractions, in agreement with its localisation in both polysomal fractions and fractions containing RNA granules (**Figure 6.1C**). This is consistent with roles for PABP in maintaining mRNA stability throughout the mRNA lifecycle, i.e. in mRNA transport as well as regulating mRNA translation.

L10 ribosomal protein showed a similar distribution to PABP – very low in monosomal fractions of 0 – 15% sucrose, and higher at 20 – 50% sucrose (**Figure 6.1D**). Its presence in polysomal fractions where active translation is ongoing is expected, whereas its abundance within the densest sucrose fractions, where RNA granules reside, is more surprising.

Finally, SOD2, a mitochondrial protein was used to further verify the expected distribution of cellular components through the gradient. Consistent with the relative density of mitochondria, this protein was detected in 0 – 20% sucrose fractions (**Figure 6.1E**). Furthermore, SOD2 was absent from polysomal and dense neuronal fractions, consistent with previous findings of Krichevsky and Kosik (2001).

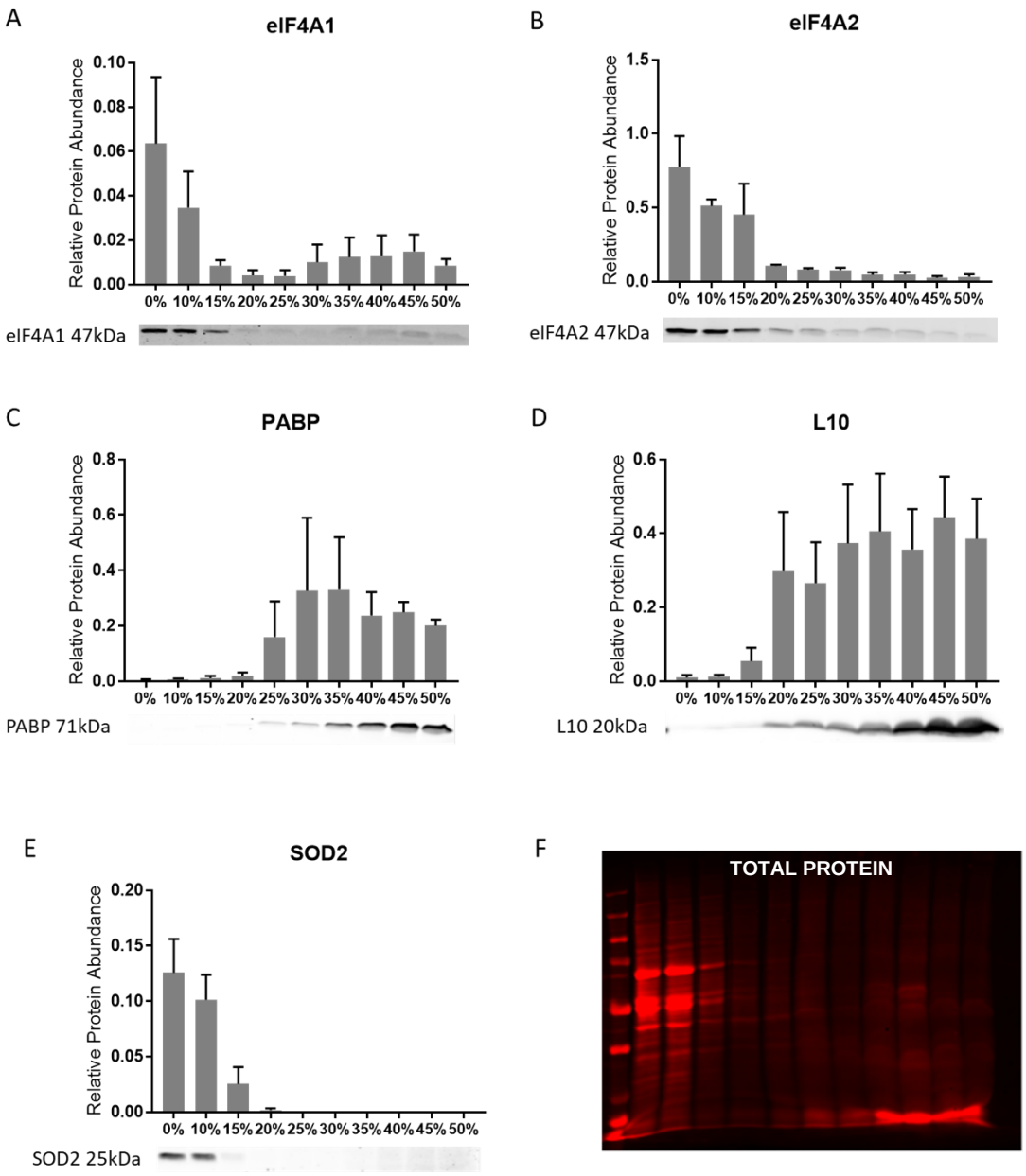

Figure 6.1: Distribution profiles of eIF4A1, eIF4A2, PABP, L10, SOD2 and total protein to characterise sucrose gradient mediated neuronal cell fractionation. Cortical neuronal cell cultures were translationally arrested by 100 µg/ml cycloheximide at DIV28, then harvested. Neuronal lysate was fractionated by sucrose density mediated fractionation, protein was extracted from each fraction and subject to western blot (**Materials and Methods**). Total protein per fraction was quantified using REVERT Total Protein stain after transfer. The blots were incubated with antibodies against **A** eIF4A1, **B** eIF4A2, **C** PABP, **D** L10 or **E** SOD2. After incubation with the appropriate IRDye conjugated secondary antibody the immunoblot was scanned at multiple intensities with the LI-COR Odyssey Infrared Imager. The signal per band was analysed in Image Studio Lite and quantified as a ratio to REVERT Total Protein Stain (**F** representative REVERT total protein stain). Plotted are the average relative protein abundances from 4 protein gradients. Graphs show mean ± SEM.

Whilst assessing the overall protein abundance using REVERT staining of freshly transferred membranes, it was evident that most proteins were present in the lower sucrose density fractions (**Figure 6.1F**). Therefore, the enrichment of our proteins of interest within denser fractions is clearly distinct and specific.

6.3 Are RBPs with known roles in neuronal RNA transport and/or translational regulation within similar sucrose gradient fractions as miR135b or miR137 and their mRNA targets?

6.3.1 IMP1

IMP1 localisation within the sucrose gradient has two peaks within dense and light fractions. This localisation is consistent with its proposed dual functions in regulating

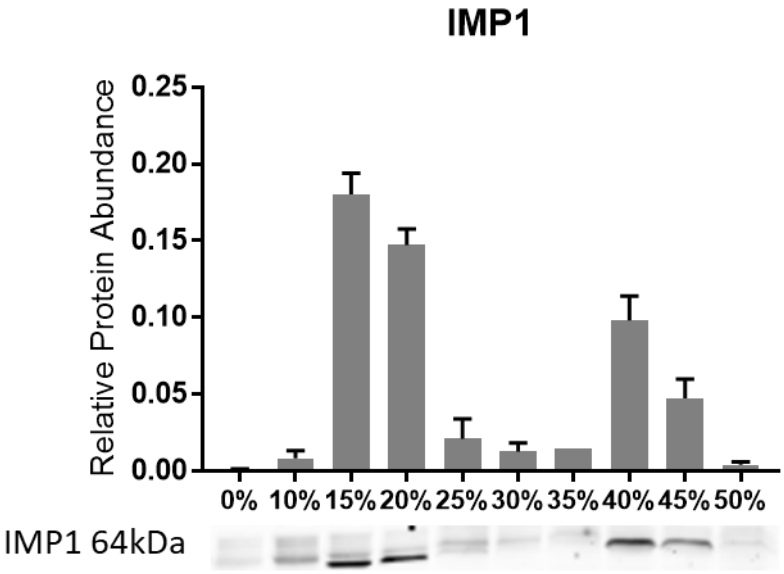

Figure 6.2: IMP1 is localised throughout the gradient in translating and dense fractions after sucrose density gradient mediated fractionation. Cortical neuronal cell cultures were translationally arrested by 100 µg/ml cycloheximide at DIV28, then harvested. Neuronal lysate was fractionated by sucrose density mediated fractionation, protein was extracted from each fraction and subject to western blot. Total protein per fraction was quantified using REVERT Total Protein stain after transfer. The blot was incubated with anti-IMP1 (1:1000). After incubation with IRDye conjugated secondary antibody the immunoblot was scanned at multiple intensities with the LI-COR Odyssey Infrared Imager. The signal per band was analysed in Image Studio Lite and quantified as a ratio to REVERT Total Protein Stain. IMP1 localisation in the gradient shows two peaks in lighter and dense fractions consistent with its role in translational repression and RNA transport. Data are pooled from 2 protein gradients. Graphs show mean ± SEM.

RNA transport and mRNA translation, respectively (**Figure 6.2**) (Zhang et al., 2001, Hüttelmaier et al., 2005). Both miR135b and miR137 demonstrated increased localisation to 40 – 45% sucrose fractions after overexpression; this compartmentalisation overlaps with the second peak of IMP1 enrichment (**Figure 4.2 and 4.4**). Furthermore, these are the same fractions in which the majority of miR135b and miR137 target mRNAs are distributed. These findings could be considered preliminary evidence for the cooperation of these microRNAs with IMP1 in regulating mRNA transport and signal-dependent translation.

6.3.2 FMRP

FMRP was detected in all cellular fractions. It is present in the densest sucrose fractions which would be consistent with a role in RNA granules, but it is not enriched there. The

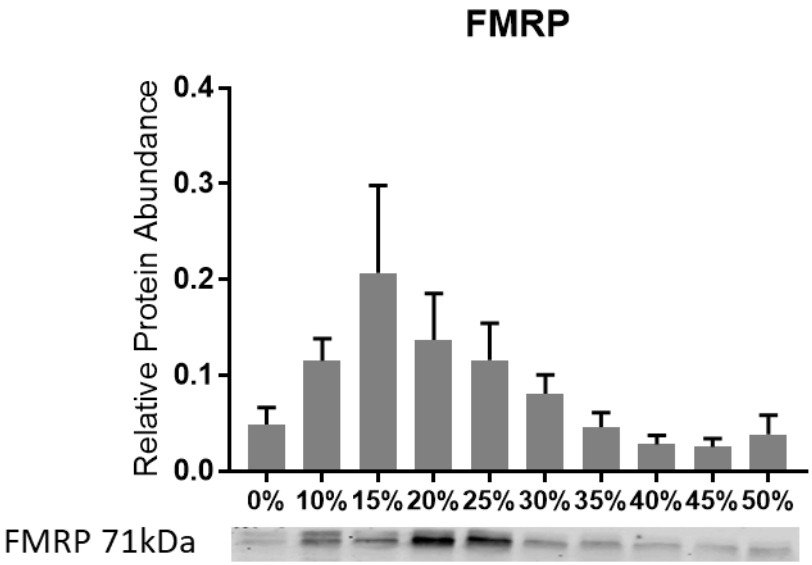

Figure 6.3: FMRP is localised throughout the gradient in translating and dense fractions after sucrose density gradient mediated fractionation. Cortical neuronal cell cultures were translationally arrested by 100 µg/ml cycloheximide at DIV28, then harvested. Neuronal lysate was fractionated by sucrose density mediated fractionation, protein was extracted from each fraction and subject to western blot. Total protein per fraction was quantified using REVERT Total Protein stain after transfer. The blot was incubated with anti-FMRP (1:25000). After incubation with IRDye conjugated secondary antibody the immunoblot was scanned at multiple intensities with the LI-COR Odyssey Infrared Imager. The signal per band was analysed in Image Studio Lite and quantified as a ratio to REVERT Total Protein Stain. FMRP is localised throughout the gradient, predominantly in translating fractions consistent with a role in translational repression. Data are pooled from 4 protein gradients. Graphs show mean ± SEM.

highest levels of FMRP being observed in less dense fractions can be attributed to its important role in translational repression by stalling elongation (**Figure 6.3**) (Darnell and Klann, 2013). Interestingly, miR137 also shows an endogenous peak of distribution in the 15% sucrose fraction, which overlaps with the peak of FMRP levels (**Figure 4.4 and 6.3**). It was somewhat surprising to note that IMP1 and FMRP had such distinct biochemical distributions, given that their reported functions are similar.

6.3.3 SMN

SMN is known to bind to mRNAs both directly and indirectly to fulfil roles in regulating RNA transport and translation (Ottesen et al., 2018). I observed SMN to be most highly enriched within actively translating sucrose density fractions (20% and 25%) (Costa and Willis, 2017, Khalil et al., 2018, Wang et al., 2018). SMN is not enriched in fractions where miR135b and miR137 are most abundant, nor is SMN enriched in the densest cellular

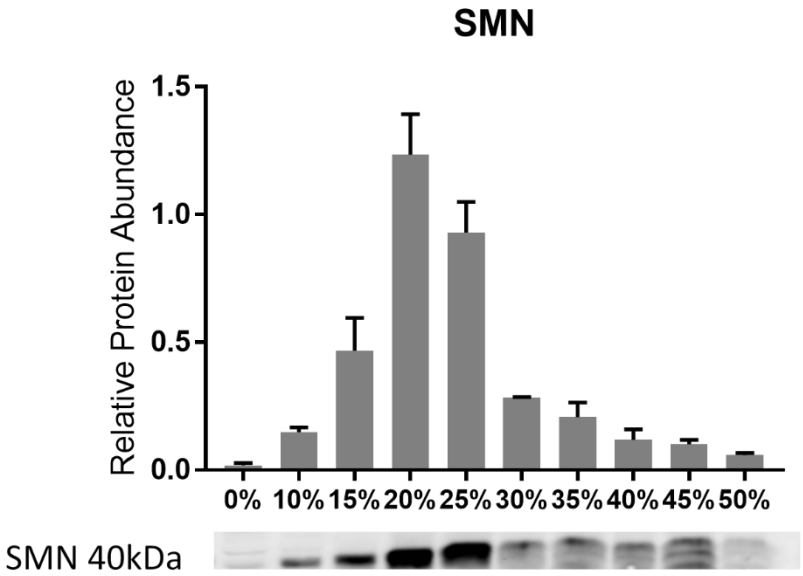

Figure 6.4: SMN protein is enriched within translating fractions and present in dense fractions within the fractions after sucrose density gradient mediated fractionation. Cortical neuronal cell cultures were translationally arrested by 100 µg/ml cycloheximide at DIV28, then harvested. Neuronal lysate was fractionated by sucrose density mediated fractionation, protein was extracted from each fraction and subject to western blot. Total protein per fraction was quantified using REVERT Total Protein stain after transfer. The blot was incubated with anti-SMN (1:5000). After incubation with IRDye conjugated secondary antibody the immunoblot was scanned at multiple intensities with the LI-COR Odyssey Infrared Imager. The signal per band was analysed in Image Studio Lite and quantified as a ratio to REVERT Total Protein Stain. SMN is predominantly localised in actively translating fractions. Data are pooled from 2 protein gradients. Graphs show mean ± SEM.

fractions (**Figure 6.4**). However, despite a lack of enrichment in denser fractions, SMN is present throughout the gradient.

6.3.4 MOV10

In my experiments, MOV10 was clearly enriched in the denser fractions of the gradient (**Figure 6.5**); this was our expected result, given its previously characterised role as a neurite enriched RBP thus a potential component of mRNA- and microRNA-containing granules regulating RNA transport and translation. The distribution of MOV10 overlaps considerably with the distributions of miR135b and miR137 (**Figure 4.2, 4.4 and 6.5**). This is a particularly exciting result, because it supports our hypothesis that MOV10 may work in conjunction with miR135b and miR137 to regulate the expression of their target mRNAs, both within RNA granules and at the synapse (Banerjee et al., 2009).

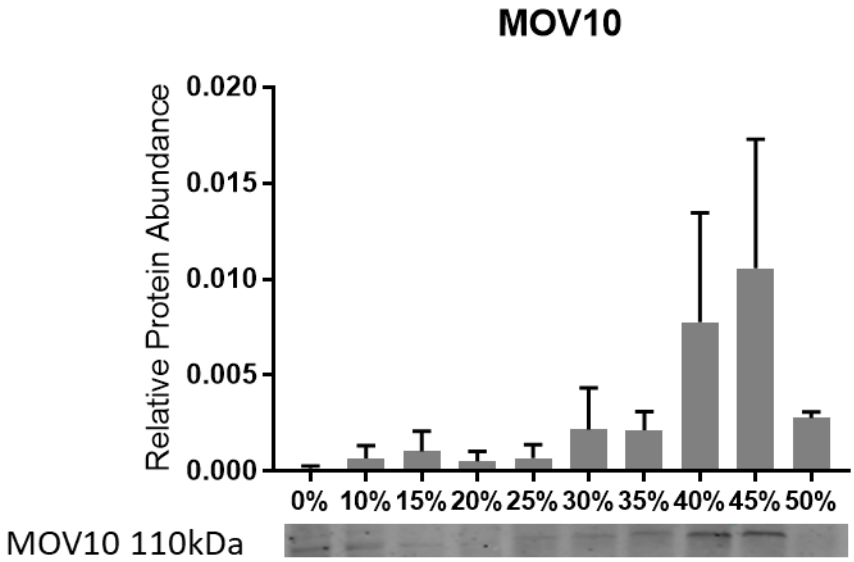

Figure 6.5: MOV10 protein is enriched within dense fractions after sucrose density gradient mediated fractionation. Cortical neuronal cell cultures were translationally arrested by 100 µg/ml cycloheximide at DIV28, then harvested. Neuronal lysate was fractionated by sucrose density mediated fractionation, protein was extracted from each fraction and subject to western blot. Total protein per fraction was quantified using REVERT Total Protein stain after transfer. The blot was incubated with anti-MOV10 (1:800). After incubation with IRDye conjugated secondary antibody the immunoblot was scanned at multiple intensities with the LI-COR Odyssey Infrared Imager. The signal per band was analysed in Image Studio Lite and quantified as a ratio to REVERT Total Protein Stain. MOV10 is enriched within denser fractions of the sucrose gradient overlapping with miR135b and miR137 localisation following their overexpression. Data are pooled from 3 protein gradients. Graphs show mean ± SEM.

6.4 Discussion

6.4.1 Distribution of components of the basal translational machinery compared to miR135b and miR137

Translation initiation factors eIF4A1 and eIF4A2 were mainly present within less dense fractions of the sucrose gradient consistent with their localisation in monosomal fractions where they would facilitate translation initiation (**Figure 6.1A and 6.1B**). Both of these helicases are expressed in the brain, but eIF4A2 is more abundant than eIF4A1 in human brain tissues (Galicia-Vázquez et al., 2012). The RBP HuD is shown to increase the levels of both eIF4A1 and eIF4A2 to promote protein synthesis to govern neuronal cell fate and plasticity in motor neurons (Tebaldi et al., 2018). Therefore, the regulation of these proteins has been previously connected to neuron-specific activities.

eIF4A2 is also known to have roles in microRNA mediated gene regulation. Meijer et al., (2013) established that RISC-associated eIF4A2 was responsible for translational silencing through its preferential association with the MIF4G domain of the CCR4-NOT deadenylation complex. This study provides evidence for microRNA mediated translation inhibition via inhibition of helicase activity during translation initiation. This was a conceptual advance in understanding microRNA mediated mRNA regulation by demonstrating that translational repression could be controlled independently of mRNA degradation.

Given the previously described roles of eIF4A2 protein in translational repression, we had postulated that it might have a role in preventing ectopic protein expression during microRNA-dependent mRNA transport. Moreover, this could have predicted it to differ in its expression profile compared to eIF4A1. The evidence that I obtained does not definitively clarify this issue, however. Both proteins were present but not abundant in denser fractions containing RNA granules in comparison to fractions undergoing translation initiation (**Figure 6.1A and 6.1B**). Moreover, whilst we hypothesised that eIF4A2, which is neuron-enriched, might selectively fulfil this function, its abundance

decreased in the denser fractions of the gradient (**Figure 6.1B**). In contrast, eIF4A1 does show a second, wider peak between 30 – 50% sucrose (**Figure 6.1A**). However, eIF4A2 was more abundant than eIF4A1 overall, and hence, whilst eIF4A2 is not enriched in denser fractions it appears to be more abundant in these fractions than eIF4A1. These results might suggest the eIF4A2 preferentially co-distributes with the microRNAs of interest and their targets localised between 40 – 45% sucrose, compared to eIF4A1 (**Figure 6.1A and 6.1B**). However, my experiments were conducted primarily to qualitatively validate the localisation of proteins of interest within the sucrose gradient. Further experiments will therefore be required to more specifically evaluate a differential eIF4A1 and eIF4A2 function in this context.

PABP exhibited a pattern of localisation almost reciprocal to that of eIF4A1 and eIF4A2. Whilst PABP was largely absent from lighter fractions, it was enriched within both actively translating and dense fractions (**Figure 6.1C**). This was surprising to us, given its well-established role in preparing mRNAs for translation initiation. PABP is present in the gradient within fractions where miR135b, miR137 and their targets were also present – this potential co-distribution is in line with a possible role for PABP in facilitating interactions between a microRNA-loaded RISC complex and its target mRNAs (Moretti et al., 2012). This would be consistent with previous data showing that the extent of microRNA repression is proportional to poly(A) tail length (Moretti et al., 2012). Therefore, we suggest a paradigm whereby PABP might recruit the microRNA-loaded RISC complex and remain associated to the poly(A) tail to confer mRNA stability during transport, protecting the target from deadenylation. Also, if microRNAs are involved in neuronal mRNA transport, their mRNA targets would likely need to be translated readily when they reach their destination, in which PABP would be required.

Likewise, L10 ribosomal protein was present within both translating and dense fractions (**Figure 6.1D**). Its abundance within polysomal fractions is expected given its role in active mRNA translation. The presence of L10 in dense fractions, however, was unexpected (**Figure 6.1D**). We therefore considered previous literature to explain this result. Krichevsky and Kosik (2001) also found that the ribosomal protein RPS6 was present in denser sucrose gradient fractions. Moreover, they suggested that RNA granules resembled ribosomal clusters (Krichevsky and Kosik, 2001). Furthermore, other

groups characterising components of RNA transport granules have also shown them to contain ribosomal proteins (Elvira et al., 2006). Taken together with these previous studies and with my finding that PABP was also localised to dense fractions, the enrichment of ribosomal components within denser fractions of the gradient is consistent with support of local protein synthesis by translation of transported mRNAs in neurites or synapses (Biever et al., 2020).

6.4.2 Distribution of specialised neuronal RBPs compared to miR135b and miR137

We investigated the localisation of specialised RBPs known to have an involvement in regulating mRNA transport and translation in neurons. This was in order to gain insight as to whether they might demonstrate a distribution consistent with cooperative roles with miR135b or miR137. IMP1 demonstrated a clear localisation within fractions 40 – 45% of the sucrose gradient like miR137 and miR135b and their targets. In contrast, FMRP was not enriched in the densest fractions of the gradient where the microRNA-mRNA pairs were co-distributed. FMRP has been shown to act in conjunction with other proteins investigated here, including IMP1, SMN and MOV10 (Rackham and Brown, 2004, Piazzon et al., 2008, Kenny et al., 2014). However, these proteins show differing profiles of distribution within the gradients. FMRP showed a distribution most similar to that of SMN.

SMN was observed to be most enriched within translating sucrose density fractions, but less enriched in fractions associated with miR135b- and miR137- mRNA pairs and the denser fractions associated with RNA granules (Krichevsky and Kosik, 2001). Given that SMN is most associated with RNA transport (rather than the regulation of translation), this result was somewhat surprising to us. Nonetheless, SMN was present in nearly all cellular fractions, including dense fractions. Therefore, despite it demonstrating a qualitatively different distribution profile, SMN is co-distributed in dense fractions alongside miR135b and miR137 (**Figure 4.2, 4.4 and 6.4**). This was of interest to us, given that many mRNA targets of microRNAs 135b and 137 are presynaptic, therefore are interesting candidates for SMN-dependent axonal transport. A dysfunction in SMN as seen in SMA has a detrimental effect on the localisation of axonal mRNAs; SMA leads to alterations in synaptic proteins, including the developmental downregulation of the

presynaptic miR137 target, Syt1, in the neuromuscular junctions of the most vulnerable muscles (Tejero et al., 2016). SMN is also known to interact with both IMP1 and FMRP, which might suggest the formation of a multi-protein complex to regulate mRNA transport (Piazzon et al., 2008, Fallini et al., 2014).

MOV10 was primarily present in the denser fractions of the gradient at 40% – 45% sucrose, co-distributing in the same fractions as to both miR135b and miR137. MOV10 has an established role in RISC complex assembly and reversible microRNA mediated translational repression at synapses (Tomari et al., 2004, Meister et al., 2005, Banerjee et al., 2009). This makes MOV10 an interesting candidate to explore in the context of miR135b- and miR137-dependent functions (Zappulo et al., 2017).

Taken together, these results show the characterisation of the sucrose gradient alongside the distribution of proteins with known and key involvements in RNA transport. The RBPs described are differentially localised in fractions where our microRNAs of interest and their targets are enriched.

6.4.2.1 Possible interpretations for differential protein distributions following sucrose gradient fractionation

The heterogeneous localisations of RBPs within the sucrose gradient may be relevant to their differential functions in regulating various functional aspects of mRNA transport and translation outside the cell soma.

Firstly, the mRNA must be translationally repressed prior to its transport from the cell body. mRNAs must be then be sorted into distinct populations of RNA granules to direct their transport to the appropriate sub-cellular domains i.e. the postsynapse versus the presynapse, with distinct sets of RBPs being expected to regulate this segregation (Tubing et al., 2010). The RBPs investigated here, including FMRP and IMP1 are known to interact with molecular motors which couple translational repression to RNA granule transport (Davidovic et al., 2007, Doyle and Kiebler, 2011, Song et al., 2015). The mRNA contained in granules must also be maintained in a translationally repressed state during transport. Finally, the appropriate proteins must be present to reverse translational repression and permit protein synthesis after the RNA granule arrives at its destination.

Moreover, translational repression might be reversed constitutively or in a signal-dependent manner.

The distributions of PABP and L10 in dense fractions may indicate their co-packaging into RNA granules to participate in reversing microRNA mediated inhibition of translation. Likewise, IMP1 and MOV10 show substantial localisation in fractions consistent with RNA transport or sequestration granules. IMP1 also shows a substantial localisation in lower density ribosome containing fractions; this could either represent inhibition of translational initiation or potentially monosomal translation (Biever et al., 2020).

Interestingly, a high enrichment is also seen for FMRP in less dense fractions, including monosomal fractions, thereby overlapping in its expression with IMP1 and SMN (**Figure 6.2, 6.3 and 6.4**). FMRP dysfunction in FXS might lead to a dysregulation in the repression and localisation of its mRNA targets, with downstream effects on neuronal connectivity (Mazroui et al., 2002, Sudhakaran et al., 2014).

Interestingly, FMRP and MOV10 have a known cooperative relationship in microRNA mediated translational repression; FMRP recruits MOV10 to mRNA targets, where MOV10 then proceeds to unwind the mRNA's secondary structure to expose microRNA recognition elements to Ago2 binding (Kenny et al., 2014). However, FMRP binding to an RNA close to the MOV10 binding site hinders the helicase activity of MOV10 therefore eliminating microRNA mediated translational repression (Kenny et al., 2014). FMRP is usually regarded as a translational repressor of transcripts, but this model proposes that under certain molecular conditions it may promote translation. Though they are enriched in different fractions, there is overlap of these two RBPs throughout the sucrose gradient (**Figure 6.3 and 6.5**).

Perhaps the most surprising compartmentalisation of all is the enrichment of SMN in polysomal fractions. One possibility is that this localisation represents a qualitatively different functional role to that of the other RBPs studied.

6.4.3 Development of a working model for the activities of miR135b and miR137 based on density gradient profile results

We propose that microRNAs 135b and 137 co-exist with and regulate the transport and localised translation of their mRNA targets, in conjunction with specific RBPs (**Figure 6.6**). The coordinated localisation of mRNAs, based on their structures and sequence characteristics, and RBPs, based on their own targeting sequences and macromolecular interactions are presumed to be crucial to the proper targeting of microRNA-mRNA pairs to RNA granules. Furthermore, this may couple together the necessary effectors to regulate the transport of RNA granules to specific cellular sub-compartments and eventually the reversal of microRNA mediated repression of mRNA targets to allow their translation. RNA transport will allow the creation of a local transcriptome. We can further assess the functional participation of specific RBPs in microRNA mediated target regulation by miR135b and miR137 by utilising microscopic imaging and biochemical techniques. It will be crucial to determine which microRNAs, target mRNAs and RBPs interact with each other to elucidate the mechanisms underlying this complex neuronal subcellular expression process.

7 Chapter 7: Cytological and biochemical evidence for roles of miR135b and miR137 in mRNA transport

7.1 Introduction

mRNA is transcribed from DNA by RNA polymerase II; the resultant pre-mRNA is capped at the 5' end, the exons are spliced and the 3' end is polyadenylated to form the mature mRNA (Fong and Bentley, 2001). The mature mRNA is exported to the cytoplasm from the nucleus, where it is either translated, degraded or translationally repressed to be transported (Martin and Ephrussi, 2009, Doyle and Kiebler, 2011).

mRNA transport to sites distant from the cell body is crucial in neurons to maintain their polarity and regulate synaptic plasticity. During transport, mRNAs are sequestered away from translating ribosomes, sorted into RNA granules which associate with motor proteins and are transported to their correct destinations (Krichevsky and Kosik, 2001, Kanai et al., 2004, Elvira et al., 2006, Kiebler and Bassell, 2006). Once mRNAs reach their destination, the translational repression can be reversed in a signal-dependent manner; in neurons this can regulate synaptic plasticity and neuronal connectivity.

Given that microRNAs 135b and 137 participate in non-degrading microRNA-target interactions and co-exist with their respective targets in neurons, we hypothesised that these microRNAs might play a role in maintaining translational repression of mRNAs during their transport. Moreover, mRNA targets of miR135b and miR137 have defined synaptic roles, which suggests that they might be involved in both axonal and dendritic transport.

In the previous chapter I demonstrated that specific RBPs, including SMN and MOV10, were detected in dense cellular fractions of cortical neurons, consistent with their localisation in RNA granules. Furthermore, this localisation within sucrose density gradients overlapped with the microRNAs themselves. There are heterogeneous populations of RNA transport granules; two of such subpopulations are distinguished as Stau2 positive or Btz positive (Fritzsche et al., 2013). MOV10, however, associates with both types of granules, suggesting its function might be crucial in RNA transport granule function in general (Fritzsche et al., 2013).

MOV10 is a neurite-enriched RNA helicase that mediates translational repression and can control the local translation of mRNAs in a microRNA-RISC associated manner (Banerjee et al., 2009, Zappulo et al., 2017). It is highly expressed in the brain during development (E18 to P14), but demonstrates a more restricted pattern of brain expression in adulthood (Skariah et al., 2017). Sequencing of MOV10-associated mRNAs showed functional clusters with terms including axonal guidance and neuronal projections (Skariah et al., 2017). Moreover the *Drosophila* orthologue of MOV10, Armitage, has been shown to regulate the translation of kinesin heavy chain and CAMKII mRNAs, while also supporting transport of the latter (Ashraf et al., 2006).

SMN has a known role in both assembly and transport of axonal RNA granules, along with regulating local translation in axonal terminals. SMN interacts with RNAs both directly and indirectly via other RBPs (Li et al., 2014a, Ottesen et al., 2018). There are a range of axonally localised RNAs which are proposed to interact directly with SMN within transport granules (Rage et al., 2013). Reduced SMN due to mutations or deletions in the *SMN1* gene are seen in SMA, where *SMN2,* a truncated version of the protein, cannot fully compensate for the loss. In this neurodegenerative condition, there are defects at the neuromuscular junction which cause skeletal muscle denervation, ostensibly due to defective RNA transport (Martinez-Hernandez et al., 2013).

Taken together, MOV10 is a key component of RNA granules which has the capacity to regulate local translation in a microRNA-dependent manner, and SMN is a key protein that may bring together the necessary components for axonal RNA transport. Furthermore, these two proteins share binding interactions with the same proteins i.e. FMRP, and thus both proteins might be operating together in the context of miR135b and miR137 target mRNA regulation (Piazzon et al., 2008, Kute et al., 2019).

Double-label fluorescence in-situ hybridisation combined with immunocytochemistry (FISH/ICC) was employed to assess the colocalisation of microRNA-mRNA pairs and MOV10 or SMN. FISH has previously been employed by other groups to visualise RNA localisation within RNA granules (Repici et al., 2019). In addition, immunoprecipitation (IP) was employed to determine whether miR135b or miR137 and their mRNA targets associated with either MOV10 or SMN biochemically.

7.2 Visualisation of RNA binding proteins within cortical neurites

7.2.1 Validating conditions for low density neuronal cultures

Previous experiments had shown that the cellular immunolabeling profiles for RBPs MOV10, SMN, IMP1 and FMRP overlapped with Tau, a marker of neuronal processes (data not presented). However, the high density of neurons in these cultures (seeded on coverslips at a density of $3x10^5$ cells/ml) made it difficult to discern individual neurites. I therefore sought to establish a protocol to create cultures with a lower neuronal density.

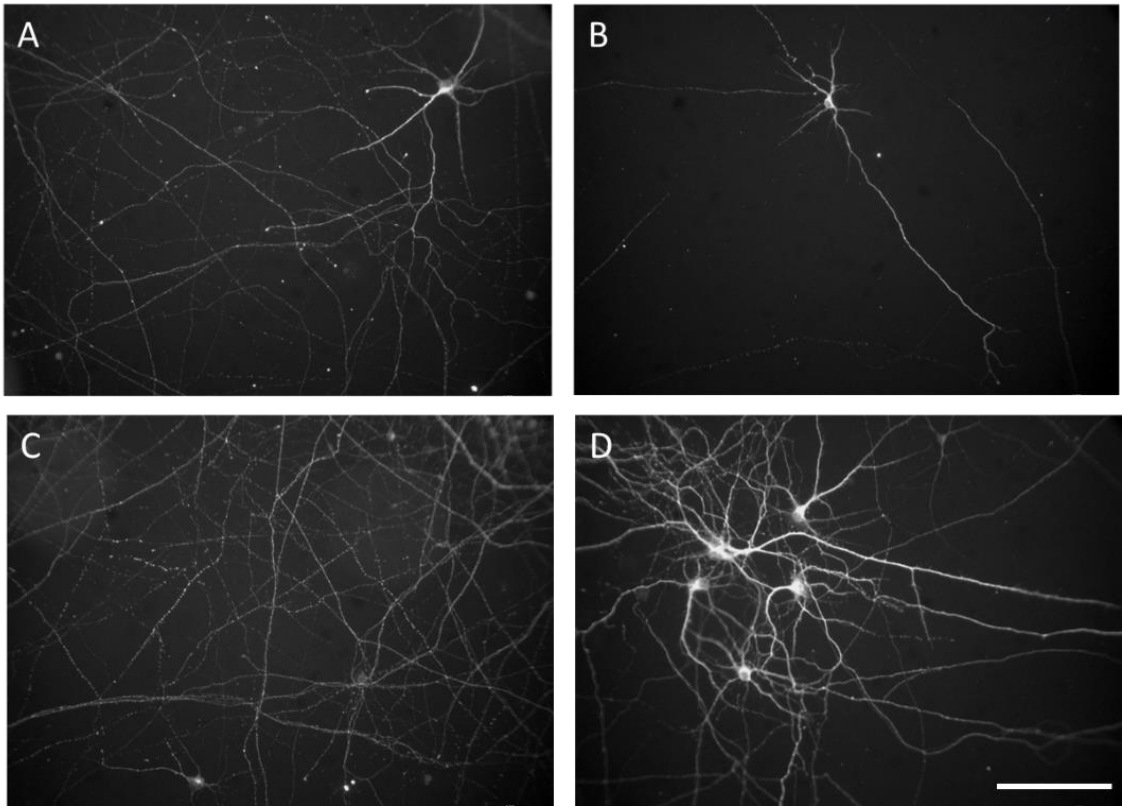

Figure 7.1: Low-density neuronal cultures allow for better visualisation of neuronal processes. Cortical neurons were cultured at a density of $1x10^4$ cells/ml in supplemented Neurobasal Media with additional 10% heat-inactivated horse serum for 7 days. At DIV14, neurons were fixed in 4% PFA/PBS for 5 minutes at room temperature, then blocked and permeabilised in 4% Goat Serum and 0.3% Triton X-100 in PBS for 60 minutes. Followed by overnight incubation at 4°C in blocking solution with Mouse anti-Tau antibody (1:500) with constant rocking. Coverslips were washed 3 times with PBS then incubated for 90 minutes at room temperature with appropriate secondary antibodies (Goat anti-Mouse AlexaFluor 488, 1:1000), washed again and mounted on slides with Fluoromount-G + DAPI. Neuronal processes are clearly discernible within low-density cultures. Images were taken at 20x on Nikon EFD-3 with CoolLED pE-300 LED illumination. Scale bar 100 µm.

Low density neuronal cultures can be difficult to maintain due to lack of trophic support (Lu et al., 2016). My aim was to reduce the cell density by 30-fold, to $1x10^4$ cells/ml. To promote the survival of neurons at a low-density, the cells were cultured with additional serum supplementation to provide short-term trophic support, and to allow glial cells to grow in parallel to provide further trophic support (Pyka et al., 2011). This method of neuronal culture allowed for the survival of low-density cultures and a better visualisation of individual neuronal processes (**Figure 7.1**).

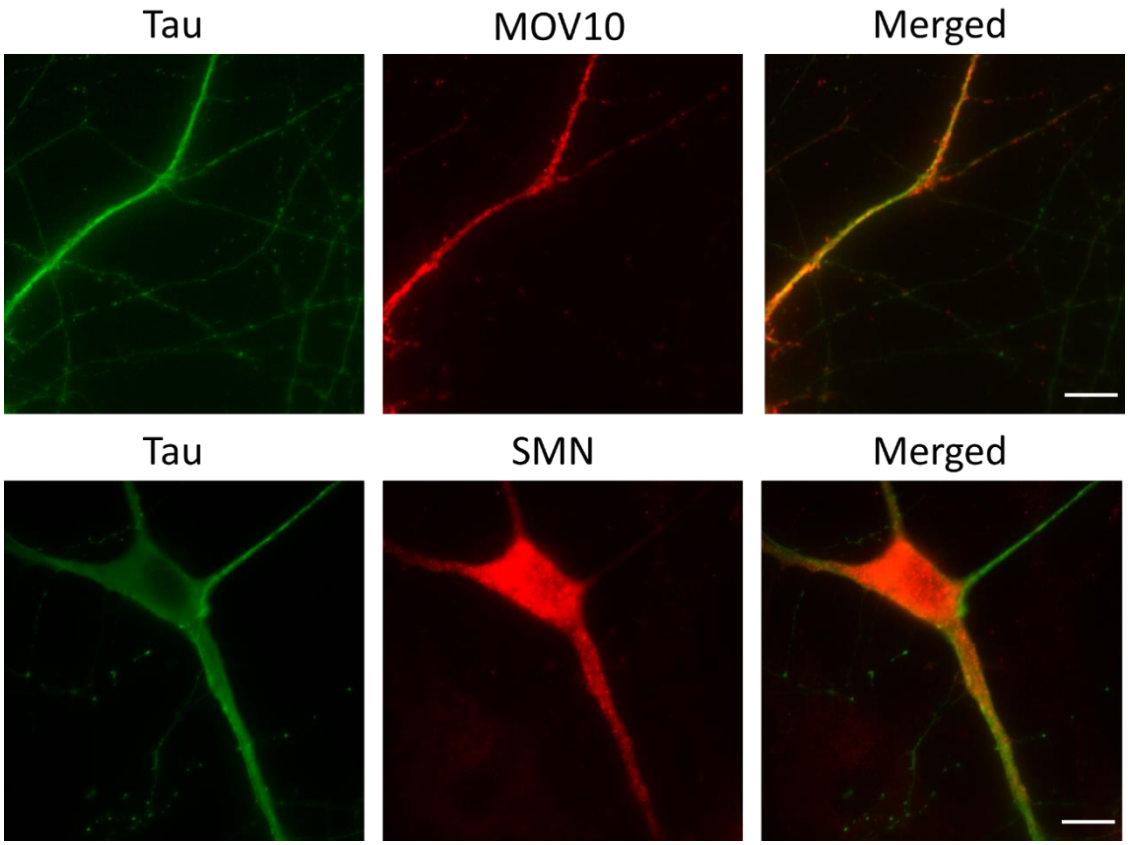

Figure 7.2: MOV10 and SMN are present in neuronal processes, shown by their overlap with Tau. Fixed, blocked and permeabilised low-density neuronal cultures were incubated at 4°C in blocking solution with 1:500 Rabbit anti-MOV10 and 1:500 Mouse anti-Tau or 1:250 Mouse anti-SMN and 1:500 Rabbit anti-Tau overnight. Coverslips were washed 3 times with PBS then incubated for 90 minutes at room temperature with appropriate secondary antibodies (Goat anti-Mouse AlexaFluor 488, Goat anti-Rabbit AlexaFluor 488, Goat anti-Mouse AlexaFluor 647 or Goat anti-Rabbit AlexaFluor 647) and washed again. Coverslips were mounted with Fluoromount-G. Both MOV10 and SMN are present in Tau positive neuronal processes. Images were taken at 100x on Nikon Eclipse Ti, scale bar = 10 µm.

I examined whether MOV10 and SMN were present in neuronal processes as defined by colocalisation with Tau positivity, as would be expected if they were directing the transport of mRNAs which encode for proteins that function remote from the cell body. **Figure 7.2** shows that both MOV10 and SMN immunostainings overlap with Tau within neuronal cell bodies and neuronal processes in low-density cultures. Interestingly, there are Tau positive processes in which MOV10 staining is absent. This would suggest that MOV10 only regulates transport in certain cortical neuronal processes. Nevertheless, the overlap between Tau and these proteins serves as a proxy to examine the potential co-localisation of microRNAs 135b and 137 and their targets within RNA granules regulating mRNA transport to sites remote from the neuronal cell body.

7.2.2 FISH/ICC method used for visualisation and analysis of microRNA-mRNA-protein complexes

FISH/ICC was employed to identify and analyse the overlap between miR135b and miR137 and their target mRNAs (*Bsn*/*Vamp2* and *Syt1*, respectively) within neuronal processes of low-density neuronal cultures immunolabeled with either MOV10 or SMN. Any observed overlap between the microRNA, mRNA and protein might be indicative of them creating a biochemical complex together. This technique of visualisation also allows identification of where in the neurons these potential complexes are present e.g. proximal to the cell bodies and/or in the distal processes.

Using the ViewRNA Cell Plus Assay, immunocytochemistry was combined with bDNA signal amplification to simultaneously detect proteins and RNAs. bDNA signal amplification has a high signal to noise ratio and facilitate imaging of low-abundance molecules (Battich et al., 2013). The images obtained were analysed on a macro designed on ImageJ (**Materials and Methods** and **Appendix 1**).

7.3 Are miR135b, *Vamp2* mRNA and MOV10 colocalised within neuronal processes?

The localisation of miR135b and its mRNA target *Vamp2*, encoding an important presynaptic vesicle protein, was investigated in MOV10-immunopositive neurons. Qualitatively, MOV10 (purple) was visualised within the neuronal cell body and neuronal processes (**Figure 7.3**). Though MOV10 labelling is generally diffuse, the presence of

some brighter spots/puncta suggests its visualisation in RNA granules. *Vamp2* mRNA (green) puncta are frequent within the cell body but can be traced all the way through to distal neuronal processes, consistent with *Vamp2* mRNA transport (**Figure 7.3**). miR135b-labeled puncta (red) were less abundant than those labelled for *Vamp2*; they show a distribution within and proximal to neuronal cell bodies and a less frequent visualisation in neuronal processes. When qualitatively assessing the overlap of miR135b and *Vamp2* within MOV10 positive neurons, the signals do not colocalise exclusively; this could suggest that they a) undergo some independent transport and functions or b) the labelling process is inefficient (**Figure 7.3**).

Quantitative analysis was conducted on 40 images obtained from FISH/ICC experiments using the macro designed in FIJI (**Materials and Methods and Appendix 1**). Images were chosen based on the ability to identify neuronal structures i.e. cell bodies and extending processes. When interpreting these data, the potential error introduced due to inefficient labelling of microRNA and mRNA species during FISH had to be taken into consideration. This would consequently lead to an underestimate in the number of overlapping species as presented in **Figure 7.4** and **Tables 7.1 and 7.2**. Therefore, though my interpretations are valid according to visible, detectable puncta, the caveat remains that the mRNA and microRNA species might not all be labelled. Taking this into consideration, it was deemed inappropriate to draw statistical conclusions from the quantitative data obtained.

A

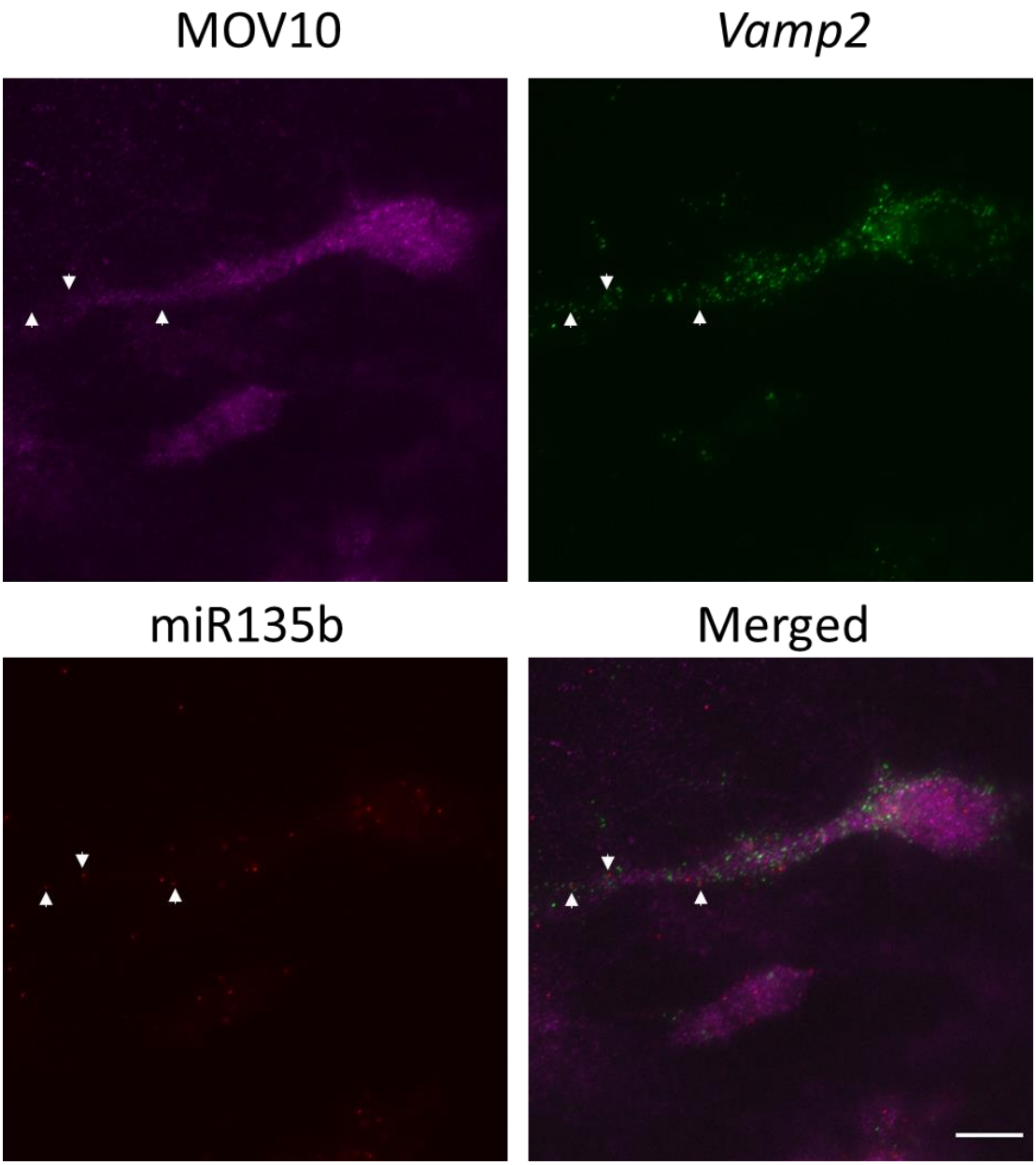

B

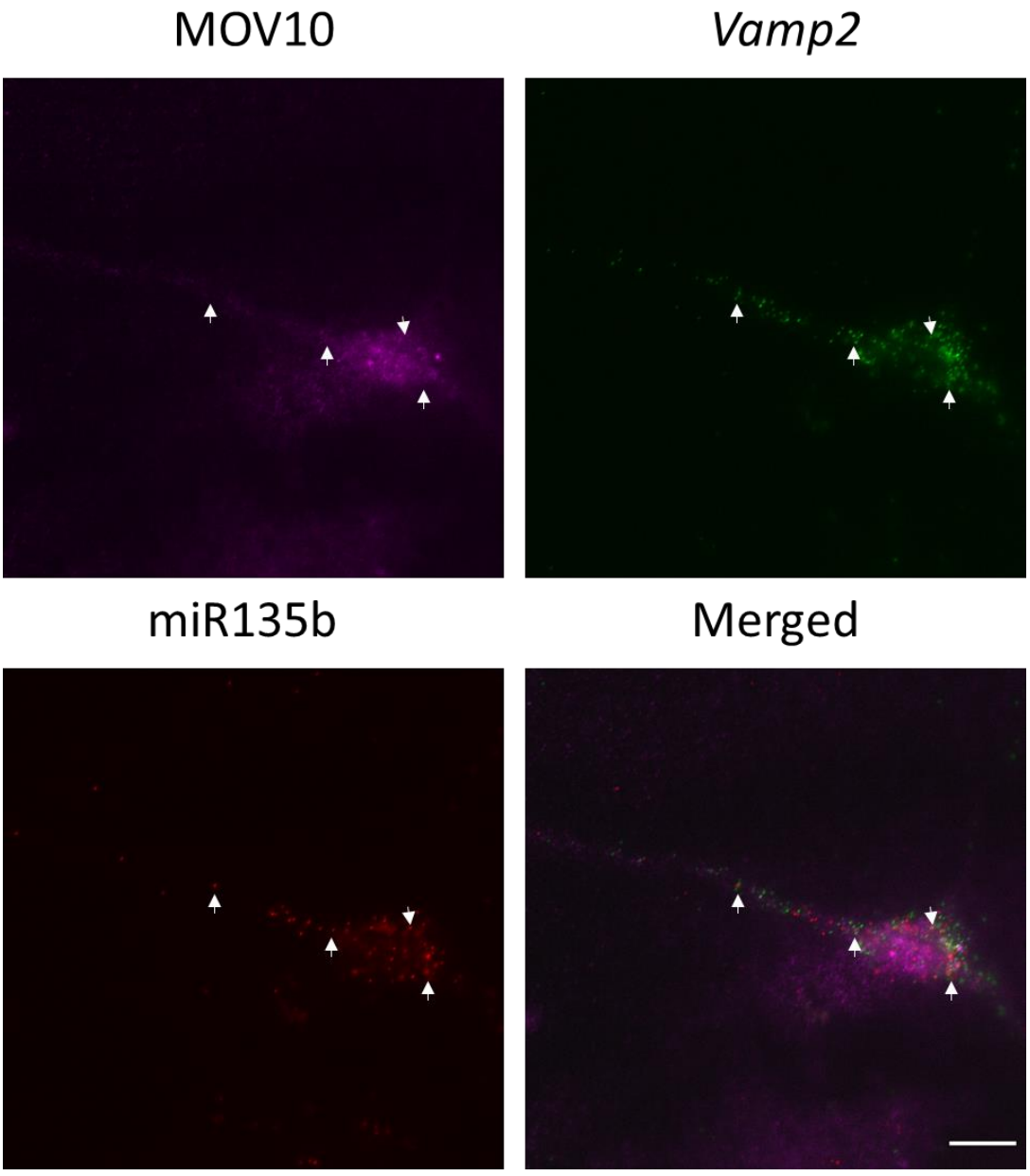

C

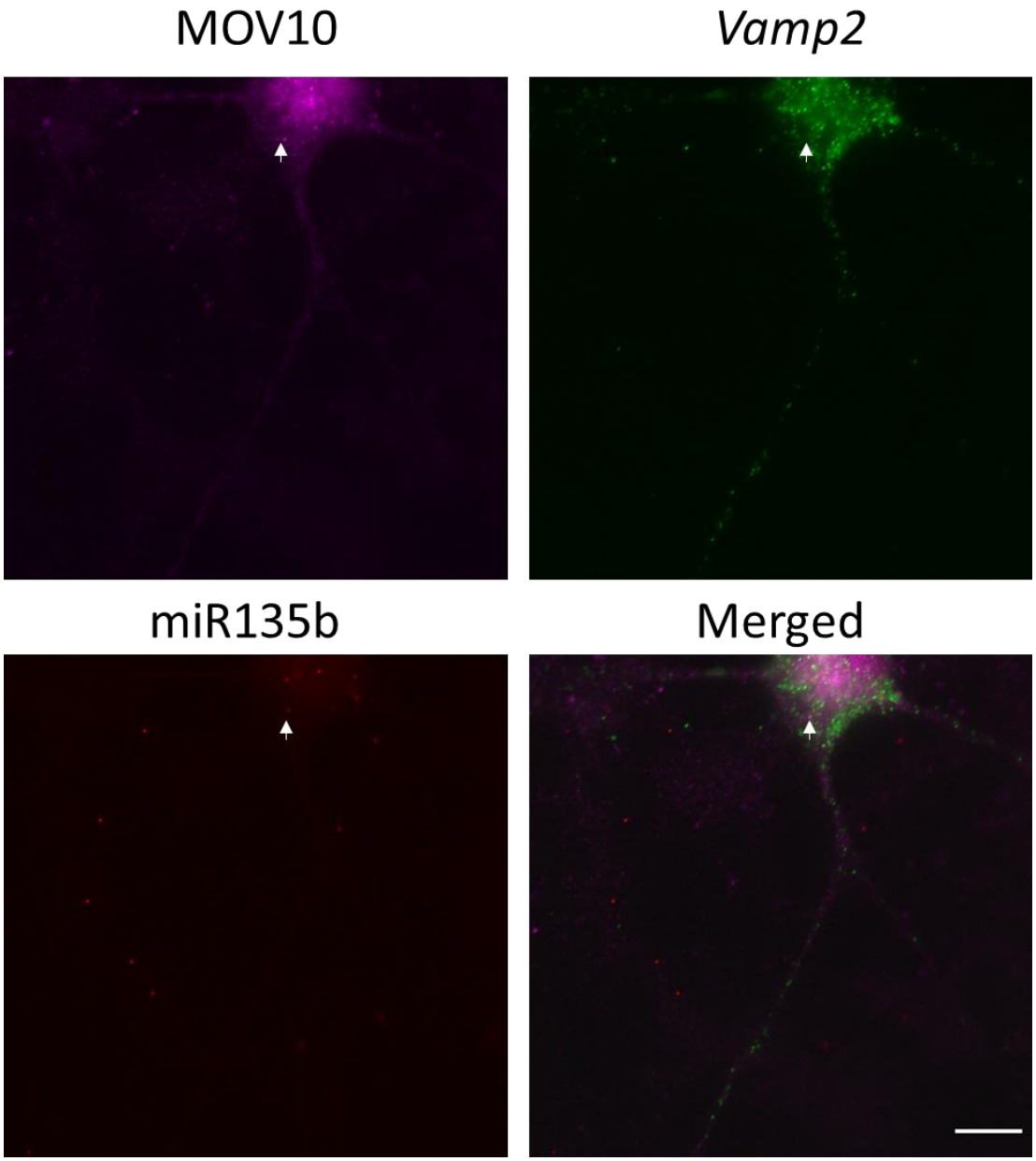

Figure 7.3: miR135b and *Vamp2* localisation within MOV10 positive neuronal processes. A, B and C Low-density neuronal cultures were subject to FISH/ICC using an antibody against MOV10 and ViewRNA Cell Plus Assay probes against miR135b and *Vamp2*. Coverslips were mounted with Fluoromount-G. Images were taken at 100x on Nikon Eclipse Ti, scale bar = 10 µm. miR135b and *Vamp2* are present in MOV10 positive neuronal subdomains. Co-labelled structures proximal to the cell body and within neuronal processes are highlighted by white arrows.

This analysis highlighted that miR135b puncta are less abundant than both *Vamp2* and MOV10, corroborating my qualitative observations (**Figure 7.4A**). MOV10 puncta were the most abundant, with there being over twice as many as compared to *Vamp2* puncta (**Figure 7.4B**).

Quantification of overlapping puncta showed that there were similar numbers of both miR135b + *Vamp2* and miR135b + MOV10 overlapping pairs (**Figure 7.4B**). *Vamp2* + MOV10 are the most abundant overlapping pair (**Figure 7.4B**). The least abundant overlap was between miR135b, *Vamp2* and MOV10 together (**Figure 7.4B**). The percentage of total puncta within all images overlapping with any other population of puncta were analysed, further breaking down the results obtained in **Figure 7.4B**.

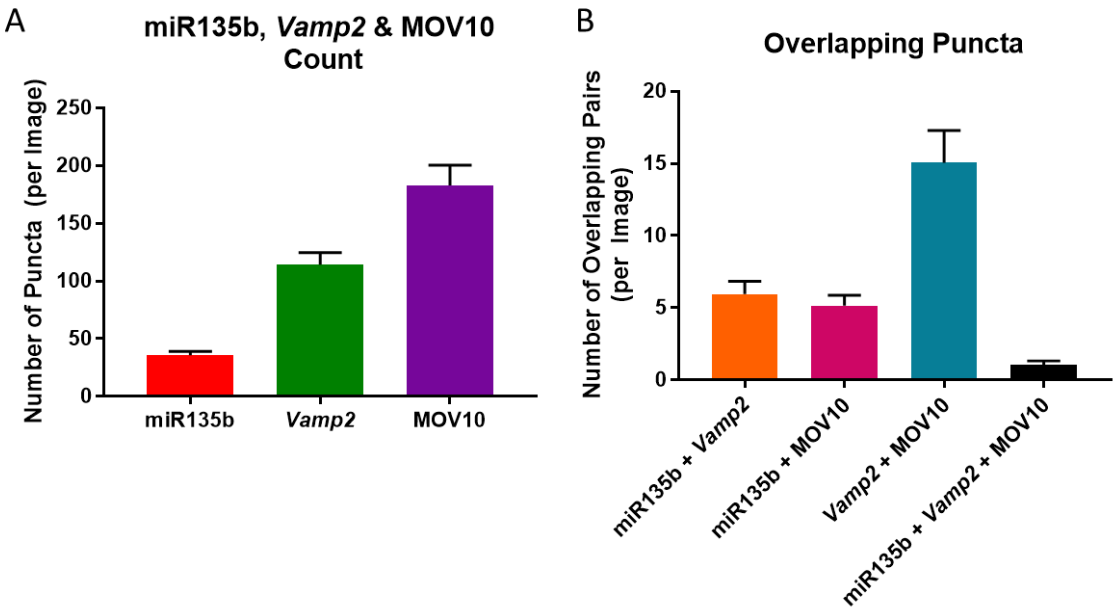

Figure 7.4: Abundance of miR135b, *Vamp2* and MOV10 puncta and the frequency of their overlap. **A** MOV10 puncta are more abundant than both miR135b puncta and *Vamp2* puncta. *Vamp2* puncta are however more abundant than miR135b puncta in MOV10 positive processes. **B** *Vamp2* and MOV10 overlapping pairs are more abundant than any other combination of overlap. miR135b puncta overlaps to a similar extent with either *Vamp2* or MOV10. The least abundant overlap is between all three miR135b, *Vamp2* and MOV10, suggesting that they are more likely to function independently of at least one component in potentially different types of granules. N = 40, graphs show mean ± SEM.

The percentages of miR135b puncta overlapping with either *Vamp2* or MOV10 puncta were similar (**Table 7.1**), consistent with the overlapping puncta shown in **Figure 7.4B**. *Vamp2* puncta and MOV10 puncta preferentially overlap with each other compared to miR135b (**Table 7.1**).

	% Overlap		
	miR135b	***Vamp2***	**MOV10**
miR135b		6.0 ± 0.9	3.4 ± 0.6
Vamp2	18.0 ± 2.5		9.2 ± 1.2
MOV10	16.9 ± 2.5	15.8 ± 2.4	

Table 7.1: The percentages of miR135b, *Vamp2* and MOV10 overlapping with any other species. There is a small difference in the percentage of miR135b puncta overlapping with either *Vamp2* or MOV10. However, there is a higher percentage of *Vamp2* puncta overlapping with MOV10 compared to miR135b. Similarly, the percentage MOV10 puncta overlapping with *Vamp2* is higher than the percentage of puncta overlapping with miR135b. N = 40, data show mean ± SEM.

Of all three molecules, MOV10 had the smallest percentage of puncta overlapping with both other populations (**Table 7.2**). A larger percentage of the total, detectable miR135b puncta contribute to the triple overlap compared to either *Vamp2* or MOV10, which could be attributed to their relative frequencies of detection.

	% Overlap		
	miR135b	***Vamp2***	**MOV10**
***Vamp2* + MOV10**	3.6 ± 1.0		
miR135b + MOV10		1.0 ± 0.3	
miR135b + *Vamp2*			0.7 ± 0.2

Table 7.2: The percentages of miR135b, *Vamp2* and MOV10 overlapping with any other pair of puncta. Every population of puncta has the fewest proportion of puncta contributing to the overlap with both other populations of puncta. However, a larger percentage of total miR135b puncta overlap to the triple overlap compared to *Vamp2* or MOV10. N = 40, data show mean ± SEM.

The data presented in **Tables 7.1 and 7.2** show that only a fraction of the total population of puncta overlap with that of the other populations. However, this observation could suggest that miR135b, *Vamp2* and MOV10 may function independently of each other. Since limitations in the sensitivity of detection by FISH/ICC might result in an underrepresentation of any overlapping combination, however, we refrained from making statistical conclusions. Nonetheless, these images provided

qualitative evidence that MOV10, *Vamp2* mRNA and miR135b could exist in the same restricted cellular compartments.

7.4 Are miR135b, *Vamp2* and SMN present together within neuronal processes?

miR135b, *Vamp2* and SMN FISH/ICC co-labelled puncta were analysed, representing a potentially different population of RNA granules.

Qualitatively, SMN (purple) is diffusely expressed throughout the labelled neurons – it is highly concentrated around the cell body, with some bright punctate staining within neuronal processes (**Figure 7.5**). Within SMN-positive neurons, *Vamp2* mRNA (green) predominantly surrounds the cell body, but is also detected along neuronal processes, perhaps indicative of its transport (**Figure 7.5**). miR135b puncta (red) are far less abundant than *Vamp2* and SMN. miR135b puncta are present mostly within the cell body, and a few puncta can be detected within processes (**Figure 7.5**). miR135b and *Vamp2* sometimes overlap in their expression within SMN positive neuronal processes (white arrows, **Figure 7.5**). This could indicate that there are miR135b-independent transport mechanisms or that the labelling process is inefficient, and we are unable to detect all overlapping species.

miR135b-, *Vamp2*- and SMN- positive structures, abundances and their overlap were qualitatively and quantitatively analysed within 27 images obtained from FISH/ICC experiments using the macro designed in FIJI (**Materials and Methods** and **Appendix 1**). Images were chosen based on the ability to identify neuronal structures i.e. cell bodies and extending processes. When interpreting these data, the potential error introduced due to inefficient labelling of microRNA and mRNA species during FISH had to be taken into consideration. This would consequently lead to an underestimation in the number of overlapping species. Taking this into consideration, it was inappropriate to draw statistical conclusions from the quantitative data obtained, instead I will comment on observed trends regarding overlapping puncta.

A

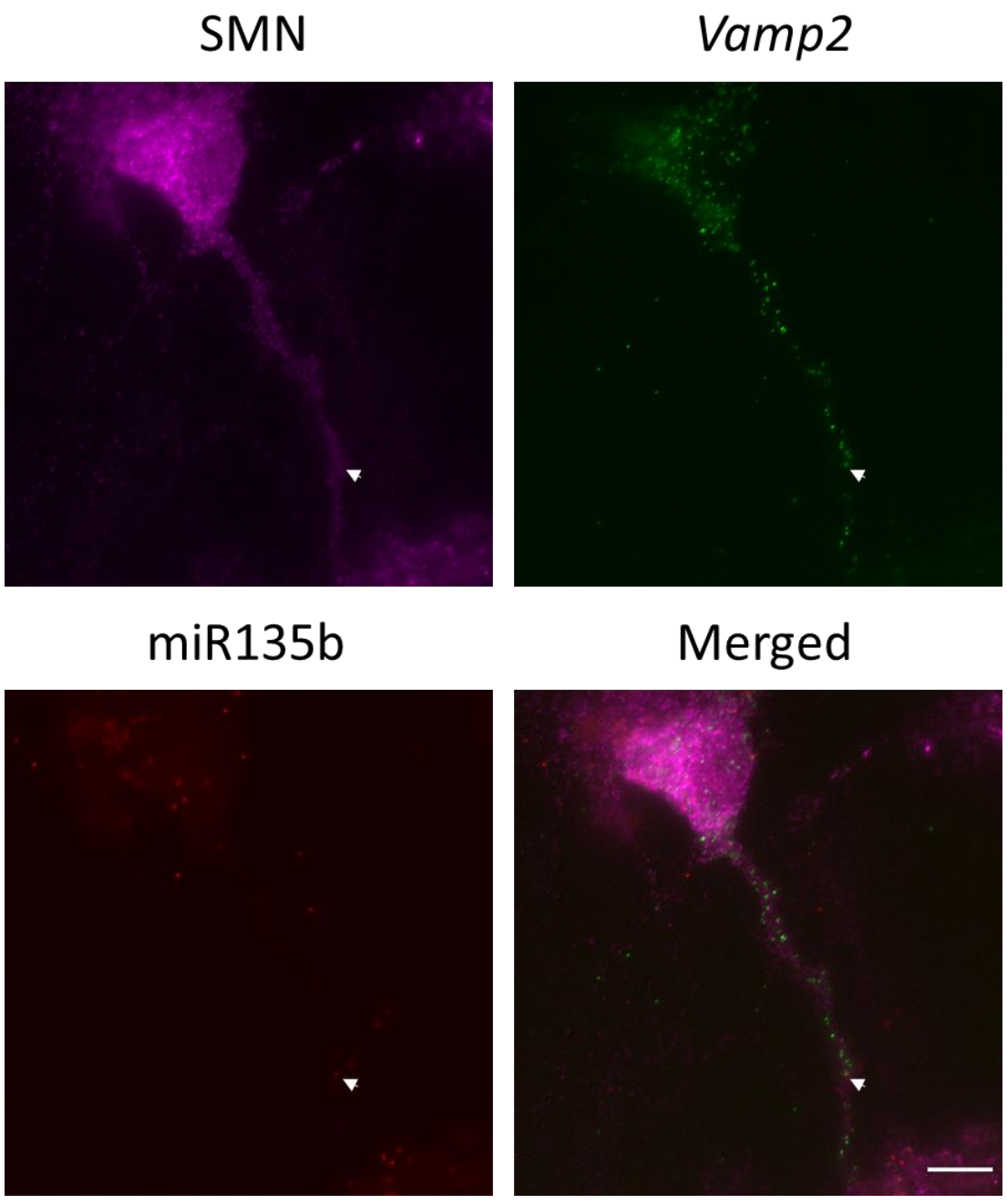

B

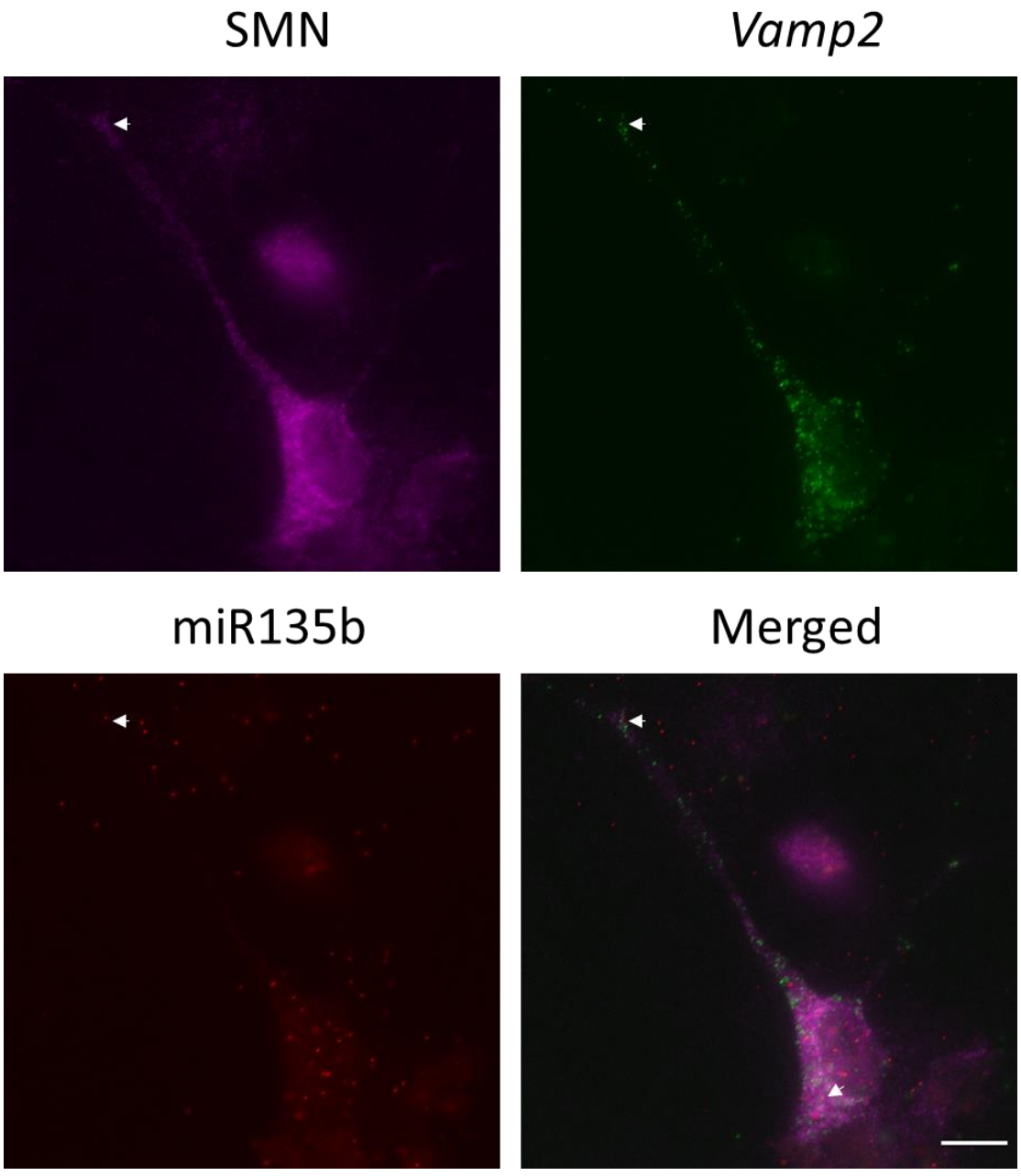

C

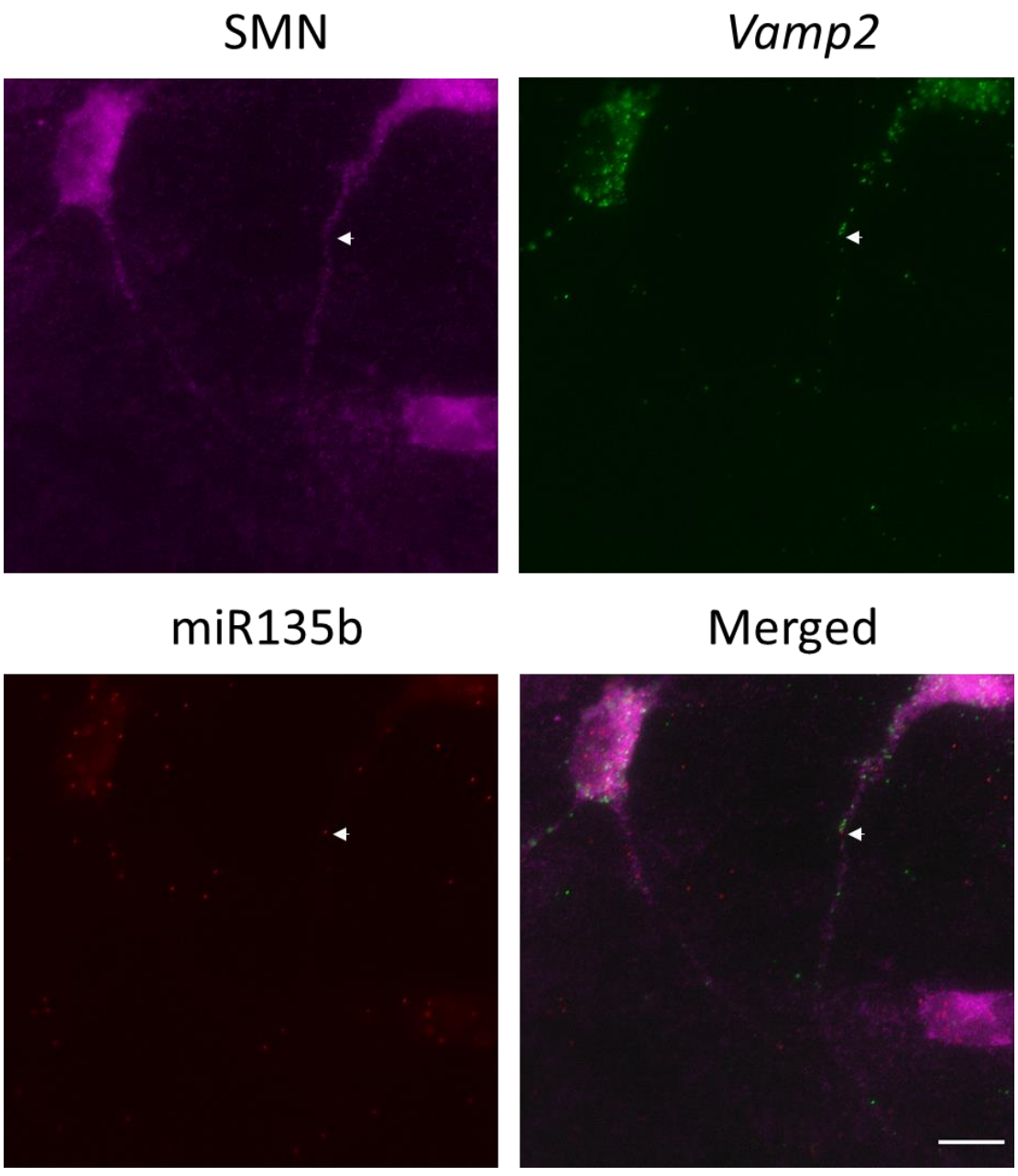

Figure 7.5: miR135b and *Vamp2* localisation within SMN positive neuronal processes. A, B and C Low-density neuronal cultures on coverslips were subject to FISH/ICC using antibodies against SMN and ViewRNA Cell Plus Assay probes against miR135b and *Vamp2*. Images were taken at 100x on Nikon Eclipse Ti, scale bar = 10 µm. miR135b and *Vamp2* are present in SMN positive neuronal subdomains. Co-labelled structures are highlighted by white arrows.

In line with the qualitative observations, SMN puncta were the most abundant, followed by *Vamp2* puncta and finally miR135b puncta (**Figure 7.6A**). A similar number of miR135b puncta overlapped with either *Vamp2* or SMN puncta (**Figure 7.6B**). *Vamp2* and SMN overlapped with each other more often than any of the other combinations, whilst the overlap between miR135b, *Vamp2* and SMN all together was least observed (**Figure 7.6B**). At face value, this might suggest that miR135b and SMN positive RNA granules might not be the most common form of *Vamp2* transport. However, the lack of overlap could alternatively be attributed to a lack of efficient labelling of microRNA/mRNA species through FISH.

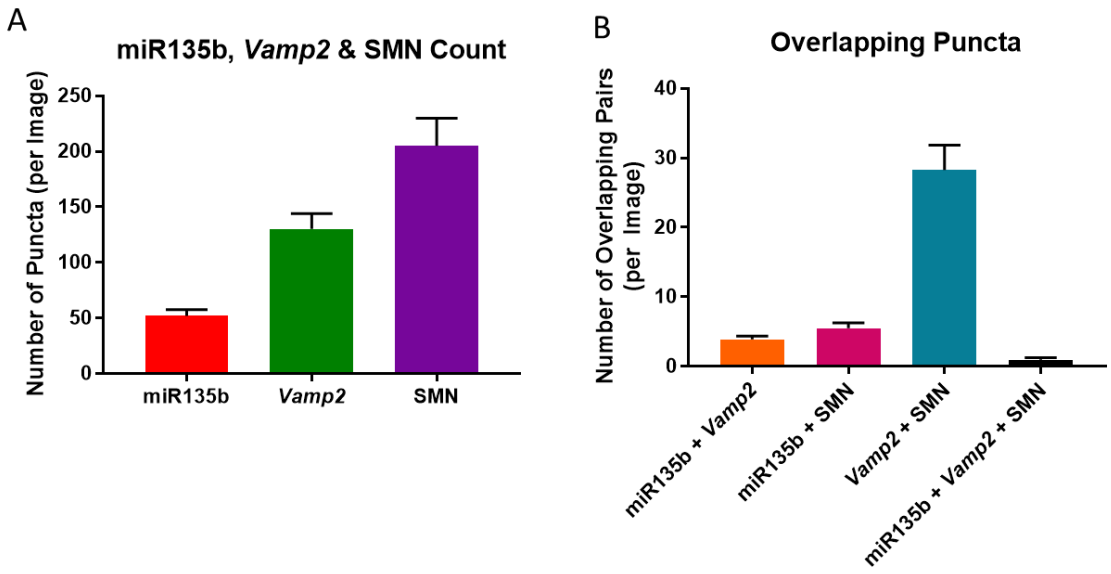

Figure 7.6: Abundance of miR135b, Vamp2 and SMN puncta and the frequency of their overlap. SMN puncta the most abundant. Vamp2 puncta are more abundant than miR135b puncta in SMN positive processes. **B** Vamp2 and SMN overlapping puncta are the most abundant. miR135b puncta overlap with either *Vamp2* or SMN in similar proportions. The least abundant overlap is between all three miR135b, *Vamp2* and SMN, suggesting that they are more likely to function independently of at least one component in potentially different kinds of granules. N = 27, graphs show mean ± SEM.

Next, the percentage of total puncta contributing to each potential overlapping combination was analysed, to assess whether detectable miR135b, *Vamp2* or SMN puncta preferentially overlapped with each other. The percentage of miR135b puncta overlapping with SMN was higher than the percentage overlapping with *Vamp2* (**Table 7.3**). There is a higher percentage of *Vamp2* and SMN puncta overlapping with each

other compared to with miR135b (**Table 7.3**). This result is reciprocated by a larger percentage of SMN puncta overlapping with *Vamp2* compared to miR135b (**Table 7.3**). However, these percentages need to also consider the relevant labelling events.

	% Overlap		
	miR135b	***Vamp2***	**SMN**
miR135b		3.7 ± 0.6	3.3 ± 0.6
Vamp2	8.6 ± 1.2		15.6 ± 1.7
SMN	12.0 ± 1.9	22.8 ± 2.0	

Table 7.3: The percentages of miR135b, *Vamp2* and SMN overlapping with any other species. A similar percentage of miR135b puncta overlaps with either *Vamp2* or SMN. A higher percentage of *Vamp2* puncta overlap with SMN compared to miR135b. Similarly, the percentage SMN puncta overlapping with *Vamp2* were higher than the percentage overlapping with miR135b. N = 27, data show mean ± SEM.

The percentage contribution from the total pool of puncta to a triple overlap was the least abundant combination observed (**Figure 7.6**). A larger percentage of miR135b contributed to the triple overlap compared to the percentages of *Vamp2* or SMN (**Table 7.4**). This can be reconciled by the overall abundance of each type of puncta.

	% Overlap		
	miR135b	***Vamp2***	**SMN**
***Vamp2* + SMN**	1.9 ± 0.6		
miR135b + SMN		0.7 ± 0.2	
miR135b + *Vamp2*			0.6 ± 0.1

Table 7.4: The percentages of miR135b, *Vamp2* and SMN overlapping with any other pair of puncta. Every population of puncta is least likely to overlap with both other populations of puncta (data in **Table 7.3**). The data here show that a larger percentage of total miR135b puncta contribute to the triple overlap compared to the percentage of *Vamp2* or SMN puncta. N = 27, data show mean ± SEM.

Furthermore, it is clear from the data provided in **Tables 7.3 and 7.4** that only a fraction of the total population of observable puncta overlap with the other populations. Limitations in the sensitivity of detection by FISH/ICC might account for an underrepresentation of any overlapping combination. However, this observation could alternatively suggest that miR135b, *Vamp2* and SMN may function independently of each other. Nonetheless, the overall miR135b, *Vamp2* and SMN colocalisation suggests

a positive relationship. To obtain more definitive conclusions, however, a more efficient method of microRNA/mRNA labelling must be employed to get a more sensitive representation of overlapping puncta.

7.5 Are miR135b, *Bsn* and MOV10 present together within neuronal processes?

To corroborate other results obtained within this thesis (**Chapter 7.8.3**), the potential coexistence between miR135b and its presynaptic target *Bsn* in MOV10 positive neurons was explored. *Bsn* is a presynaptic scaffolding protein, involved in organising the presynaptic structure to regulate proper neurotransmitter release; *Bsn* itself is speculated to have specific involvement in recruiting synaptic vesicles to release sites (Hallermann et al., 2010, Gundelfinger et al., 2015). Colocalisation of all three species could be indicative of them forming an RNA granule together, with miR135b and MOV10 perhaps regulating mRNA transport and signal-dependent translation.

FISH/ICC images were analysed to qualitatively identify the localisation of miR135b and *Bsn* puncta within neurons, particularly within neuronal processes immunolabelled for MOV10. Though MOV10 staining (purple) is diffuse throughout neuronal structures, there are brighter spots of staining which could represent potential sequestration into RNA granules (**Figure 7.7**). *Bsn* mRNA puncta (green) are present proximal to the cell body, with few puncta present at sites distal from the cell body. miR135b puncta (red) are also primarily closer to the cell body with only a few puncta within neuronal process-like structures. *Bsn* and miR135b puncta seem to be present in similar numbers, in contrast to miR135b target *Vamp2*, which was labelled much more frequently than miR135b. This could be attributed to inefficient *Bsn* mRNA labelling, a lower overall expression of *Bsn* mRNA or a lesser need for *Bsn* mRNA transport.

A

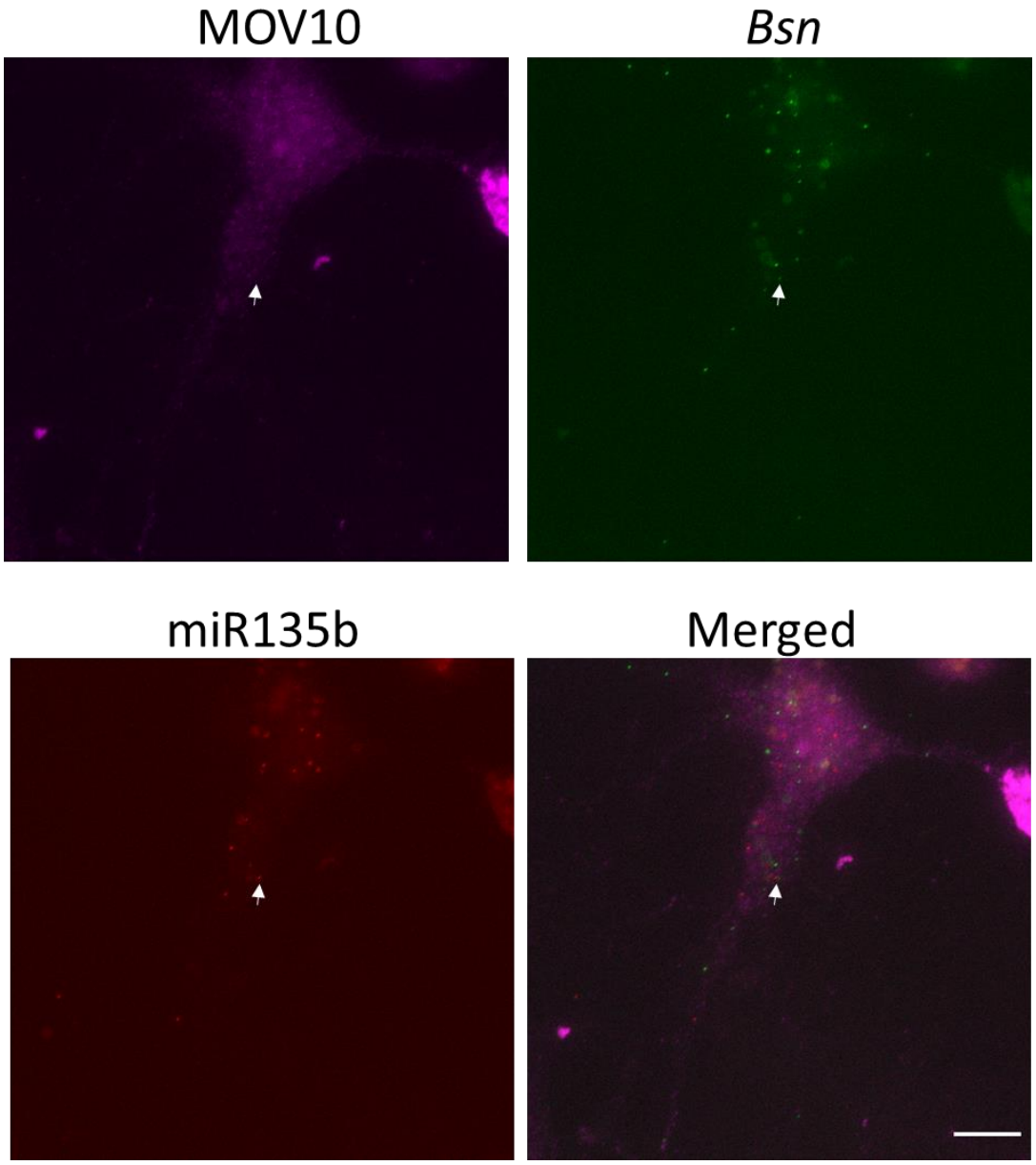

B

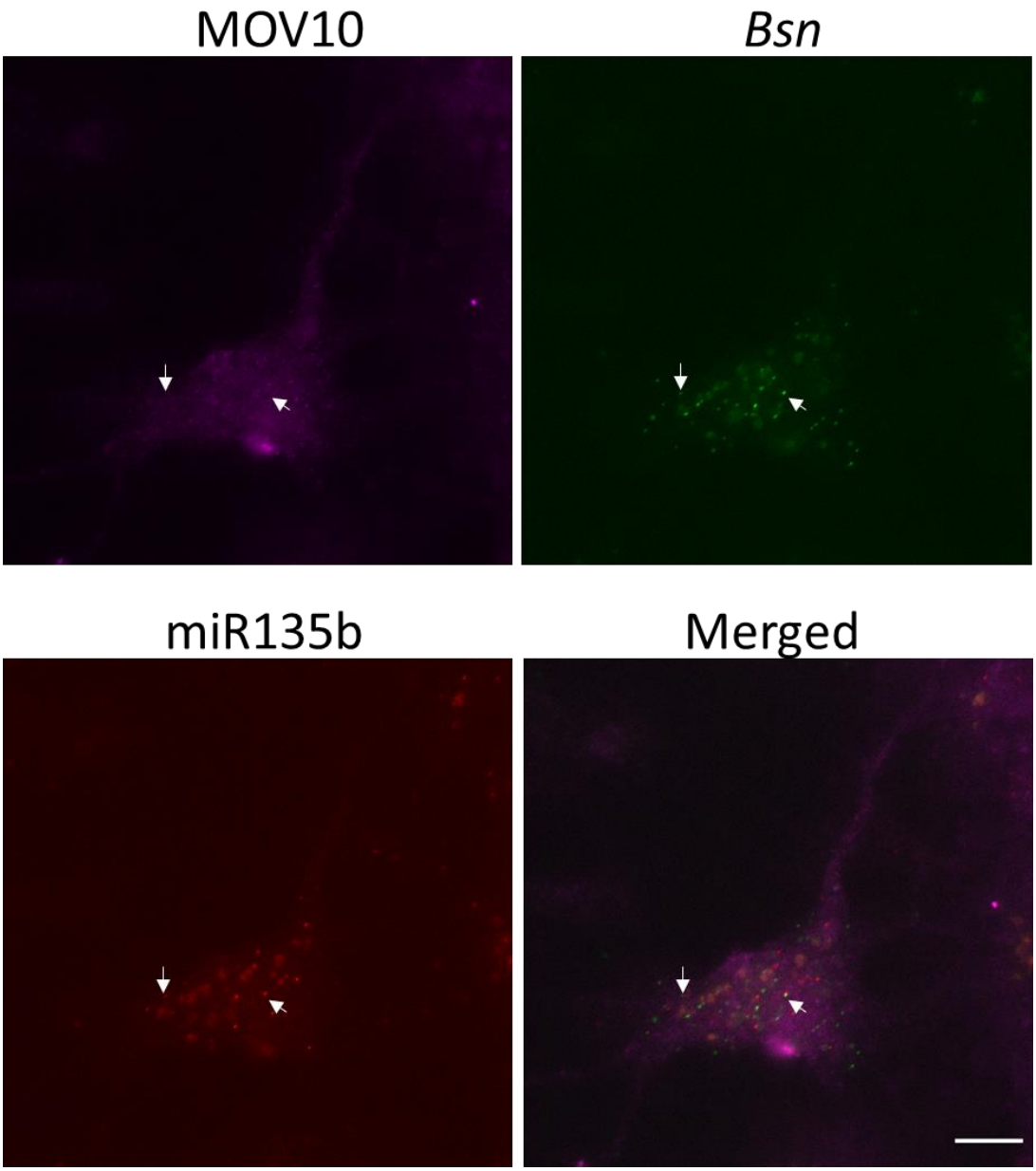

C

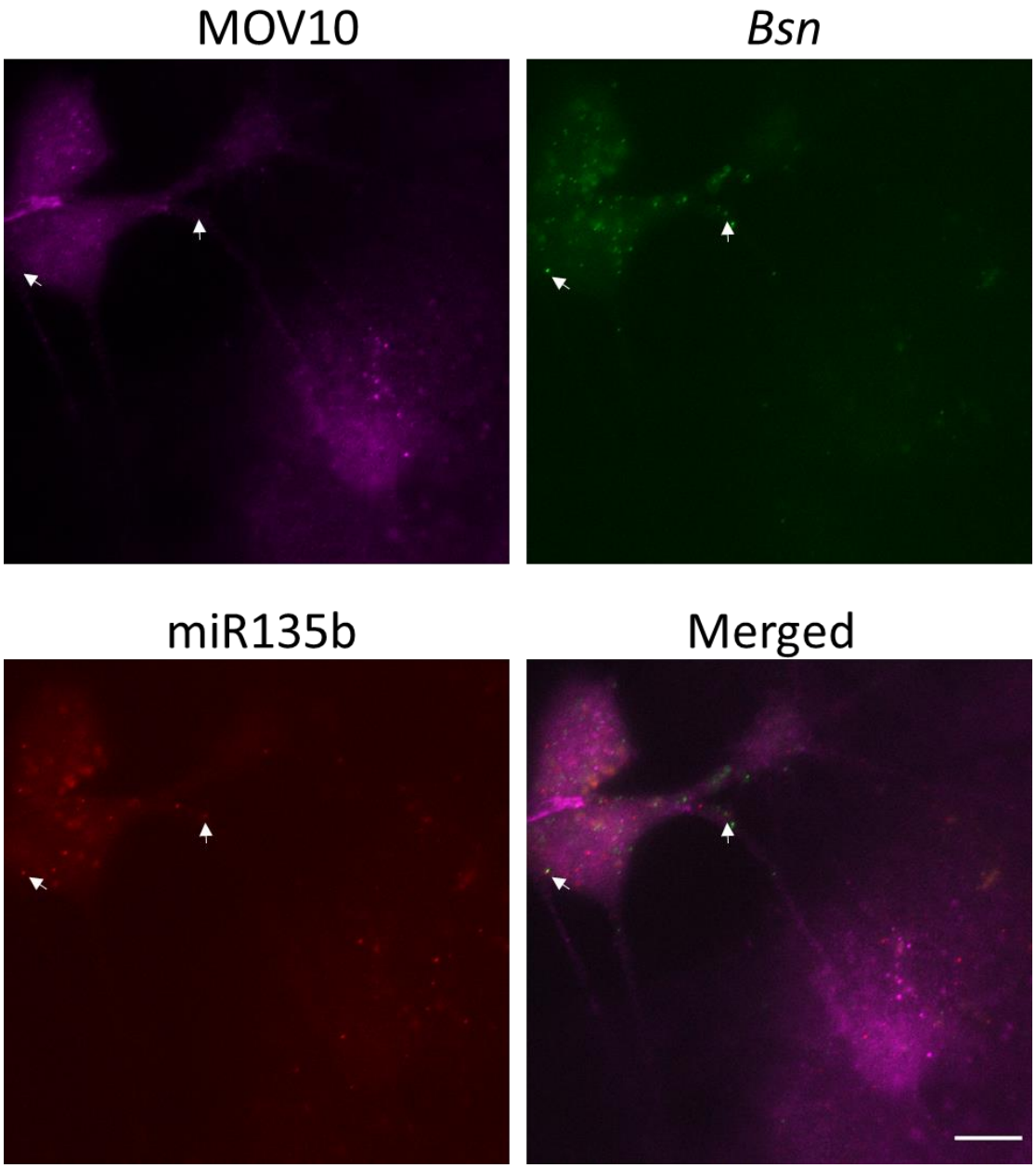

Figure 7.7: miR135b and *Bsn* co-exist within MOV10 positive neurons, primarily proximal to the cell body. A, B and C Low-density neuronal cultures on coverslips were subject to FISH/ICC using antibodies against MOV10 and ViewRNA Cell Plus Assay probes against miR135b and *Bsn*. Coverslips were mounted with Fluoromount-G. Images were taken at 100x on Nikon Eclipse Ti, scale bar = 10 µm. miR135b and *Bsn* are present in MOV10 positive neuronal subdomains. Co-labelled structures proximal to the cell body are highlighted by white arrows.

Compared to previous FISH/ICC experiments with miR135b, there are areas of blurred microRNA and mRNA staining which could not be precisely focused. Despite this, brighter and focused miR135b and *Bsn* puncta are observed to colocalise together (white arrows) within and in proximity to MOV10-positive neuronal cell bodies (**Figure 7.7**). One possibility is that miR135b might not facilitate *Bsn* transport to sites distal from the cell body, but instead act as a 'loading-mechanism' into potential granules. Similarly, miR135b and *Bsn* signals are not observed to exclusively colocalise with each other in MOV10 positive processes. This could be indicative of independent functions or may alternatively be attributed to inefficient labelling via FISH/ICC and/or poor clarity of the microscopic recording.

65 images were quantitatively analysed from FISH/ICC experiments in order to evaluate the extent of overlap between miR135b and *Bsn* within MOV10 positive neurons using the macro designed in FIJI (**Materials and Methods** and **Appendix 1**). Images were chosen based on the ability to identify neuronal structures i.e. cell bodies and extending processes.

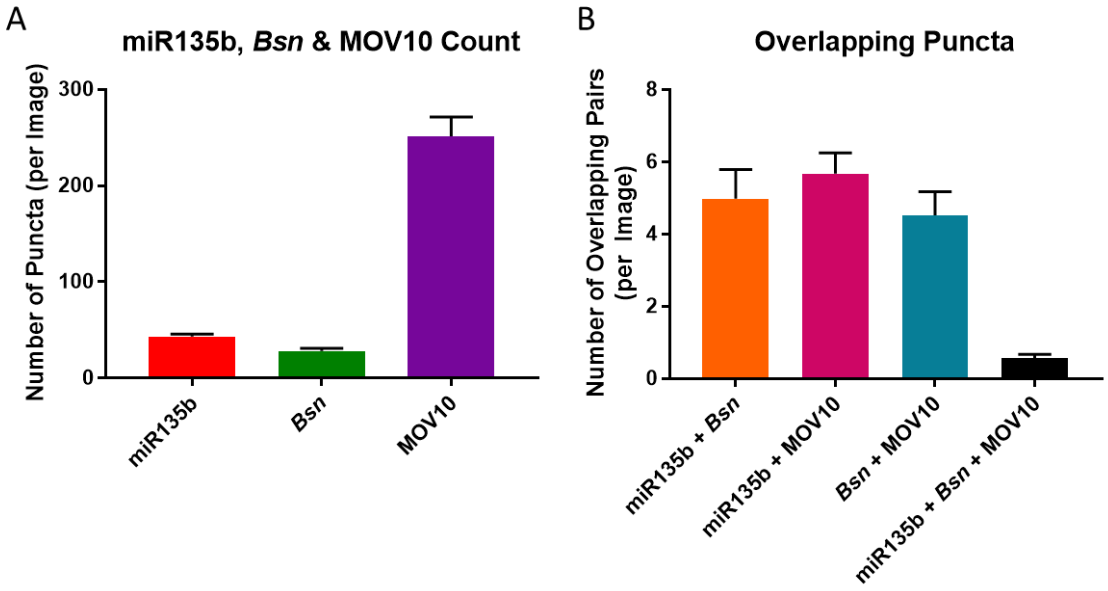

Figure 7.8: Abundance of miR135b, *Bsn* and MOV10 puncta and the frequency of their overlap. miR135b puncta and *Bsn* puncta are both less abundant than MOV10 puncta. **B** miR135b + *Bsn*, miR135b + MOV10 and *Bsn* + MOV10 overlapping pairs are the most frequently observed, compared to an overlap between all three populations. This suggests that miR135b, *Bsn* and MOV10 are more likely to function independently of at least one component in potentially different types of granules. N = 65, graphs show mean ± SEM.

My interpretations are based on detectable puncta. Considering the possibility of inefficient microRNA and mRNA labelling via FISH, no statistically based conclusions were made from the quantitative data obtained. Instead, I will comment on observed trends in species overlap.

MOV10 puncta are most abundant within the images analysed compared to miR135b and *Bsn* (**Figure 7.8A**). Surprisingly, *Bsn* puncta are less abundant than miR135b. Quantification of overlapping puncta identified that an overlap between miR135b, *Bsn* and MOV10 together is the least observed (**Figure 7.8B**).

The percentage contribution of each population of puncta (miR135b, *Bsn* or MOV10) to each overlapping combination was further analysed. There were only small differences in the percentages of either miR135b, *Bsn* or MOV10 puncta overlapping with either of the other labelled species (**Table 7.5**).

	% Overlap		
	miR135b	***Bsn***	**MOV10**
miR135b		15.3 ± 2.3	2.9 ± 0.3
Bsn	13.2 ± 1.9		2.3 ± 0.3
MOV10	15.6 ± 1.6	17.3 ± 2.3	

Table 7.5: The percentages of miR135b, *Bsn* and MOV10 overlapping with any other species. Similar percentages of each labelled population of puncta, miR135b, *Bsn* or MOV10, co-segregate with any other labelled population in pairs N = 65, data show mean ± SEM.

When analysing the triple overlap, where observed, there were only slight differences between the percentage of miR135b or *Bsn* puncta overlapping with *Bsn* + MOV10 or miR135b + MOV10 respectively (**Table 7.6**). MOV10 contributed the least percentage from its total pool of puncta to an overlap with both miR135b and *Bsn* (**Table 7.6**). This again, could be attributed to the relative abundances of each of these populations of labelled puncta (**Figure 7.8). Tables 7.5 and 7.6** that only a fraction of the total population of observable puncta overlap with the other populations. Limitations in the sensitivity of detection by FISH/ICC might account for an underrepresentation of any overlapping combination of miR135b, *Bsn* and MOV10. To obtain more definitive conclusions, however, a more efficient method of microRNA/mRNA labelling must be employed to get a more sensitive representation of overlapping puncta.

	% Overlap		
	miR135b	***Bsn***	**MOV10**
***Bsn* + MOV10**	2.0 ± 0.4		
miR135b + MOV10		3.2 ± 1.1	
miR135b + *Bsn*			0.3 ± 0.07

Table 7.6: The percentages of miR135b, *Bsn* and MOV10 overlapping with any other pair of puncta. The smallest percentages of total labelled puncta contribute to a triple overlap between miR135b, *Bsn* and MOV10. A slightly higher proportion of *Bsn* puncta contribute to this overlapping condition compared to miR135b. MOV10 puncta contribute the lowest percentage of total puncta to a triple overlap. N = 65, data show mean ± SEM.

7.6 Are miR137, *Syt1* and MOV10 present together within neuronal processes?

In keeping with the theme of important presynaptic proteins, for miR137, its interaction with and the localisation of its mRNA target *Syt1* was examined, firstly within MOV10 positive neurons. Neurotransmitter release is dependent on presynaptic calcium binding to the calcium-sensor, *Syt1*, therefore its transport to the pre-synapse and its translation will be important for neuronal connectivity (Xu et al., 2009, Südhof, 2013). In these conditions, FISH/ICC was carried out with target probe-sets complementary to miR137 and *Syt1*, and an antibody against MOV10.

Qualitative observations of FISH/ICC images highlighted that MOV10 (purple) is present heavily within the neuronal cell body and is additionally identified within neuronal processes (**Figure 7.9**). Though this staining is quite diffuse, there are brighter spots/punctate expression of MOV10 which suggest localisation in RNA granules. *Syt1* mRNA (green) signal is abundant within and surrounding the cell body, with only a few puncta present in neuronal processes (**Figure 7.9**). This could suggest that this mRNA is not constitutively transported along neuronal processes, where *Syt1* protein transport could be more predominant. miR137 staining (red) was less abundant than either MOV10 or *Syt1*, mostly surrounding the cell body and a minority of puncta being

A

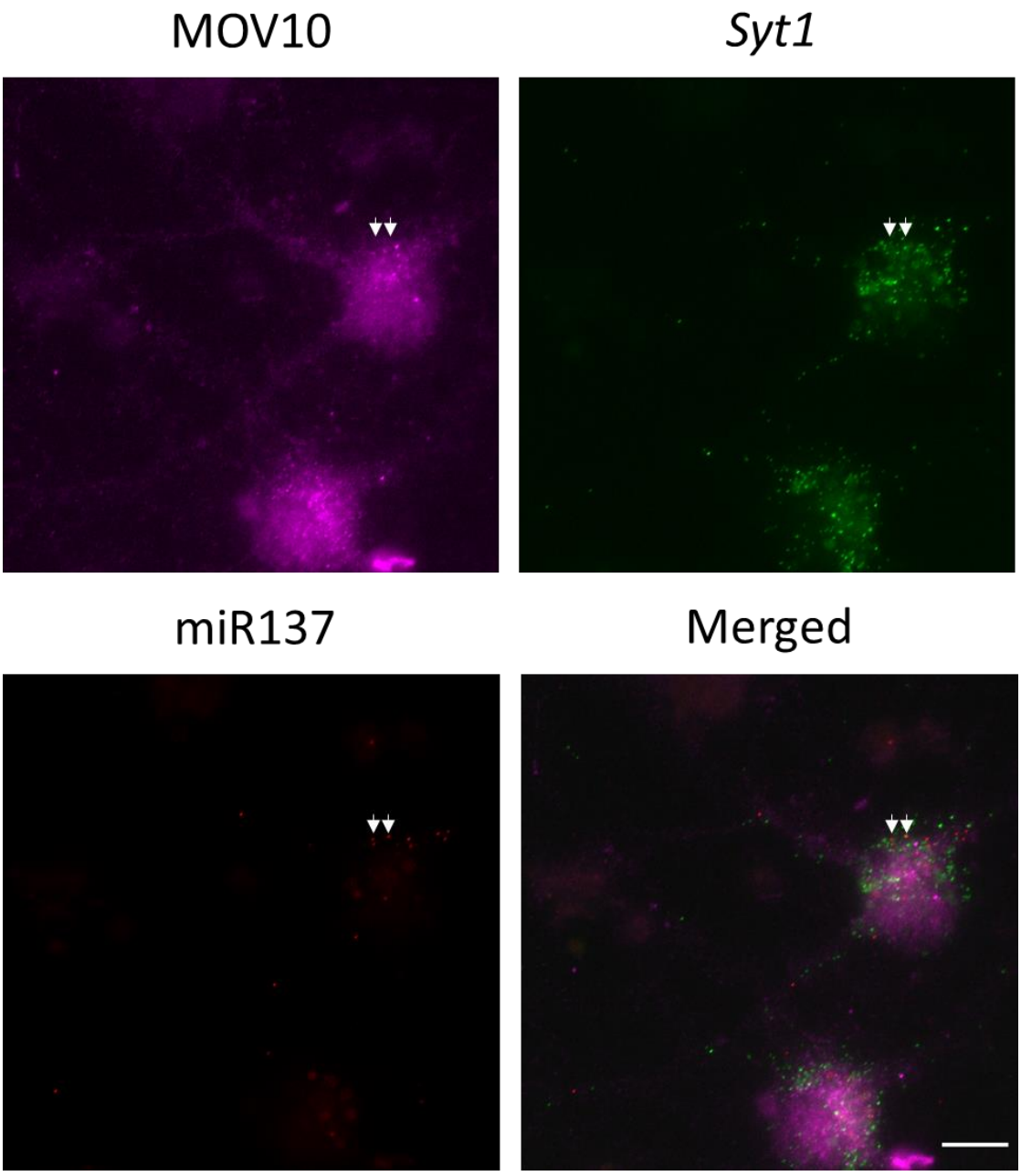

B

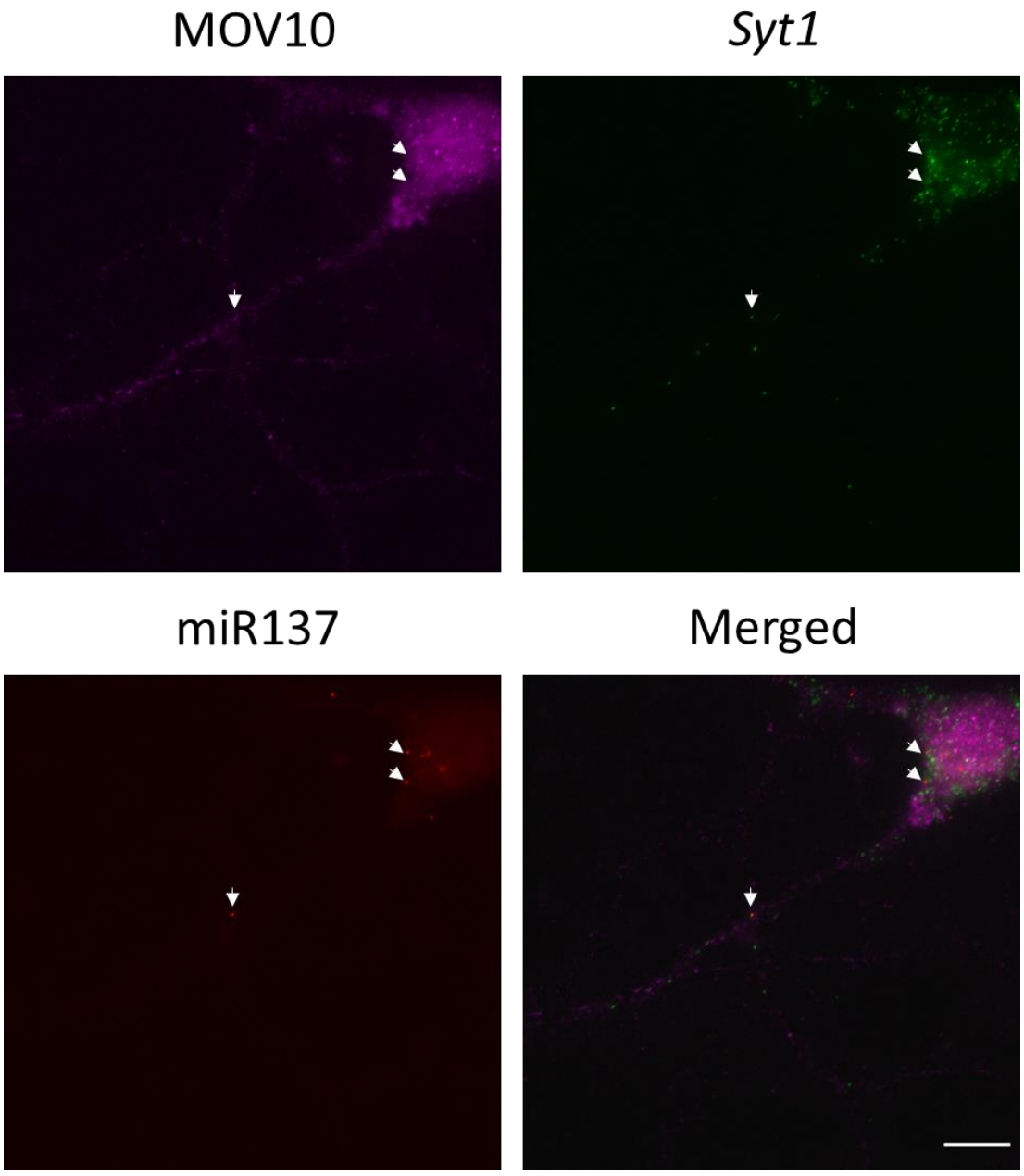

C

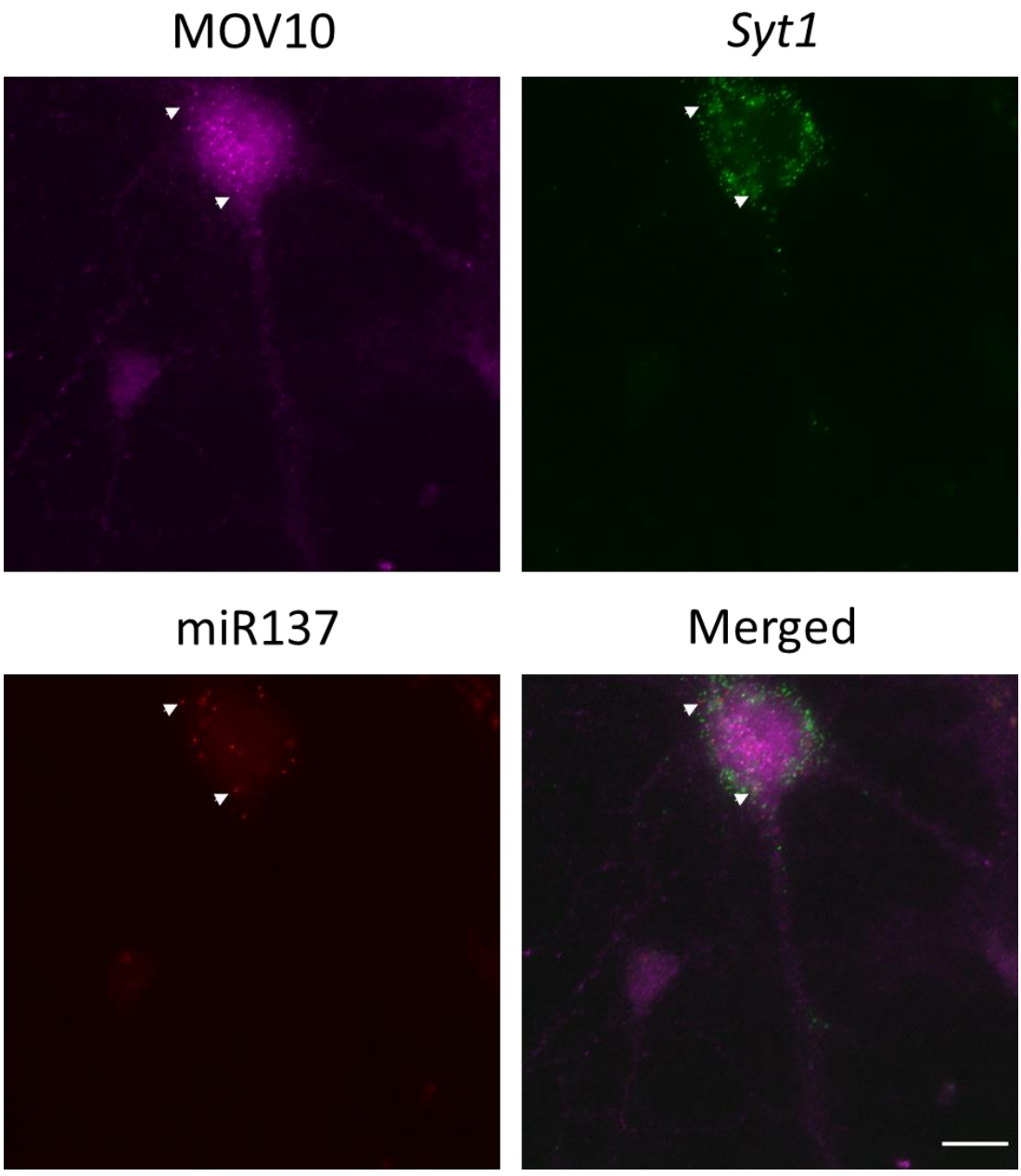

Figure 7.9: miR137 and *Syt1* localisation within MOV10 positive neuronal processes. A, B and C Low-density neuronal cultures on coverslips were subject to FISH/ICC using an antibody against MOV10 and ViewRNA Cell Plus Assay probes against miR137 and *Syt1*. Coverslips were mounted with Fluoromount-G. Images were taken at 100x on Nikon Eclipse Ti, scale bar = 10 µm. miR137 and *Syt1* are present in MOV10 positive neuronal subdomains. Co-labelled structures proximal to the cell body and within neuronal processes are highlighted by white arrows.

present in neuronal processes (**Figure 7.9**). miR137 and *Syt1* do overlap in MOV10 positive neuronal processes (white arrows, **Figure 7.9**). This is perhaps indicative of co-transport to sites remote from the cell body. When qualitatively assessing the overlap of miR137 and *Syt1* within MOV10 positive neurons, the signals do not colocalise exclusively; most overlapping instances are proximal to the cell body, where the microRNA first targets the mRNA. This could suggest that either miR137 and *Syt1* undergo some independent transport and functions or the labelling process is inefficient and is insufficient in identifying all overlapping pairs.

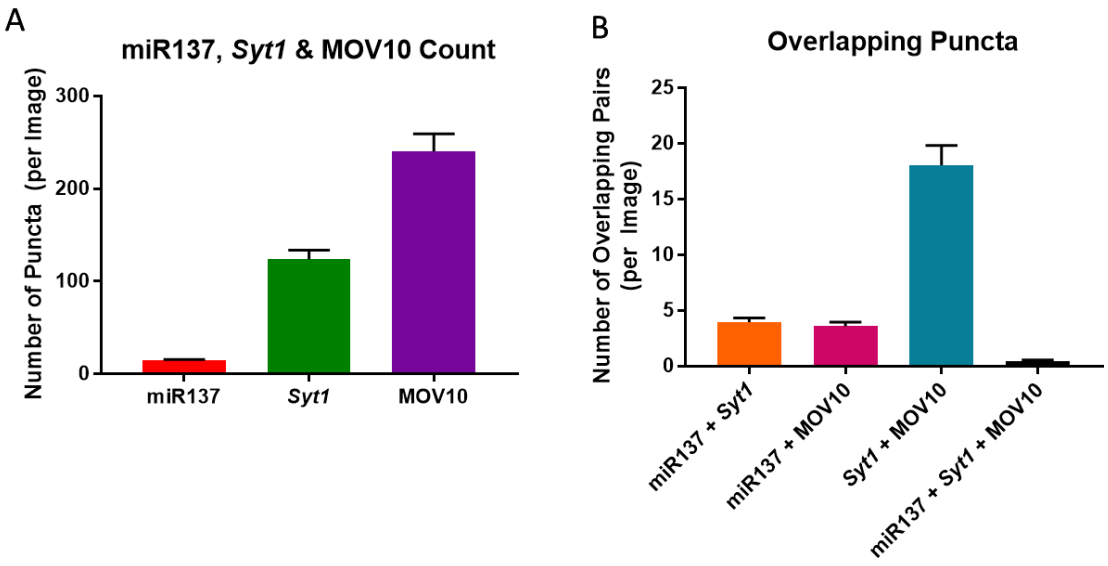

Figure 7.10: Abundance of miR137, *Syt1* and MOV10 puncta and the frequency of their overlap. A miR137 puncta are the least abundant. *Syt1* puncta are more abundant than miR137, but less so than MOV10 labelled puncta. **B** *Syt1* and MOV10 puncta overlap more with each other than they do with miR137. A similar number of miR137 puncta overlap with either *Syt1* or MOV10. The least abundant overlap is between all three miR137, *Syt1* and MOV10, suggesting that they are more likely to function independently of at least one component in potentially different kinds of granules. N = 68, graphs show mean ± SEM.

A total of 68 images obtained from FISH/ICC were quantitatively analysed to determine the extent of overlap between miR137, MOV10 and *Syt1* experiments using the macro designed in FIJI (**Materials and Methods and Appendix 1**). Images were selected based on the identification of neuronal structures, as stained by MOV10. When interpreting these data, the potential error introduced due to inefficient labelling of microRNA and

mRNA species during FISH had to be taken into consideration. Therefore, no statistically based conclusions were drawn.

The numbers of puncta in each overlapping condition were analysed. MOV10 and *Syt1* most abundantly overlapped with each other, whereas the least abundant overlap was between all three miR137, *Syt1* and MOV10 (**Figure 7.10B**). A similar number of miR137 puncta overlapped with either *Syt1* or MOV10 (**Figure 7.10B**).

To further investigate the results in **Figure 7.10B**, the percentage contribution of each population of puncta (miR137, *Syt1* or MOV10) to each overlapping combination was analysed. A similar percentage of total miR137 puncta co-segregate with either *Syt1* or MOV10 (**Table 7.7**). Whereas both *Syt1* and MOV10 overlap with each other preferentially compared to their overlap with miR137 (**Table 7.7**). This could be related to their relative abundances or due to inefficiencies in labelling (**Figure 7.10**).

	% Overlap		
	miR137	***Syt1***	**MOV10**
miR137		4.1 ± 0.6	2.1 ± 0.3
Syt1	29.7 ± 3.7		8.8 ± 0.7
MOV10	26.7 ± 3.2	15.8 ± 1.3	

Table 7.7: The percentages of miR137, *Syt1* and MOV10 overlapping with any other species. A similar percentage of miR137 puncta overlaps with either *Syt1* or MOV10. A higher percentage of *Syt1* puncta overlap with MOV10 compared to miR137. A larger percentage of MOV10 puncta overlap with *Syt1* compared to with miR137. N = 68, data show mean ± SEM.

miR137, *Syt1* and MOV10 least abundantly co-exist altogether. When analysing the percentage contributions from the total pool of miR137, *Syt1* and MOV10 puncta it was evident that a larger percentage of miR137 contributes to the triple overlap compared to MOV10 (**Table 7.8**). This could suggest independent functions, representing granules which are not reliant of MOV10- or miR137-mediated translational repression, or those transporting other mRNA cargoes (**Figure 7.10**). However, this could be attributed to an inefficient microRNA or mRNA labelling process via FISH.

	% Overlap		
	miR137	***Syt1***	**MOV10**
***Syt1* + MOV10**	3.8 ± 0.9		
miR137 + MOV10		0.7 ± 0.2	
miR137 + *Syt1*			0.2 ± 0.1

Table 7.8: The percentage of miR137, *Syt1* and MOV10 overlapping with any other pair of puncta. Every population of puncta is least likely to overlap with both other populations of puncta (data in **Table 7.7**). The data here show that miR137 puncta are more likely to contribute to a triple overlap compared to *Syt1* or MOV10 – this could be indicative of their relative abundances. N = 68, data show mean ± SEM.

The data in **Tables 7.7 and 7.8** suggest that miR137, *Syt1* and MOV10 may also interact with other microRNAs, mRNAs or proteins which have not been considered here, in differing populations of RNA granules. Alternatively, if all species haven't been efficiently labelled this might be an underrepresentation of a potential overlap of miR137 and *Syt1* pairs in MOV10 positive RNA granules.

7.7 Are miR137, *Syt1* & SMN present together within neuronal processes?

The population of miR137 and *Syt1* puncta that might co-exist with the axonal transport protein SMN were imaged and analysed using an SMN antibody in the FISH/ICC protocol. An overlap between miR137 and *Syt1* in SMN positive neurons could suggest SMN to act in conjunction with miR137-*Syt1* pairs to regulate their transport.

Qualitative analysis of the images obtained via FISH/ICC showed SMN staining (purple) to be diffuse throughout the neuron, with some punctate expression which could be representative of aggregation into structures characteristic of RNA granules (**Figure 7.11**). *Syt1* mRNA signal (green) surrounds the cell body, with some localisation in the proximal neuronal process and very few puncta at sites distal from the cell body (**Figure 7.11**). A similar pattern was observed for miR137 labelling, which was observed predominantly closer to the cell body and rarely at sites remote from the cell body, with the caveat that very few total puncta are observed (**Figure 7.11**). There are few instances where miR137 and *Syt1* overlap in their expression within SMN positive neurons (white arrows) within cell body regions. This could suggest independent functions of miR137

A

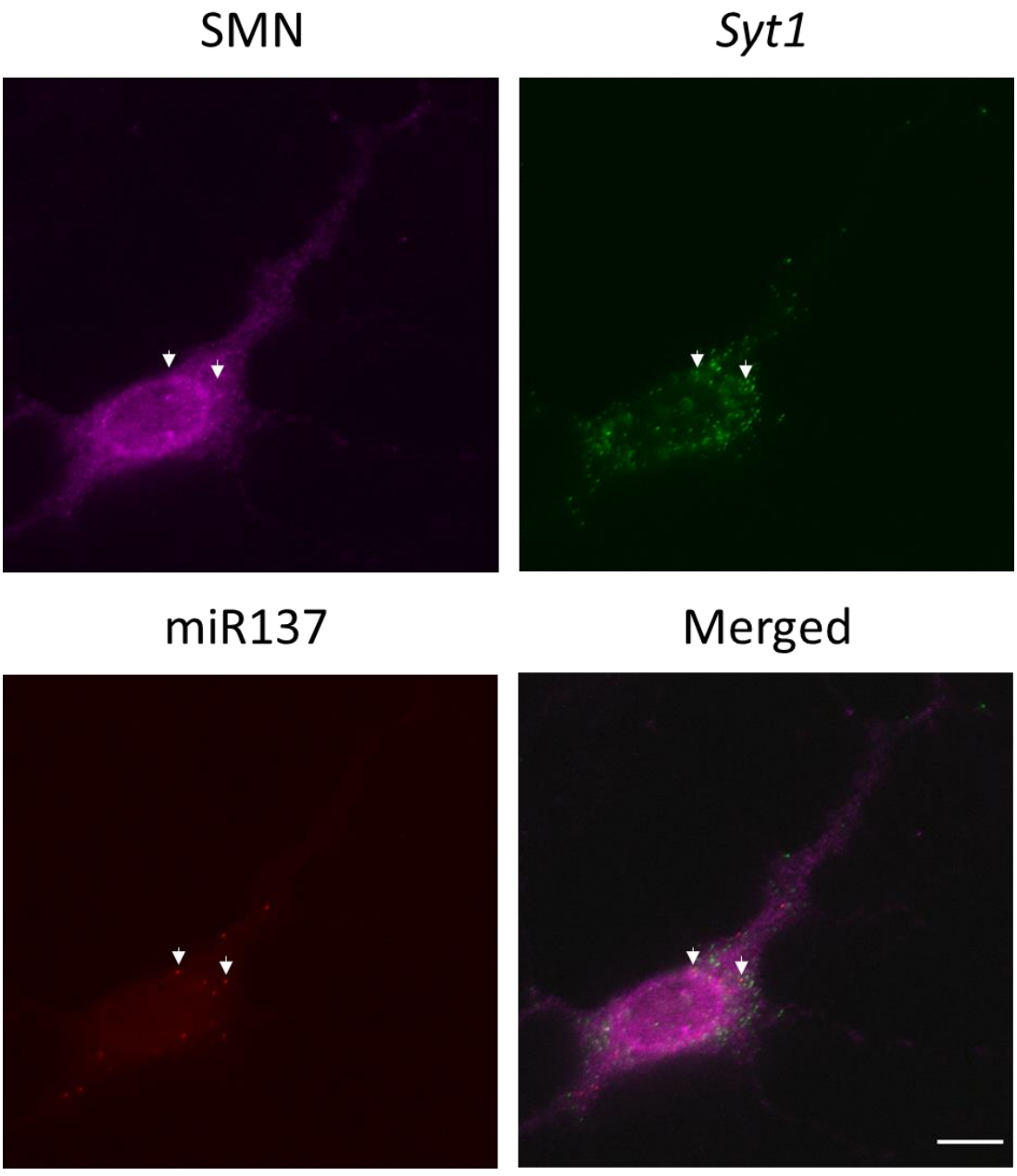

B

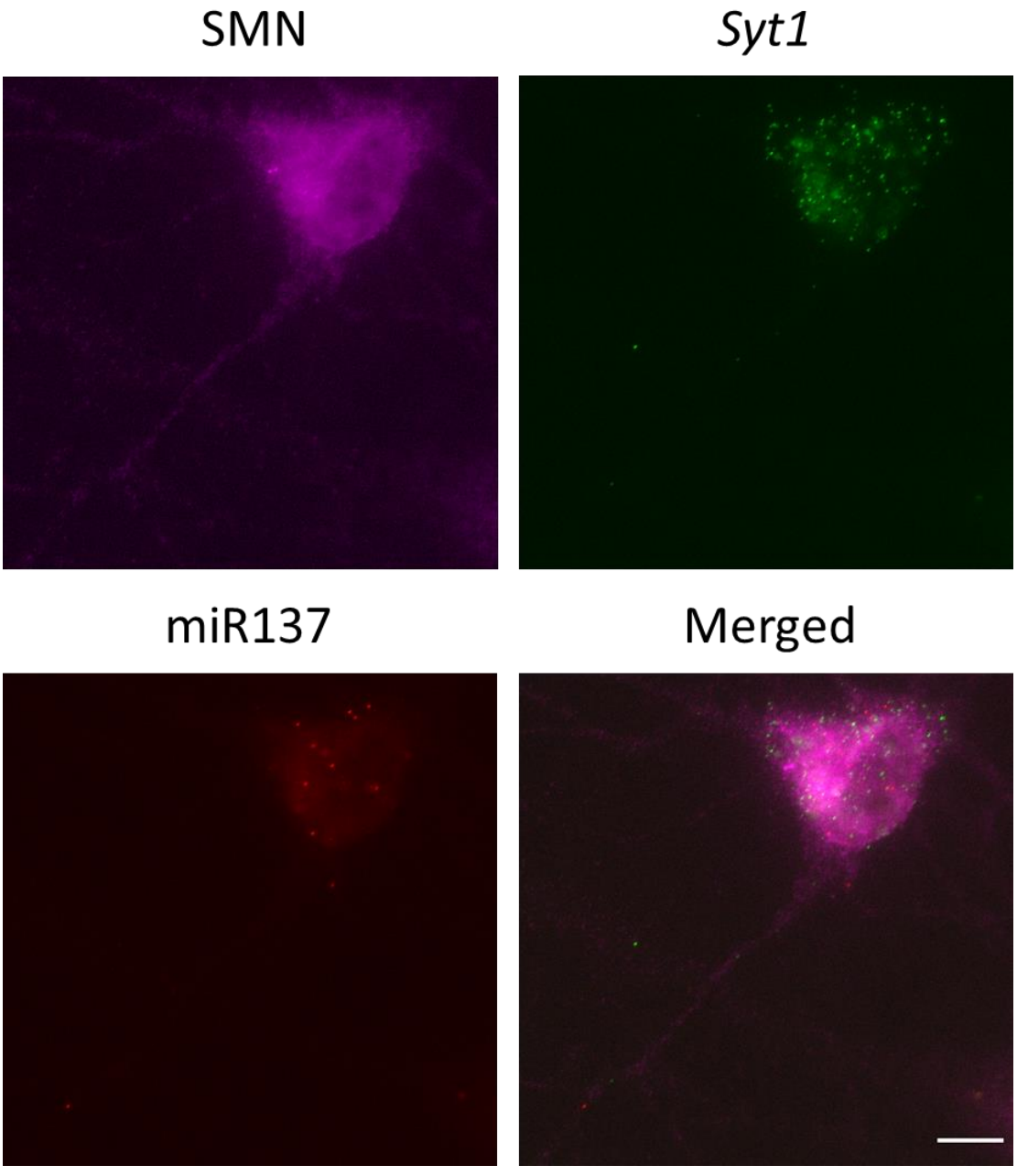

C

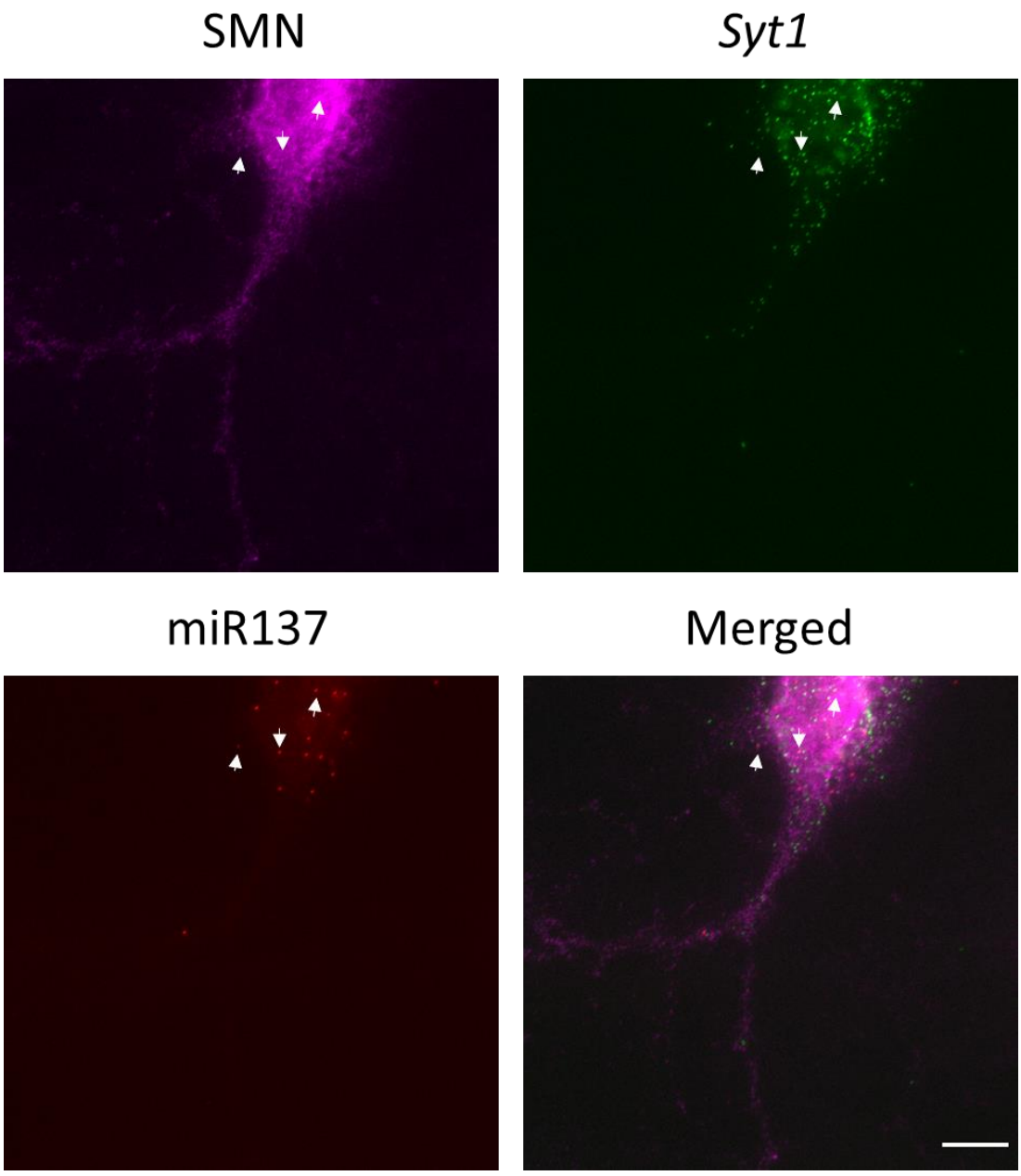

Figure 7.11: miR137 and *Syt1* localisation within SMN positive neurons. A, B and C Low-density neuronal cultures on coverslips were subject to FISH/ICC using an antibody against SMN and ViewRNA Cell Plus Assay probes against miR137 and *Syt1*. Coverslips were mounted with Fluoromount-G. Images were taken at 100x on Nikon Eclipse Ti, scale bar = 10 µm. miR137 and *Syt1* are present in SMN positive neuronal subdomains. Co-labelled structures proximal to the cell body and within neuronal processes are highlighted by white arrows.

and *Syt1* or could indicate inefficient labelling via FISH of microRNA and mRNA species. Alternatively, the colocalisation of the two species mostly in cell bodies could indicate miR137 action at that site.

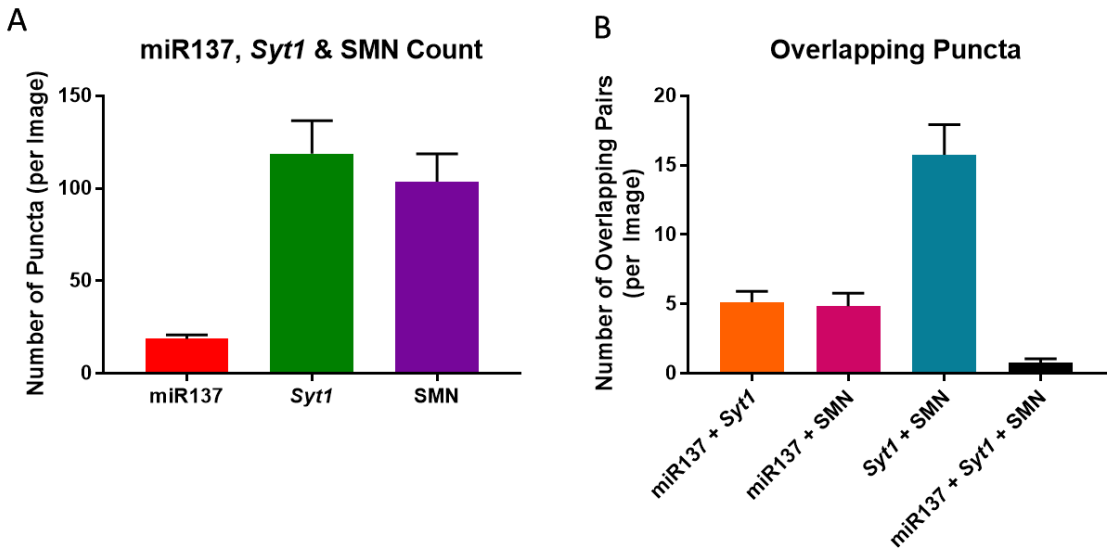

Figure 7.12: Abundance of miR137, *Syt1* and SMN puncta and the frequency of their overlap. miR137 puncta are the least abundant. *Syt1* puncta are more abundant than quantified SMN puncta. **B** *Syt1* and SMN puncta overlap more with each other than they do with miR137. A similar number of miR137 puncta overlap with either *Syt1* or SMN. The least abundant overlap is between all three miR137, *Syt1* and SMN, suggesting that they are more likely to function independently of at least one component in potentially different kinds of granules. N = 21, graphs show mean ± SEM.

21 images obtained from FISH/ICC experiments were used to analyse the potential overlap of miR137, *Syt1* and SMN puncta within neurons that are positive for SMN using the macro designed in FIJI (**Materials and Methods** and **Appendix 1**). Images were chosen based on the ability to identify neuronal structures. When interpreting these data, the limitations in the sensitivity of detection by FISH/ICC had to be considered to account for an underrepresentation of any overlapping combination. My interpretations are based on the detected and quantified puncta, but I have not drawn statistically based conclusions from the data obtained.

miR137 puncta are least abundant compared to *Syt1* and SMN, of which similar numbers were detected (**Figure 7.12A**). miR137 + *Syt1*, and miR137 + SMN were the least abundant overlapping pairs, consistent with the limited miR137 signal (**Figure 7.12B**). *Syt1* + SMN were the most abundant overlapping pair (**Figure 7.12B**). The least extent

of overlap was observed between all three, miR137, *Syt1* and SMN puncta, suggesting that this potential mechanism of microRNA-RBP mediated transport might only regulate a specialised subset of *Syt1* RNA transport in cortical neurons (**Figure 7.12B**). However, as previously mentioned, the limitation of inefficient microRNA-mRNA labelling via FISH may confound these observations.

The percentage contribution of each type of puncta (miR137, *Syt1* and SMN) to each overlapping combination was then analysed. This was to assess whether miR137, *Syt1* or SMN co-exist with any of the other two types of puncta. miR137 strongly overlaps with both *Syt1* and SMN (**Table 7.9**). *Syt1* and SMN have the largest percentages of their puncta overlapping with each other (**Table 7.9**).

	% Overlap		
	miR137	***Syt1***	**SMN**
miR137		5.6 ±1.1	7.1 ± 2.7
Syt1	27.6 ± 3.5		16.4 ± 2.0
SMN	27.7 ± 5.6	23.1 ± 5.3	

Table 7.9: The percentage of miR137, *Syt1* and SMN overlapping with any other species. There is an almost equal percentage of miR137 puncta overlapping with either *Syt1* or SMN. A higher percentage of *Syt1* puncta overlap with SMN compared to miR137. A larger percentage of SMN puncta overlap with Syt1 compared to with miR137. N = 68, data show mean ± SEM.

The least percentages of all three miR137, *Syt1* and SMN contributed to triple overlapping signals (**Table 7.10**). This could suggest that these three species preferentially exist in pairs. A larger percentage of miR137 puncta contributed the most to this overlap compared to *Syt1* or SMN, which could be attributed to their relative frequencies of detection (**Table 7.10**). As observed in all other conditions, only a proportion of total labelled miR137, *Syt1* and SMN puncta overlap in any condition (**Tables 7.9 and 7.10**). This again suggests functions of all three populations independent of each other, perhaps in differing populations of transport granules. Furthermore, miR137 regulation of *Syt1* transport in conjunction with SMN might not function as a

preferred method of mRNA transport. However, this observation may be a consequence of inefficient microRNA or mRNA labelling, which cannot be ruled out.

	% Overlap		
	miR137	***Syt1***	**SMN**
***Syt1* + SMN**	4.8 ± 2.3		
miR137 + SMN		1.6 ± 0.8	
miR137 + *Syt1*			0.5 ± 0.2

Table 7.10: The percentages of miR137, *Syt1* and SMN overlapping with any other pair of puncta. Every population of puncta is least likely to overlap with both other populations of puncta (data in **Table 7.9**). The data here show that there is a higher percentage of miR137 puncta contributing to the triple overlap compared to *Syt1* or SMN. N = 68, data show mean ± SEM.

7.8 Are miR135b, miR137 and their targets co-immunoprecipitated with RNA-binding proteins?

FISH/ICC allowed visualisation of microRNA-mRNA pairs within neurons positive for either MOV10 or SMN by labelling microRNA and mRNA molecules using complementary target probes coupled to bDNA amplification. However, due to inefficiencies in FISH labelling we cannot be certain that the observed overlap was representative of the entire population and, moreover it was inconclusive about whether the microRNA, mRNA and protein are biochemically interacting with each other.

In order to circumvent the limitations of FISH/ICC, in parallel, IP experiments were conducted. IP permits the analysis of both protein and RNA binding partners of a protein of interest. This could suggest a biochemical interaction which, in my experiments, could be indicative of an RNA granule containing microRNA-mRNA pairs, alongside RBPs, to regulate RNA transport and translation. To this end, both MOV10 and SMN were immunoprecipitated from cortical neuronal lysates using specific antibodies (**Materials & Methods**). Subsequently, their interactions with either miR135b or miR137 and their respective mRNA targets were analysed.

7.8.1 Confirmation of immunoprecipitation

Western blotting was used to confirm that IP experiments using specific antibodies enriched for either MOV10 or SMN compared to an IgG control antibody (**Figure 7.15**). Both MOV10 and SMN proteins were detected within input fractions (lysate prior to IP), and immunoprecipitated fractions (**Figure 7.13**). Neither protein was detected after IP with a control IgG antibody raised in the same species as the MOV10 or SMN antibodies. This validated the specificity of MOV10 and SMN antibody binding, and the IP of their respective antigens from cortical neuronal lysate.

7.8.2 Are microRNAs 135b or 137 co-immunoprecipitated with either MOV10 or SMN?

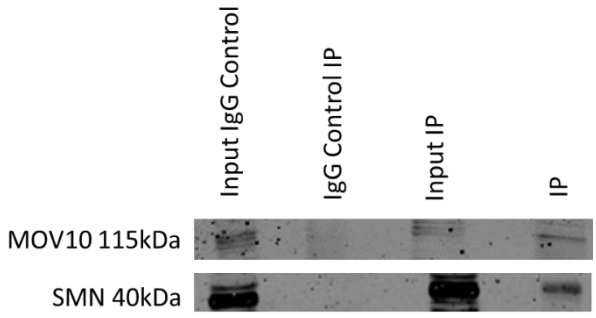

Figure 7.13: Positive control to show that MOV10 and SMN proteins are enriched following their IP. Cortical neuronal cells were harvested at DIV21, 3 plates were harvested per condition. Diluted lysate was incubated overnight at 4°C with 4 µg of SMN or MOV10 antibody, or for control conditions with 4 µg of Normal IgG from mouse or rabbit serum. The following day, the antigen-antibody lysate was incubated for 2 hours at 4°C with Dynabeads Protein G. The antigen was eluted from the resulting Dynabeads-antigen-antibody complex for analysis via western blot. The blot was incubated with anti-MOV10 (1:800) or anti-SMN (1:500). After incubation with appropriate IRDye conjugated secondary antibodies the immunoblot was scanned at multiple intensities with the LI-COR Odyssey Infrared Imager.

After validating that both MOV10 and SMN were successfully immunoprecipitated from cortical neuronal lysates, their interactions with miR135b and miR137 were analysed downstream. Based on the success of miR135b or miR137 co-IP with either MOV10 or SMN proteins, their target mRNA association with these RBPs were also explored.

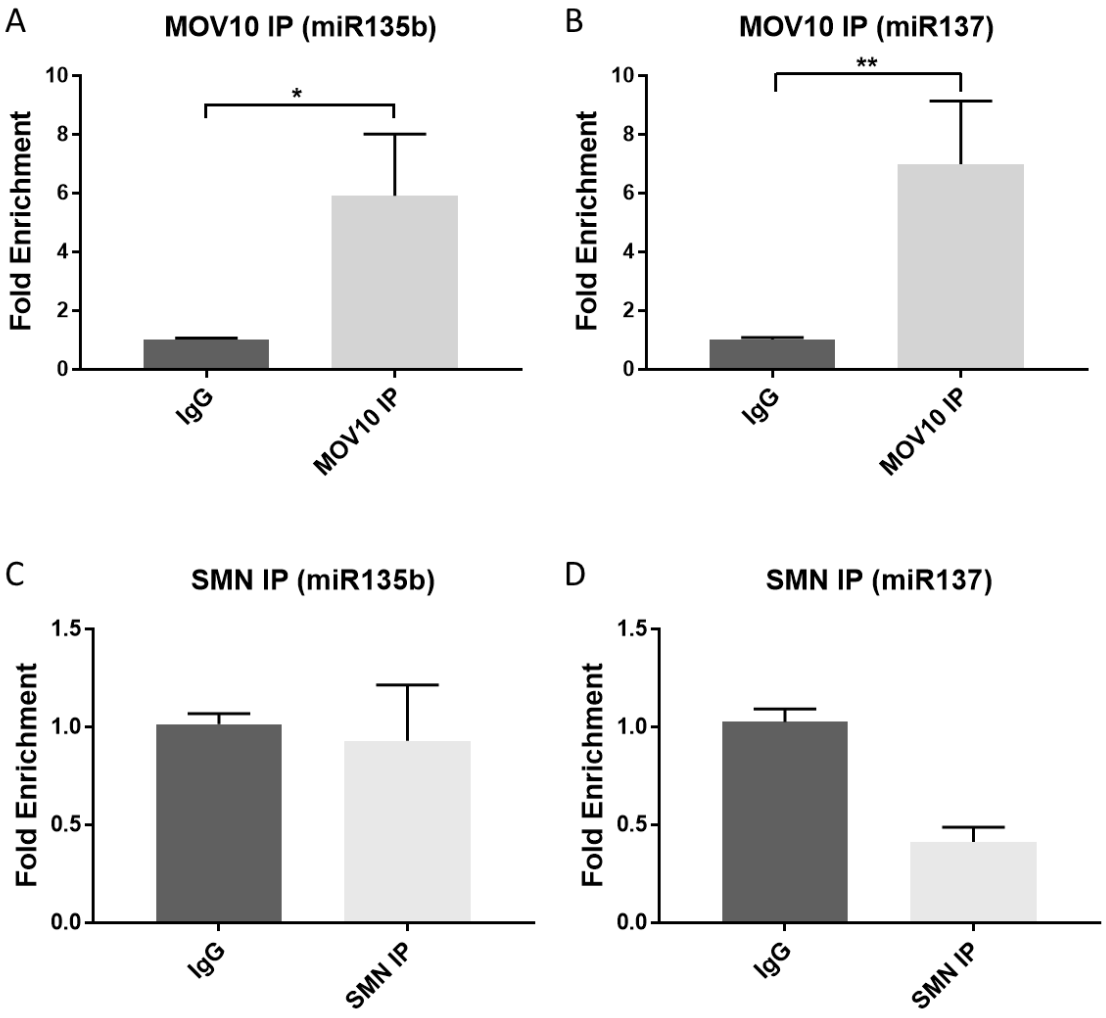

Figure 7.14: miR135b and miR137 were co-immunoprecipitated with MOV10, but not with SMN. Reverse transcription qPCR was employed from the immunoprecipitated product following MOV10 or SMN IP from cortical neuronal cultures. This was in order to analyse whether miR135b or miR137 were present in potential MOV10 or SMN positive RNA granules. MOV10 IP significantly enriches for **A** miR135b ($p < 0.05$, one-tailed unpaired t-test, n = 5 biological replicates) and **B** miR137 ($p < 0.01$, one-tailed unpaired t-test, n = 3 biological replicates). SMN IP does not significantly enrich for **C** miR135b (one-tailed unpaired t-test, n = 4 biological replicates) or **D** miR137 (one-tailed unpaired t-test, n = 4 biological replicates). This suggests both microRNAs to be present in MOV10 positive RNA granules, but absent or not directly interacting with SMN in another population of granules. Fold enrichment was calculated relative to IgG. Data are displayed as mean ± SEM.

SMN IP from cortical neuronal cultures did not enrich for either miR135b or miR137 (**Figure 7.14C and D**). This result indicates that SMN does not physically interact with either miR135b or miR137. This could suggest that SMN does not regulate the axonal localisation of miR135b-target or miR137-target pairs as is suggested with its regulation

of other mRNAs in the literature (Fallini et al., 2016). Due to this result, the interactions between SMN and microRNA target mRNAs were not further explored.

In contrast, MOV10 IP significantly enriched for both miR135b (**Figure 7.14A**) and miR137 (**Figure 7.14B**). This suggests that these microRNAs and MOV10 physically interact (directly or indirectly). Similar to its role in regulating Lypla1 translation together with miR138, MOV10 might impart signal-dependent regulation of translation on miR135b and miR137 target mRNAs (Banerjee et al., 2009).

7.8.3 Are miR135b's mRNA targets co-enriched with MOV10?

After validating that MOV10 IP enriches for miR135b, I chose to explore whether any of its mRNA targets were additionally present within the RNA extracted from the immunoprecipitated product.

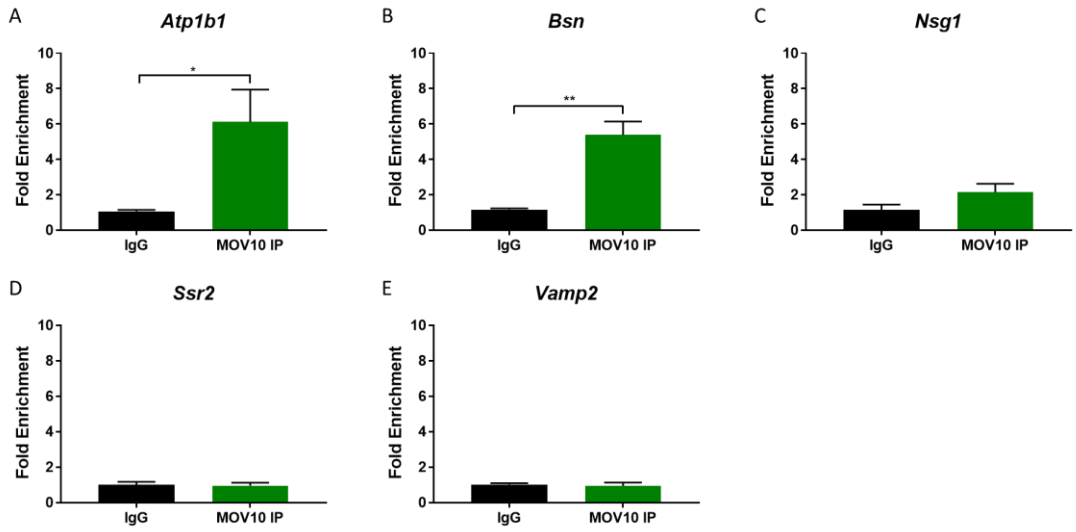

Figure 7.15: MOV10 IP significantly enriches for miR135b mRNA targets', *Atp1b1* and *Bsn*. Reverse transcription qPCR was employed from the immunoprecipitated product following MOV10 IP from cortical neuronal cultures. This was in order to analyse whether miR135b's mRNA targets were present in MOV10 positive RNA granules. MOV10 IP significantly enriched for both **A** *Atp1b1* ($p < 0.05$, n = 5 biological replicates) and **B** *Bsn* ($p < 0.01$, n = 5 biological replicates). However, MOV10 IP did not significantly enrich for **C** *Nsg1* (n = 4 biological replicates), **D** *Vamp2* (n = 4 biological replicates, in technical triplicates) or **E** *Ssr2* (n = 3 biological replicates) ($p > 0.05$ in all cases). Fold enrichment was calculated relative to IgG. Unpaired one-tailed t-test data are displayed as mean ± SEM.

There was a significant enrichment of the miR135b target mRNA *Atp1b1* in MOV10 IPs ($p < 0.05$, **Figure 7.15A**). Atp1b1 does not have a specific synaptic role but it functions to create and maintain an electrochemical gradient across the plasma membrane of excitable cells (Johar et al., 2012). MOV10 IP also enriched for *Bsn* mRNA, encoding a presynaptic scaffolding protein which regulates neurotransmitter release ($p < 0.01$, **Figure 7.15B**) (Gundelfinger et al., 2015). This result suggests that MOV10 and miR135b might interact with and regulate the translation and transport of *Atp1b1* and *Bsn* mRNAs, including the expression of these proteins in a signal-dependent manner.

Nsg1, *Ssr2* and *Vamp2* were not significantly enriched in MOV10 IPs ($p > 0.05$) (**Figure 7.15C, 7.15D and 7.15E**); this result does not infer that these mRNAs do not localise into RNA granules but instead suggests that they may not interact with MOV10.

7.8.4 Are miR137's mRNA targets co-enriched with MOV10?

Following the observation that MOV10 IP enriched for miR137, it was assessed whether any of its mRNA targets were associated with MOV10. MOV10 IP enriched for the majority of miR137 targets, again suggesting a potential co-existence of miR137 and these targets within MOV10 positive RNA granules.

Though their functions in the brain have not been entirely elucidated, *Ankrd12* ($p < 0.01$) and *Fam126b* ($p < 0.01$) were significantly enriched after MOV10 IP (**Figure 7.16A and 7.16H**). This could provide basis for further research into the functions of these mRNAs and their transport. The other targets of miR137 which were significantly enriched by MOV10 IP, included *Sept3* ($p < 0.0001$), *Syt1* ($p < 0.01$) and *Slc6a1* ($p < 0.01$) (**Figure 7.16B, 7.16D and 7.16F**), all of which have known presynaptic roles; therefore, their synaptic expression will be important to neuronal function.

Neither *Lrrn3*, *Ptpn5* or *Gabra1* were enriched upon MOV10 IP ($p > 0.05$) (**Figure 7.16C, 7.16E and 7.16G**). Again, this result does not necessarily infer that these mRNA targets of miR137 do not localise into RNA granules but instead suggests that they may not interact with MOV10. One caveat of these results is that limited replicates were performed because the experiments were both time- and resource-intensive.

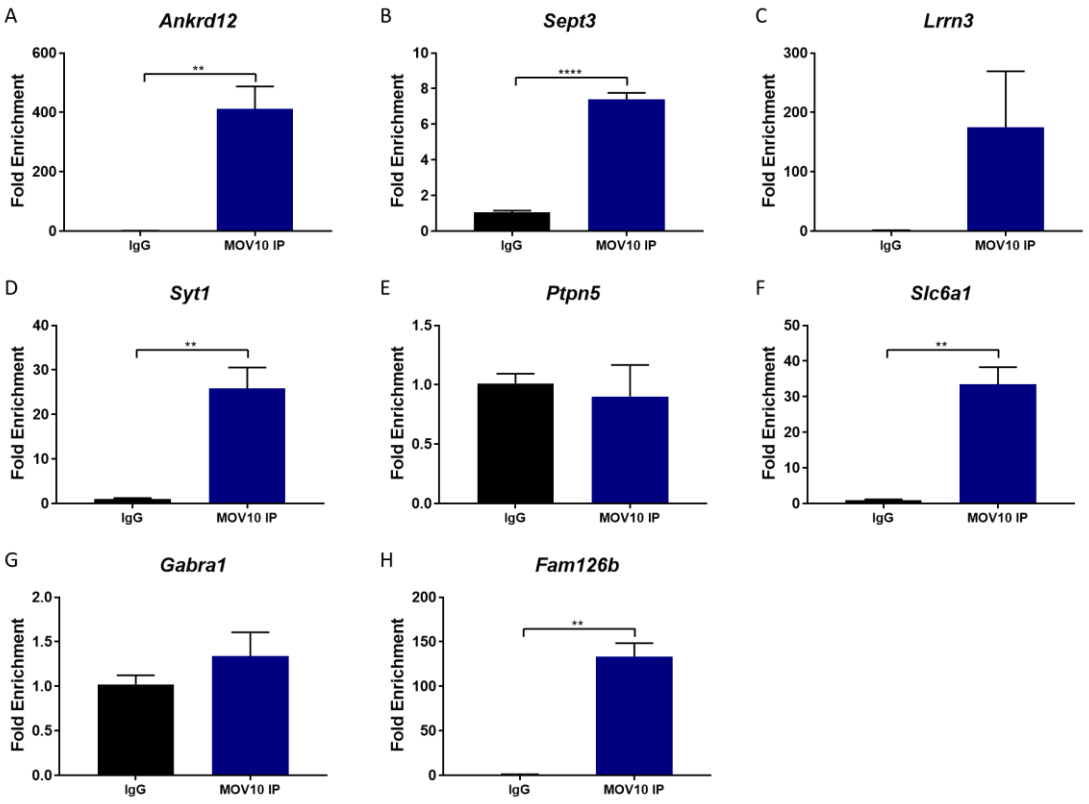

Figure 7.16: MOV10 IP significantly enriches for multiple miR137 target mRNAs. Reverse transcription qPCR was employed from the immunoprecipitated product following MOV10 IP from cortical neuronal cultures. This was in order to analyse whether miR137's mRNA targets were present in MOV10 positive RNA granules. MOV10 IP significantly enriched for **A** *Ankrd12* ($p < 0.01$, n = 3 biological replicates), **B** *Sept3* ($p < 0.0001$, n = 2 biological replicates), **C** *Syt1* ($p < 0.01$, n = 2 biological replicates), **F** *Slc6a1* ($p < 0.01$, n = 3 biological replicates) and **H** *Fam126b* ($p < 0.01$, n = 2 biological replicates). However, MOV10 IP did not significantly enrich for **C** *Lrrn3* (n = 3 biological replicates), **E** *Ptpn5* (n = 2 biological replicates) or **G** *Gabra1* (n = 2 biological replicates) ($p > 0.05$ in all cases). Fold enrichment was calculated relative to IgG. Unpaired one-tailed t-test data are displayed as mean ± SEM.

7.9 Discussion

I aimed to cytologically and biochemically assess the interaction between miR135b or miR137 and their mRNA targets and RBPs of interest. Many targets of miR135b and miR137 have important synaptic roles, therefore their transport and regulated translation within pre- and postsynaptic regions might be essential to proper neuronal function.

Firstly, this was approached by FISH/ICC imaging and analysis, to observe the potential co-localisation microRNAs and their target mRNAs, combined with labelling by

antibodies labelling RBPs of interest. To this end, miR135b and its targets *Vamp2* or *Bsn*, and miR137 with its target *Syt1* were investigated within neurons which were positive for MOV10 or SMN. In FISH/ICC experiments, microRNA-mRNA pairs were predominantly localised closer the cell body regions compared to distal neuronal processes (**Figure 7.3, 7.5, 7.7, 7.9 and 7.11**). These observations could infer that microRNA-loaded RISC complexes translationally repress targets within the cell body and/or proximal neuronal process. The mRNA might be loaded into RNA granules, where the microRNA dissociates, and translational repression might be maintained by a variety of other *trans*-acting factors, such as RBPs. Experiments to elucidate the necessity of microRNA mediated translational repression during mRNA transport and signal-dependent translation will be helpful in resolving this question.

microRNA, mRNAs and RBPs were not exclusively observed to exist together, which could suggest functions independent of each other (**Figure 7.3, 7.5, 7.7, 7.9 and 7.11**). However, as mentioned throughout my considerations of these analyses, there are limitations observed with the FISH/ICC labelling. It was not possible with the type of microscopy utilised to identify if the microRNA, mRNA and RBPs were only colocalised in space or if they were biochemically interacting. Confocal microscopy was not utilised in my experiments, due to the difficulty in locating regions of interest.

Moreover, there are inefficiencies inherent to FISH labelling of RNA species, particularly microRNAs. This could lead to an underrepresentation of labelled, thus detectable, RNA puncta. Furthermore, microRNAs themselves are very small RNA molecules, therefore the probability of them diffusing out of the cells prior to fixation is high and could lead to an underrepresentation of the number of microRNA present within the neurons. A further limitation to consider for these experiments is the binding specificity of microRNA probe-sets, where they may also hybridise to the pre-microRNA. This could suggest that this method labels both mature and precursor microRNAs. Furthermore, the potential presence of microRNA-mRNA pairs in RNA transport complexes may hinder the probe sets and amplifiers binding to complementary sequences.

Taken together, there were limitations in the FISH/ICC experiments to detect colocalising microRNA-mRNA pairs in neurons positive for MOV10 and SMN. Alternative approaches in the future could include microRNA overexpression to reconcile the low

numbers of microRNAs detected in these experiments. microRNA overexpression by lentiviral transduction might be necessary in order to detect any potential overlap between microRNA-mRNA pairs. Moreover, more sensitive, super-resolution microscopy techniques which are better at resolving the spatial dimension, such as Stochastic Optical Reconstruction Microscopy (STORM) may allow better detection of microRNA-mRNA pairs at a single-molecular level in neuronal processes (Bates et al., 2013).

To reconcile these difficulties, IP experiments were conducted to investigate biochemical interactions between the RBPs of interest, miR135b and miR137 and their respective mRNA targets. Moreover, the microRNA TaqMan assays are specific to the detection and amplification of mature microRNAs. The results obtained suggest that miR135b and miR137 do not biochemically interact directly or indirectly with SMN, despite many of their target mRNAs having a presynaptic role within neurons (**Figure 7.14**).

In contrast, miR137 and miR135b both biochemically interact with MOV10, evidenced by their enrichment in MOV10 IPs (**Figure 7.14**). MOV10 has a previously identified role in microRNA mediated translational repression, and the reversal of this phenomenon. MOV10 functions in unwinding RNA to facilitate microRNA-loaded RISC binding and to regulate signal-dependent translation of a subset of dendritically localised mRNAs (Meister et al., 2005, Banerjee et al., 2009, Kenny et al., 2019). This includes the reversal of miR138 repression of *Lypla1* mRNA by NMDA receptor activation and the consequent degradation of MOV10 by the proteasome (Banerjee et al., 2009). Furthermore, the presence of MOV10 is shown to be necessary for microRNA mediated mRNA targeting in both Drosophila and mammalian cells (Tomari et al., 2004, Meister et al., 2005). Accordingly, the finding that both miR135b and miR137 are co-immunoprecipitated with MOV10 suggests their specific biochemical interaction.

Furthermore, MOV10 IP enriched for miR135b's targets *Atp1b1* ($p < 0.05$) and *Bsn* ($p < 0.01$) (**Figure 7.15**). The potential regulation of *Atp1b1* transport by both miR135b and MOV10 within RNA granules could be important within neurons to maintain resting membrane potential to eventually propagate action potentials at sites close to the synapse (Johar et al., 2012). Bsn is localised to and delineates the active zones of central

and peripheral synapses and is thus an obvious potential regulator of synaptic plasticity (Gundelfinger et al., 2015).

The majority of miR137's targets were enriched following MOV10 IP. *Ankrd12* ($p < 0.01$) and *Fam126b* ($p < 0.01$), whose functions aren't entirely elucidated in the brain, were enriched after MOV10 IP (**Figure 7.16**). Interestingly, *Ankrd12* is elevated in the serum of schizophrenia patients; a psychiatric disorder which is linked to dysregulated miR137 expression (Thomas et al., 2018, Smirnova et al., 2019). *Sept3* ($p < 0.0001$), *Syt1* ($p < 0.01$) and *Slc6a1* ($p < 0.01$) mRNAs were all enriched after MOV10 IP (**Figure 7.16**). Proper targeting of *Slc6a1* is essential, and a dysfunction in this can lead to epilepsy and intellectual disability, perhaps by initiating excitotoxicity (Cai et al., 2019). Furthermore, single nucleotide polymorphisms in the *Syt1* gene impairs synaptic vesicle fusion (Baker et al., 2018). *Sept3* knock-out impedes presynaptic neurotransmission by decreasing synaptic proteins, including Syt1 (Tsang et al., 2008). Dysfunction of these genes leads to disease phenotypes, potentially due to a dysregulation of miR137 itself (Tsang et al., 2008, Baker et al., 2018, Cai et al., 2019).

These results suggest that MOV10 biochemically interacts with both miR135b and miR137, and a subset of their targets, most of which are localised to the pre-synapse. This suggests a role for MOV10 in assisting translational repression and regulating the signal-dependent translation of neuritic mRNAs following transport (Banerjee et al., 2009). This lends credibility to our hypothesis that microRNAs in conjunction with specific RBPs could be involved in controlling the transport of synaptically localised neuronal mRNAs, to spatiotemporally regulate their translation. Going forward, to obtain more definitive conclusions, further IP experiments and a more efficient method of microRNA/mRNA labelling must be employed to obtain a more sensitive method to visualise overlapping puncta.

Heterogenous populations of RNA granules are known to exist, which suggest that miR135b and miR137 could associate with several different RBPs. Therefore, the mRNAs investigated here that were not enriched in MOV10 IP could segregate into a separate population of granules not positive for MOV10. Further experiments would need to be conducted to identify each population of RNA granule, perhaps through detecting microRNAs and mRNAs associated with specific RBPs following IP.

8 Chapter 8: Discussion

The Luthi-Carter group has previously shown that the expression levels of a number of neuronal microRNAs, including miR135b and miR137, are positively correlated with their target mRNAs in neuronal cells. These findings, together with further experimental testing, indicated that these neuronal microRNAs do not behave in the canonical manner of directing their targets' degradation but might instead co-exist with their target mRNAs (Jovičić, 2011). Furthermore, Jovičić (2011) demonstrated that both microRNAs decreased the fraction of their targets associated with translating ribosomes. My thesis attempted to further validate the positively correlated relationships between miR135b and miR137 and their mRNA targets, to elucidate the potential function of their co-existence and explore the translational regulation of their targets.

8.1 Target-directed dynamics of microRNA and mRNA target pairs

Target directed microRNA degradation (TDMD) is a phenomenon where extensive complementary pairing between a microRNA and its mRNA target beyond the seed sequence can trigger microRNA degradation. TDMD is predicted to occur between over 1000 microRNA-mRNA pairs, and is observed in the brain to restrict the expression of certain microRNAs to particular regions, for example NREP restricts its targeting microRNA, miR29b's, expression to the cerebellum in mice (Bitetti et al., 2018). Interestingly, this highlights a method by which a microRNA can be spatiotemporally restricted, perhaps to regulate cellular function, mirroring the effect that microRNAs are posed to have on their own targets (Jovičić et al., 2013).

It is reported that microRNA degradation in TDMD is preceded by modifications to the microRNA's 3' end, altering its stability. These modifications include tailing and trimming (Fuchs Wightman et al., 2018). Tailing is the addition of non-templated nucleotides, commonly adenosine or uridine by Poly(A) Polymerases or Terminal Uridylyl Transferases, respectively, to the 3' end of the microRNA (Modepalli and Moran, 2017). Tailing can occur whilst the microRNA is still attached to the RISC complex, and this may lead to its dissociation (Fuchs Wightman et al., 2018). However, it has been argued that

dissociation of the 3’ end of the microRNA from RISC might be necessary to allow access to tailing enzymes (Modepalli and Moran, 2017). These modifications have been shown to direct the degradation of metazoan pre- and mature microRNAs (Fuchs Wightman et al., 2018). Furthermore, microRNAs undergoing TDMD are often subject to trimming where nucleotides are removed from the 3’ end, again to alter microRNA stability (Ameres et al., 2010). The investigation of TDMD in human cell lines has shown a potential involvement of the Terminal Uridylyl Transferase TUT1 and a 3’ to 5’ exoribonuclease DIS3L2 (Haas et al., 2016). However, recent work from the Bartel group highlights that tailing and trimming of a microRNA do not necessarily lead to its decay and this pathway might be microRNA and/or cell type specific, rather than a global microRNA decay mechanism (Kingston and Bartel, 2019).

With reference to previous literature, a mechanism of target-mediated microRNA protection (TMMP) has been described previously in *C. elegans*. Chatterjee and Grosshans (2009) described that only mature single stranded microRNAs were degraded in the 5’ to 3’ direction by the exoribonuclease, XRN2, however microRNA duplexes were not. This provided evidence for mature microRNA degradation after strand seperation, therefore the authors speculated whether microRNA-mRNA complementary binding could serve to protect a mature microRNA from degradation (Chatterjee and Grosshans, 2009). To this end, a synthetic UTR containing binding sites to the *C. elegans* microRNA Let-7 was introduced into larvae and shown to stabilise mature Let-7 microRNA, this was also true for miR237 (Chatterjee and Grosshans, 2009). The authors suggested that TMMP could regulate microRNA homeostasis; low target abundance would trigger microRNA degradation by XRN2 to prevent a toxic accumulation, but the presence of a target would protect and maintain microRNA abundance (Chatterjee and Grosshans, 2009).

This group went on to evidence that expression of a target mRNA or depletion of XRN2 or related XRN1 could promote the accumulation of microRNA passenger strands (Chatterjee et al., 2011). Usually, the guide strand of the microRNA duplex is selected and loaded onto RISC based on the relative thermodynamic stability of the 5’ end, whereas the passenger strand is degraded (Meijer et al., 2014). However, miR241’s passenger strand is less thermodynamically stable compared to the guide strand at the

5’ end; introduction of complementary mRNAs within in vivo and in vitro models of *C. elegans* protected both strands of miR241 (Chatterjee et al., 2011). Despite this, the guide strand of miR241 was preferentially loaded into RISC, showing a mechanism of RISC loading and strand selection beyond thermodynamic asymmetry (Chatterjee et al., 2011).

Furthermore, Chatterjee et al., (2011) provided further evidence of TMMP by demonstrating that overexpressing one of two microRNAs with overlapping target sets (Let-7 and miR84) negatively affected the abundance of the other. This study also showed that increasing the abundance of specific mRNA targets protects microRNAs which would otherwise be degraded by either XRN1 or XRN2 in *C. elegans* (Chatterjee et al., 2011). Recent work has evidenced TMMP in a human U2OS cell line, where limited mRNA target abundance caused microRNA instability and turnover, whereas microRNAs with abundant seed matched targets were stably encorporated into the RISC complex (Pitchiaya et al., 2017). This was extended to show that microinjection of an ‘anti-miR’, a construct complementary to microRNAs to prevent their binding to targets, was also protective (Pitchiaya et al., 2017).

TMMP provides a functional mechanism to add diversity to microRNA mediated gene regulation by protecting and potentially upregulating the abundance of a microRNA which is usually degraded, either due to strand selection or due to a lack of targets. TMMP might provide a mechanism of microRNA ‘arm-switching’ from the guide to passenger strand to regulate the translation of a different subset of genes (Chatterjee et al., 2011). Furthermore, the degradation of microRNAs lacking targets could provide cells with a ‘clear-out’ mechanism, to ensure only microRNAs with targets are encorporated into RISC.

8.2 Previous evidence for facilitatory regulation of mRNA targets by microRNAs

The previous work by Jovičić (2011), described a co-existence between multiple microRNAs, including miR135b and miR137, with their respective mRNA targets. This requires consideration of possible non-degrading microRNA-target interactions. Moreover, the results that I have collected show that these microRNAs are facilitatory

rather than inhibitory to their target mRNA and protein levels. These findings prompted me to review the literature with a view toward uncovering other previous evidence for positive, rather than negative, for microRNA mediated gene regulation.

Post-transcriptional stabilisation of mRNA targets by microRNAs has been described in HEK293 cells (Vasudevan and Steitz, 2007). AU-rich elements (ARE) are cis-elements within the 3' UTR of an mRNA which allow regulatory control of mRNA decay, translation and mRNA export; proteins which bind to AREs can affect mRNA stability (Vasudevan et al., 2007). Inducing cellular quiescence increased 3' UTR ARE dependent translational activation of TNFα in conjunction with FXR1-iso-a and Ago2 (Vasudevan and Steitz, 2007). In addition, 5 microRNAs which target the ARE upregulated TNFα mRNA translation by recruiting Ago2 and FXR1-iso-a during cell cycle arrest (Vasudevan and Steitz, 2007, Vasudevan et al., 2007). These studies provide evidence for differential microRNA activity depending on the cell cycle, with translational repression dominating in proliferating cells and translational activation in nondividing cells (Vasudevan et al., 2007, Vasudevan and Steitz, 2007).

This was extended to *X. laevis* oocytes, where the authors hoped to establish whether microRNA mediated translational activation was important in maintaining the naturally quiescent oocyte in an immature state (Mortensen et al., 2011). Genes selectively expressed in the immature oocyte include *Myt1* Kinase; it was shown that miR16 upregulated this mRNA through non-seed matched base pairing, whereas depletion of *Myt1* or miR16 triggered the loss of oocyte immaturity (Mortensen et al., 2011). Within immature oocytes, GW182, an important RISC associated scaffolding protein which brings together factors regulating translational repression and mRNA degradation was not associated to Ago proteins (Mortensen et al., 2011). This would suggest that immature, cell-cycle arrested cells create a microRNA-loaded RISC devoid of GW182 to promote translational activation, in conjunction with AGO2 and FXR1-iso-a (Vasudevan and Steitz, 2007, Mortensen et al., 2011).

microRNA mediated target activation has been described in the brain; however, this was again via non-canonical microRNA-target pairing. miR346 was shown to upregulate *RIP140* mRNA by binding to its 5'UTR in an Ago2-independent manner in the mouse brain (Tsai et al., 2009). More recently, miR346 was shown in human primary neurons

and HeLa cells to target the 5' UTR of the *Amyloid Precursor Protein* (*APP*) mRNA to upregulate its translation, and thereby amyloid-beta (Aβ) production, in an Ago2 dependent manner (Long et al., 2019). This target site overlapped with an iron-response element and an interleukin-1 acute box element, which interact with IRP1 and various cytokines, respectively (Long et al., 2019). These results provided possible new modes of inhibiting the miR346 and APP interaction that could decrease Aβ production in Alzheimer's disease.

Recent evidence shows miR135b to upregulate the expression of its targets *RASAL2* and *Atp1b1* in pancreatic cancer, to act as a tumour suppressor, contrary to other literature (Yin et al., 2019). However, this interaction invoked base pairing beyond the seed sequence of the microRNA. Furthermore, a study which aimed to investigated gene networks disturbed in Schizophrenia showed that up- or down-regulation of miR137 bidirectionally regulated 500 genes (Olde Loohuis et al., 2017). However, this study did not control for indirect regulation of targets, and many identified genes did not contain seed sites, suggesting non-canonical interactions with miR137 (Olde Loohuis et al., 2017).

Though these studies show evidence for non-degrading microRNA-target interactions or microRNA mediated translational activation, this is often due to microRNA-target pairing within the 5' UTR, in AREs or non-seed matched pairing. Though it can be argued that mature neuronal cells are not proliferating and may resemble quiescent cells, in contrast to the claims of Vasudevan and Steitz (2007), microRNA mediated translational repression has been demonstrated more frequently than activation within the brain (Kosik, 2006).

8.3 miR135b and miR137 protect, rather than oppose, the expression of their mRNA targets

This thesis provides further evidence for miR135b and miR137's co-existence with and/or positive regulation of the abundances of their mRNA targets via canonical 3'UTR seed-matched base pairing within neurons. I attempted to further validate the relationship between miR135b and miR137 and their respective mRNA targets, to elucidate the potential function of their co-existence and explore the translational

regulation of their targets. I propose this relationship may be based on the formation of RNA granules, which may serve to regulate RNA transport within neurons. Since neurons are highly polarised cells whose function is dependent on the segregation of proteins and mRNA to different cellular sub-compartments, this regime would serve an obvious purpose. Moreover, strengthening and weakening of connections between neurons through signal-dependent mRNA translation is known to modulate the connectivity and plasticity of any synapse in the brain. Given that many of the mRNA targets of microRNAs 135b and 137 have important roles at synapses (as outlined in **Table 8.1**), their spatiotemporally restricted microRNA mediated regulation of translation might also be key in regulating neuronal connectivity.

Corroborating the results of Jovičić (2011), overexpression of either miR135b or miR137 did not decrease the levels of their target mRNAs or proteins. Instead, overexpression of both of these microRNAs either maintained or positively modulated the abundances of their target mRNAs (**Figure 3.4 and 3.5**). This suggests the existence of a mechanism for microRNA mediated mRNA protection. This interpretation was further corroborated in my subsequent experiments.

An increase in mRNA upon microRNA overexpression suggests an increased pool available for protein translation. Subsequent experiments showed that the dynamics between mRNA and protein levels varied by microRNA and target. No increases were observed in miR135b target protein Bsn or in miR137 target proteins Ptpn5 and Gabra1 (**Figure 3.7B, 3.8A and 3.8B**). In contrast, miR137 overexpression caused its target Syt1 to be significantly increased at both the mRNA and protein levels in cortical neurons under our experimental conditions (**Figure 3.8**). These findings do not definitively prove that neuronal microRNAs facilitate their target mRNAs' translation but nonetheless support this possibility. Furthermore, as evidenced by other groups, the formation of a non-canonical microRNA-RISC complex (for example one devoid of GW182) may result in the translational activation over repression (Vasudevan et al., 2007, Mortensen et al., 2011). It could therefore be suggested that miR137 and Syt1 interact via a translationally activating RISC under the conditions of my experiments.

	Target	Function	Disease Implications	Key References
miR135b	***Atp1b1***	• β_1 subunit of neuronal Na^+/K^+ ATPase which restores the resting membrane potential after action potential induced depolarisation • *Atp1b1* expression is directly correlated to neuronal activity and controlled by transcription factors NRF-1 and Sp4	• Decreased in depression in humans and animal models • Decreased in stress • Decreased in traumatic brain injury induced seizures	(Silva et al., 2011, Johar et al., 2012, Johar et al., 2014, de Lores Arnaiz and Ordieres, 2014)
	Bsn	• Presynaptic scaffolding protein which delineates synaptic active zones to regulate neurotransmitter release • Might be involved in synaptic vesicle recruitment	• Mutation in *Bsn* implicated in hereditary and sporadic progressive supranuclear palsy	(Hallermann et al., 2010, Gundelfinger et al., 2015, Yabe et al., 2018)
	Nsg1	• Regulates trafficking and recycling of dendritic neuronal receptors (including transferrin and GluR2 receptors)	• Interacts with APP with potential involvement in Alzheimer's disease progression	(Steiner et al., 2002, Norstrom et al., 2010, Yap et al., 2017)
	Ssr2	• Signal sequence receptor, which regulates protein translocation across the endoplasmic reticulum membrane.	• Highly expressed in subset of human melanomas promoting cancer progression	(Chinen et al., 1995, van Battum et al., 2018, Garg et al., 2016, Ho et al., 2016)
	Vamp2	• Controls synaptic vesicle fusion to neuronal presynaptic membrane • Proteolysed by tetanus toxin	• *Vamp2* mRNA and protein significantly increased after long-term antidepressant treatment • Mutated with implications in neurodevelopmental disorders: ID, axial hypotonia, autistic features, epilepsy and visual impairment	(Schiavo et al., 1992, Yamada et al., 2002, Honardoost et al., 2016, Salpietro et al., 2019)

miR137	***Ankrd12***	• Ankyrin repeat domain-containing protein • Unclear functions, but may repress nuclear receptors by recruiting HDACs	• Elevated in schizophrenia and bipolar disorder patient sera	(Zhang et al., 2004, Smirnova et al., 2019)
	Sept3	• Presynaptic GTPase, selectively expressed in neurons • Involved in neurite outgrowth and synaptic vesicle trafficking	• Polymorphisms in *Sept3* are associated with Alzheimer's Diseases	(Takehashi et al., 2004, Tsang et al., 2008)
	Lrrn3	• Brain enriched leucine rich repeat protein • Role in developing and maintaining the nervous system • Expressed in developing ganglia and motor neurons	• Polymorphisms associated with ASD • Downregulated in blood in Parkinson's Disease	(Ishii et al., 1996, Sousa et al., 2010, Jiang et al., 2019, Sakharkar et al., 2019)
	Syt1	• Presynaptic calcium sensor that coordinates neurotransmitter release	• Potential involvement in schizophrenia • Downregulated in nerve terminals at the neuromuscular junction in SMA	(Xu et al., 2009, Südhof, 2013, Siegert et al., 2015, Tejero et al., 2016, He et al., 2018a)
	Ptpn5	• Regulates AMPA and NMDA receptor endocytosis • Abundant in striatal and cortical neurons	• Increased expression in Alzheimer's Disease related Aβ accumulation and increased NMDAR endocytosis leading to cognitive defecit • Elevated levels in postmortem Schizophrenic brains • Decreased in Huntington's disease striatum	(Lombroso et al., 1991, Boulanger et al., 1995, Yang et al., 2012a, Karasawa and Lombroso, 2014)
	Slc6a1	• Voltage dependent GABA Transporter 1, responsible for presynaptic GABA re-uptake	• Loss of function causes epilepsy with mild to moderate ID – these phenotypes can present independently	(Carvill et al., 2015, Johannesen et al., 2018, Cai et al., 2019)
	Gabra1	• Alpha-1 subunit of the GABA-A receptor which receives GABA neurotransmitter at the postsynaptic membrane	• Mutated in patients with epilepsy	(Hernandez et al., 2019)
	Fam126b	• Member of leukodystrophy protein family *Fam126* • Subunit of phosphotidyl inositol-4-kinase	• Mutations could lead to a defective myelin sheath as with *Fam126a*	(Gazzerro et al., 2012, Baskin et al., 2016)

Table 8.1: miR135b and miR137 mRNA targets, functions, and implications in neurological and or psychiatric disorders. Many mRNA targets of both miR135b and miR137 have roles at the synapse in regulating neurotransmitter receptors and neurotransmission. Furthermore, the dysregulation of these mRNAs has implications in neurological and psychiatric disease phenotypes, often related to disorders arising with microRNA dysfunction i.e. miR135b in depression and Alzheimer's Disease and miR137 in Schizophrenia, ASD and ID. Further investigation would give rise to whether mRNA related disorders are as a result of ineffective microRNA targeting.

In contrast to my results, two papers describe miR137 to negatively regulate its targets in the hippocampus, including *Syt1*, with consequences in synapse formation and impaired synaptic transmission (Siegert et al., 2015, He et al., 2018a). When exploring the effect of miR137 overexpression in cultured hippocampal neurons, I observed no difference in Gabra1 or Syt1 protein levels (consistent with (He et al., 2018a) (**Figure 3.8 and 3.9**). In contrast to results in cortical neurons, Ptpn5 protein was significantly increased in cultured hippocampal neurons after miR137 overexpression, perhaps to modulate hippocampal synaptic plasticity by neurotransmitter receptor endocytosis at the postsynaptic membrane (**Table 8.1**) (Yang et al., 2006). Though, in my experimental systems, miR137 did not degrade its targets in either brain region explored, these results may point towards a potential target and context dependent role of this microRNA.

Going forward, further exploring the effect of microRNA overexpression on targets at both the mRNA and protein level under different experimental conditions and understanding the cue-dependent switching of microRNA regulation regimes might shed light into their contextual regulation of gene expression in the brain. This might be key in neuronal function and dysfunction in pathological conditions. Furthermore, investigating the RISC components which co-segregate with different microRNA-target regulatory regimes could aid in identifying the other components necessary to direct translational repression over activation or degradation.

8.4 miR135b and miR137 appear to co-exist with their mRNA targets in RNA granules

I have demonstrated that miR135b and miR137 co-exist with and/or positively regulate their target mRNAs and proteins within the same cell type. I next explored the

hypothesis that microRNAs and their targets exist in the same sub-cellular compartments. This phenomenon was analysed biochemically with sucrose gradient fractionation and immunoprecipitation and in-situ via FISH/ICC.

8.4.1 Distribution of microRNAs in subcellular fractions

My biochemical analysis was based on that of Krichevsky and Kosik (2001), who had previously identified RNA granules resembling tightly packed ribosomes that sedimented to denser fractions than polysomes in sucrose gradient fractionations. The packed granular structures they isolated broke down after KCl-mediated neuronal depolarisation and was coupled with a shift in their resident mRNAs moving into translating ribosomal fractions; this suggested that these granules were dynamic compartments responsible for regulating mRNA translation. Therefore, we postulated that such RNA granules could contain factors responsible for regulating the transport of translationally repressed RNAs to neuronal sub-compartments remote from the cell body. miR135b and miR137 demonstrate characteristics consistent with participating in this neuronal function.

miR135b and its mRNA targets' abundances were increased in denser sucrose fractions upon microRNA overexpression, perhaps highlighting a sequestration into RNA granules (**Figure 4.2 and 4.3**). miR135b target mRNAs are expressed both within translating and denser sucrose gradient fractions, suggesting their constitutive translation coupled with their association into fractions containing RNA granules. Importantly, miR135b was enriched within similar fractions to its mRNA targets, further implying their co-existence.

Endogenous miR137 was mainly present in lighter fractions but was significantly enriched in dense fractions after its overexpression (**Figure 4.4**). It is generally held that microRNAs first encounter and exert their repression on their targets during translation initiation; thus the presence of miR137 in monosomal fractions could be indicative of this (Chendrimada et al., 2007, Kiriakidou et al., 2007, Meijer et al., 2013). miR137 targets were localised in dense fractions, highlighting potential sequestration into RNA granules under both control and microRNA overexpression conditions (**Figure 4.5**). Moreover, miR137 and its targets showed increased overlap within the gradient upon microRNA overexpression, which suggests their co-existence (**Figure 4.5**). Moreover,

microRNA overexpression shifted mRNA expression towards polysomal fractions, which is consistent with the increases in Syt1 and Ptpn5 target proteins as observed in **Figures 3.7** and **3.8**.

8.4.2 Examination of protein components of neuronal RNA granules

Interestingly, proteins with a known involvement in RNA translational regulation and transport were shown to be present in similar fractions after sucrose gradient fractionation compared to both microRNAs and their targets. Of these, SMN (**Figure 6.4**) and MOV10 (**Figure 6.5**) were chosen to investigate further due to their roles in axonal mRNA transport and the reversal of microRNA mediated translational repression, respectively (Banerjee et al., 2009, Ottesen et al., 2018).

8.4.3 SMN

SMN protein regulates the transport of axonal mRNAs, and as such has been shown to travel rapidly and bidirectionally along axons within neuronal cultures (Zhang et al., 2003). In line with this, SMN interacts with RNAs through a non-canonical RNA binding motif and also binds multiple RBPs, including FMRP and IMP1 (as investigated in **Figure 6.2 and 6.3**). It has therefore been purported to assemble the necessary set of RNA transport granule components (Fallini et al., 2012, Ottesen et al., 2018) . Furthermore, the RBP FMRP interacts with both SMN and translationally repressed mRNAs in a microRNA dependent manner, which might provide a link between SMN and microRNA mediated transport (Höck et al., 2007, Piazzon et al., 2008, Cheever and Ceman, 2009, Wan et al., 2017). Some mRNA targets of both miR135b and miR137 investigated here (**Table 8.1**) have presynaptic roles, therefore investigating their relationships to this protein and thus axonal transport was an interesting pursuit.

Somewhat surprisingly, SMN was primarily enriched within polysomal fractions but nonetheless was present in denser fractions (**Figure 6.4**), consistent with its interaction with FMRP and its presence in RNA transport granules. Importantly, this also highlighted a pattern overlapping with microRNAs and their targets. Immunocytochemistry highlighted that SMN was present throughout our primary neurons, and overlapped with Tau staining, consistent with the literature (**Figure 7.2**) (Piazzon et al., 2008). In FISH/ICC experiments, neuronal processes stained for SMN were positive for both

miR135b and miR137, and microRNA labelling in neurites did occasionally overlap with bright SMN puncta (**Figure 7.7 and 7.13**). miR135b target Vamp2 was also visualised throughout neuronal processes positive for SMN (**Figure 7.7**). In contrast, the overlap between SMN and the miR137 target mRNA Syt1 was much less frequent (**Figure 7.13**). These experiments were therefore relatively inconclusive regarding a role for SMN in miR135b's and miR137's activities

To compensate for limitations in the FISH/ICC experiments and to validate that the overlap observed in-situ was due to a physical interaction between SMN, microRNAs and mRNAs, SMN immunoprecipitation experiments were carried out from cortical neuronal lysates. Here, it was evident that SMN did not biochemically interact with either miR135b or miR137 (**Figure 7.18**). It is nonetheless possible that SMN might transport other neuronal microRNAs and their targets that behave similarly to miR135b and miR137.

8.4.4 MOV10

MOV10 is a neurite enriched, RISC complex-associated helicase with known involvement in the signal-dependent reversal of microRNA mediated translational repression (Meister et al., 2005, Ashraf et al., 2006, Banerjee et al., 2009, Zappulo et al., 2017). MOV10 associated mRNAs, consistent with those investigated here, predominantly cluster with terms including axonal guidance and neuronal projections (Skariah et al., 2017). Furthermore, MOV10 was shown to associate with two distinct populations of RNA granules, suggesting its crucial role in RNA granule regulation (Fritzsche et al., 2013). Ashraf and colleagues showed that the Drosophila homologue of MOV10 controlled the synaptic transport and translation of CaMKII (Ashraf et al., 2006). Therefore, it was postulated that this protein might function in conjunction with the microRNA-mRNA pairs investigated here to regulate the transport and spatiotemporal translation of synaptic components.

MOV10 was primarily expressed within denser fractions of the sucrose gradient, consistent with its compartmentalisation in RNA granules (**Figure 6.5**). Furthermore, MOV10 immunostaining overlapped in its expression with Tau in both the cell body and neuronal processes (**Figure 7.2**), highlighting its neurite enrichment and potential role

in RNA transport. Both miR135b and miR137 and their respective targets were found to be present in MOV10 positive neuronal processes in FISH/ICC mainly within and proximal to the cell body with some expression in the distal neuronal process (**Figure 7.5, 7.9, 7.11**).

The observed overlap between miR135b/miR137, their targets and MOV10 within neurons required validation due to limitations in the FISH/ICC labelling rendering these experiments inconclusive. This was achieved by MOV10 immunoprecipitation from cortical neuronal lysates. Both miR135b and miR137 showed a significant enrichment within the immunoprecipitated product compared to an IgG control IP (**Figure 7.18**). Interestingly, two miR135b targets (*Atp1b1* and *Bsn*, **Figure 7.19**) and five miR137 targets (*Ankrd12*, *Sept3*, *Syt1*, *Slc6a1* and *Fam126b*, **Figure 7.20**) were also significantly enriched by MOV10 IP. The results therefore indicate that these microRNAs interact in complex with MOV10 to potentially regulate the transport and the reversal of their targets' translational repression in a signal-dependent manner at synapses (Ashraf et al., 2006, Banerjee et al., 2009) (**Table 8.1**).

8.4.5 Possible non-canonical effects of miR135b and miR137 overexpression

Whilst miR135b and miR137 were shown to maintain or upregulate the levels of their own targets. miR137 was shown the decrease the abundances and the translational profile of two mRNA's which it should not canonically target via its seed sequence. miR137 overexpression led to a significant decrease in *Egr1* and *Nr4a1* mRNA compared to untransduced control cells, this was coupled with a decrease of these mRNAs within denser sucrose fractions following sucrose gradient fractionation (**Figure 5.2 and 5.4**).

On analysis of the mRNA sequences, *Egr1* was found to contain two 5-base sequences complementary to the miR137 seed sequence (**Table 5.1**), however it is shown that pairing between nucleotides 2 – 8 flanked by an adenosine at position 1 is often necessary for a microRNA-target effect (Lewis et al., 2005). Non-canonical microRNA-mRNA pairing has often been linked to microRNA sequestration, so did not explain the effect of miR137 on *Egr1* and *Nr4a1* (Wang, 2014). Though this does not rule out that miR137 may be employing a different indirect, non-canonical, mRNA targeting mechanism.

However, it was shown that miR137 targeted mRNAs which acted upstream of *Egr1* and *Nr4a1*. TargetScan and ENCORI showed miR137 to target *NAB2* which endogenously represses *Egr1*, and *MEF2A* which usually induces *Nr4a1* expression (Kumbrink et al., 2005, Shalizi et al., 2006, Bhattacharyya et al., 2013, Chen et al., 2014b). However, this shows that miR137 would need to differentially regulate NAB2 and MEF2A in order to achieve the degradation of *Egr1* and *Nr4a1*, respectively, as highlighted in my results. The possibility that the changes in *Egr1* and *Nr4a1* gene expression observed on miR137 overexpression may be due to the indirect effects of prolonged microRNA overexpression, for example by regulating neuronal cell activity, cannot be disregarded.

Interestingly, taken together, the results here show that miR137 does not direct the degradation of its own targets which were investigated in this project, but provides evidence for miR137 overexpression to direct the degradation of other mRNAs through either non-canonical or indirect mechanisms.

8.5 Further consideration of potential cooperative roles for neuronal microRNAs, mRNAs and MOV10 in RNA granules

My results provide evidence for non-degrading microRNA-target relationships between miR135b and miR137 and their respective mRNA targets. The microRNA-mRNA pairs are colocalised in overlapping fractions after sucrose gradient fractionation together with MOV10. Immunoprecipitation experiments provide evidence for miR135b and miR137's biochemical association with MOV10 together with a subset of each of their respective targets. These experiments provide evidence for miR135b or miR137 and their targets to be sequestered into RNA granules containing MOV10 protein.

I propose that there are two possible consequences for this localisation of microRNA-target pairs into RNA granules: firstly, to direct the transport of microRNA-mRNA pairs away from the neuronal cell body, and secondly, to aid in the formation of a translationally repressed reservoir of mRNAs close to synaptic sites to facilitate signal-dependent spatiotemporal protein synthesis (**Table 8.1**).

8.5.1 RNA transport

RNA transport is observed in a variety of different organisms in order to maintain discrete cellular subdomains, whether in the budding yeast or patterning the axis of *Drosophila* during development (Bertrand et al., 1998, Kiebler and Bassell, 2006). mRNA transport occurs in neuronal cell processes (axons and dendrites) to localise synaptic mRNAs to their necessary locations (Doyle and Kiebler, 2011). The transport of the mRNAs investigated here to synaptic sites will be crucial to their functions. To ensure their correct transport, these mRNAs will contain cis-element 'zip-codes' within their UTRs (Martin and Ephrussi, 2009, Doyle and Kiebler, 2011). For example, the binding of IMP1 (a trans-factor) to the cis-element in the 3'UTR of *β-actin* mRNA is a major facilitatory event in its transport (Hüttelmaier et al., 2005). An mRNA to be transported may contain multiple cis-elements and therefore might be bound to by a variety of trans-acting factors, comprising both microRNAs and RBPs.

MOV10 and FMRP are enriched within populations of Stau2 positive or Btz positive RNA granules, shown to link translational repression and transport (Fritzsche et al., 2013). Importantly, these RNA granules are very heterogenous, which highlights the importance of both MOV10 and FMRP within the granules in providing a core function. Furthermore, MOV10 is shown to interact with FMRP to regulate microRNA binding; the proximity of MOV10 and FMRP binding sites on a target 3'UTR can facilitate or inhibit microRNA mediated translational repression (Kenny et al., 2014). Importantly, FMRP and MOV10 may work in conjunction with microRNAs to control mRNA translation, which will be particularly important during transport. More recently, a link has been established between MOV10, FMRP and Ago2 in controlling NMDA triggered signal-dependent translation. The authors show FMRP to be crucial for MOV10 mediated translational regulation; furthermore, they demonstrated that NMDA receptor activation leads to the phosphorylation and dissociation of FMRP and AGO2 from the targeted mRNA, whilst MOV10 and the targeted mRNA become associated with polysomes (Kute et al., 2019). Importantly, this provides evidence that MOV10 might be acting to both inhibit and promote the translation of its target mRNAs, contextually.

RBPs binding the 3'UTRs of transcripts to be localised also provide affinity to molecular motors; for example FMRP is shown to directly couple itself and its target mRNAs to the molecular motor kinesin (Dictenberg et al., 2008). Furthermore, neuronal RNA transport granules were shown to bind directly to KIF5 and dynein to regulate their transport (Kanai et al., 2004, Elvira et al., 2006). In *Drosophila*, the MOV10 homologue Armitage was shown to regulate the translation of kinesin heavy chain protein, which the authors speculated might be the mechanism by which Armitage is able to regulate transport; this has not been explored further in vertebrate systems, however (Ashraf et al., 2006).

During transport, the mRNA must be maintained translationally repressed by RBPs and microRNAs to avoid aberrant protein expression. Once having reached their destination the mRNAs must be released for translation in a regulated manner.

8.5.2 Signal-dependent translation

Blocking protein synthesis perturbs long-term memory formation (Flexner et al., 1963). Protein synthesis at the synapse appears to be an important feature in the stabilising of memory by modulating synaptic connection structures and signal strength in a short timescale. This provides the framework for synaptic plasticity, the process by which synaptic strength can be strengthened (LTP) or weakened (LTD) over time (Malenka and Bear, 2004). Human diseases arise from the disruption of translation in neurons, including Alzheimer's Disease, ASD and FXS (Buffington et al., 2014).

Local translation at the synapse modulates individual neuronal connections. Synapses can be tagged to promote their acquisition of mRNAs which can be locally translated (Frey and Morris, 1997). During LTP, synapses become tagged to receive proteins/to attract local translation to modulate synaptic plasticity, however In the absence of *de novo* protein synthesis, the later phase of LTP was abolished (Frey and Morris, 1997). The process of RNA transport in the brain could however be more dynamic, as explained by the 'sushi-belt' model. Here, it is suggested that mRNAs are constantly trafficked bidirectionally within transport granules, where synapses which require a particular mRNA can recruit the granule and facilitate the translation of its cargo mRNA (Doyle and Kiebler, 2011).

Monosomes (single ribosomes) and translation factors are known to be localised at sites close to axonal and dendritic synapses (Biever et al., 2020). Monosomal translation provides a 'space-saving' mechanism of protein production (Biever et al., 2020). Specific transcripts appear to have a propensity for monosomal translation, polysomal translation or both (Biever et al., 2020). Interestingly, *Bsn* is an mRNA that is preferentially associated with monosomes.

Many studies have highlighted RBPs which control both transport to and translation at the synapse, including IMP1 and FMRP (Fernandez-Moya et al., 2014). For example, translational repression imparted on *β-actin* by IMP1 can be reversed upon Src-kinase phosphorylation of IMP1 (Hüttelmaier et al., 2005). Whilst metabotropic glutamate receptor activation regulates the reversible translational inhibition of the postsynaptic protein, PSD95, in a miR125a, phosphorylated FMRP and Ago2 dependent manner (Muddashetty et al., 2011, Fernandez-Moya et al., 2014).

miR125a is one of a number of microRNAs known to exist alongside synapse-enriched proteins and mRNAs in synapses, to modulate the local transcriptome thus synaptic structure and connectivity. For example, Schratt et al., (2006) showed that miR134 regulates dendritic spine volume by translationally repressing *Limk1*, an interaction which is reversed upon BDNF signalling. Moreover, miR138 represses the translation of *Lypla1* mRNA, which can reversed in a MOV10 dependent manner by NMDA signalling (Banerjee et al., 2009).

Interestingly, pre-microRNAs can also be localised to and processed locally in dendrites (Schratt et al., 2006, Bicker et al., 2013). It was shown that the loop structure within pre-miR134 served as a platform for the binding of DHX36 to prevent its synaptic processing by Dicer, thereby regulating its conversion into mature miR134. Moreover, this processing was regulated in an NMDA-dependent manner in dendrites (Lugli et al., 2005, Bicker et al., 2013, Hu and Li, 2017). These findings indicate that translational control by microRNAs can be positively or negatively regulated at the synapse in a signal-dependent manner.

8.5.3 Roles for miR135b-MOV10 and miR137-MOV10 RNA granules

The binding of multiple RBPs and microRNAs to an RNA molecule provides complex mechanisms for regulating its translational repression and intercellular transport. MOV10 might facilitate the unwinding of mRNAs to be targeted to expose the complementary seed sequence to allow miR135b or miR137 binding. In conjunction with other RBPs and motor proteins this will lead to the microRNA-target pair to be localised to RNA granules to be transported. This can be seen as analogous to MOV10's orthologue in *Drosophila,* which regulates *CAMKII* mRNA transport and translation. MOV10's interaction with FMRP also provides a potential key link to its transport and translational regulation of microRNA-bound mRNAs (Ashraf et al., 2006, Dictenberg et al., 2008, Kute et al., 2019).

I consider here that upon transport of an RNA granule there are two eventualities. Depending on the need of the neuron, the translational repression of the mRNA target during its transport can be reversed promptly upon reaching its destination to modulate synaptic connectivity in line with a steady state of the neuron's activity. Here, the translational repression imparted on the target will be transient, whereby no change in global mRNA abundances may be observed. Alternatively, an RNA granule may reside in the synapse maintaining the translational repression of the cargo mRNA in a microRNA-RBP dependent manner; this would create an mRNA reservoir to facilitate signal-dependent translation i.e. stimulated by NMDA receptor activation. In this situation there may be an accumulation of mRNA with increasing microRNA abundance, with little change in protein abundance or possibly an increase in protein abundance dependent on reaching the threshold required to reverse translational repression.

Since many targets of miR135b and miR137 have important roles in modulating neuronal connectivity and were colocalised with MOV10, this seems to be an obvious candidate translational co-regulator. However, there were a subset of synaptic targets for each microRNA which did not co-immunoprecipitate with MOV10, which suggests that these may be transported in some other, MOV10-independent manner (Fritzsche et al., 2013).

8.5.3.1 miR135b

In the brain, miR135b has known and suspected links to neuropsychiatric and neurodegenerative disorders including depression, PTSD, Parkinson's Disease, Alzheimer's Disease and Schizophrenia (Issler et al., 2014, Rossi et al., 2014, Fernandez-Santiago et al., 2015, Zhang et al., 2016, Sillivan et al., 2019). Its pri-microRNA is transcribed from a region which is a susceptibility locus for bipolar disorder (Issler et al., 2014). Outside the brain miR135b has been implicated in oncogenesis. miR135b contributes to cancers throughout the body, with its overexpression directly correlated to the ability of cancerous cells to form tumours (Khatri and Subramanian, 2013). It is unknown whether this relates to an abnormal expression of miR135b or an extension of its normal function in these tissues.

Consistent with a pro-survival activity, gene regulation by miR135b in the brain seems to be largely neuroprotective. miR135b positively increases the capacity for axon growth and regeneration through its inhibition of an inhibitory factor, *KLF4* (van Battum et al., 2018). miR135b also increases serotonin levels in monoaminergic neurons (Issler et al., 2014). Furthermore, miR135b negatively regulates *DISC1* mRNA, a gene which is a risk factor for schizophrenia and mood disorders (Rossi et al., 2014). In Alzheimer's Disease, miR135b negatively regulates *BACE1* which decreases the accumulation of β-amyloid – a loss of miR135b could exacerbate the progression of this neurodegenerative disorder (Zhang et al., 2016).

Though miR135b is clearly important for brain health, it has thus far been reported that it acts through negatively regulating its mRNA targets via a canonical mechanism (Eichhorn et al., 2014). My research clearly demonstrates that this is not the case for any of the targets investigated here, at least under these experimental conditions in cortical neurons. Instead, miR135b overexpression was shown to either maintain or significantly increase the abundance of its mRNA targets. The mode by which miR135b regulates its targets might be dependent on cellular context or mRNA-directed features. Specifically, in the case of *Bsn*, miR135b overexpression increased the pool of *Bsn* mRNA, which was one of two mRNA targets biochemically associated to MOV10. This suggests that *Bsn* mRNA transport is coupled to the creation of a reserve pool of *Bsn* mRNA. The reversal

of miR135b mediated translational repression could lead to a large upregulation in Bsn protein, perhaps to regulate the delineation of presynaptic active zones. It was not possible in my experiments to discriminate whether a subset of synapses might have been facilitated in this manner.

8.5.3.2 miR137

miR137 also appears to have roles in regulating the stability and transport of its mRNA targets in cortical and hippocampal neurons. Interestingly, it was also present in translating ribosomal fractions and increased the levels of some of its target proteins. With such an apparently complex role of this microRNA in regulating its target mRNA and protein expression, it is not surprising that its dyshomeostasis could be detrimental to proper neuronal function (Willemsen et al., 2011). SNPs in the *MIR137HG* are known to be associated with Schizophrenia, with the major risk allele *rs1625579* producing reduced miR137 (Ripke et al., 2011). Furthermore, microdeletions within the host gene are linked to vulnerability to ASD and ID, again associated with a decrease in miR137 and its precursors (Willemsen et al., 2011). Corroborating this finding in an experimental system, a conditional knock-out of miR137 in mice led to the presentation of behaviours mimicking ASD (Cheng et al., 2018). Schizophrenia, ASD and ID are all neurodevelopmental conditions, further highlighting the importance of miR137 during brain development.

Furthermore, alongside targets investigated here, many other schizophrenia associated genes are potential miR137 targets whose dysregulation might negatively impact LTP and axonal guidance during neurodevelopment (Wright et al., 2013). Proteins within the PI3K-Akt-mTOR pathway are putative miR137 targets. miR137 targets the *ErbB* receptor, when bound by Nrg1 triggers this pathway which is crucial in regulating synaptic plasticity, neurite outgrowth, learning and memory (Thomas et al., 2017). This group showed that the inhibition of endogenous miR137 negatively affected BDNF and Nrg1 stimulated activation of the PI3K-Akt-mTOR pathway with consequent effects on mRNA translation, glutamate receptor expression and neurite outgrowth (Thomas et al., 2017). Dysregulation of this pathway and reduced neuronal connectivity is evident in schizophrenic patients, suggesting that miR137 might be crucial in regulating cellular

pathways necessary for neuronal health, alongside facilitating the transport and translation of mRNAs involved in synaptic connectivity.

Though it might seem logical that increasing miR137 in the brain could have positive effects, this is not the case. Evidence in the literature shows that miR137 overexpression in the hippocampus caused reduced synaptic spine density and synaptic vesicle numbers together with decreased LTP and learning behaviour (Siegert et al., 2015, He et al., 2018a). Moreover, transgenic mice overexpressing miR137 in neurons driven by the Thy-1 promoter displayed phenotypes consistent with Schizophrenia, including social and cognitive deficits and altered brain architecture within the prefrontal cortex (Arakawa et al., 2019). However, in all of these studies, the effects of miR137 overexpression were reported to occur through target mRNA degradation (Siegert et al., 2015, He et al., 2018a).

In contrast, I have shown consistently that miR137 coexists with its targets in cultured cortical neurons, either maintaining or increasing their mRNA and protein abundances. However, taking together my results and the available literature suggests that miR137 might potentially regulate its targets differently depending on the context (e.g. between brain regions, at different developmental stages, etc.). I hypothesised that this may be due to the real-time thresholds of signals necessary for the reversal of translational repression, or the presence of a non-canonical RISC which may activate translation rather than degradation. Previous groups have shown that this may be mediated through the absence of GW182 interactions, therefore the abolition of the coupling between repression, deadenylation, decapping and degradation (Mortensen et al., 2011).

Evidence in the literature suggests that upregulation or downregulation of miR137 can have adverse consequences on brain function (Thomas et al., 2018). This suggests that the levels of miR137 must be tightly controlled. As for miR135b, the association between the neurite enriched MOV10 and miR137 could provide a missing link contributing to the transport and signal-dependent translation and transport of its mRNA targets.

8.6 Future Directions

8.6.1 Age and context dependent roles of miR135b and miR137

My work has shown non-degrading relationships between miR135b and miR137 and their targets when investigated in E16 cortical neuronal cultures. However, I have speculated that differences in microRNA mediated translational regulation observed by myself and other groups could be due to developmental age, model system and brain region. Therefore, investigating the effects of microRNA overexpression on their targets in animals of varying developmental and postnatal stages could provide more of an insight as to how these microRNAs regulate gene expression over time. Furthermore, this could be extended to assessing microRNA-mRNA relationship profiles in various brain regions. Another interesting route would be to investigate the consequences of non-degrading microRNA-target relationships on the protein expression of a wider range of mRNA targets.

8.6.2 RISC complex components to direct translational repression versus translational activation

Evidence has emerged for decreased GW182 association with AGO proteins in the RISC complex to direct microRNA mediated translational activation over degradation in quiescent cells (Mortensen et al., 2011). Though neurons might be characterised as quiescent, microRNA mediated translational repression coupled to degradation has been widely described (Kosik, 2006). However, my work shows evidence for microRNA mediated mRNA upregulation, which is coupled to translational activation for Syt1 and Ptpn5 in cortical and hippocampal neurons, respectively.

Future experiments to elucidate which members of the RISC complex associate with miR135b and miR137 in immunoprecipitation experiments could provide evidence for specific factors directing alternate microRNA regimes. For example, complexes directing degradation may differ from those directing translational repression, compared to those directing translational upregulation. This would provide scope for elucidating the full repetoire of microRNA mechanisms.

8.6.3 Investigation of factors regulating RNA granule transport

As noted above, mRNA must be transported in a translationally repressed granule in order to reach a strictly compartmentalised localisation within a neuron. This is key in regulating neuronal polarity. My experiments have provided evidence for a biochemical association between the RBP MOV10, known to regulate translation, to both miR135b and miR137 and a subset of their respective targets (Banerjee et al., 2009). Though this protein is neurite enriched, its direct links to transport as part of an RNA granule are limited. I have speculated that its links to FMRP based on previous literature might fulfil a key association in the transport continuum (Ashraf et al., 2006, Zappulo et al., 2017, Kute et al., 2019). Therefore, it would be interesting to assess whether FMRP associates with the potential microRNA-mRNA-MOV10 granules identified in my work. This could be via immunoprecipitation or immunocytological experiments, both to provide a biochemical and visual basis for this functional RNA granule localisation within this experimental system.

8.6.4 miR135b and miR137 overexpression effects on neuronal connectivity

This thesis has highlighted a positive regulation of miR135b and miR137 on their targets. However, there were time and resource limitations on my ability to perform studies to explore the functional aspects of this relationship.

To this end, multi-electrode arrays could be used to assess the effect of microRNA overexpression on neuronal network connectivity. These provide platforms for extracellular recordings of cultured neurons to allow the measurement of extracellular field potentials elicited by a neuronal network. The changes in extracellular field potentials by miR135b and miR137 overexpression could be measured, to provide a direct indication on any potential consequences in neuronal connectivity. Overexpression of miR137 is reported to inflict synaptic defects when carrying out whole cell recordings from the hippocampus (either cultured neurons or from slices) (Siegert et al., 2015, He et al., 2018a). The effect of miR135b or miR137 modulation has not been assessed using MEAs and might provide useful insight as to how these microRNAs regulate synaptic plasticity.

8.6.5 Do miR135b and miR137 regulate the signal-dependent translation of their target mRNAs?

Some conditions under which microRNA mediated translational repression can be reversed in a signal-dependent manner are known to be directly regulated by MOV10 (Banerjee et al., 2009). Photoconvertible florescent reporters could be utilised to investigate the necessity of miR135b and miR137 in regulating the signal-dependent translation of their mRNA targets. This was attempted during the final year of my experiments, however the cloning of the photoconvertible reporters was not achieved in time. The envisaged experiments were for the coding sequence for the photoconvertible fluorescent protein, Dendra2, to be ligated to 3' UTRs of miR135b and miR137 mRNA targets. In addition, Dendra2 would also be ligated to 3' UTRs which have had their microRNA seed sequence (the 7-mer sequence to which the microRNA binds) mutated as a negative control. This would allow determination of whether RNA transport and signal-dependent translation is dependent on the microRNA binding to its mRNA target and the reversal thereof.

Dendra2 fluoresces green (excitation/emission: 490/507), and upon UV irradiation or photoconversion by the 488nm laser, is converted irreversibly to fluoresce red (excitation/emission: 553/573) (Chudakov et al., 2007). Dendra2 has been altered from the original protein, Dendra, by an A224V mutation which causes it to fluoresce brighter at both green and red wavelengths (Chudakov et al., 2007). This protein has successfully been employed by other groups to investigate mRNA transport and protein translation in both mice and zebrafish (Pilaz et al., 2016, Torvund-Jensen et al., 2018).

Upon transfection of the Dendra2-3'UTR constructs into neuronal cells, the transport of reporter-UTRs and local protein translation could have been monitored in real-time. Prior to the application of a signal to reverse translational repression, all translated Dendra2 constructs would be photoconverted to red. The resultant translation of protein (green fluorescence) upon application of a signal, i.e. NMDA, could then be monitored in real time. Using this methodology, a variety of different factors could be analysed, including the signals necessary to reverse microRNA mediated translational

repression, the dosage of identified signals, and the localisation of translated protein in-vitro.

Alongside the signal-dependent translation of mRNA targets, microRNA levels themselves are altered during LTP and LTD. The differential modulation of microRNAs during these plasticity behaviours could be another way in which long-lasting changes at the synapse are implemented. Many microRNAs have been shown to be upregulated at specific timepoints after chemical LTP or metabotropic glutamate receptor dependent LTD in the hippocampus (Park and Tang, 2009). The authors suggest that microRNA upregulation during synaptic plasticity behaviours are to reduce protein synthesis (Park and Tang, 2009).

miR135b has been identified in dendritic spines, and was additionally shown to be upregulated at the pri- and mature level in hippocampal neurons after LTD (Hu et al., 2014). Inhibiting miR135b prevents shrinkage in dendritic spines upon NMDA-induced LTD, miR135b imparts this by negatively regulating complexin-1 and -2 which usually regulate AMPA receptor exocytosis (Hu et al., 2014). Furthermore, pre-microRNAs are shown to localise to dendrites and be processed by Dicer into mature microRNAs in a signal-dependent manner to modulate the local transcriptome (Lugli et al., 2005, Bicker et al., 2013). Going forward, the axonal and dendritic localisation of both pre-miR135b and pre-miR137, and their signal-dependent maturation could be analysed in a similar way as performed by Bicker et al., (2013) to identify whether the pre-microRNAs themselves might be poised locally in neuronal terminals to modulate the effects of their targets.

Synaptic plasticity at the dendritic postsynaptic terminal has been heavily studied, but axonal plasticity less so. Bicker et al., (2013) noted that pre-miR137 was not localised to the dendritic compartment, but this does not rule out pre- or mature miR137 being localised to the presynaptic compartment where it could in turn regulate many of its presynaptic targets. This possibility merits further investigation.

8.6.6 Investigating off-target effects of microRNA overexpression

My experiments provided evidence for significant apparent off-target effects of miR137 in its regulation of miR124 targets *Egr1* and *Nr4a1*. These results could be explained by

miR137's targeting of *NAB2*, which negatively regulates *Egr1* expression and *MEF2A*, which positively regulates *Nr4a1* expression. However, experimental evidence to corroborate that miR137 positively regulates *NAB2* and negatively regulates *MEF2A* mRNAs will be necessary to elucidate if this was indeed the pathway which led to the degradation of *Egr1* and *Nr4a1* mRNAs following miR137 overexpression. This could be investigated via qPCR and western blot analysis of NAB2 and MEF2A abundances following miR137 overexpression compared to untransduced cells. These experiments could provide evidence for miR137's participating in canonical and non-degrading microRNA regimes within cortical neurons.

However, should miR137 overexpression not have the predicted effects on either *NAB2* or *MEF2A* mRNAs, some other non-canonical miR137 targeting of *Egr1* and *Nr4a1* mRNAs would need to be investigated further. This could be achieved by exploring the effect of microRNA overexpression on overall neuronal activity, and its consequent modulation on gene expression.

8.7 Concluding Remarks

This thesis has highlighted novel roles for neuron-enriched microRNAs miR135b and miR137 on the regulation of their mRNA targets. In contrast to the previous literature, I have described a novel mechanism for microRNA mediated target protection which is mediated by 3' UTR microRNA-target interactions. I have shown that miR135b and miR137 co-exist with and/or positively modulate the expression of their target mRNAs, with either no effect or a positive modulation on their consequent translation.

Here, I propose a model (**Figure 8.1**) whereby miR135b and miR137 are packaged into RNA granules positive for the protein MOV10. MOV10 and its associated RBPs may facilitate the sorting of translationally repressed microRNA-mRNA pairs into distinct populations of RNA granules, which are transported to sites remote from the cell body, for example the pre- and postsynaptic terminals (consistent with the roles of many miR135b- and miR137- mRNA targets). This translational repression can be reversed in a signal-dependent manner in order to modulate synaptic and neuronal connectivity. Furthermore, RNA granule transport may also serve to form a reservoir of mRNAs poised

at the synapse to modulate synaptic connectivity following a signal-dependent reversal of translational repression.

I also postulate that the modulation of microRNA-mRNA binding might be threshold- and context-dependent. This would explain the effect of microRNA overexpression on Syt1 protein translation and Ptpn5 protein translation in the cortex and hippocampus, respectively. The microRNA mediated increase in translation of these mRNAs potentially occurs at a basal state in different brain regions. Therefore, I suggest that the character of the signal received by a synapse may have differential effects on whether translational repression is reversed, or possibly even to facilitate microRNA mediated mRNA degradation instead. The signals and thresholds to facilitate or reverse translational repression or to direct mRNA degradation may vary by cell type, brain region or developmental stage. Moreover, these consequences will have varying effects on synaptic plasticity throughout the brain, i.e. the regulation of LTP and LTD dependent on a microRNA and its subset of localised targets. This heterogeneity of potential

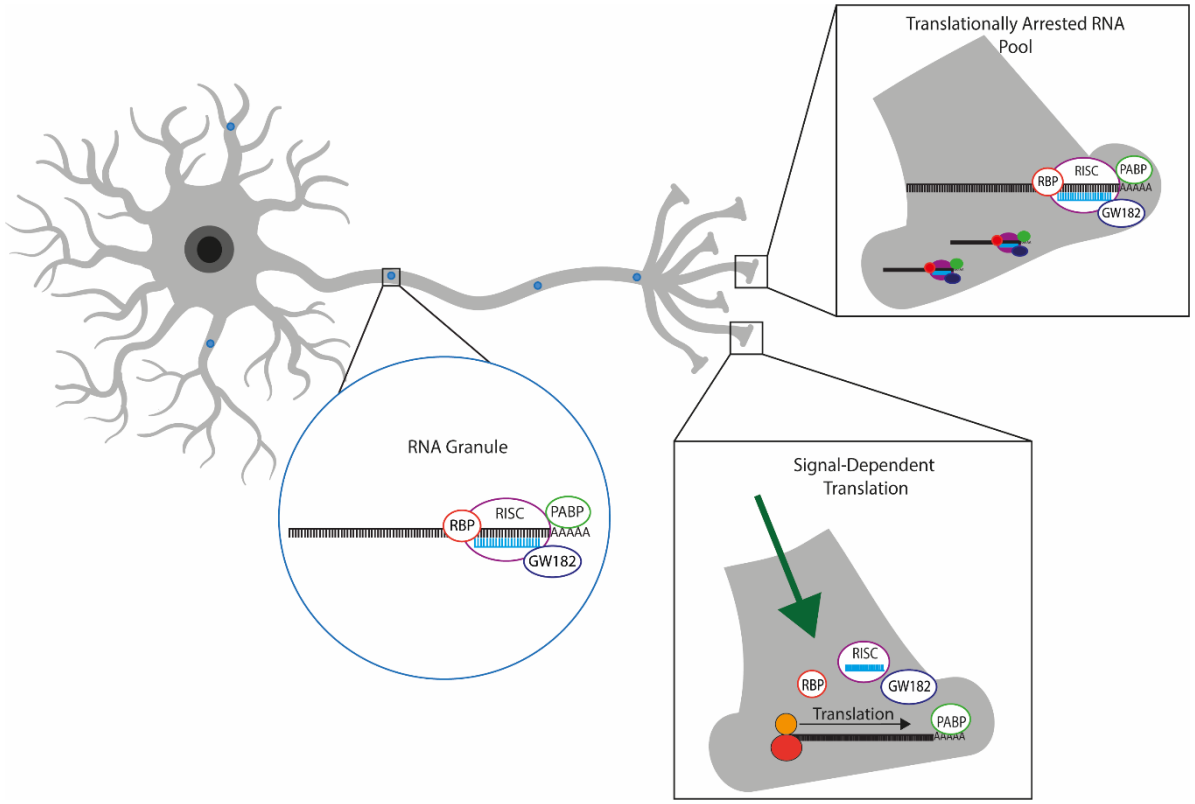

Figure 8.1: Model of neuronal RNA transport. mRNA and protein localisation are ways in which neurons maintain their polarity. Due to the specialised structure of the cell, asymmetric localisation of protein and mRNA are necessary to maintain the identity of neuronal cellular sub-compartments. To facilitate mRNA transport, mRNA must be rendered translationally silent by RBPs and other translational regulators (e.g. microRNAs). Together, they are sorted into specialised granules to be transported via molecular motors to sites remote from the cell body. Upon reaching the destination the translationally repressed mRNA will be anchored to the local cytoskeleton, likely forming a pool of mRNA to be translated. Upon the receival of a signal to the axonal/dendritic compartment, the RBP/microRNA mediated translational repression will be alleviated. Protein synthesis can occur in a discrete location in a to modulate neuronal connectivity, hence synaptic plasticity (Wilhelm and Vale, 1993, Kosik and Krichevsky, 2002, Kiebler and Bassell, 2006, Bramham and Wells, 2007).

microRNA activities provides scope for a flexible and dynamic gene regulatory role for neuronal microRNAs and their targets in influencing neuronal connectivity.

The proper functions of miR135b and miR137 are important in brain health. Should these microRNAs be crucial in regulating RNA transport, any dysfunction could result in ectopic protein expression within the brain. If proteins cannot be translated where and when required during neurodevelopment this will lead to issues in synaptic connectivity and eventual pathological phenotypes as observed with miR137 dysfunction in schizophrenia, ASD and ID (Thomas et al., 2018). Furthermore, alongside the positive modulation of mRNAs investigated here, these microRNAs might be involved in inhibiting the expression of genes which exacerbate disease phenotypes as observed with miR135b in its regulation of *DISC1* and *BACE1* (Rossi et al., 2014, Zhang et al., 2016). The variance in the interactions of one microRNA on its many targets is an important way in which the brain can control post-transcriptional gene expression, which will be essential in maintaining neuronal health and neuronal circuitry.

It is plausible that the mechanism of microRNA-mRNA interaction may change throughout development to accommodate the differing needs of a mature brain. However, if neuronal connectivity is dysfunctional as a result of microRNA abnormalities during development, the needs of the mature brain will consequently be altered.

Future experiments exploring the functional consequences of miR135b and miR137 overexpression on neuronal network connectivity, and their role in modulating signal-dependent translation will be crucial in exploring the roles fulfilled by microRNA-mRNA coexistence. Furthermore, investigating the regulation of mRNA targets by miR135b and miR137 at different developmental stages will be key in elucidating the dynamic role of these microRNAs in the brain throughout life.

9 Appendix 1

9.1 ImageJ macro for FISH/ICC puncta quantification

9.1.1 'Puncta Analysis' macro

```
* Macro code to select stained puncta on images with up to 4 colour channels

* Selects puncta and does some simple analysis (count, average size)

* Also identifies and counts areas of overlap between channels

* Requires installation of Biovoxxel update site for convoluted background subtraction

*/


// Global Variables


minDia=0.2;

maxDia=3;

bins=100;

threshold=0.1;

filterRadius=9;

chan=newArray(5);

chan[1]=true;

chan[2]=true;

chan[3]=false;

chan[4]=true;


// Main
```

```
curImage=getTitle();


Dialog.create("Image Processing Parameters");
	Dialog.setInsets(0, 0, 0);
	Dialog.addMessage("Puncta Parameters");
	Dialog.addMessage("Puncta diameter");
	Dialog.addNumber("Minimum (um)",minDia);
	Dialog.addNumber("Maximum (um)",maxDia);
	Dialog.addNumber("Filter radius (um)",filterRadius);
	Dialog.addMessage("Threshold Parameters");
	Dialog.addNumber("Bins",bins);
	Dialog.addToSameRow();
	Dialog.addNumber("Max % change",threshold);


	Dialog.setInsets(0, 0, 0);
	Dialog.addMessage("Tick box to include channel");
	Dialog.addCheckbox("Channel 1",chan[1]);
	Dialog.addCheckbox("Channel 2",chan[2]);
	Dialog.addCheckbox("Channel 3",chan[3]);
	Dialog.addCheckbox("Channel 4",chan[4]);


Dialog.show();
```

```
minDia=Dialog.getNumber();
maxDia=Dialog.getNumber();
filterRadius=Dialog.getNumber();
bins=Dialog.getNumber();
threshold=Dialog.getNumber();
ch1=Dialog.getCheckbox();
ch2=Dialog.getCheckbox();
ch3=Dialog.getCheckbox();
ch4=Dialog.getCheckbox();

mergeString="";

for (i=1;i<=4;i++){
	if (chan[i]==true){
		detectPuncta(curImage,i,minDia,maxDia,bins,threshold);
		mergeString=mergeString + "c"+i+"=[Mask of wChan"+i+"] ";
	};
};

run("Merge Channels...", mergeString+ "create");
rename(curImage+"_Puncta");
punctaImage=getTitle();
```

```
reportPunctaOverlap(chan,punctaImage);


//End Main Code


//Functions


function reportPunctaOverlap(checkCh,image){
	n=1;
	if (isOpen("Coloc")!=true){
		getDimensions(width, height, channels, slices, frames);
		getPixelSize(unit, pixelWidth, pixelHeight);
		newImage("Coloc", "8-bit black", width, height, 1);
		setVoxelSize(pixelWidth, pixelHeight, 1, "um");
	};


	for(i=1;i<=4;i++){
		if (checkCh[i]==true){
			selectWindow(image);
			run("Duplicate...", "duplicate channels="+n);
			rename("Channel"+i);
			changeValues(1,255,pow(2,i-1));
			imageCalculator("Add", "Coloc","Channel"+i);
			close("Channel"+i);
```

```
                n=n+1;
            };
        };

        for(i=1;i<16;i++){
            setThreshold(i,i);
            run("Analyze Particles...", "size=0-infinity display clear summarize");
            chComb=toBinary(i);
            while (lengthOf(chComb)<4){
                chComb="0"+chComb;
            };
            Table.set("Slice",Table.size-1,chComb);
        };

}


function detectPuncta(image,chan,lowLimit,highLimit,maxBins,th){
        print("Channel: "+chan);
        selectWindow(image);
        Stack.setChannel(chan);
        run("Select None");
```

```
	run("Duplicate...", "title=wChan"+chan);
	run("Convoluted Background Subtraction", "convolution=Gaussian radius="+filterRadius);

	getMinAndMax(min, max);
	nBins=(max-min)/maxBins;
	getHistogram(values, counts, nBins,min,max);
	getDimensions(width, height, channels, slices, frames);
	i=0;
	total=0;
	while ((counts[i]-counts[i+1])>(width*height*(th/100))){
		print(i,counts[i],counts[i+1],(counts[i]-counts[i+1])/(width*height));
		i=i+1;
	};
	getPixelSize(unit, pixelWidth, pixelHeight);
	run("Median...", "radius="+lowLimit/pixelWidth);
	setThreshold(i*100, max);
	setOption("BlackBackground", true);
	run("Convert to Mask");
	run("Watershed");
	print(pow(lowLimit/2,2)*PI);
	print(pow(highLimit/2,2)*PI);
	run("Analyze Particles...", "size="+pow(lowLimit/2,2)*PI+"-"+pow(highLimit/2,2)*PI+" show=Masks display clear include summarize");
```

```
        close("wChan"+chan);
}
```

9.1.2 'Puncta Analysis' macro automation

```
dir1 = getDirectory("Source Directory");
list = getFileList(dir1);
dir2 = getDirectory("Destination Directory");
for (i=0; i<list.length; i++) {
        path = dir1 + list[i];
        open(path);
        title1 = getTitle();
        title2 = File.nameWithoutExtension;
        runMacro("PunctaAnalysis_v1");
        selectWindow(title2+".tif_Puncta");
        saveAs("Tiff", dir2+title2+"_Puncta.tif");
        selectWindow("Summary");
        saveAs("Results", dir2+title2+"_summary.csv");
        selectWindow(title2+"_summary.csv");
        run("Close");
        run("Close All");

}
run("Close All")
```

10 Bibliography

ADHIKARI, P., OROZCO, D., RANDHAWA, H. & WOLF, F. W. 2019. Mef2 induction of the immediate early gene Hr38/Nr4a is terminated by Sirt1 to promote ethanol tolerance. *Genes, Brain and Behavior,* 18**,** e12486.

AGARWAL, V., BELL, G. W., NAM, J. W. & BARTEL, D. P. 2015. Predicting effective microRNA target sites in mammalian mRNAs. *Elife,* 4.

ALAMI, N. H., SMITH, R. B., CARRASCO, M. A., WILLIAMS, L. A., WINBORN, C. S., HAN, S. S. W., KISKINIS, E., WINBORN, B., FREIBAUM, B. D., KANAGARAJ, A., CLARE, A. J., BADDERS, N. M., BILICAN, B., CHAUM, E., CHANDRAN, S., SHAW, C. E., EGGAN, K. C., MANIATIS, T. & TAYLOR, J. P. 2014. Axonal transport of TDP-43 mRNA granules is impaired by ALS-causing mutations. *Neuron,* 81**,** 536-543.

AMERES, S. L., HORWICH, M. D., HUNG, J.-H., XU, J., GHILDIYAL, M., WENG, Z. & ZAMORE, P. D. 2010. Target RNA-directed trimming and tailing of small silencing RNAs. *Science (New York, N.Y.),* 328**,** 1534-1539.

ANNAMNEEDI, A., CALISKAN, G., MULLER, S., MONTAG, D., BUDINGER, E., ANGENSTEIN, F., FEJTOVA, A., TISCHMEYER, W., GUNDELFINGER, E. D. & STORK, O. 2018. Ablation of the presynaptic organizer Bassoon in excitatory neurons retards dentate gyrus maturation and enhances learning performance. *Brain Struct Funct,* 223**,** 3423-3445.

ARAKAWA, Y., YOKOYAMA, K., TASAKI, S., KATO, J., NAKASHIMA, K., TAKEYAMA, M., NAKATANI, A. & SUZUKI, M. 2019. Transgenic mice overexpressing miR-137 in the brain show schizophrenia-associated behavioral deficits and transcriptome profiles. *PLoS One,* 14**,** e0220389.

ASHRAF, S. I., MCLOON, A. L., SCLARSIC, S. M. & KUNES, S. 2006. Synaptic Protein Synthesis Associated with Memory Is Regulated by the RISC Pathway in Drosophila. *Cell,* 124**,** 191-205.

ASIMINAS, A., JACKSON, A. D., LOUROS, S. R., TILL, S. M., SPANO, T., DANDO, O., BEAR, M. F., CHATTARJI, S., HARDINGHAM, G. E., OSTERWEIL, E. K., WYLLIE, D. J. A., WOOD, E. R. & KIND, P. C. 2019. Sustained correction of associative learning deficits after brief, early treatment in a rat model of Fragile X Syndrome. *Science Translational Medicine,* 11**,** eaao0498.

AUYEUNG, V. C., ULITSKY, I., MCGEARY, S. E. & BARTEL, D. P. 2013. Beyond secondary structure: primary-sequence determinants license pri-miRNA hairpins for processing. *Cell,* 152**,** 844-58.

BAEK, D., VILLEN, J., SHIN, C., CAMARGO, F. D., GYGI, S. P. & BARTEL, D. P. 2008. The impact of microRNAs on protein output. *Nature,* 455**,** 64-71.

BAHRAMI, S. & DRABLØS, F. 2016. Gene regulation in the immediate-early response process. *Advances in Biological Regulation,* 62**,** 37-49.

BAI, R., LI, D., SHI, Z., FANG, X., GE, W. & ZHENG, S. 2013. Clinical significance of Ankyrin repeat domain 12 expression in colorectal cancer. *Journal of Experimental & Clinical Cancer Research,* 32**,** 35.

BAKER, K., GORDON, S. L., MELLAND, H., BUMBAK, F., SCOTT, D. J., JIANG, T. J., OWEN, D., TURNER, B. J., BOYD, S. G., ROSSI, M., AL-RAQAD, M., ELPELEG, O., PECK, D., MANCINI, G. M. S., WILKE, M., ZOLLINO, M., MARANGI, G., WEIGAND, H., BORGGRAEFE, I., HAACK, T., STARK, Z., SADEDIN, S., TAN, T. Y., JIANG, Y., GIBBS, R. A., ELLINGWOOD, S., AMARAL, M., KELLEY, W., KURIAN, M. A., COUSIN, M. A.

& RAYMOND, F. L. 2018. SYT1-associated neurodevelopmental disorder: a case series. *Brain,* 141**,** 2576-2591.

BANERJEE, S., NEVEU, P. & KOSIK, K. S. 2009. A Coordinated Local Translational Control Point at the Synapse Involving Relief from Silencing and MOV10 Degradation. *Neuron,* 64**,** 871-884.

BARTEL, D. P. 2004. MicroRNAs: genomics, biogenesis, mechanism, and function. *Cell,* 116**,** 281-97.

BARTEL, D. P. 2009. MicroRNAs: target recognition and regulatory functions. *Cell,* 136**,** 215-33.

BASKIN, J. M., WU, X., CHRISTIANO, R., OH, M. S., SCHAUDER, C. M., GAZZERRO, E., MESSA, M., BALDASSARI, S., ASSERETO, S., BIANCHERI, R., ZARA, F., MINETTI, C., RAIMONDI, A., SIMONS, M., WALTHER, T. C., REINISCH, K. M. & DE CAMILLI, P. 2016. The leukodystrophy protein FAM126A (hyccin) regulates PtdIns(4)P synthesis at the plasma membrane. *Nat Cell Biol,* 18**,** 132-8.

BATES, M., JONES, S. A. & ZHUANG, X. 2013. Stochastic optical reconstruction microscopy (STORM): a method for superresolution fluorescence imaging. *Cold Spring Harb Protoc,* 2013**,** 498-520.

BATTICH, N., STOEGER, T. & PELKMANS, L. 2013. Image-based transcriptomics in thousands of single human cells at single-molecule resolution. *Nature Methods,* 10**,** 1127.

BENTLEY, M. & BANKER, G. 2016. The cellular mechanisms that maintain neuronal polarity. *Nat Rev Neurosci,* 17**,** 611-622.

BERNSTEIN, P., PELTZ, S. W. & ROSS, J. 1989. The poly(A)-poly(A)-binding protein complex is a major determinant of mRNA stability in vitro. *Mol Cell Biol,* 9**,** 659-70.

BERTRAND, E., CHARTRAND, P., SCHAEFER, M., SHENOY, S. M., SINGER, R. H. & LONG, R. M. 1998. Localization of ASH1 mRNA particles in living yeast. *Mol Cell,* 2**,** 437-45.

BHATTACHARYYA, S., FANG, F., TOURTELLOTTE, W. & VARGA, J. 2013. Egr-1: new conductor for the tissue repair orchestra directs harmony (regeneration) or cacophony (fibrosis). *The Journal of pathology,* 229**,** 286-297.

BICKER, S., KHUDAYBERDIEV, S., WEISS, K., ZOCHER, K., BAUMEISTER, S. & SCHRATT, G. 2013. The DEAH-box helicase DHX36 mediates dendritic localization of the neuronal precursor-microRNA-134. *Genes Dev,* 27**,** 991-6.

BIEVER, A., GLOCK, C., TUSHEV, G., CIIRDAEVA, E., DALMAY, T., LANGER, J. D. & SCHUMAN, E. M. 2020. Monosomes actively translate synaptic mRNAs in neuronal processes. *Science,* 367.

BITETTI, A., MALLORY, A. C., GOLINI, E., CARRIERI, C., CARRENO GUTIERREZ, H., PERLAS, E., PEREZ-RICO, Y. A., TOCCHINI-VALENTINI, G. P., ENRIGHT, A. J., NORTON, W. H. J., MANDILLO, S., O'CARROLL, D. & SHKUMATAVA, A. 2018. MicroRNA degradation by a conserved target RNA regulates animal behavior. *Nat Struct Mol Biol,* 25**,** 244-251.

BOULANGER, L. M., LOMBROSO, P. J., RAGHUNATHAN, A., DURING, M. J., WAHLE, P. & NAEGELE, J. R. 1995. Cellular and molecular characterization of a brain-enriched protein tyrosine phosphatase. *J Neurosci,* 15**,** 1532-44.

BRAMHAM, C. R. & WELLS, D. G. 2007. Dendritic mRNA: transport, translation and function. *Nat Rev Neurosci,* 8**,** 776-789.

BRAUN, J. E., HUNTZINGER, E. & IZAURRALDE, E. 2013. The role of GW182 proteins in miRNA-mediated gene silencing. *Adv Exp Med Biol,* 768**,** 147-63.

BUFFINGTON, S. A., HUANG, W. & COSTA-MATTIOLI, M. 2014. Translational control in synaptic plasticity and cognitive dysfunction. *Annual review of neuroscience,* 37**,** 17-38.

BURACK, M. A., SILVERMAN, M. A. & BANKER, G. 2000. The role of selective transport in neuronal protein sorting. *Neuron,* 26**,** 465-72.

CAI, K., WANG, J., EISSMAN, J., NWOSU, G., SHEN, W., LIANG, H. C., LI, X. J., ZHU, H. X., YI, Y. H., SONG, J., XU, D., DELPIRE, E., LIAO, W. P., SHI, Y. W. & KANG, J. Q. 2019. A missense mutation in SLC6A1 associated with Lennox-Gastaut syndrome impairs GABA transporter 1 protein trafficking and function. *Exp Neurol,* 320**,** 112973.

CARVILL, G. L., MCMAHON, J. M., SCHNEIDER, A., ZEMEL, M., MYERS, C. T., SAYKALLY, J., NGUYEN, J., ROBBIANO, A., ZARA, F., SPECCHIO, N., MECARELLI, O., SMITH, R. L., LEVENTER, R. J., MØLLER, R. S., NIKANOROVA, M., DIMOVA, P., JORDANOVA, A., PETROU, S., HELBIG, I., STRIANO, P., WECKHUYSEN, S., BERKOVIC, S. F., SCHEFFER, I. E. & MEFFORD, H. C. 2015. Mutations in the GABA Transporter SLC6A1 Cause Epilepsy with Myoclonic-Atonic Seizures. *Am J Hum Genet,* 96**,** 808-15.

CHANDRADOSS, S. D., SCHIRLE, N. T., SZCZEPANIAK, M., MACRAE, I. J. & JOO, C. 2015. A Dynamic Search Process Underlies MicroRNA Targeting. *Cell,* 162**,** 96-107.

CHATTERJEE, S., FASLER, M., BUSSING, I. & GROSSHANS, H. 2011. Target-mediated protection of endogenous microRNAs in C. elegans. *Dev Cell,* 20**,** 388-96.

CHATTERJEE, S. & GROSSHANS, H. 2009. Active turnover modulates mature microRNA activity in Caenorhabditis elegans. *Nature,* 461**,** 546-9.

CHEEVER, A. & CEMAN, S. 2009. Phosphorylation of FMRP inhibits association with Dicer. *Rna.* United States.

CHEN, Y., BOLAND, A., KUZUOGLU-OZTURK, D., BAWANKAR, P., LOH, B., CHANG, C. T., WEICHENRIEDER, O. & IZAURRALDE, E. 2014a. A DDX6-CNOT1 complex and W-binding pockets in CNOT9 reveal direct links between miRNA target recognition and silencing. *Mol Cell,* 54**,** 737-50.

CHEN, Y., WANG, Y., ERTURK, A., KALLOP, D., JIANG, Z., WEIMER, R. M., KAMINKER, J. & SHENG, M. 2014b. Activity-induced Nr4a1 regulates spine density and distribution pattern of excitatory synapses in pyramidal neurons. *Neuron,* 83**,** 431-443.

CHENDRIMADA, T. P., FINN, K. J., JI, X., BAILLAT, D., GREGORY, R. I., LIEBHABER, S. A., PASQUINELLI, A. E. & SHIEKHATTAR, R. 2007. MicroRNA silencing through RISC recruitment of eIF6. *Nature,* 447**,** 823-8.

CHENG, Y., WANG, Z. M., TAN, W., WANG, X., LI, Y., BAI, B., LI, Y., ZHANG, S. F., YAN, H. L., CHEN, Z. L., LIU, C. M., MI, T. W., XIA, S., ZHOU, Z., LIU, A., TANG, G. B., LIU, C., DAI, Z. J., WANG, Y. Y., WANG, H., WANG, X., KANG, Y., LIN, L., CHEN, Z., XIE, N., SUN, Q., XIE, W., PENG, J., CHEN, D., TENG, Z. Q. & JIN, P. 2018. Partial loss of psychiatric risk gene Mir137 in mice causes repetitive behavior and impairs sociability and learning via increased Pde10a. *Nat Neurosci,* 21**,** 1689-1703.

CHI, S. W., ZANG, J. B., MELE, A. & DARNELL, R. B. 2009. Argonaute HITS-CLIP decodes microRNA-mRNA interaction maps. *Nature,* 460**,** 479-486.

CHINEN, K., SUDO, K., TAKAHASHI, E. & NAKAMURA, Y. 1995. Isolation and mapping of the human beta-signal sequence receptor gene (SSR2). *Cytogenet Cell Genet,* 70**,** 215-7.

CHUDAKOV, D. M., LUKYANOV, S. & LUKYANOV, K. A. 2007. Tracking intracellular protein movements using photoswitchable fluorescent proteins PS-CFP2 and Dendra2. *Nature Protocols,* 2**,** 2024.

CIAFRÈ, S. A. & GALARDI, S. 2013. microRNAs and RNA-binding proteins: A complex network of interactions and reciprocal regulations in cancer. *RNA Biol,* 10**,** 934-42.

CONACO, C., OTTO, S., HAN, J. J. & MANDEL, G. 2006. Reciprocal actions of REST and a microRNA promote neuronal identity. *Proc Natl Acad Sci U S A,* 103**,** 2422-7.

COSTA, C. J. & WILLIS, D. E. 2017. To the End of the Line: Axonal mRNA transport and local translation in health and neurodegenerative disease. *Developmental neurobiology*.

CROWLEY, J. J., COLLINS, A. L., LEE, R. J., NONNEMAN, R. J., FARRELL, M. S., ANCALADE, N., MUGFORD, J. W., AGSTER, K. L., NIKOLOVA, V. D., MOY, S. S. & SULLIVAN, P. F. 2015. Disruption of the microRNA 137 primary transcript results in early embryonic lethality in mice. *Biological psychiatry,* 77**,** e5-e7.

DARNELL, J. C. & KLANN, E. 2013. The Translation of Translational Control by FMRP: Therapeutic Targets for Fragile X Syndrome. *Nat Neurosci,* 16**,** 1530-6.

DAVIDOVIC, L., JAGLIN, X. H., LEPAGNOL-BESTEL, A.-M., TREMBLAY, S., SIMONNEAU, M., BARDONI, B. & KHANDJIAN, E. W. 2007. The fragile X mental retardation protein is a molecular adaptor between the neurospecific KIF3C kinesin and dendritic RNA granules. *Human Molecular Genetics,* 16**,** 3047-3058.

DE LORES ARNAIZ, G. R. & ORDIERES, M. G. L. 2014. Brain Na(+), K(+)-ATPase Activity In Aging and Disease. *International journal of biomedical science : IJBS,* 10**,** 85-102.

DICTENBERG, J. B., SWANGER, S. A., ANTAR, L. N., SINGER, R. H. & BASSELL, G. J. 2008. A direct role for FMRP in activity-dependent dendritic mRNA transport links filopodial-spine morphogenesis to fragile X syndrome. *Dev Cell,* 14**,** 926-39.

DOYLE, M. & KIEBLER, M. A. 2011. Mechanisms of dendritic mRNA transport and its role in synaptic tagging. *EMBO J,* 30**,** 3540-52.

DUCLOT, F. & KABBAJ, M. 2017. The Role of Early Growth Response 1 (EGR1) in Brain Plasticity and Neuropsychiatric Disorders. *Frontiers in Behavioral Neuroscience,* 11**,** 35.

EICHHORN, S. W., GUO, H., MCGEARY, S. E., RODRIGUEZ-MIAS, R. A., SHIN, C., BAEK, D., HSU, S. H., GHOSHAL, K., VILLEN, J. & BARTEL, D. P. 2014. mRNA destabilization is the dominant effect of mammalian microRNAs by the time substantial repression ensues. *Mol Cell,* 56**,** 104-15.

ELVIRA, G., WASIAK, S., BLANDFORD, V., TONG, X. K., SERRANO, A., FAN, X., DEL RAYO SANCHEZ-CARBENTE, M., SERVANT, F., BELL, A. W., BOISMENU, D., LACAILLE, J. C., MCPHERSON, P. S., DESGROSEILLERS, L. & SOSSIN, W. S. 2006. Characterization of an RNA granule from developing brain. *Mol Cell Proteomics,* 5**,** 635-51.

FABIAN, M. R. & SONENBERG, N. 2012. The mechanics of miRNA-mediated gene silencing: a look under the hood of miRISC. *Nat Struct Mol Biol,* 19**,** 586-93.

FALLINI, C., BASSELL, G. J. & ROSSOLL, W. 2012. Spinal muscular atrophy: the role of SMN in axonal mRNA regulation. *Brain Res,* 1462**,** 81-92.

FALLINI, C., DONLIN-ASP, P. G., ROUANET, J. P., BASSELL, G. J. & ROSSOLL, W. 2016. Deficiency of the Survival of Motor Neuron Protein Impairs mRNA Localization and Local Translation in the Growth Cone of Motor Neurons. *J Neurosci,* 36**,** 3811-20.

FALLINI, C., ROUANET, J. P., DONLIN-ASP, P. G., GUO, P., ZHANG, H., SINGER, R. H., ROSSOLL, W. & BASSELL, G. J. 2014. Dynamics of survival of motor neuron (SMN) protein interaction with the mRNA-binding protein IMP1 facilitates its trafficking into motor neuron axons. *Dev Neurobiol,* 74**,** 319-332.

FALLINI, C., ZHANG, H., SU, Y., SILANI, V., SINGER, R. H., ROSSOLL, W. & BASSELL, G. J. 2011. The survival of motor neuron (SMN) protein interacts with the mRNA-binding protein HuD and regulates localization of poly(A) mRNA in primary motor neuron axons. *J Neurosci,* 31**,** 3914-25.

FENG, W. & ZHANG, M. 2009. Organization and dynamics of PDZ-domain-related supramodules in the postsynaptic density. *Nature Reviews Neuroscience,* 10**,** 87-99.

FERNANDEZ-MOYA, S. M., BAUER, K. E. & KIEBLER, M. A. 2014. Meet the players: local translation at the synapse. *Front Mol Neurosci,* 7**,** 84.

FERNANDEZ-SANTIAGO, R., CARBALLO-CARBAJAL, I., CASTELLANO, G., TORRENT, R., RICHAUD, Y., SANCHEZ-DANES, A., VILARRASA-BLASI, R., SANCHEZ-PLA, A., MOSQUERA, J. L., SORIANO, J., LOPEZ-BARNEO, J., CANALS, J. M., ALBERCH, J., RAYA, A., VILA, M., CONSIGLIO, A., MARTIN-SUBERO, J. I., EZQUERRA, M. & TOLOSA, E. 2015. Aberrant epigenome in iPSC-derived dopaminergic neurons from Parkinson's disease patients. *EMBO Mol Med,* 7**,** 1529-46.

FILIPOWICZ, W., BHATTACHARYYA, S. N. & SONENBERG, N. 2008. Mechanisms of post-transciptional regulation by microRNAs: are the answers in sight? *Nature Reviews Genetics* 9**,** 102-14.

FIORE, R., KHUDAYBERDIEV, S., CHRISTENSEN, M., SIEGEL, G., FLAVELL, S. W., KIM, T. K., GREENBERG, M. E. & SCHRATT, G. 2009. Mef2-mediated transcription of the miR379-410 cluster regulates activity-dependent dendritogenesis by fine-tuning Pumilio2 protein levels. *Embo j,* 28**,** 697-710.

FLEXNER, J. B., FLEXNER, L. B. & STELLAR, E. 1963. Memory in mice as affected by intracerebral puromycin. *Science,* 141**,** 57-9.

FONG, N. & BENTLEY, D. L. 2001. Capping, splicing, and 3' processing are independently stimulated by RNA polymerase II: different functions for different segments of the CTD. *Genes & development,* 15**,** 1783-1795.

FREY, U. & MORRIS, R. G. 1997. Synaptic tagging and long-term potentiation. *Nature,* 385**,** 533-6.

FRITZSCHE, R., KARRA, D., BENNETT, K. L., ANG, F. Y., HERAUD-FARLOW, J. E., TOLINO, M., DOYLE, M., BAUER, K. E., THOMAS, S., PLANYAVSKY, M., ARN, E., BAKOSOVA, A., JUNGWIRTH, K., HORMANN, A., PALFI, Z., SANDHOLZER, J., SCHWARZ, M., MACCHI, P., COLINGE, J., SUPERTI-FURGA, G. & KIEBLER, M. A. 2013. Interactome of two diverse RNA granules links mRNA localization to translational repression in neurons. *Cell Rep,* 5**,** 1749-62.

FUCHS WIGHTMAN, F., GIONO, L. E., FEDEDA, J. P. & DE LA MATA, M. 2018. Target RNAs Strike Back on MicroRNAs. *Frontiers in genetics,* 9**,** 435-435.

FUKAO, A., MISHIMA, Y., TAKIZAWA, N., OKA, S., IMATAKA, H., PELLETIER, J., SONENBERG, N., THOMA, C. & FUJIWARA, T. 2014. MicroRNAs Trigger

Dissociation of eIF4AI and eIF4AII from Target mRNAs in Humans. *Molecular Cell,* 56**,** 79-89.

FUKAYA, T. & TOMARI, Y. 2011. PABP is not essential for microRNA-mediated translational repression and deadenylation in vitro. *The EMBO journal,* 30**,** 4998-5009.

GALICIA-VÁZQUEZ, G., CENCIC, R., ROBERT, F., AGENOR, A. Q. & PELLETIER, J. 2012. A cellular response linking eIF4AI activity to eIF4AII transcription. *RNA (New York, N.Y.),* 18**,** 1373-1384.

GARG, B., PATHRIA, G., WAGNER, C., MAURER, M. & WAGNER, S. N. 2016. Signal Sequence Receptor 2 is required for survival of human melanoma cells as part of an unfolded protein response to endoplasmic reticulum stress. *Mutagenesis,* 31**,** 573-582.

GARNEAU, N. L., WILUSZ, J. & WILUSZ, C. J. 2007. The highways and byways of mRNA decay. *Nat Rev Mol Cell Biol,* 8**,** 113-126.

GAZZERRO, E., BALDASSARI, S., GIACOMINI, C., MUSANTE, V., FRUSCIONE, F., LA PADULA, V., BIANCHERI, R., SCARFÌ, S., PRADA, V., SOTGIA, F., DUNCAN, I. D., ZARA, F., WERNER, H. B., LISANTI, M. P., NOBBIO, L., CORRADI, A. & MINETTI, C. 2012. Hyccin, the molecule mutated in the leukodystrophy hypomyelination and congenital cataract (HCC), is a neuronal protein. *PLoS One,* 7**,** e32180.

GEBERT, L. F. R. & MACRAE, I. J. 2019. Regulation of microRNA function in animals. *Nature Reviews Molecular Cell Biology,* 20**,** 21-37.

GERMAN, M. A., LUO, S., SCHROTH, G., MEYERS, B. C. & GREEN, P. J. 2009. Construction of Parallel Analysis of RNA Ends (PARE) libraries for the study of cleaved miRNA targets and the RNA degradome. *Nat Protoc,* 4**,** 356-62.

GRIFFITHS-JONES, S., HUI, J. H., MARCO, A. & RONSHAUGEN, M. 2011. MicroRNA evolution by arm switching. *EMBO Rep,* 12**,** 172-7.

GRIMSON, A., FARH, K. K., JOHNSTON, W. K., GARRETT-ENGELE, P., LIM, L. P. & BARTEL, D. P. 2007. MicroRNA targeting specificity in mammals: determinants beyond seed pairing. *Mol Cell,* 27**,** 91-105.

GROSS, C., YAO, X., ENGEL, T., TIWARI, D., XING, L., ROWLEY, S., DANIELSON, S. W., THOMAS, K. T., JIMENEZ-MATEOS, E. M., SCHROEDER, L. M., PUN, R. Y. K., DANZER, S. C., HENSHALL, D. C. & BASSELL, G. J. 2016. MicroRNA-Mediated Downregulation of the Potassium Channel Kv4.2 Contributes to Seizure Onset. *Cell Rep,* 17**,** 37-45.

GU, S. & KAY, M. A. 2010. How do miRNAs mediate translational repression? *Silence,* 1**,** 11.

GUNDELFINGER, E. D., REISSNER, C. & GARNER, C. C. 2015. Role of Bassoon and Piccolo in Assembly and Molecular Organization of the Active Zone. *Front Synaptic Neurosci,* 7**,** 19.

GUO, H., INGOLIA, N. T., WEISSMAN, J. S. & BARTEL, D. P. 2010. Mammalian microRNAs predominantly act to decrease target mRNA levels. *Nature,* 466**,** 835-840.

HA, M. & KIM, V. N. 2014. Regulation of microRNA biogenesis. *Nature Reviews,* 15**,** 509-24.

HAAS, G., CETIN, S., MESSMER, M., CHANE-WOON-MING, B., TERENZI, O., CHICHER, J., KUHN, L., HAMMANN, P. & PFEFFER, S. 2016. Identification of factors involved in target RNA-directed microRNA degradation. *Nucleic acids research,* 44**,** 2873-2887.

HAINES, B. P., GUPTA, R., JONES, C. M., SUMMERBELL, D. & RIGBY, P. W. 2005. The NLRR gene family and mouse development: Modified differential display PCR identifies NLRR-1 as a gene expressed in early somitic myoblasts. *Dev Biol,* 281**,** 145-59.

HALLERMANN, S., FEJTOVA, A., SCHMIDT, H., WEYHERSMULLER, A., SILVER, R. A., GUNDELFINGER, E. D. & EILERS, J. 2010. Bassoon speeds vesicle reloading at a central excitatory synapse. *Neuron,* 68**,** 710-23.

HAN, J., LEE, Y., YEOM, K. H., KIM, Y. K., JIN, H. & KIM, V. N. 2004. The Drosha-DGCR8 complex in primary microRNA processing. *Genes Dev,* 18**,** 3016-27.

HARDINGHAM, G. E. & BADING, H. 2010. Synaptic versus extrasynaptic NMDA receptor signalling: implications for neurodegenerative disorders. *Nature Reviews Neuroscience,* 11**,** 682-696.

HARDINGHAM, G. E., FUKUNAGA, Y. & BADING, H. 2002. Extrasynaptic NMDARs oppose synaptic NMDARs by triggering CREB shut-off and cell death pathways. *Nat Neurosci,* 5**,** 405-14.

HE, E., LOZANO, M. A. G., STRINGER, S., WATANABE, K., SAKAMOTO, K., DEN OUDSTEN, F., KOOPMANS, F., GIAMBERARDINO, S. N., HAMMERSCHLAG, A., CORNELISSE, L. N., LI, K. W., VAN WEERING, J., POSTHUMA, D., SMIT, A. B., SULLIVAN, P. F. & VERHAGE, M. 2018a. MIR137 schizophrenia-associated locus controls synaptic function by regulating synaptogenesis, synapse maturation and synaptic transmission. *Hum Mol Genet,* 27**,** 1879-91.

HE, M., LIU, Y., WANG, X., ZHANG, M. Q., HANNON, G. J. & HUANG, Z. J. 2012. Cell-type-based analysis of microRNA profiles in the mouse brain. *Neuron,* 73**,** 35-48.

HE, R.-Q., YANG, X., LIANG, L., CHEN, G. & MA, J. 2018b. MicroRNA-124-3p expression and its prospective functional pathways in hepatocellular carcinoma: A quantitative polymerase chain reaction, gene expression omnibus and bioinformatics study. *Oncology letters,* 15**,** 5517-5532.

HELWAK, A., KUDLA, G., DUDNAKOVA, T. & TOLLERVEY, D. 2013. Mapping the human miRNA interactome by CLASH reveals frequent noncanonical binding. *Cell,* 153**,** 654-65.

HERCULANO-HOUZEL, S. 2009. The human brain in numbers: a linearly scaled-up primate brain. *Front Hum Neurosci,* 3**,** 31.

HERNANDEZ, C. C., XIANGWEI, W., HU, N., SHEN, D., SHEN, W., LAGRANGE, A. H., ZHANG, Y., DAI, L., DING, C., SUN, Z., HU, J., ZHU, H., JIANG, Y. & MACDONALD, R. L. 2019. Altered inhibitory synapses in de novo GABRA5 and GABRA1 mutations associated with early onset epileptic encephalopathies. *Brain,* 142**,** 1938-1954.

HO, T.-T., HE, X., MO, Y.-Y. & BECK, W. T. 2016. Transient resistance to DNA damaging agents is associated with expression of microRNAs-135b and -196b in human leukemia cell lines. *International journal of biochemistry and molecular biology* [Online], 7. Available: http://europepmc.org/abstract/MED/27570640Available: http://europepmc.org/articles/PMC4981649?pdf=renderAvailable: http://europepmc.org/articles/PMC4981649 [Accessed 2016].

HOFTMAN, G. D., VOLK, D. W., BAZMI, H. H., LI, S., SAMPSON, A. R. & LEWIS, D. A. 2015. Altered cortical expression of GABA-related genes in schizophrenia: illness progression vs developmental disturbance. *Schizophr Bull,* 41**,** 180-91.

HONARDOOST, M., AREFIAN, E., SOLEIMANI, M., SOUDI, S. & SAROOKHANI, M. R. 2016. Development of Insulin Resistance through Induction of miRNA-135 in C2C12 Cells. *Cell journal,* 18**,** 353-361.

HU, Z. & LI, Z. 2017. miRNAs in synapse development and synaptic plasticity. *Current opinion in neurobiology,* 45**,** 24-31.

HU, Z., YU, D., GU, Q.-H., YANG, Y., TU, K., ZHU, J. & LI, Z. 2014. miR-191 and miR-135 are required for long-lasting spine remodelling associated with synaptic long-term depression. *Nature communications,* 5**,** 3263-3263.

HUBBARD, T., BARKER, D., BIRNEY, E., CAMERON, G., CHEN, Y., CLARK, L., COX, T., CUFF, J., CURWEN, V., DOWN, T., DURBIN, R., EYRAS, E., GILBERT, J., HAMMOND, M., HUMINIECKI, L., KASPRZYK, A., LEHVASLAIHO, H., LIJNZAAD, P., MELSOPP, C., MONGIN, E., PETTETT, R., POCOCK, M., POTTER, S., RUST, A., SCHMIDT, E., SEARLE, S., SLATER, G., SMITH, J., SPOONER, W., STABENAU, A., STALKER, J., STUPKA, E., URETA-VIDAL, A., VASTRIK, I. & CLAMP, M. 2002. The Ensembl genome database project. *Nucleic Acids Res,* 30**,** 38-41.

HÖCK, J., WEINMANN, L., ENDER, C., RÜDEL, S., KREMMER, E., RAABE, M., URLAUB, H. & MEISTER, G. 2007. Proteomic and functional analysis of Argonaute-containing mRNA-protein complexes in human cells. *EMBO reports,* 8**,** 1052-1060.

HÜTTELMAIER, S., ZENKLUSEN, D., LEDERER, M., DICTENBERG, J., LORENZ, M., MENG, X., BASSELL, G. J., CONDEELIS, J. & SINGER, R. H. 2005. Spatial regulation of β-actin translation by Src-dependent phosphorylation of ZBP1. *Nature,* 438**,** 512-515.

ISHII, N., WANAKA, A. & TOHYAMA, M. 1996. Increased expression of NLRR-3 mRNA after cortical brain injury in mouse. *Brain Res Mol Brain Res,* 40**,** 148-52.

ISSLER, O., HARAMATI, S., PAUL, E. D., MAENO, H., NAVON, I., ZWANG, R., GIL, S., MAYBERG, H. S., DUNLOP, B. W., MENKE, A., AWATRAMANI, R., BINDER, E. B., DENERIS, E. S., LOWRY, C. A. & CHEN, A. 2014. MicroRNA 135 is essential for chronic stress resiliency, antidepressant efficacy, and intact serotonergic activity. *Neuron,* 83**,** 344-60.

IVANOV, A., MIKHAILOVA, T., ELISEEV, B., YERAMALA, L., SOKOLOVA, E., SUSOROV, D., SHUVALOV, A., SCHAFFITZEL, C. & ALKALAEVA, E. 2016. PABP enhances release factor recruitment and stop codon recognition during translation termination. *Nucleic acids research,* 44**,** 7766-7776.

IWAKAWA, H.-O. & TOMARI, Y. 2015. The Functions of MicroRNAs: mRNA Decay and Translational Repression. *Trends in Cell Biology,* 25**,** 651-665.

IWASAKI, S., KOBAYASHI, M., YODA, M., SAKAGUCHI, Y., KATSUMA, S., SUZUKI, T. & TOMARI, Y. 2010. Hsc70/Hsp90 chaperone machinery mediates ATP-dependent RISC loading of small RNA duplexes. *Mol Cell,* 39**,** 292-9.

JACKSON, R. J., HELLEN, C. U. T. & PESTOVA, T. V. 2010. The mechanism of eukaryotic translation initiation and principles of its regulation. *Nature Reviews Molecular Cell Biology,* 11**,** 113-127.

JEANNETEAU, F., BARRERE, C., VOS, M., DE VRIES, C. J. M., ROUILLARD, C., LEVESQUE, D., DROMARD, Y., MOISAN, M. P., DURIC, V., FRANKLIN, T. C., DUMAN, R. S., LEWIS, D. A., GINSBERG, S. D. & ARANGO-LIEVANO, M. 2018. The Stress-Induced Transcription Factor NR4A1 Adjusts Mitochondrial Function and Synapse Number in Prefrontal Cortex. *J Neurosci,* 38**,** 1335-1350.

JIA, X., WANG, F., HAN, Y., GENG, X., LI, M., SHI, Y., LU, L. & CHEN, Y. 2016. miR-137 and miR-491 Negatively Regulate Dopamine Transporter Expression and Function in Neural Cells. *Neurosci Bull,* 32**,** 512-522.

JIANG, F., WU, Q., SUN, S., BI, G. & GUO, L. 2019. Identification of potential diagnostic biomarkers for Parkinson's disease. *FEBS open bio,* 9**,** 1460-1468.

JIMENEZ-MATEOS, E. M., BRAY, I., SANZ-RODRIGUEZ, A., ENGEL, T., MCKIERNAN, R. C., MOURI, G., TANAKA, K., SANO, T., SAUGSTAD, J. A., SIMON, R. P., STALLINGS, R. L. & HENSHALL, D. C. 2011. miRNA Expression profile after status epilepticus and hippocampal neuroprotection by targeting miR-132. *Am J Pathol,* 179**,** 2519-32.

JIN, H. Y. & XIAO, C. 2015. MicroRNA Mechanisms of Action: What have We Learned from Mice? *Front Genet,* 6.

JIN, X. T., GALVAN, A., WICHMANN, T. & SMITH, Y. 2011. Localization and Function of GABA Transporters GAT-1 and GAT-3 in the Basal Ganglia. *Front Syst Neurosci,* 5**,** 63.

JOHANNESEN, K. M., GARDELLA, E., LINNANKIVI, T., COURAGE, C., DE SAINT MARTIN, A., LEHESJOKI, A. E., MIGNOT, C., AFENJAR, A., LESCA, G., ABI-WARDE, M. T., CHELLY, J., PITON, A., MERRITT, J. L., 2ND, RODAN, L. H., TAN, W. H., BIRD, L. M., NESPECA, M., GLEESON, J. G., YOO, Y., CHOI, M., CHAE, J. H., CZAPANSKY-BEILMAN, D., REICHERT, S. C., PENDZIWIAT, M., VERHOEVEN, J. S., SCHELHAAS, H. J., DEVINSKY, O., CHRISTENSEN, J., SPECCHIO, N., TRIVISANO, M., WEBER, Y. G., NAVA, C., KEREN, B., DOUMMAR, D., SCHAEFER, E., HOPKINS, S., DUBBS, H., SHAW, J. E., PISANI, L., MYERS, C. T., TANG, S., PAL, D. K., MILLICHAP, J. J., CARVILL, G. L., HELBIG, K. L., MECARELLI, O., STRIANO, P., HELBIG, I., RUBBOLI, G., MEFFORD, H. C. & MOLLER, R. S. 2018. Defining the phenotypic spectrum of SLC6A1 mutations. *Epilepsia,* 59**,** 389-402.

JOHAR, K., PRIYA, A. & WONG-RILEY, M. T. 2012. Regulation of Na(+)/K(+)-ATPase by nuclear respiratory factor 1: implication in the tight coupling of neuronal activity, energy generation, and energy consumption. *J Biol Chem,* 287**,** 40381-90.

JOHAR, K., PRIYA, A. & WONG-RILEY, M. T. T. 2014. Regulation of Na(+)/K(+)-ATPase by neuron-specific transcription factor Sp4: implication in the tight coupling of energy production, neuronal activity and energy consumption in neurons. *The European journal of neuroscience,* 39**,** 566-578.

JOHN, B., ENRIGHT, A. J., ARAVIN, A., TUSCHL, T., SANDER, C. & MARKS, D. S. 2004. Human MicroRNA targets. *PLoS Biol,* 2**,** e363.

JOHNSTON, R. J. & HOBERT, O. 2003. A microRNA controlling left/right neuronal asymmetry in Caenorhabditis elegans. *Nature,* 426**,** 845-9.

JONAS, S. & IZAURRALDE, E. 2015. Towards a molecular understanding of microRNA-mediated gene silencing. *Nat Rev Genet,* 16**,** 421-33.

JOVIČIĆ, A. 2011. *Unique Cell-Type Specific Distributions and Functions of Brain MicroRNAs.* Ph.D., EPFL.

JOVIČIĆ, A., ROSHAN, R., MOISOI, N., PRADERVAND, S., MOSER, R., PILLAI, B. & LUTHI-CARTER, R. 2013. Comprehensive expression analyses of neural cell-type-specific miRNAs identify new determinants of the specification and maintenance of neuronal phenotypes. *The Journal of Neuroscience,* 33**,** 5127-5137.

KAHVEJIAN, A., ROY, G. & SONENBERG, N. 2001. The mRNA closed-loop model: the function of PABP and PABP-interacting proteins in mRNA translation. *Cold Spring Harb Symp Quant Biol,* 66**,** 293-300.

KANAI, Y., DOHMAE, N. & HIROKAWA, N. 2004. Kinesin transports RNA: isolation and characterization of an RNA-transporting granule. *Neuron,* 43**,** 513-25.

KARASAWA, T. & LOMBROSO, P. J. 2014. Disruption of striatal-enriched protein tyrosine phosphatase (STEP) function in neuropsychiatric disorders. *Neuroscience research,* 89**,** 1-9.

KENNY, P. J., KIM, M., SKARIAH, G., NIELSEN, J., LANNOM, M. C. & CEMAN, S. 2019. The FMRP–MOV10 complex: a translational regulatory switch modulated by G-Quadruplexes. *Nucleic Acids Research,* 48**,** 862-878.

KENNY, P. J., ZHOU, H., KIM, M., SKARIAH, G., KHETANI, R. S., DRNEVICH, J., ARCILA, M. L., KOSIK, K. S. & CEMAN, S. 2014. MOV10 and FMRP regulate AGO2 association with microRNA recognition elements. *Cell Rep,* 9**,** 1729-41.

KHALIL, B., MORDERER, D., PRICE, P. L., LIU, F. & ROSSOLL, W. 2018. mRNP assembly, axonal transport, and local translation in neurodegenerative diseases. *Brain Res*.

KHATRI, R. & SUBRAMANIAN, S. 2013. MicroRNA-135b and Its Circuitry Networks as Potential Therapeutic Targets in Colon Cancer. *Frontiers in oncology,* 3**,** 268-268.

KIEBLER, M. A. & BASSELL, G. J. 2006. Neuronal RNA granules: movers and makers. *Neuron,* 51**,** 685-90.

KING, H. A. & GERBER, A. P. 2016. Translatome profiling: methods for genome-scale analysis of mRNA translation. *Brief Funct Genomics,* 15**,** 22-31.

KINGSTON, E. R. & BARTEL, D. P. 2019. Global analyses of the dynamics of mammalian microRNA metabolism. *Genome Res,* 29**,** 1777-1790.

KIRIAKIDOU, M., TAN, G. S., LAMPRINAKI, S., DE PLANELL-SAGUER, M., NELSON, P. T. & MOURELATOS, Z. 2007. An mRNA m7G cap binding-like motif within human Ago2 represses translation. *Cell,* 129**,** 1141-51.

KISLAUSKIS, E. H., ZHU, X. & SINGER, R. H. 1994. Sequences responsible for intracellular localization of beta-actin messenger RNA also affect cell phenotype. *J Cell Biol,* 127**,** 441-51.

KLAUCK, S. M., FELDER, B., KOLB-KOKOCINSKI, A., SCHUSTER, C., CHIOCCHETTI, A., SCHUPP, I., WELLENREUTHER, R., SCHMÖTZER, G., POUSTKA, F., BREITENBACH-KOLLER, L. & POUSTKA, A. 2006. Mutations in the ribosomal protein gene RPL10 suggest a novel modulating disease mechanism for autism. *Molecular Psychiatry,* 11**,** 1073-1084.

KNOWLES, R. B., SABRY, J. H., MARTONE, M. E., DEERINCK, T. J., ELLISMAN, M. H., BASSELL, G. J. & KOSIK, K. S. 1996. Translocation of RNA granules in living neurons. *J Neurosci,* 16**,** 7812-20.

KOSIK, K. S. 2006. The neuronal microRNA system. *Nature Reviews Neuroscience,* 7**,** 911-20.

KOSIK, K. S. & KRICHEVSKY, A. M. 2002. The Message and the Messenger: Delivering RNA in Neurons. *Science's STKE,* 2002**,** pe16-pe16.

KRICHEVSKY, A. M. & KOSIK, K. S. 2001. Neuronal RNA Granules: A Link between RNA Localization and Stimulation-Dependent Translation. *Neuron,* 32**,** 683-696.

KROL, J., LOEDIGE, I. & FILIPOWICZ, W. 2010. The widespread regulation of microRNA biogenesis, function and decay. *Nat Rev Genet,* 11**,** 597-610.

KUMBRINK, J., GERLINGER, M. & JOHNSON, J. P. 2005. Egr-1 induces the expression of its corepressor nab2 by activation of the nab2 promoter thereby establishing a negative feedback loop. *J Biol Chem,* 280**,** 42785-93.

KUTE, P. M., RAMAKRISHNA, S., NEELAGANDAN, N., CHATTARJI, S. & MUDDASHETTY, R. S. 2019. NMDAR mediated translation at the synapse is regulated by MOV10 and FMRP. *Molecular Brain,* 12**,** 65.

KYE, M.-J., LIU, T., LEVY, S. F., XU, N. L., GROVES, B. B., BONNEAU, R., LAO, K. & KOSIK, K. S. 2007. Somatodendritic microRNAs identified by laser capture and multiplex RT-PCR. *RNA (New York, N.Y.),* 13**,** 1224-1234.

LAGOS-QUINTANA, M., RAUHUT, R., LENDECKEL, W. & TUSCHL, T. 2001. Identification of novel genes coding for small expressed RNAs. *Science,* 294**,** 853-8.

LARSSON, O. & NADON, R. 2013. Re-analysis of genome wide data on mammalian microRNA-mediated suppression of gene expression. *Translation (Austin),* 1**,** e24557.

LAU, N. C., LIM, L. P., WEINSTEIN, E. G. & BARTEL, D. P. 2001. An abundant class of tiny RNAs with probable regulatory roles in Caenorhabditis elegans. *Science,* 294**,** 858-62.

LEE, R., FEINBAUM, R. & AMBROS, V. 1993. The C. elegans heterochronic gene lin-4 encodes small RNAs with antisense complementarity to lin-14. *Cell,* 75**,** 843-54.

LEE, R. C. & AMBROS, V. 2001. An extensive class of small RNAs in Caenorhabditis elegans. *Science,* 294**,** 862-4.

LEE, Y., KIM, M., HAN, J., YEOM, K.-H., LEE, S., BAEK, S. H. & KIM, V. N. 2004. MicroRNA genes are transcribed by RNA polymerase II. *The EMBO journal,* 23**,** 4051-4060.

LEWIS, B. P., BURGE, C. B. & BARTEL, D. P. 2005. Conserved seed pairing, often flanked by adenosines, indicates that thousands of human genes are microRNA targets. *Cell,* 120**,** 15-20.

LI, D. K., TISDALE, S., LOTTI, F. & PELLIZZONI, L. 2014a. SMN control of RNP assembly: from post-transcriptional gene regulation to motor neuron disease. *Seminars in cell & developmental biology,* 32**,** 22-29.

LI, J.-H., LIU, S., ZHOU, H., QU, L.-H. & YANG, J.-H. 2014b. starBase v2.0: decoding miRNA-ceRNA, miRNA-ncRNA and protein-RNA interaction networks from large-scale CLIP-Seq data. *Nucleic acids research,* 42**,** D92-D97.

LI, Z. & LANGHANS, S. A. 2015. Transcriptional regulators of Na,K-ATPase subunits. *Front Cell Dev Biol,* 3**,** 66.

LIANG, S., BELLATO, H. M., LORENT, J., LUPINACCI, F. C. S., OERTLIN, C., VAN HOEF, V., ANDRADE, V. P., ROFFÉ, M., MASVIDAL, L., HAJJ, G. N. M. & LARSSON, O. 2018. Polysome-profiling in small tissue samples. *Nucleic acids research,* 46**,** e3-e3.

LIU, B. & QIAN, S.-B. 2016. Characterizing inactive ribosomes in translational profiling. *Translation (Austin, Tex.),* 4**,** e1138018-e1138018.

LIU, J., CARMELL, M. A., RIVAS, F. V., MARSDEN, C. G., THOMSON, J. M., SONG, J. J., HAMMOND, S. M., JOSHUA-TOR, L. & HANNON, G. J. 2004. Argonaute2 is the catalytic engine of mammalian RNAi. *Science,* 305**,** 1437-41.

LIU, J., RIVAS, F. V., WOHLSCHLEGEL, J., YATES, J. R., 3RD, PARKER, R. & HANNON, G. J. 2005. A role for the P-body component GW182 in microRNA function. *Nat Cell Biol,* 7**,** 1261-6.

LOMBROSO, P. J., MURDOCH, G. & LERNER, M. 1991. Molecular characterization of a protein-tyrosine-phosphatase enriched in striatum. *Proc Natl Acad Sci U S A,* 88**,** 7242-6.

LONG, J. M., MALONEY, B., ROGERS, J. T. & LAHIRI, D. K. 2019. Novel upregulation of amyloid-β precursor protein (APP) by microRNA-346 via targeting of APP mRNA

5’-untranslated region: Implications in Alzheimer’s disease. *Molecular Psychiatry,* 24**,** 345-363.

LU, W. T., WILCZYNSKA, A., SMITH, E. & BUSHELL, M. 2014. The diverse roles of the eIF4A family: you are the company you keep. *Biochem Soc Trans,* 42**,** 166-72.

LU, Z., PIECHOWICZ, M. & QIU, S. 2016. A Simplified Method for Ultra-Low Density, Long-Term Primary Hippocampal Neuron Culture. *J Vis Exp*.

LUGLI, G., LARSON, J., MARTONE, M. E., JONES, Y. & SMALHEISER, N. R. 2005. Dicer and eIF2c are enriched at postsynaptic densities in adult mouse brain and are modified by neuronal activity in a calpain-dependent manner. *J Neurochem,* 94**,** 896-905.

MACKENZIE, I. R. A. & RADEMAKERS, R. 2008. The role of transactive response DNA-binding protein-43 in amyotrophic lateral sclerosis and frontotemporal dementia. *Current opinion in neurology,* 21**,** 693-700.

MALENKA, R. C. & BEAR, M. F. 2004. LTP and LTD: an embarrassment of riches. *Neuron,* 44**,** 5-21.

MALKA-MAHIEU, H., NEWMAN, M., DESAUBRY, L., ROBERT, C. & VAGNER, S. 2017. Molecular Pathways: The eIF4F Translation Initiation Complex-New Opportunities for Cancer Treatment. *Clin Cancer Res,* 23**,** 21-25.

MARTIN, K. C. & EPHRUSSI, A. 2009. mRNA Localization: Gene Expression in the Spatial Dimension. *Cell,* 136**,** 719.

MARTINEZ-HERNANDEZ, R., BERNAL, S., ALSO-RALLO, E., ALIAS, L., BARCELO, M. J., HEREU, M., ESQUERDA, J. E. & TIZZANO, E. F. 2013. Synaptic defects in type I spinal muscular atrophy in human development. *J Pathol,* 229**,** 49-61.

MATHONNET, G., FABIAN, M. R., SVITKIN, Y. V., PARSYAN, A., HUCK, L., MURATA, T., BIFFO, S., MERRICK, W. C., DARZYNKIEWICZ, E., PILLAI, R. S., FILIPOWICZ, W., DUCHAINE, T. F. & SONENBERG, N. 2007. MicroRNA inhibition of translation initiation in vitro by targeting the cap-binding complex eIF4F. *Science,* 317**,** 1764-7.

MAZROUI, R., HUOT, M. E., TREMBLAY, S., FILION, C., LABELLE, Y. & KHANDJIAN, E. W. 2002. Trapping of messenger RNA by Fragile X Mental Retardation protein into cytoplasmic granules induces translation repression. *Hum Mol Genet,* 11**,** 3007-17.

MEIJER, H. A., KONG, Y. W., LU, W. T., WILCZYNSKA, A., SPRIGGS, R. V., ROBINSON, S. W., GODFREY, J. D., WILLIS, A. E. & BUSHELL, M. 2013. Translational repression and eIF4A2 activity are critical for microRNA-mediated gene regulation. *Science,* 340**,** 82-5.

MEIJER, H. A., SMITH, E. M. & BUSHELL, M. 2014. Regulation of miRNA strand selection: follow the leader? *Biochem Soc Trans,* 42**,** 1135-40.

MEISTER, G., LANDTHALER, M., PETERS, L., CHEN, P. Y., URLAUB, H., LÜHRMANN, R. & TUSCHL, T. 2005. Identification of Novel Argonaute-Associated Proteins. *Current Biology,* 15**,** 2149-2155.

MIKL, M., VENDRA, G. & KIEBLER, M. A. 2011. Independent localization of MAP2, CaMKIIα and β-actin RNAs in low copy numbers. *EMBO Reports,* 12**,** 1077-1084.

MODEPALLI, V. & MORAN, Y. 2017. Evolution of miRNA Tailing by 3' Terminal Uridylyl Transferases in Metazoa. *Genome biology and evolution,* 9**,** 1547-1560.

MORETTI, F., KAISER, C., ZDANOWICZ-SPECHT, A. & HENTZE, M. W. 2012. PABP and the poly(A) tail augment microRNA repression by facilitated miRISC binding. *Nat Struct Mol Biol,* 19**,** 603-8.

MORTENSEN, R. D., SERRA, M., STEITZ, J. A. & VASUDEVAN, S. 2011. Posttranscriptional activation of gene expression in Xenopus laevis oocytes by microRNA-protein complexes (microRNPs). *Proc Natl Acad Sci U S A,* 108**,** 8281-6.

MUDDASHETTY, R. S., NALAVADI, V. C., GROSS, C., YAO, X., XING, L., LAUR, O., WARREN, S. T. & BASSELL, G. J. 2011. Reversible inhibition of PSD-95 mRNA translation by miR-125a, FMRP phosphorylation, and mGluR signaling. *Mol Cell,* 42**,** 673-88.

NEO, W. H., YAP, K., LEE, S. H., LOOI, L. S., KHANDELIA, P., NEO, S. X., MAKEYEV, E. V. & SU, I. H. 2014. MicroRNA miR-124 controls the choice between neuronal and astrocyte differentiation by fine-tuning Ezh2 expression. *J Biol Chem,* 289**,** 20788-801.

NILSSON, S., HELOU, K., WALENTINSSON, A., SZPIRER, C., NERMAN, O. & STÅHL, F. 2001. Rat–Mouse and Rat–Human Comparative Maps Based on Gene Homology and High-Resolution Zoo-FISH. *Genomics,* 74**,** 287-298.

NORSTROM, E. M., ZHANG, C., TANZI, R. & SISODIA, S. S. 2010. Identification of NEEP21 as a ss-amyloid precursor protein-interacting protein in vivo that modulates amyloidogenic processing in vitro. *J Neurosci,* 30**,** 15677-85.

NOTTROTT, S., SIMARD, M. J. & RICHTER, J. D. 2006. Human let-7a miRNA blocks protein production on actively translating polyribosomes. *Nat Struct Mol Biol,* 13**,** 1108-14.

NYATHI, Y., WILKINSON, B. M. & POOL, M. R. 2013. Co-translational targeting and translocation of proteins to the endoplasmic reticulum. *Biochimica et Biophysica Acta (BBA) - Molecular Cell Research,* 1833**,** 2392-2402.

OLDE LOOHUIS, N. F. M., NADIF KASRI, N., GLENNON, J. C., VAN BOKHOVEN, H., HÉBERT, S. S., KAPLAN, B. B., MARTENS, G. J. M. & ASCHRAFI, A. 2017. The schizophrenia risk gene MIR137 acts as a hippocampal gene network node orchestrating the expression of genes relevant to nervous system development and function. *Progress in neuro-psychopharmacology & biological psychiatry,* 73**,** 109-118.

OTTESEN, E. W., SINGH, N. N., LUO, D. & SINGH, R. N. 2018. High-affinity RNA targets of the Survival Motor Neuron protein reveal diverse preferences for sequence and structural motifs. *Nucleic acids research,* 46**,** 10983-11001.

PARK, C. S. & TANG, S.-J. 2009. Regulation of microRNA Expression by Induction of Bidirectional Synaptic Plasticity. *Journal of Molecular Neuroscience,* 38**,** 50-56.

PASQUINELLI, A., REINHART, B., SLACK, F., MARTINDALE, M., KURODA, M., MALLER, B., HAYWARD, D., BALL, E., DEGNAN, B., MÜLLER, P., SPRING, J., SRINIVASAN, A., FISHMAN, M., FINNERTY, J., CORBO, J., LEVINE, M., LEAHY, P., DAVIDSON, E. & RUVKUN, G. 2000. Conservation of the sequence and temporal expression of let-7 heterochronic regulatory RNA. *Nature,* 408**,** 86-9.

PETER, B., WIJSMAN, E. M., NATO, A. Q., JR., UNIVERSITY OF WASHINGTON CENTER FOR MENDELIAN, G., MATSUSHITA, M. M., CHAPMAN, K. L., STANAWAY, I. B., WOLFF, J., ODA, K., GABO, V. B. & RASKIND, W. H. 2016. Genetic Candidate Variants in Two Multigenerational Families with Childhood Apraxia of Speech. *PLOS ONE,* 11**,** e0153864.

PETERSEN, C. P., BORDELEAU, M. E., PELLETIER, J. & SHARP, P. A. 2006. Short RNAs repress translation after initiation in mammalian cells. *Mol Cell,* 21**,** 533-42.

PIAZZON, N., RAGE, F., SCHLOTTER, F., MOINE, H., BRANLANT, C. & MASSENET, S. 2008. In vitro and in cellulo evidences for association of the survival of motor neuron complex with the fragile X mental retardation protein. *J Biol Chem,* 283**,** 5598-610.

PILAZ, L. J., LENNOX, A. L., ROUANET, J. P. & SILVER, D. L. 2016. Dynamic mRNA Transport and Local Translation in Radial Glial Progenitors of the Developing Brain. *Curr Biol,* 26**,** 3383-3392.

PILLAI, R. S., BHATTACHARYYA, S. N., ARTUS, C. G., ZOLLER, T., COUGOT, N., BASYUK, E., BERTRAND, E. & FILIPOWICZ, W. 2005. Inhibition of translational initiation by Let-7 MicroRNA in human cells. *Science,* 309**,** 1573-6.

PITCHIAYA, S., HEINICKE, L. A., PARK, J. I., CAMERON, E. L. & WALTER, N. G. 2017. Resolving Subcellular miRNA Trafficking and Turnover at Single-Molecule Resolution. *Cell Reports,* 19**,** 630-642.

POULOPOULOS, A., ARAMUNI, G., MEYER, G., SOYKAN, T., HOON, M., PAPADOPOULOS, T., ZHANG, M., PAARMANN, I., FUCHS, C., HARVEY, K., JEDLICKA, P., SCHWARZACHER, S. W., BETZ, H., HARVEY, R. J., BROSE, N., ZHANG, W. & VAROQUEAUX, F. 2009. Neuroligin 2 drives postsynaptic assembly at perisomatic inhibitory synapses through gephyrin and collybistin. *Neuron,* 63**,** 628-42.

PRASAD, A., BHARATHI, V., SIVALINGAM, V., GIRDHAR, A. & PATEL, B. K. 2019. Molecular Mechanisms of TDP-43 Misfolding and Pathology in Amyotrophic Lateral Sclerosis. *Frontiers in Molecular Neuroscience,* 12**,** 25.

PRATT, A. J. & MACRAE, I. J. 2009. The RNA-induced Silencing Complex: A Versatile Gene-silencing Machine. *J Biol Chem,* 284**,** 17897-901.

PRICE, T. J., FLORES, C. M., CERVERO, F. & HARGREAVES, K. M. 2006. The RNA binding and transport proteins staufen and fragile X mental retardation protein are expressed by rat primary afferent neurons and localize to peripheral and central axons. *Neuroscience,* 141**,** 2107-16.

PRINGLE, E. S., MCCORMICK, C. & CHENG, Z. 2019. Polysome Profiling Analysis of mRNA and Associated Proteins Engaged in Translation. *Curr Protoc Mol Biol,* 125**,** e79.

PYKA, M., BUSSE, C., SEIDENBECHER, C., GUNDELFINGER, E. D. & FAISSNER, A. 2011. Astrocytes are crucial for survival and maturation of embryonic hippocampal neurons in a neuron-glia cell-insert coculture assay. *Synapse,* 65**,** 41-53.

RACKHAM, O. & BROWN, C. M. 2004. Visualization of RNA-protein interactions in living cells: FMRP and IMP1 interact on mRNAs. *The EMBO journal,* 23**,** 3346-3355.

RAGE, F., BOULISFANE, N., RIHAN, K., NEEL, H., GOSTAN, T., BERTRAND, E., BORDONNE, R. & SORET, J. 2013. Genome-wide identification of mRNAs associated with the protein SMN whose depletion decreases their axonal localization. *Rna,* 19**,** 1755-66.

RAMANATHAN, A., ROBB, G. B. & CHAN, S.-H. 2016. mRNA capping: biological functions and applications. *Nucleic acids research,* 44**,** 7511-7526.

RASCHKE, S., GUAN, J. & ILIAKIS, G. 2009. Application of alkaline sucrose gradient centrifugation in the analysis of DNA replication after DNA damage. *Methods Mol Biol,* 521**,** 329-42.

RECZKO, M., MARAGKAKIS, M., ALEXIOU, P., GROSSE, I. & HATZIGEORGIOU, A. G. 2012. Functional microRNA targets in protein coding sequences. *Bioinformatics,* 28**,** 771-6.

REINHART, B. J., SLACK, F. J., BASSON, M., PASQUINELLI, A. E., BETTINGER, J. C., ROUGVIE, A. E., HORVITZ, H. R. & RUVKUN, G. 2000. The 21-nucleotide let-7 RNA regulates developmental timing in Caenorhabditis elegans. *Nature,* 403**,** 901-6.

REMENYI, J., HUNTER, C. J., COLE, C., ANDO, H., IMPEY, S., MONK, C. E., MARTIN, K. J., BARTON, G. J., HUTVAGNER, G. & ARTHUR, J. S. 2010. Regulation of the miR-212/132 locus by MSK1 and CREB in response to neurotrophins. *Biochem J,* 428**,** 281-91.

REPICI, M., HASSANJANI, M., MADDISON, D. C., GARÇÃO, P., CIMINI, S., PATEL, B., SZEGÖ É, M., STRAATMAN, K. R., LILLEY, K. S., BORSELLO, T., OUTEIRO, T. F., PANMAN, L. & GIORGINI, F. 2019. The Parkinson's Disease-Linked Protein DJ-1 Associates with Cytoplasmic mRNP Granules During Stress and Neurodegeneration. *Mol Neurobiol,* 56**,** 61-77.

RIPKE, S., SANDERS, A. R., KENDLER, K. S., LEVINSON, D. F., SKLAR, P., HOLMANS, P. A., LIN, D.-Y., DUAN, J., OPHOFF, R. A., ANDREASSEN, O. A., SCOLNICK, E., CICHON, S., ST. CLAIR, D., CORVIN, A., GURLING, H., WERGE, T., RUJESCU, D., BLACKWOOD, D. H. R., PATO, C. N., MALHOTRA, A. K., PURCELL, S., DUDBRIDGE, F., NEALE, B. M., ROSSIN, L., VISSCHER, P. M., POSTHUMA, D., RUDERFER, D. M., FANOUS, A., STEFANSSON, H., STEINBERG, S., MOWRY, B. J., GOLIMBET, V., DE HERT, M., JÖNSSON, E. G., BITTER, I., PIETILÄINEN, O. P. H., COLLIER, D. A., TOSATO, S., AGARTZ, I., ALBUS, M., ALEXANDER, M., AMDUR, R. L., AMIN, F., BASS, N., BERGEN, S. E., BLACK, D. W., BØRGLUM, A. D., BROWN, M. A., BRUGGEMAN, R., BUCCOLA, N. G., BYERLEY, W. F., CAHN, W., CANTOR, R. M., CARR, V. J., CATTS, S. V., CHOUDHURY, K., CLONINGER, C. R., CORMICAN, P., CRADDOCK, N., DANOY, P. A., DATTA, S., DE HAAN, L., DEMONTIS, D., DIKEOS, D., DJUROVIC, S., DONNELLY, P., DONOHOE, G., DUONG, L., DWYER, S., FINK-JENSEN, A., FREEDMAN, R., FREIMER, N. B., FRIEDL, M., GEORGIEVA, L., GIEGLING, I., GILL, M., GLENTHØJ, B., GODARD, S., HAMSHERE, M., HANSEN, M., HANSEN, T., HARTMANN, A. M., HENSKENS, F. A., HOUGAARD, D. M., HULTMAN, C. M., INGASON, A., JABLENSKY, A. V., JAKOBSEN, K. D., JAY, M., JÜRGENS, G., KAHN, R. S., KELLER, M. C., KENIS, G., KENNY, E., KIM, Y., KIROV, G. K., KONNERTH, H., KONTE, B., KRABBENDAM, L., KRASUCKI, R., et al. 2011. Genome-wide association study identifies five new schizophrenia loci. *Nature Genetics,* 43**,** 969-976.

ROSSI, M., KILPINEN, H., MUONA, M., SURAKKA, I., INGLE, C., LAHTINEN, J., HENNAH, W., RIPATTI, S. & HOVATTA, I. 2014. Allele-specific regulation of DISC1 expression by miR-135b-5p. *European Journal of Human Genetics,* 22**,** 840-843.

RUSSO, A. 2020. Understanding the mammalian TRAP complex function(s). *Open biology,* 10**,** 190244-190244.

SABA, R., STORCHEL, P. H., AKSOY-AKSEL, A., KEPURA, F., LIPPI, G., PLANT, T. D. & SCHRATT, G. M. 2012. Dopamine-regulated microRNA MiR-181a controls GluA2 surface expression in hippocampal neurons. *Mol Cell Biol,* 32**,** 619-32.

SAKAMOTO, K. & CROWLEY, J. J. 2018. A comprehensive review of the genetic and biological evidence supports a role for MicroRNA-137 in the etiology of schizophrenia. *Am J Med Genet B Neuropsychiatr Genet,* 177**,** 242-256.

SAKHARKAR, M. K., KASHMIR SINGH, S. K., RAJAMANICKAM, K., MOHAMED ESSA, M., YANG, J. & CHIDAMBARAM, S. B. 2019. A systems biology approach towards the

identification of candidate therapeutic genes and potential biomarkers for Parkinson's disease. *PLOS ONE,* 14**,** e0220995.

SALPIETRO, V., MALINTAN, N. T., LLANO-RIVAS, I., SPAETH, C. G., EFTHYMIOU, S., STRIANO, P., VANDROVCOVA, J., CUTRUPI, M. C., CHIMENZ, R., DAVID, E., DI ROSA, G., MARCE-GRAU, A., RASPALL-CHAURE, M., MARTIN-HERNANDEZ, E., ZARA, F., MINETTI, C., KRIOUILE, Y., EL KHORASSANI, M., AGUENNOUZ, M., KARASHOVA, B., AVDJIEVA, D., KATHOM, H., TINCHEVA, R., VAN MALDERGEM, L., NACHBAUER, W., BOESCH, S., ARNING, L., TIMMANN, D., CORMAND, B., PÉREZ-DUEÑAS, B., PIRONTI, E., GORAYA, J. S., SULTAN, T., KIRMANI, S., IBRAHIM, S., JAN, F., MINE, J., BANU, S., VEGGIOTTI, P., FERRARI, M. D., VERROTTI, A., MARSEGLIA, G. L., SAVASTA, S., GARAVAGLIA, B., SCUDERI, C., BORGIONE, E., DIPASQUALE, V., CUTRUPI, M. C., PORTARO, S., SANCHEZ, B. M., PINEDA-MARFA', M., MUNELL, F., MACAYA, A., BOLES, R., HEIMER, G., PAPACOSTAS, S., MANOLE, A., MALINTAN, N., ZANETTI, M. N., HANNA, M. G., ROTHMAN, J. E., KULLMANN, D. M., HOULDEN, H., BELLO, O. D., DE ZORZI, R., FORTUNA, S., DAUBER, A., ALKHAWAJA, M., MANKAD, K., VITOBELLO, A., THOMAS, Q., MAU-THEM, F. T., FAIVRE, L., MARTINEZ-AZORIN, F., PRADA, C. E. & KRISHNAKUMAR, S. S. 2019. Mutations in the Neuronal Vesicular SNARE VAMP2 Affect Synaptic Membrane Fusion and Impair Human Neurodevelopment. *The American Journal of Human Genetics,* 104**,** 721-730.

SAMBANDAN, S., AKBALIK, G., KOCHEN, L., RINNE, J., KAHLSTATT, J., GLOCK, C., TUSHEV, G., ALVAREZ-CASTELAO, B., HECKEL, A. & SCHUMAN, E. M. 2017. Activity-dependent spatially localized miRNA maturation in neuronal dendrites. *Science,* 355**,** 634-637.

SCHIAVO, G., BENFENATI, F., POULAIN, B., ROSSETTO, O., POLVERINO DE LAURETO, P., DASGUPTA, B. R. & MONTECUCCO, C. 1992. Tetanus and botulinum-B neurotoxins block neurotransmitter release by proteolytic cleavage of synaptobrevin. *Nature,* 359**,** 832-5.

SCHIRLE, N. T., SHEU-GRUTTADAURIA, J., CHANDRADOSS, S. D., JOO, C. & MACRAE, I. J. 2015. Water-mediated recognition of t1-adenosine anchors Argonaute2 to microRNA targets. *Elife,* 4.

SCHRATT, G. 2009. microRNAs at the synapse. *Nature Reviews Neuroscience,* 10**,** 842.

SCHRATT, G. M., TUEBING, F., NIGH, E. A., KANE, C. G., SABATINI, M. E., KIEBLER, M. & GREENBERG, M. E. 2006. A brain-specific microRNA regulates dendritic spine development. *Nature,* 439**,** 283-9.

SCHULLER, A. P. & GREEN, R. 2018. Roadblocks and resolutions in eukaryotic translation. *Nature Reviews Molecular Cell Biology,* 19**,** 526-541.

SHALIZI, A., GAUDILLIÈRE, B., YUAN, Z., STEGMÜLLER, J., SHIROGANE, T., GE, Q., TAN, Y., SCHULMAN, B., HARPER, J. W. & BONNI, A. 2006. A Calcium-Regulated MEF2 Sumoylation Switch Controls Postsynaptic Differentiation. *Science,* 311**,** 1012.

SHENG, M. & KIM, E. 2011. The postsynaptic organization of synapses. *Cold Spring Harb Perspect Biol,* 3.

SIEGERT, S., SEO, J., KWON, E. J., RUDENKO, A., CHO, S., WANG, W., FLOOD, Z., MARTORELL, A. J., ERICSSON, M., MUNGENAST, A. E. & TSAI, L. H. 2015. The schizophrenia risk gene product miR-137 alters presynaptic plasticity. *Nat Neurosci,* 18**,** 1008-16.

SILLIVAN, S. E., JAMIESON, S., DE NIJS, L., JONES, M., SNIJDERS, C., KLENGEL, T., JOSEPH, N. F., KRAUSKOPF, J., KLEINJANS, J., VINKERS, C. H., BOKS, M. P. M., GEUZE, E., VERMETTEN, E., BERRETTA, S., RESSLER, K. J., RUTTEN, B. P. F., RUMBAUGH, G. & MILLER, C. A. 2019. MicroRNA regulation of persistent stress-enhanced memory. *Mol Psychiatry*.

SILVA, L. F., HOFFMANN, M. S., RAMBO, L. M., RIBEIRO, L. R., LIMA, F. D., FURIAN, A. F., OLIVEIRA, M. S., FIGHERA, M. R. & ROYES, L. F. 2011. The involvement of Na+, K+-ATPase activity and free radical generation in the susceptibility to pentylenetetrazol-induced seizures after experimental traumatic brain injury. *J Neurol Sci,* 308**,** 35-40.

SKARIAH, G., SEIMETZ, J., NORSWORTHY, M., LANNOM, M. C., KENNY, P. J., ELRAKHAWY, M., FORSTHOEFEL, C., DRNEVICH, J., KALSOTRA, A. & CEMAN, S. 2017. Mov10 suppresses retroelements and regulates neuronal development and function in the developing brain. *BMC biology,* 15**,** 54-54.

SMIRNOVA, L., SEREGIN, A., BOKSHA, I., DMITRIEVA, E., SIMUTKIN, G., KORNETOVA, E., SAVUSHKINA, O., LETOVA, A., BOKHAN, N., IVANOVA, S. & ZGODA, V. 2019. The difference in serum proteomes in schizophrenia and bipolar disorder. *BMC Genomics,* 20**,** 535.

SONENBERG, N. & HINNEBUSCH, A. G. 2009. Regulation of translation initiation in eukaryotes: mechanisms and biological targets. *Cell,* 136**,** 731-45.

SONG, T., ZHENG, Y., WANG, Y., KATZ, Z., LIU, X., CHEN, S., SINGER, R. H. & GU, W. 2015. Specific interaction of KIF11 with ZBP1 regulates the transport of beta-actin mRNA and cell motility. *J Cell Sci,* 128**,** 1001-10.

SOUSA, I., CLARK, T. G., HOLT, R., PAGNAMENTA, A. T., MULDER, E. J., MINDERAA, R. B., BAILEY, A. J., BATTAGLIA, A., KLAUCK, S. M., POUSTKA, F., MONACO, A. P. & INTERNATIONAL MOLECULAR GENETIC STUDY OF AUTISM, C. 2010. Polymorphisms in leucine-rich repeat genes are associated with autism spectrum disorder susceptibility in populations of European ancestry. *Molecular Autism,* 1**,** 7.

STARK, A., BRENNECKE, J., BUSHATI, N., RUSSELL, R. B. & COHEN, S. M. 2005. Animal MicroRNAs confer robustness to gene expression and have a significant impact on 3'UTR evolution. *Cell,* 123**,** 1133-46.

STEINER, P., SARRIA, J. C., GLAUSER, L., MAGNIN, S., CATSICAS, S. & HIRLING, H. 2002. Modulation of receptor cycling by neuron-enriched endosomal protein of 21 kD. *J Cell Biol,* 157**,** 1197-209.

SUDHAKARAN, I. P., HILLEBRAND, J., DERVAN, A., DAS, S., HOLOHAN, E. E., HÜLSMEIER, J., SAROV, M., PARKER, R., VIJAYRAGHAVAN, K. & RAMASWAMI, M. 2014. FMRP and Ataxin-2 function together in long-term olfactory habituation and neuronal translational control. *Proceedings of the National Academy of Sciences,* 111**,** E99-E108.

SUDHOF, T. C. 2012. The presynaptic active zone. *Neuron,* 75**,** 11-25.

SUDHOF, T. C. 2013. Neurotransmitter release: the last millisecond in the life of a synaptic vesicle. *Neuron,* 80**,** 675-90.

SUN, Y., LUO, Z. M., GUO, X. M., SU, D. F. & LIU, X. 2015. An updated role of microRNA-124 in central nervous system disorders: a review. *Front Cell Neurosci,* 9**,** 193.

SÜDHOF, T. C. 2013. A molecular machine for neurotransmitter release: synaptotagmin and beyond. *Nature Medicine,* 19**,** 1227.

SÜDHOF, T. C. 2018. Towards an Understanding of Synapse Formation. *Neuron,* 100**,** 276-293.

TAKANO, T., XU, C., FUNAHASHI, Y., NAMBA, T. & KAIBUCHI, K. 2015. Neuronal polarization. *Development,* 142**,** 2088-2093.

TAKEHASHI, M., ALIOTO, T., STEDEFORD, T., PERSAD, A. S., BANASIK, M., MASLIAH, E., TANAKA, S. & UEDA, K. 2004. Septin 3 gene polymorphism in Alzheimer's disease. *Gene expression,* 11**,** 263-270.

TEBALDI, T., ZUCCOTTI, P., PERONI, D., KOHN, M., GASPERINI, L., POTRICH, V., BONAZZA, V., DUDNAKOVA, T., ROSSI, A., SANGUINETTI, G., CONTI, L., MACCHI, P., D'AGOSTINO, V., VIERO, G., TOLLERVEY, D., HUTTELMAIER, S. & QUATTRONE, A. 2018. HuD Is a Neural Translation Enhancer Acting on mTORC1-Responsive Genes and Counteracted by the Y3 Small Non-coding RNA. *Mol Cell,* 71**,** 256-270.e10.

TEJERO, R., LOPEZ-MANZANEDA, M., ARUMUGAM, S. & TABARES, L. 2016. Synaptotagmin-2, and -1, linked to neurotransmission impairment and vulnerability in Spinal Muscular Atrophy. *Hum Mol Genet,* 25**,** 4703-4716.

TENGA, A., BEARD, J. A., TAKWI, A., WANG, Y. M. & CHEN, T. 2016. Regulation of Nuclear Receptor Nur77 by miR-124. *PLoS One,* 11.

THOMAS, K. T., ANDERSON, B. R., SHAH, N., ZIMMER, S. E., HAWKINS, D., VALDEZ, A. N., GU, Q. & BASSELL, G. J. 2017. Inhibition of the Schizophrenia-Associated MicroRNA miR-137 Disrupts Nrg1α Neurodevelopmental Signal Transduction. *Cell Reports,* 20**,** 1-12.

THOMAS, K. T., GROSS, C. & BASSELL, G. J. 2018. microRNAs Sculpt Neuronal Communication in a Tight Balance That Is Lost in Neurological Disease. *Frontiers in Molecular Neuroscience,* 11.

THOMSON, S. R., SEO, S. S., BARNES, S. A., LOUROS, S. R., MUSCAS, M., DANDO, O., KIRBY, C., WYLLIE, D. J. A., HARDINGHAM, G. E., KIND, P. C. & OSTERWEIL, E. K. 2017. Cell-Type-Specific Translation Profiling Reveals a Novel Strategy for Treating Fragile X Syndrome. *Neuron,* 95**,** 550-563.e5.

TOGNINI, P. & PIZZORUSSO, T. 2012. MicroRNA212/132 family: Molecular transducer of neuronal function and plasticity. *The International Journal of Biochemistry & Cell Biology,* 44**,** 6-10.

TOLOSA, E., BOTTA-ORFILA, T., MORATÓ, X., CALATAYUD, C., FERRER-LORENTE, R., MARTÍ, M.-J., FERNÁNDEZ, M., GAIG, C., RAYA, Á., CONSIGLIO, A., EZQUERRA, M. & FERNÁNDEZ-SANTIAGO, R. 2018. MicroRNA alterations in iPSC-derived dopaminergic neurons from Parkinson disease patients. *Neurobiology of Aging,* 69**,** 283-291.

TOMARI, Y., DU, T., HALEY, B., SCHWARZ, D. S., BENNETT, R., COOK, H. A., KOPPETSCH, B. S., THEURKAUF, W. E. & ZAMORE, P. D. 2004. RISC Assembly Defects in the Drosophila RNAi Mutant armitage. *Cell,* 116**,** 831-841.

TORVUND-JENSEN, J., STEENGAARD, J., ASKEBJERG, L. B., KJAER-SORENSEN, K. & LAURSEN, L. S. 2018. The 3'UTRs of Myelin Basic Protein mRNAs Regulate Transport, Local Translation and Sensitivity to Neuronal Activity in Zebrafish. *Front Mol Neurosci,* 11**,** 185.

TSAI, N. P., LIN, Y. L. & WEI, L. N. 2009. MicroRNA mir-346 targets the 5'-untranslated region of receptor-interacting protein 140 (RIP140) mRNA and up-regulates its protein expression. *Biochem J,* 424**,** 411-8.

TSANG, C. W., FEDCHYSHYN, M., HARRISON, J., XIE, H., XUE, J., ROBINSON, P. J., WANG, L. Y. & TRIMBLE, W. S. 2008. Superfluous role of mammalian septins 3 and 5 in neuronal development and synaptic transmission. *Mol Cell Biol,* 28**,** 7012-29.

TUBING, F., VENDRA, G., MIKL, M., MACCHI, P., THOMAS, S. & KIEBLER, M. A. 2010. Dendritically localized transcripts are sorted into distinct ribonucleoprotein particles that display fast directional motility along dendrites of hippocampal neurons. *J Neurosci,* 30**,** 4160-70.

VAN BATTUM, E. Y., VERHAGEN, M. G., VANGOOR, V. R., FUJITA, Y., DERIJCK, A., O'DUIBHIR, E., GIULIANI, G., DE GUNST, T., ADOLFS, Y., LELIEVELD, D., EGAN, D., SCHAAPVELD, R. Q. J., YAMASHITA, T. & PASTERKAMP, R. J. 2018. An Image-Based miRNA Screen Identifies miRNA-135s As Regulators of CNS Axon Growth and Regeneration by Targeting Kruppel-like Factor 4. *J Neurosci,* 38**,** 613-630.

VAROQUEAUX, F., JAMAIN, S. & BROSE, N. 2004. Neuroligin 2 is exclusively localized to inhibitory synapses. *Eur J Cell Biol,* 83**,** 449-56.

VASUDEVAN, S. & STEITZ, J. A. 2007. AU-rich-element-mediated upregulation of translation by FXR1 and Argonaute 2. *Cell,* 128**,** 1105-1118.

VASUDEVAN, S., TONG, Y. & STEITZ, J. A. 2007. Switching from Repression to Activation: MicroRNAs Can Up-Regulate Translation. *Science,* 318**,** 1931.

VO, N., KLEIN, M. E., VARLAMOVA, O., KELLER, D. M., YAMAMOTO, T., GOODMAN, R. H. & IMPEY, S. 2005. A cAMP-response element binding protein-induced microRNA regulates neuronal morphogenesis. *Proc Natl Acad Sci U S A,* 102**,** 16426-31.

WAN, R. P., ZHOU, L. T., YANG, H. X., ZHOU, Y. T., YE, S. H., ZHAO, Q. H., GAO, M. M., LIAO, W. P., YI, Y. H. & LONG, Y. S. 2017. Involvement of FMRP in Primary MicroRNA Processing via Enhancing Drosha Translation. *Mol Neurobiol,* 54**,** 2585-2594.

WANG, B., PAN, L., WEI, M., WANG, Q., LIU, W. W., WANG, N., JIANG, X. Y., ZHANG, X. & BAO, L. 2015. FMRP-Mediated Axonal Delivery of miR-181d Regulates Axon Elongation by Locally Targeting Map1b and Calm1. *Cell Rep,* 13**,** 2794-807.

WANG, E. T., TALIAFERRO, J. M., LEE, J. A., SUDHAKARAN, I. P., ROSSOLL, W., GROSS, C., MOSS, K. R. & BASSELL, G. J. 2016. Dysregulation of mRNA Localization and Translation in Genetic Disease. *J Neurosci,* 36**,** 11418-26.

WANG, W., GUO, Y., HE, L., CHEN, C., LUO, J., MA, Y., LI, J., YANG, Y., YANG, Q., DU, C., ZHANG, Y., LI, Z., XU, X., TIAN, X. & WANG, X. 2018. Overexpression of miRNA-137 in the brain suppresses seizure activity and neuronal excitability: A new potential therapeutic strategy for epilepsy. *Neuropharmacology,* 138**,** 170-181.

WANG, X. 2014. Composition of seed sequence is a major determinant of microRNA targeting patterns. *Bioinformatics (Oxford, England),* 30**,** 1377-1383.

WELLS, S. E., HILLNER, P. E., VALE, R. D. & SACHS, A. B. 1998. Circularization of mRNA by Eukaryotic Translation Initiation Factors. *Molecular Cell,* 2**,** 135-140.

WIGHTMAN, B., HA, I. & RUVKUN, G. 1993. Posttranscriptional regulation of the heterochronic gene lin-14 by lin-4 mediates temporal pattern formation in C. elegans. *Cell,* 75**,** 855-862.

WILCZYNSKA, A. & BUSHELL, M. 2015. The complexity of miRNA-mediated repression. *Cell Death and Differentiation,* 22**,** 22-33.

WILCZYNSKA, A., GILLEN, S. L., SCHMIDT, T., MEIJER, H. A., JUKES-JONES, R., LANGLAIS, C., KOPRA, K., LU, W.-T., GODFREY, J. D., HAWLEY, B. R., HODGE, K., ZANIVAN, S., CAIN, K., LE QUESNE, J. & BUSHELL, M. 2019. eIF4A2 drives repression of

translation at initiation by Ccr4-Not through purine-rich motifs in the 5'UTR. *Genome Biology,* 20**,** 262.

WILHELM, J. E. & VALE, R. D. 1993. RNA on the move: the mRNA localization pathway. *J Cell Biol,* 123**,** 269-74.

WILLEMSEN, M. H., VALLES, A., KIRKELS, L. A., MASTEBROEK, M., OLDE LOOHUIS, N., KOS, A., WISSINK-LINDHOUT, W. M., DE BROUWER, A. P., NILLESEN, W. M., PFUNDT, R., HOLDER-ESPINASSE, M., VALLEE, L., ANDRIEUX, J., COPPENS-HOFMAN, M. C., RENSEN, H., HAMEL, B. C., VAN BOKHOVEN, H., ASCHRAFI, A. & KLEEFSTRA, T. 2011. Chromosome 1p21.3 microdeletions comprising DPYD and MIR137 are associated with intellectual disability. *J Med Genet,* 48**,** 810-8.

WOLF, J. & PASSMORE, L. A. 2014. mRNA deadenylation by Pan2-Pan3. *Biochem Soc Trans,* 42**,** 184-7.

WRIGHT, C., TURNER, J. A., CALHOUN, V. D. & PERRONE-BIZZOZERO, N. 2013. Potential Impact of miR-137 and Its Targets in Schizophrenia. *Front Genet,* 4**,** 58.

XU, J., PANG, Z. P., SHIN, O.-H. & SÜDHOF, T. C. 2009. Synaptotagmin-1 functions as a Ca2+ sensor for spontaneous release. *Nature neuroscience,* 12**,** 759-766.

YABE, I., YAGUCHI, H., KATO, Y., MIKI, Y., TAKAHASHI, H., TANIKAWA, S., SHIRAI, S., TAKAHASHI, I., KIMURA, M., HAMA, Y., MATSUSHIMA, M., FUJIOKA, S., KANO, T., WATANABE, M., NAKAGAWA, S., KUNIEDA, Y., IKEDA, Y., HASEGAWA, M., NISHIHARA, H., OHTSUKA, T., TANAKA, S., TSUBOI, Y., HATAKEYAMA, S., WAKABAYASHI, K. & SASAKI, H. 2018. Mutations in bassoon in individuals with familial and sporadic progressive supranuclear palsy-like syndrome. *Scientific reports,* 8**,** 819-819.

YAMADA, M., TAKAHASHI, K., TSUNODA, M., NISHIOKA, G., KUDO, K., OHATA, H., KAMIJIMA, K., HIGUCHI, T. & MOMOSE, K. 2002. Differential expression of VAMP2/synaptobrevin-2 after antidepressant and electroconvulsive treatment in rat frontal cortex. *The Pharmacogenomics Journal,* 2**,** 377-382.

YANG, C.-H., HUANG, C.-C. & HSU, K.-S. 2006. Novelty exploration elicits a reversal of acute stress-induced modulation of hippocampal synaptic plasticity in the rat. *The Journal of physiology,* 577**,** 601-615.

YANG, C.-H., HUANG, C.-C. & HSU, K.-S. 2012a. A Critical Role for Protein Tyrosine Phosphatase Nonreceptor Type 5 in Determining Individual Susceptibility to Develop Stress-Related Cognitive and Morphological Changes. *The Journal of Neuroscience,* 32**,** 7550-7562.

YANG, Y., SHU, X., LIU, D., SHANG, Y., WU, Y., PEI, L., XU, X., TIAN, Q., ZHANG, J., QIAN, K., WANG, Y. X., PETRALIA, R. S., TU, W., ZHU, L. Q., WANG, J. Z. & LU, Y. 2012b. EPAC null mutation impairs learning and social interactions via aberrant regulation of miR-124 and Zif268 translation. *Neuron,* 73**,** 774-88.

YAP, C. C., DIGILIO, L., MCMAHON, L. & WINCKLER, B. 2017. The endosomal neuronal proteins Nsg1/NEEP21 and Nsg2/P19 are itinerant, not resident proteins of dendritic endosomes. *Sci Rep,* 7**,** 10481.

YATES, A. D., ACHUTHAN, P., AKANNI, W., ALLEN, J., ALLEN, J., ALVAREZ-JARRETA, J., AMODE, M. R., ARMEAN, I. M., AZOV, A. G., BENNETT, R., BHAI, J., BILLIS, K., BODDU, S., MARUGÁN, J. C., CUMMINS, C., DAVIDSON, C., DODIYA, K., FATIMA, R., GALL, A., GIRON, C. G., GIL, L., GREGO, T., HAGGERTY, L., HASKELL, E., HOURLIER, T., IZUOGU, O. G., JANACEK, S. H., JUETTEMANN, T., KAY, M., LAVIDAS, I., LE, T., LEMOS, D., MARTINEZ, J. G., MAUREL, T., MCDOWALL, M.,

MCMAHON, A., MOHANAN, S., MOORE, B., NUHN, M., OHEH, D. N., PARKER, A., PARTON, A., PATRICIO, M., SAKTHIVEL, M. P., ABDUL SALAM, A. I., SCHMITT, B. M., SCHUILENBURG, H., SHEPPARD, D., SYCHEVA, M., SZUBA, M., TAYLOR, K., THORMANN, A., THREADGOLD, G., VULLO, A., WALTS, B., WINTERBOTTOM, A., ZADISSA, A., CHAKIACHVILI, M., FLINT, B., FRANKISH, A., HUNT, S. E., IISLEY, G., KOSTADIMA, M., LANGRIDGE, N., LOVELAND, J. E., MARTIN, F. J., MORALES, J., MUDGE, J. M., MUFFATO, M., PERRY, E., RUFFIER, M., TREVANION, S. J., CUNNINGHAM, F., HOWE, K. L., ZERBINO, D. R. & FLICEK, P. 2019. Ensembl 2020. *Nucleic Acids Research,* 48**,** D682-D688.

YEOM, K. H., MITCHELL, S., LINARES, A. J., ZHENG, S., LIN, C. H., WANG, X. J., HOFFMANN, A. & BLACK, D. L. 2018. Polypyrimidine tract-binding protein blocks miRNA-124 biogenesis to enforce its neuronal-specific expression in the mouse. *Proc Natl Acad Sci U S A,* 115**,** E11061-e11070.

YIN, L., XIAO, X., GEORGIKOU, C., LUO, Y., LIU, L., GLADKICH, J., GROSS, W. & HERR, I. 2019. Sulforaphane Induces miR135b-5p and Its Target Gene, RASAL2, thereby Inhibiting the Progression of Pancreatic Cancer. *Molecular Therapy - Oncolytics,* 14**,** 74-81.

YOO, A. S., SUN, A. X., LI, L., SHCHEGLOVITOV, A., PORTMANN, T., LI, Y., LEE-MESSER, C., DOLMETSCH, R. E., TSIEN, R. W. & CRABTREE, G. R. 2011. MicroRNA-mediated conversion of human fibroblasts to neurons. *Nature,* 476**,** 228-231.

ZAPPULO, A., VAN DEN BRUCK, D., CIOLLI MATTIOLI, C., FRANKE, V., IMAMI, K., MCSHANE, E., MORENO-ESTELLES, M., CALVIELLO, L., FILIPCHYK, A., PEGUERO-SANCHEZ, E., MULLER, T., WOEHLER, A., BIRCHMEIER, C., MERINO, E., RAJEWSKY, N., OHLER, U., MAZZONI, E. O., SELBACH, M., AKALIN, A. & CHEKULAEVA, M. 2017. RNA localization is a key determinant of neurite-enriched proteome. *Nat Commun,* 8**,** 583.

ZEKRI, L., KUZUOGLU-OZTURK, D. & IZAURRALDE, E. 2013. GW182 proteins cause PABP dissociation from silenced miRNA targets in the absence of deadenylation. *Embo j,* 32**,** 1052-65.

ZHANG, A., YEUNG, P. L., LI, C. W., TSAI, S. C., DINH, G. K., WU, X., LI, H. & CHEN, J. D. 2004. Identification of a novel family of ankyrin repeats containing cofactors for p160 nuclear receptor coactivators. *J Biol Chem,* 279**,** 33799-805.

ZHANG, H. L., EOM, T., OLEYNIKOV, Y., SHENOY, S. M., LIEBELT, D. A., DICTENBERG, J. B., SINGER, R. H. & BASSELL, G. J. 2001. Neurotrophin-induced transport of a beta-actin mRNP complex increases beta-actin levels and stimulates growth cone motility. *Neuron,* 31**,** 261-75.

ZHANG, H. L., PAN, F., HONG, D., SHENOY, S. M., SINGER, R. H. & BASSELL, G. J. 2003. Active transport of the survival motor neuron protein and the role of exon-7 in cytoplasmic localization. *J Neurosci,* 23**,** 6627-37.

ZHANG, Y., XING, H., GUO, S., ZHENG, Z., WANG, H. & XU, D. 2016. MicroRNA-135b has a neuroprotective role via targeting of beta-site APP-cleaving enzyme 1. *Exp Ther Med,* 12**,** 809-814.